Surface Active Polymers as Anti-Infective and Anti-Biofouling Materials

Emily Margaret Parker

Worcester College
University of Oxford

A thesis submitted for the degree of
Doctor of Philosophy
Hilary 2012

This thesis is dedicated to my parents, Lynda and Steve, and my sister Amy.

The work described in this thesis is entirely my own, except where I have acknowledged help from a named person, or given a reference to a published source or thesis. Details of experiments not conducted by me can be found in the Acknowledgements, Chapter 6 and throughout the relevant sections. Any conclusions or analysis of data presented are my own. Text taken from another source is enclosed in quotation marks or a reference has been given.

Abstract

Surface Active Polymers as Anti-infective and Anti-biofouling Materials

Emily Margaret Parker, Worcester College, University of Oxford

Thesis submitted for the degree of D.Phil, Hilary Term 2012

This thesis is concerned with the chemical modification of polymers in the preparation of a library of materials which exhibit altered surface properties as a result of the surface chemical functionality, with particular emphasis on the development of materials that control biofouling and are antibacterial. Chemical modification of crosslinked polystyrene, in film and microsphere form, was carried out by carbene insertion followed by diazonium coupling. This provided access to a collection of materials with varying surface chemistry, whilst the bulk properties of the polystyrene substrates were maintained. Synthesis of the diaryldiazo and the diazonium salts used to perform the surface modifications is described, as well as the preparation and characterisation of the materials.

Analysis of the ability of the materials to adsorb and bind the protein bovine serum albumin (BSA) is presented with data obtained from two methods of observation. Quartz Crystal Microbalance with Dissipation (QCM-D) and a protein assay based on the change in optical density of a BSA/PBS solution are used to demonstrate how the specific surface chemistry of the materials influences the ability to adsorb and bind protein. The behaviour of the materials was time dependent and was rationalised with respect to the surface water contact angle and the calculated parameters polar surface area and % polar surface area of the functional groups added to the surfaces.

Finally, penicillin loaded materials were prepared and their antibacterial activity was tested against *E. coli* and *S. aureus,* demonstrating that the antibiotic is still active from within the polystyrene scaffold.

Acknowledgements

Firstly, I would like to thank Professor Mark Moloney for his support and supervision throughout my career so far. He introduced to me to scientific research during my Part II and it was a pleasure to return for my DPhil. I have learnt a lot from him and the experience has proved invaluable. I would also like to thank Dr Jon-Paul Griffiths, from Oxford Advanced Surfaces, for his input throughout.

This thesis would not have been possible without my collaborators. Geoffrey Nelson from the University of Oxford prepared the polystyrene films on the various substrates discussed in Chapter 3 as well carrying out XPS analysis of the modified substrates. The QCM-D experiments and optical microscopy were carried out by Geoffrey and I, whilst Geoffrey modelled the data to determine the change in mass and thicknesses measured during the QCM-D experiments. Dr Chris Blanford, now based at Manchester University, must be acknowledged for assisting Geoff and I in the QCM-D investigations. Professor Cleo Choong from NTU Singapore, and her research group performed the XPS, contact angle, SEM, DSC and TGA analysis of the polystyrene bead based materials discussed in Chapter 4. Professor Choong was also responsible for gathering the protein adsorption data presented in Chapter 5. Combustion analysis was outsourced to MEDAC Ltd. and further XPS analysis was performed by the Cardiff Catalysis Institute. The hole-plate bioassay experiments discussed in Chapter 5 were performed under the supervision of Wendy Sobey and Apichat Aphaiwong performed the bioassay of penicillin V in solution. I would also like to thank Dr Robert Jacobs of the University of Oxford for his assistance with the surface analysis of the materials I produced and for producing the gold coated silicon substrates modified in Chapter 3. Finally, I am very grateful to the rest of the CRL staff.

The Moloney group members past and present must be acknowledged; without whom my DPhil would not have been nearly as much fun. In particular Beth, Claire, Lawrence and Alex; Beth has kept me relatively sane for the last three and half years. My friends and family, Mum, Dad and Amy, as well as Matt have been constant source of support throughout. I appreciate and love them all enormously.

Finally, this work was made possible by the generous funding from the EPSRC and Oxford Advanced Surfaces Ltd.

Contents

Abbreviations i

Chapter 1 : Introduction 1

1.1 Biomaterials and biofouling 1

1.2 Control of biofouling 4

1.3 Surface modification techniques 21

1.4 Surface modification with diaryldiazo compounds 30

1.5 Thesis outline 44

Chapter 2 : Synthesis of organic coatings and solution phase investigations 46

2.1 Preparation of organic compounds for material modifications 46

2.2 Solution study of diazonium coupling 51

2.3 Conclusions 61

Chapter 3 : 2-D Model Study 63

3.1 Preparation of materials 63

3.2 Characterisation of surfaces 66

3.3 QCM-D analysis 72

3.4 Conclusions 87

Chapter 4 : Preparation and Characterisation of XAD-4 Based Materials 89

4.1 Choice of base material and target surface functionalities 90

4.2 Preparation of biopassive materials 91

4.3 Visual indication of diazonium coupling 93

4.4 Characterisation of biopassive materials 95

4.5 Preparation and characterisation of antibacterial materials 115

4.6 Conclusions 117

Chapter 5 : Assessment of Biological Properties 119

5.1 Protein Adsorption 119

5.2 Antibacterial materials 136

5.3 Summary 141

Chapter 6 : Experimental 144

6.1 General procedures and equipment 144

6.2 Chapter 2 146

6.3 Chapter 3 169

6.4 Chapter 4 175

6.5 Chapter 5 192

Chapter 7 : References 197

Appendix I : Combustion analysis calculations i

Appendix II : Protein Adsorption Correlations iv

Appendix III : Bioassay data and calibrations xii

Appendix IV : XPS data on disc xiv

Abbreviations

Ac	Acetate
app.	Apparent
aq.	Aqueous
Ar	Aryl
asym.	Asymmetric
ATR-IR	Attenuated total internal reflectance infra-red
Av	Avagadro's constant
BOC	*tert*-butyloxycarbonyl
BSA	Bovine serum albumin
Bu	Butyl
C. albicans	*Candida albicans*
ClogP	Calculated log of the partition coefficient
CMR	Calculated molecular refractivity
Conc.	Concentrated
COSY	2D 1H correlation spectroscopy
D	Doublet
Δ	Chemical shift
DCC	*N*,*N*'-Dicyclohexylcarbodiimide
DCM	Dichloromethane
Dd	Doublet doublet

DEPT	Distortionless enhancement by polarisation transfer
DMAP	4-(*N*,*N*-dimethylamino)pyridine
DPBS	Dulbecco's phosphate buffered saline
DSC	Differential scanning calorimetry
DVB	Divinyl benzene
E. coli	*Escherichia coli*
Eq	Equivalents
ESI	Electrospray ionisation
Et	Ethyl
FI	Field ionisation
FWHM	Full width at half maximum intensity
HMBC	Heteronuclear multibond correlation
Hr	Hour
HRMS	High resolution mass spectrometry
Hrs	Hours
HSQC	Heteronuclear single quantum Correlation
IR	Infra-red
kD	Kilo Daltons
Lit.	Literature
M	Molar
m	Multiplet

Me	Methyl
Mp	Melting point
M_r	Relative molecular mass
MSA	Molecular surface area
MW	Molecular weight
NMR	Nuclear magnetic resonance
OWLS	Optical waveguide light spectroscopy
P. aeroginosa	*Pseudomonas aeroginosa*
PBS	Phosphate buffered saline
PE	Polyethylene
PEG	Polyethylene glycol
PET	Polyethylene teraphthalate
Ppm	Parts per million
PS	Polystyrene
PSA	Polar surface area
PTFE	Polytetrafluoroethylene
q	Quartet
QCM-D	Quartz crystal microbalance dissipation
QAC	Quaternary ammonium compound
R_f	Retention factor
RT	Room Temperature

s	Singlet
S. aureus	*Staphylococcus aureus*
S. epidermidis	*Staphylococcus epidermidis*
SAM	Self-assembled monolayer
Sat.	Saturated
SD	Standard deviation
SDS	Sodium dodecyl sulfate
SEM	Scanning electron microscopy
sym.	Symmetric
T	*Tert*
T	Triplet
Tg	Glass transition temperature
TEG	Tri(ethylene glycol)
TGA	Thermal gravitational analysis
THF	Tetrahydrofuran
TLC	Thin layer chromatography
UV	Ultra violet
Wt	Weight
w/v	weight per volume
XPS	X-ray photoelectron spectroscopy

Chapter 1: Introduction

1.1 Biomaterials and biofouling

A biomaterial has been described as *'a nonviable material used in a medical device, intended to interact with biological systems'*.[1] Development and research into biomaterials has been on-going for over 60 years, with the first recorded biomaterials being documented in the 1940s. Harold Ridley noticed that the injuries associated with shards of canopy plastic embedded in the eyes of pilots were healing naturally without any further reaction from the body. He then went on to develop lenses from the canopy plastic, poly(methyl methacrylate), that could replace the natural cataractous lenses in the eye, with the first implantation occurring in 1949. Biomaterials have since been developed and used in a wide range of applications such as implants, stents, catheters, wound dressings along with hip and knee joints. Uses outside of the body include biosensors, cell culture materials, fuel cells and biofouling-resistant materials.[2]

Biofouling is the attachment and sometimes colonisation of biological molecules or organisms on surfaces. Within the body, bacteria and non-specific cell and protein adhesion are of interest in order to reduce infection and rejection associated with the use of medical implants and devices. Bacteria adhesion is also an issue of great interest outside the body, with antibacterial cleaning products and surfaces being used to reduce the development and spread of infection. Outside of the medical sector, antifouling paints are used in the marine industry to reduce colonisation on ship hulls by barnacles and algae; the increase in ship weight as a result of this leads to an increase in the fuel necessary for transport. This is especially evident in the shipping industry where the International Maritime Organisation estimated that the use of non-toxic effective antifouling coatings could reduce fuel emissions

of carbon dioxide and sulfur from 384 million tonnes to 3.6 million tonnes a year, saving the industry $60 billion per annum in fuel costs.[3] Previously, tin-based paints were applied to ship-hulls to prevent biofouling but since these paints are highly toxic to many other organisms in the marine environment, investigations are being employed to develop non-toxic alternatives.[4] Other uses of antifouling paints are to reduce the growth of mould and algae and to inhibit discolouration on outdoor walls and fences.[5,6]

1.1.1 Biomaterials in vivo

For a material to be used in biomedical applications, it must be biocompatible; biocompatibility has been defined as *'the ability of a material to perform with an appropriate host in response to a specific application'*.[7] An appropriate response is one that does not encourage infection and does not initiate a negative immune response. Upon insertion of a foreign material in the body, the area of surgical trauma is flooded with blood, and then non-specific protein adhesion occurs; protein adsorption is reversible whilst the protein is in its native state, but is irreversible after the protein has denatured, changed conformation leading to enhanced binding.[8] Cell adhesion follows protein adsorption, and this can result in the release of cytokines, signalling proteins that will result in a pro-inflammatory response. If this occurs, macrophage cells fuse together to form foreign body cells that will not disperse as long as the implant is present. The final response in this immune sequence is the formation of a wall-like structure around the implant, made of fibrous tissue that is about 50-200 μm thick. In addition, bacteria will compete with host cells to adhere to the protein adsorbed layer; once adhered, the bacteria will aggregate, and eventually a biofilm will be formed,[9] the formation and consequences of the existence of which is discussed below. The types of proteins adsorbed and their conformations on the surface of the implant dictate the type of cells that adhere to the surface. Fibrinogen is used

as a biological marker for biocompatibility as its presence on implant surfaces can result in thrombosis, the formation of blood clots, and this protein is therefore often used a standard to evaluate biocompatibility.[10]

1.1.2 Biofilms: colonisation of bacteria

Another hurdle that must be addressed in the development of biomaterials is moderation of the formation of bacterial biofilms on the surfaces of medical implants and devices; they are a major source of infection and show up to 1000 times higher tolerance to antibiotics and disinfectants compared with free forms of bacteria.[11,12] Biofilms are highly complex colonies of bacteria that are encased in a polymeric polysaccharide matrix which serves to give the biofilm structure and protection. Single bacterium aggregate on material surfaces and eventually form colonies using quorum sensing, a cell-cell communication method, to organise and develop the biofilm.[13] Failure of medical implants is most commonly due to infection, so reduction in biofilm formation and therefore infection could save the lives of hospital patients.[14,15]

Biofilms are very resilient to known methods of treatment; current antibiotics can treat infections due to planktonic bacteria effectively, however they are not active enough against biofilms; either the polysaccharide matrix prevents any penetration into the biofilm or the antibiotic cannot penetrate far enough into the biofilm. There is evidence of biofilms responding to antibiotic administration by increasing production of polysaccharide and increasing the size of the biofilm. This was observed by Hoffman *et al.*[16] who showed that exposure of *Pseudomonas aeroginosa* (*P. aeroginosa*) to the antibiotic Tobramycin actually induced biofilm formation; *P. aeroginosa* is a strain of bacteria associated with cystic fibrosis and infections stemming from the use of catheters. In addition, biofilms also release single bacteria from the colony, thus creating a source of chronic infection to the rest of the

body. The body's natural defences also struggle to combat biofilms; the presence of bacteria will induce the production of antibodies, but they are generally not effective at killing bacteria within the biofilm.[11,17] Treatment of infections resulting from biofilms usually involves removal of the device supporting the biofilm, followed by intense administration of antibiotics followed by introduction of a new device which is potentially exposed to the same problems.[9]

Whilst much of the focus has been with regard to the effects of biofilms within the body, it is noteworthy that biofilms can form on any surface; efforts to reduce biofilms are also being developed within other areas such as marine fouling and food packaging.

1.2 Control of biofouling

The necessity to control protein and cell adhesion as well as reduce biofilm formation is essential in the development of biomaterials to be used in medical applications, with control of protein and cell adhesion being essential for *in vivo* acceptance. A number of avenues are being investigated in order to control biofouling and increase the biocompatibility of surfaces. These include reducing non-specific protein and cell adhesion, creating biomimetic surfaces and tethering antimicrobials to surfaces that are toxic to bacteria or which inhibit the formation of biofilms.

Much work is going into determining how protein adhesion to material surfaces can be controlled. Proteins are made up of peptides which are linear sequences of amino acids joined by a peptide linkage. The peptides form hydrogen bonds internally and with other peptides resulting in regular structures in the form of α-helices and β-sheets, known as the secondary structure of proteins. The specific 3D arrangement of the proteins in space makes them biologically active, and their arrangement will change depending upon the

environment and the sequence of amino acids in the peptides. A polar environment will result in folding to expose the polar side chains whilst shielding the hydrophobic side chains, this is known as the hydrophobic effect. In physiological conditions the 3D structure is sustained by the hydrophobic effect, electrostatic forces between charged groups (COO^- and NH_3^+), van der Waals forces of attraction, hydrogen bonds, and disulphide bonds between different peptides and regions of the peptide.[18]

For protein adsorption at a surface to occur spontaneously, regardless of the mechanism, the change in Gibbs free energy of adsorption must be less than zero.[19]

$$\Delta G_{ads} = \Delta H_{ads} - T\Delta S_{ads} < 0$$

The adsorption of protein G on gold was investigated using a Quartz Crystal Microbalance (QCM) at three different temperatures, 296, 303 and 308 K.[20] Using the Vant Hoff relationship

$$\ln\left[\frac{K_2}{K_1}\right] = \frac{-\Delta H_{ads}}{R}\left[\frac{1}{T_2} - \frac{1}{T_1}\right]$$

where K_1 and K_2 are the equilibrium constants of adsorption and T_1 and T_2 the temperatures. The change in enthalpy of adsorption (ΔH_{ads}) was calculated to be -25 ± 6 kcal/mol, indicative of an exothermic adsorption process. Investigations into the effect of temperature on the Gibbs free energy change of adsorption (ΔG_{ads}) revealed that the adsorption followed the Langmuir isotherm, and the entropy change of adsorption (ΔS_{ads}) was calculated to be 0.52 kcal/mol.K. This indicated to the authors that entropy term had a larger contribution in driving the protein adsorption than the enthalpy term. Norde[19] demonstrated a similar outcome using caloritmetry and titration experiments to determine ΔG and ΔH of the

different sub-processes that contribute to adsorption of proteins. The adsorption of two proteins, lysozyme and α-lactalbumin, onto negatively charge polystyrene lattices were investigated and in both cases the total ΔG of adsorption was large and negative. The sub-processes investigated include association/dissociation of H^+ ions with charged groups on the protein surface, overlap of electric fields, non-electrostatic contributions to the incorporation of ions into the adsorbed layer, structural rearrangement of the protein and changes in the state of hydration of the surface such as dehydration upon protein adsorption. The dehydration of the polystyrene layer of both systems proceeded with a large increase in entropy, 0.60 kJ/mol.K, and the associated ΔG term had by far the largest contribution to the overall ΔG of adsorption at -220 kJ/mol. The total ΔG of adsorption was -280 kJ/mol for lysozyme and -400 kJ/mol for α-lactalbumin. The next largest negative ΔG contribution was due to the structural rearrangements of the protein, with ΔG terms of -60 and -200 for the lysozyme and α-lactalbumin, respectively. It is evident that for α-lactalbumin the structural rearrangement of the protein is also a major driving force along with the entropy term associated with displacement of water from the polystyrene lattice.

When considering materials that can be used as biomaterials, the following must be considered; the macroscopic or bulk properties including the mechanical properties, the microscopic surface properties including the chemical properties and topographical structure, and finally the atomic and molecular interactions the material will take part in. Kang *et al.*[10] used electropolishing to smooth the surface of stainless steel before grafting various polymers to the material. The smoother materials showed reduced adsorption of the protein fibrinogen compared to the rough analogues. However, surface chemistry is becoming increasingly dominant in controlling biomolecular adhesion and fouling, since the interfacial interactions between the surface and biomolecule are essential when considering the efficiency of a biomaterial.[7] The mechanical properties of the material are key when

designing a device since they must fulfil the needs of the application, but mechanically desirable materials are not always biocompatible. The ability to control the surface chemistry of materials allows the benefit of mechanical and biocompatible properties to be combined. There is a vast amount of research going into the control of biofouling of materials, particularly involving surface chemical modifications, as is discussed below.

1.2.1 Biopassive coatings to reduce protein and bacteria adhesion

The chemical functionality of a surface has proved to have a great influence on biofouling by inhibiting non-specific protein adhesion without being toxic, thereby making it biopassive. The functional groups on a surface affect the surface properties and will dictate conformations that proteins adopt on the surface,[21] and this has a knock-on effect in dictating the cells that adhere to the protein layer, thus influencing any further responses by the body.[2]

The effect of surface hydrophilicity, governed by the surface chemistry, on protein adsorption is well documented, with the overall conclusion being that protein adsorption increases as surfaces become more hydrophobic.[2,7,10,22] Hydrophilicity and hydrophobicity describe the wettability of a surface by water, with more hydrophilic surfaces having a higher affinity for water; water contact angles are used as a measure of wettability with smaller contact angles being indicative of hydrophilicity. Hydrophilic surfaces interact with water favourably by hydrogen bonding and the result is a network of water molecules that form a hydration layer around the material, with the extent of the hydration layer being dictated by the functional groups on the surface.[7] For protein adsorption to occur, proteins must first displace the water in order to gain access to the material surface; the stronger the surface water interactions and the greater the extent of hydration, the more difficult it is for the protein to gain access to the surface. Thus, it is hypothesised that a reduction in non-

specific protein adhesion using hydrophilic surfaces will prevent immune response reactions *in vivo* and result in materials with increased biocompatibility.[2,7,23]

The reduction of protein adhesion by hydrophilic surfaces is exemplified by a group of materials produced by the modification of silica with five different polymers, with their water contact angles demonstrating the variation in surface hydrophilicity. (**1-5**, Figure 1.1, Table 1.1).

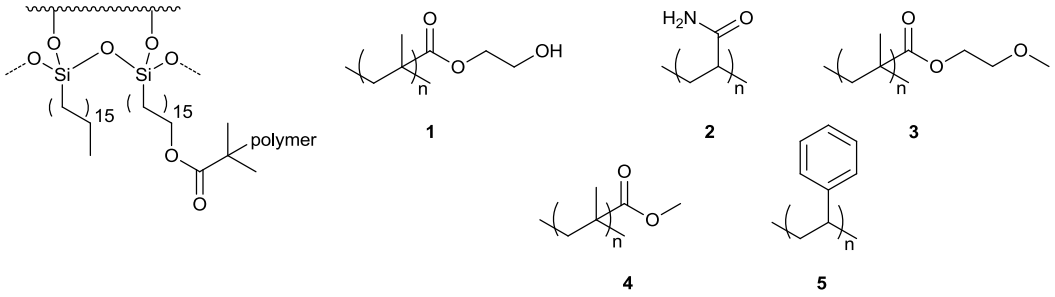

Figure 1.1: Polymer modified silica substrates.

Table 1.1: Contact angle and protein adsorption measurements for a range of silica based materials.

Material	Contact angle (degrees)	BSA adsorbed (μg nm^{-2})	Fibrinogen (μg nm^{-2})
1	25.4	4.7	0.09
2	35.5	5.7	0.14
3	64.4	1.5	0.02
4	78.3	9.2	0.20
5	98.3	13.0	0.23

The materials were exposed to fibrinogen and bovine serum albumin (BSA) and a direct correlation of decreasing protein adsorption with increasing hydrophilicity was observed in both cases, with the exception of **3** which deviated from the trend with both proteins; **3** demonstrated the smallest adsorption of all the modified materials.[23]

Materials modified with poly(ethylene glycol) (PEG) chains have proved to be exceptional in reducing protein adsorption and adhesion.[2,24] Stainless steel is a desirable material used in stents and orthopaedic implants due to good resistance and excellent mechanical properties, however, bare steel is not biocompatible. Successful modification with 3-glycidoxpropyltrimethoxysilane followed by grafting with various polymers including PEG furnished a set of materials **6**-**9** that exhibited lower protein adsorption than bare stainless steel (Figure 1.2).[10] As implied by the contact angles in Figure 1.2, all the materials are more hydrophilic than stainless steel (which has a contact angle of 78.8˚), with the PEG modified surface **6** having the smallest contact angle at 46˚, making it the most hydrophilic.

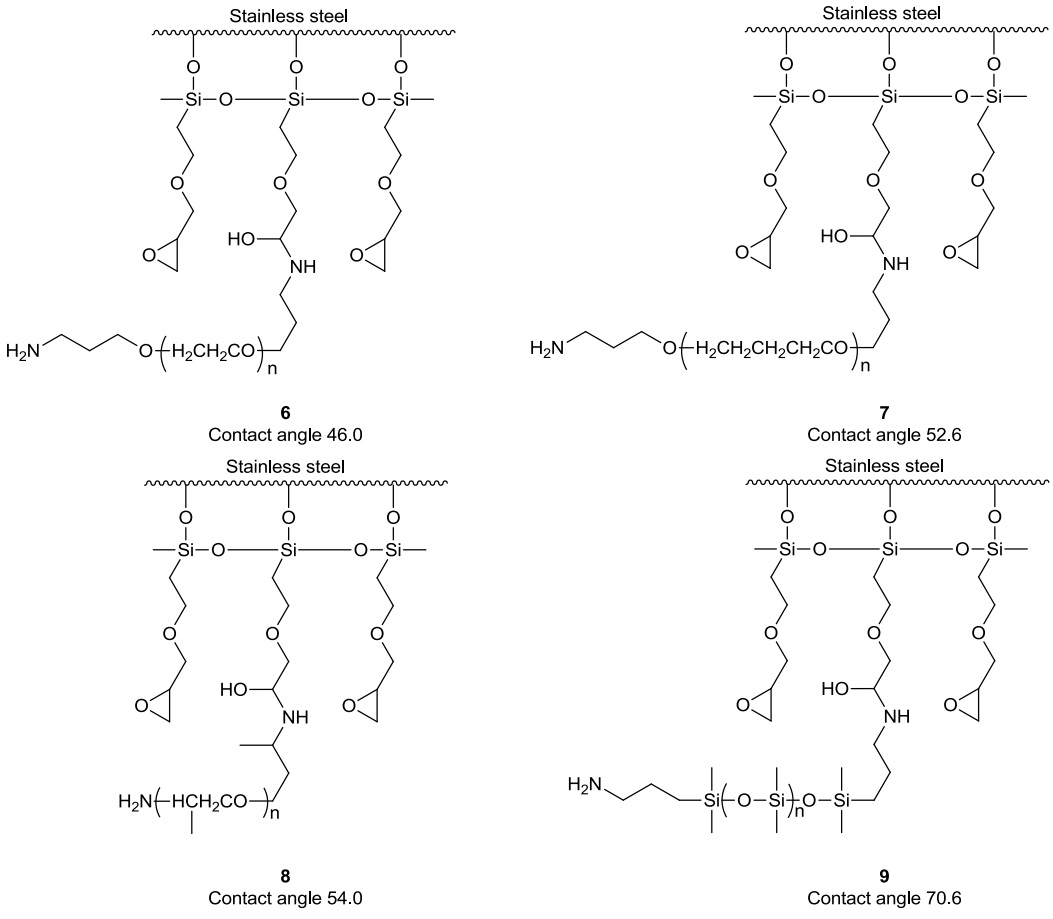

Figure 1.2: Stainless steel grafted polymers.

Fibrinogen was coupled to rhodamine succinimidyl ester, generating fluorescently tagged fibrinogen that could be observed by a fluorescent microscope as a means of quantifying protein adsorption. All the materials showed a decrease in fibrinogen adsorption by 72-83%, compared to untreated stainless steel, with the PEG surface **6** having lowest protein adsorption overall. The authors of this work also commented on the effect of using polymer chains to modify the surface; chains that are flexible suffer an entropy loss associated with compression and infiltration of the polymer chains by the proteins, which also inhibits protein adsorption. When the effect of chain density on protein adsorption was investigated using the silica coatings in Figure 1.1, it was found that the hydrophobic surfaces **4**-**5** showed no dependency on chain density; however the hydrophilic surfaces **1**-**3** exhibited decreased protein adsorption as the polymer chain density decreased. Hydrophilic polymers are much more mobile in the aqueous environment compared with the hydrophobic polymers, as the chain density increases the flexibility and freedom of the polymer chains will decrease hindering their ability to repel proteins.[23]

A disadvantage to PEG based surfaces is that the ethylene glycol moieties have a tendency to oxidize.[2,25] Consequently, Whitesides *et al.*[25] used self-assembled monolayers (SAMs) with varying terminal functionality in order to determine different functional groups that would be as effective as PEG in reducing protein adsorption (Table 1.2 below). They investigated surfaces with uniform functionality as well as mixed functionality to determine how they responded to fibrinogen, a large protein (340 kD), and lysozyme, a small (14 kD) positively charged protein. The mixed functional surfaces were achieved by mixing SAMs of a specific functionality with carboxylate terminated SAMs (CO_2H/CO_2^-). The percentage of a protein monolayer (% monolayer) was calculated from the change in response units as measured by surface plasmon resonance spectroscopy with reference to mixed alkyl SAM **11**. The most interesting candidates have been summarised below in Table 1.2.

Table 1.2: A selection protein resistant surfaces produced by Whitesides *et al.*.

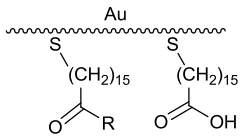 R		Advancing contact angle	% Monolayer	
			Fibrinogen	Lysozyme
10	$NH(CH_2CH_2O)_3H$	54	2	1
11	$NH(CH_2)_{11}CH_3$	156	100	100
12	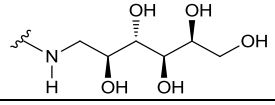	37	68	20
13	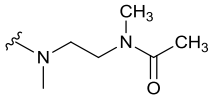	53	12	4
14	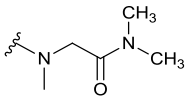	65	9	2
15	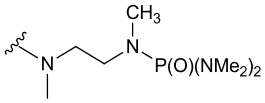	66	4	<1
16	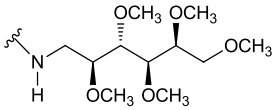	81	3	6

PEG terminated SAM **10** has % monolayer values of 2 and 1% for fibrinogen and lysozyme respectively. Materials **13-16** all have comparable protein resistance with **15** having greater resistance to lysozyme than PEG terminated material **10**. The results in Table 1.2 are for mixed SAMs, however the protein resistance was increased by using homogenous SAMs terminated with the groups used for **13-16**, although this was not true for all of the functionalities investigated. The advancing contact angles have been included; it is notable that amide **13** has a similar contact angle as PEG surface **10** but does not reduce protein adsorption as efficiently and alcohol **12** which has a very hydrophilic contact angle of 37˚ actually adsorbs high levels of both proteins. The methylated version of this surface, **16**, has a much higher contact angle but a lower level of protein adsorption; comparison of other methylated verses unmethylated surfaces consistently found that the methylated surfaces

adsorbed less protein. The authors noticed four molecular characteristics shared by functional surfaces that had a high resistance to protein adsorption; these are that the functional groups were polar, they had the capability to accept hydrogen bonding but did not contain hydrogen bonding donating groups and finally the surfaces did not have any net charge.[25] This work demonstrates that, whilst relying purely on hydrophilic surfaces does generate some coatings successful in reducing protein adsorption, the specific functional groups and how they bond is important also.

The effect of surface chemistry on the conformation of proteins has also been investigated. SAMs terminated with methyl, hydroxyl, acid and amine (CH_3, OH, COOH and NH_2) were exposed to fibronectin with the protein adsorption following the pattern OH<COOH<CH_3<NH_2. The acid and hydroxyl surfaces exhibited hydrophilic contact angles at 25˚ and 28˚, respectively, and the methyl terminated surface had a contact angle of 107˚, consistent with the trend of increasing surface wettability leading to decreasing protein adsorption. However, the amine terminated surface had a contact angle of 43˚ and broke away from this trend, presumably as the amine functionality interacts favourably with the proteins affording strong bonds. The conformations that the proteins adopted on the surfaces was investigated using a monoclonal antibody assay; the antibodies used are known to prevent protein adhesion to the central binding site of fibronectin, so that the level of antibody adhesion would be dependent on the amount of this central region that is accessible. Antibody binding followed the pattern of OH>COOH=NH_2>CH_3; the surfaces that bind protein via hydrogen bonding had high levels of antibody adsorption thus indicating that fibronectin bound to the methylated surface adopts conformations that reveal more of the central binding domain of the protein. The same pattern was observed for adsorption of integrin $\alpha_5\beta_1$ onto the fibronectin layers, whereas integrin α_v exhibited a different pattern COOH>>OH=NH_2=CH_3. Integrins are receptors that mediate cell

attachment to surrounding tissues and proteins so the effect of surface chemistry on integrin binding is of interest when considering biocompatible materials. This work was completed with the observation of MC3T3-E1 cell adhesion to the protein coated surfaces, resulting in the following trend OH>COOH>NH_2>CH_3.[21] The effect of surface chemistry on cell adhesion without protein coatings has also been investigated; polystyrene surfaces oxidised with various methods resulting in carboxylate/hydroxyl and sulfur/hydroxyl functionalised surfaces demonstrated increased cell adhesion with hamster kidney and leukocyte cells, however more detailed investigations revealed that the hydroxyl groups were necessary to increase the cell adhesion.[26]

The use of surface chemistry to inhibit biofilm formation has been widely investigated with most of the work involving antimicrobial and biomimetic surfaces that are discussed below. However, there are some examples of surface functionality affecting biofilm formation. PEG terminated surfaces have been shown to reduce bacteria adhesion, with covalently bonded PEG coatings reducing bacteria adhesion by up to two times compared with physisorbed PEG coatings.[9,27]

Figure 1.3 displays three SAMs on gold with differing functionality that were investigated by Ren *et al.* with regard to their effect on biofilm formation and bacteria adhesion.[12] Within 2 hours, bacterial adhesion to the bare gold surface was observed and biofilm formation was evident by the presence of viscous films after only 24 hours. However D-mannitol terminated SAM **18** exhibited reduced bacterial adhesion and biofilm formation with three strains of bacteria; by 24 hours, bacterial adhesion was reduced by 92.1%, 88.4% and 94.2% with *Escherichia coli* (*E. coli*), *Pseudomonas aeruginosa* (*P. aeruginosa*) and *Candida albicans* (*C. albicans*), respectively. The methylated SAM **17** showed no resistance to bacteria whilst the tri(ethylene glycol) (TEG) terminated SAM **19** showed resistance but not

to the same extent as the D-mannitol terminated surface **18**. Patterned surfaces were prepared on which a region of the surface was coated with either the D-mannitol **18** or TEG **19** SAMs and the surfaces were exposed to *E. coli*. In both cases, biofilm formation was observed in the unmodified regions but it took 7 days for the biofilms to expand into the modified areas of the TEG surface and 26 days for the D-mannitol surface. It was found that D-mannitol does not prevent biofilm formation when it is a free molecule, and the authors conclude that the solvent structure at the surface dominates in the prevention of biofilm formation. Other functional groups that reduce bacteria adhesion are phosphonates and zwitterionic groups, whilst sulfonated surfaces have increased *Staphylococcus aureus* (*S. aureus*) adhesion to polyurethane based materials.[22]

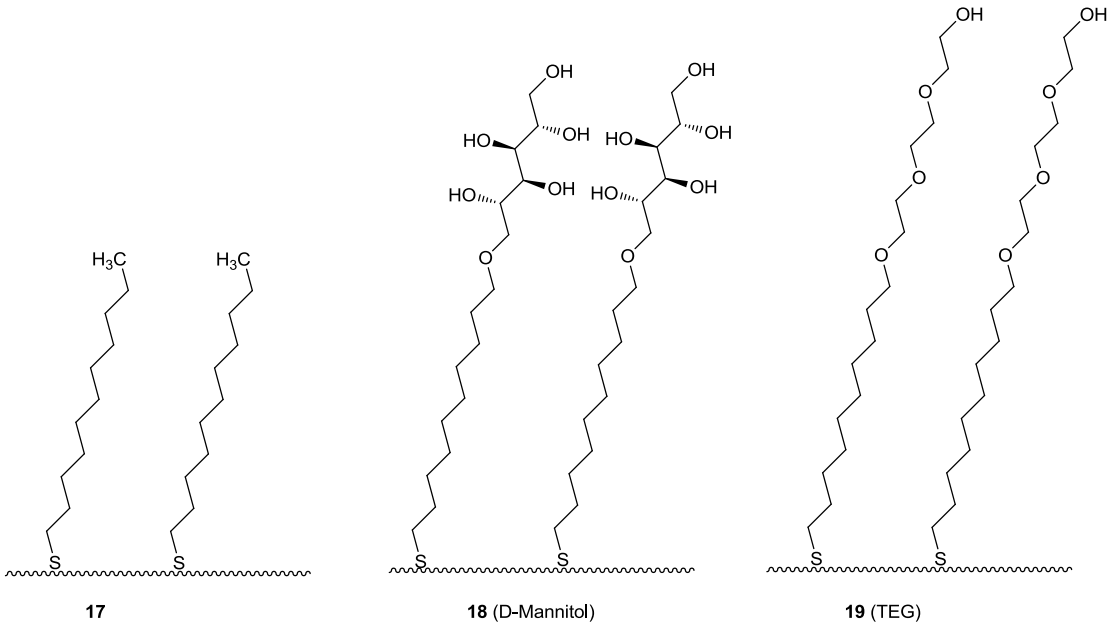

Figure 1.3: SAMs on gold used to investigate inhibition of biofilm formation.

1.2.2 Biomimetic materials to control cell adhesion

Biomimetic materials are inspired by natural biological surface properties and naturally occurring compounds that control cell adhesion, bacteria inhibition and protein adhesion. Biomimetic materials have been designed to promote specific cell adhesion and to be used as tissue engineering scaffolds that initiate a regenerative response; they can be used in the control of biofouling since both applications are aimed to reduce non-specific cell adhesion, thus decreasing immune response and rejection of the materials.[28-30] Use of biomimetic materials as tissue scaffolds is exemplified by phosphonate-containing acrylamide polymers that encouraged osteoblast cell proliferation for the use on materials that will aid bone growth and recovery. The inspiration for these materials stems from the knowledge that phosphate rich proteins initiate bone growth; it was hypothesised that phosphonate-containing polymers would imitate the mineral-protein interactions. Vinyl phosphonic acid and acrylamide were combined in varying amounts and the osteoblast cell proliferation after 7 days was measured for all of the materials. Acrylamide had 2×10^4 cells/cm^2, all of the phosphonate polymers showed greater cell proliferation, with 30% vinyl phosphonic acid proving to be optimal with 28×10^4 cells/cm^2.[29]

The control of cell adhesion using peptide motifs has been widely researched to control specific cell adhesion and discourage non-specific cell adhesion.[28,31,32] Initially, materials were coated with cell adhesive proteins such as fibronectin, collagen and laminin that would direct the cell adhesion.[33,34] However the fact that the proteins proved to be difficult to source since they are from natural organisms and need careful extraction and purification, and that the proteins were prone to degradation over time which reduced their effectiveness, all made this approach more complicated. Furthermore, the protein coatings were not stable in sterilisation conditions, heat treatment or to pH changes; all of these altered the

conformations of the proteins thus altering their cell specificity.[28] Peptide motifs commonly found in proteins also trigger specific cell adhesion and they proved to be much more resilient than proteins. A number of motifs have been found but RGD has been most extensively discussed as it directs adhesion of a broad range of cells;[28] the motif is displayed in Figure 1.4 and is made up of the arginine (R), glycine (G) and aspartic acid (D) amino acids.

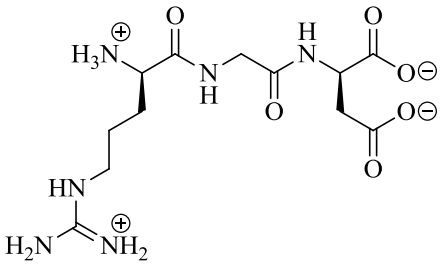

Figure 1.4: RGD motif commonly used to encourage cell specific adhesion.

Lee *et al.*[31] created SAMs terminated with acid and amine functionalities (COOH and NH_2); compared to unmodified silicon, the adhesion of K100 erythroleukemia cells was increased with the detachment strength increasing from 34.8 dyn/cm^2 to 188.3 dyn/cm^2, whilst the acid terminated surface exhibited lower adhesion strength with a detachment strength of 23.0 dyn/cm^2. Reaction of these two functional groups with the RGD tri-peptide generated surfaces that both showed increased cell adhesion, NH_2-RGD terminated surface exhibited a detachment strength of 201.1 dyn/cm^2 and COOH-RGD 37.7 dyn/cm^2. RGD modified titanium dental implants have exhibited increased adhesion of epithelial cells, fibroblasts and osteoblasts compared with PEG and RDG modified surfaces; the analogous RDG surface was analysed in order to confirm that the RGD motif was responsible for adhesion rather than the presence on the functional groups on the surface in any order.[35]

For the RGD peptide to bind cells, strong covalent attachment of the peptide to the material is needed to withstand the forces exerted by cells during binding, covalent attachment of RGD is discussed in detail below. Finally, it has been reported for the RGD containing peptides to be active, they need a certain amount of flexibility such that the RGD moiety can access the binding sites in the cells or integrins, consequently long chain linkers are commonly used to remove the peptide from the material surface.[31] It is notable that the activity of RGD is reduced when it is removed from a wider peptide sequence; furthermore the selectivity of cell binding *in vivo* is dictated by the surrounding amino acids as they influence the integrins that the peptide interacts with thus defining the cells that are adhered. For example, the YRGDG peptide on a PEG based network adhered mouse macrophage cells whilst YAVTGRGDS mediated adhesion of osteosarcoma (Balb/c 3T3) cells.[28]

1.2.3 Antibacterial surfaces

In order to contain the scope of this section, only antibacterials that are covalently bonded to material surface will discussed. Antibacterial surfaces are toxic to bacteria so reduce infection by killing the bacteria before they can aggregate and form biofilms that are more difficult to penetrate and combat. The deployment of antimicrobial peptides by small organisms is an effective method of nature's defence against infection; it was noticed that generally the peptides have a cationic group on one face of the molecule with a hydrophobic group at the other face such that the cationic group can penetrate the bacterium cell membrane without affecting the mammalian cells.[36] Kizhakkedathu *et al*.[37] obtained a selection of highly active peptides via high throughput screening and covalently attached them to titanium surfaces deposited in silica wafers via polymer brushes (Figure 1.5); the peptides chosen were active against a broad spectrum of bacteria and yeasts.

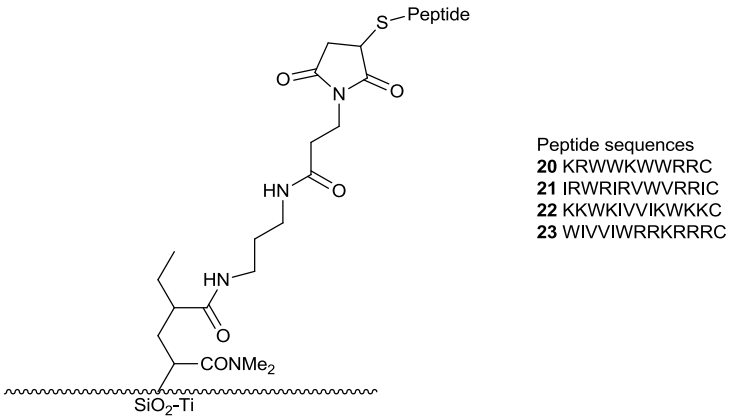

Figure 1.5: Polymer bushes terminated with antibacterial peptides.

The surfaces were exposed to *P. aeruginosa* for 7 days, after which the density of bacteria on each substrate was determined by staining. Unmodified titanium had a high density of 1268±695 bacteria per 0.35 mm^2; the bacteria coverage of the peptide terminated surfaces was at least 40% less than unmodified titanium in all cases with **23** having the smallest coverage at 8.4±6.6 bacteria per 0.35 mm^2.

Quaternary ammonium compounds (QACs) also have high levels of antibacterial activity due to the cationic quaternary ammonium moiety that is fatal to bacteria.[9,24] In solution, quaternary ammonium compounds are extremely active, although when the QACs are directly bonded to surfaces their activity is lost, and therefore a long chain spacer or linker is required to give the QACs enough flexibility and mobility to be able to penetrate the bacteria; studies have revealed that a cationic head group and a polar alkyl chain linking the cation to the surface are required for the surface to be antibacterial. Some examples can be found in Figure 1.6. In addition, no leaching of the QACs has been observed so the surface is permanently antibacterial as long as the surface is intact; **24** was tested against *S. aureus* and after 45 days of washing the polymer was still active with no leaching observed.[9] Surfaces **25** and **26** were found to be active against *S. aureus* and *E. coli*.[24] However, it is notable that quaternary ammonium compounds have shown toxicity towards human cells.[31]

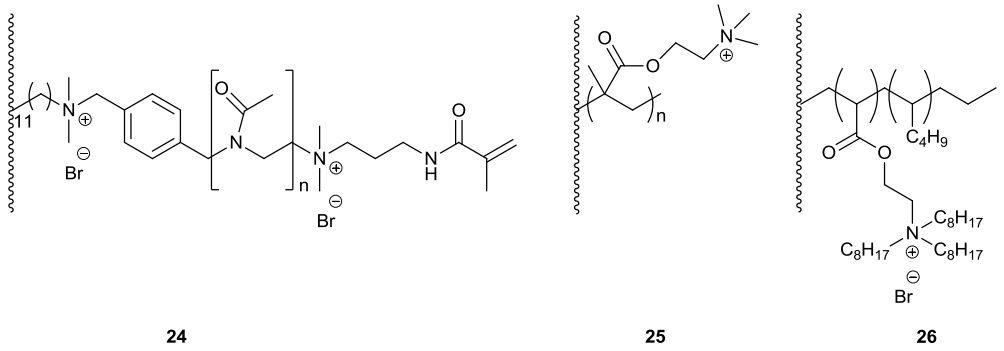

24 **25** **26**

Figure 1.6: Examples of antibacterial surfaces with quaternary ammonium compounds.

Combination of antibacterial coatings with biopassive antifouling coatings has been investigated with some success.[9] Copolymerisation of 2-(2-methoxy)ethyl methacrylate with oligo(ethylene glycol)methacrylate resulted in a hydrophilic polymer terminated with hydroxyl groups that were used to bond Magainin I, a natural antimicrobial peptide that is toxic to bacteria, to the surface. The peptide serves to kill bacteria on contact, whilst the biopassive polymer discourages fouling by preventing dead bacteria from settling on the surface, since fouling with dead bacteria will hinder the efficiency of a biocidal material.[38]

More inspiration comes from natural products that are antibacterial; halogenated furanones were isolated from Australian red algae *Delisea Pulchra* that are essential in preventing settlement of eukaryotic and prokaryotic organisms on the surface of the algae. The furanones are released onto the plant surface from vesicles situated in gland cells and are present on the surface in very small quantities, typically 10-100 ng.cm^{-2}.[39] There are two methods by which the furanones prevent fouling of bacteria, the first is by killing the bacteria on contact, thus being antibacterial, and the second is by preventing biofilm formation by stopping the quorum sensing mechanism used by the bacteria in biofilm construction; although the latter is not strictly antibacterial by toxicity, the molecules are still of interest for the reduction of fouling. Below, Figure 1.7 displays a selection on bromo-

furanones that were found to be active; **27**-**29** inhibit quorum sensing but are not lethal to bacteria whereas **30** and **31** are both toxic to bacteria on contact.[40]

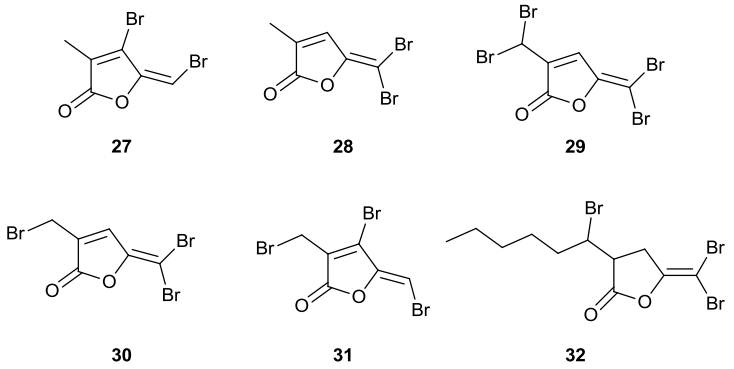

Figure 1.7: Active furanones that prevent biofilm formation.

3-(1ˈ-bromohexyl)5-dibromomethylene-2(5H)-furanone **32** was covalently attached to catheters, and biofilm formation by *Staphylococcus epidermidis* (*S. epidermidis*) was monitored *in vitro*. After 5 hours bacteria colonisation was reduced by 85% by the furanone terminated catheter compared to untreated commercially used catheters and after 24 hours the reduction went up to 78%. *In vivo* tests on sheep with the same furanone modified catheter were promising also, with a reduction in infection throughout the 84 day time period after implantation with the furanone terminated catheter compared with the control.[41] It must be noted that care must be taken in selecting furanones to be covalently bonded to materials since there have been reports of loss of activity after bonding.[42]

Finally, the covalent bonding of antibiotics to surfaces has proved to also decrease bacterial adhesion on surfaces. When penicillin was covalently bonded to polytetrafluoroethylene (PTFE), the method of attachment of which is discussed in detail below (Scheme 1.4) the amount of bacteria on the surface after being placed in a culture containing *S. aureus* was 80% less than that observed on unmodified PTFE.[43] Notably this system contained a PEG spacer that gave the penicillin freedom to move and resulted in the formation of a hydration

layer that prevents fouling. Ampicillin was covalently attached to PTFE using similar chemistry resulting in a material that showed resistance to *S. aureus*, *Enterococcus faecalis* and *Bacillus thuringiensis*.[44] PTFE is of interest due to its non-toxic and non-reactive properties, it is used in many medical applications such as soft tissue in reconstructive surgeries and orthopaedic implants.

1.3 Surface modification techniques

This section will focus on the methods for covalent surface modification of materials for the control of surface chemistry whilst the bulk properties of the base material are maintained. Polymers as biomaterials are of increasing interest since their diversity of chemical functionality provides access to a range of modified surfaces that can be utilised, in addition low-cost, ease of handling and modification are beneficial.[9]

1.3.1 Adding functionality to 'inert' materials

Surface functionality can be introduced onto polymers and other materials using a range of surface treatment techniques. Wet chemical treatments can take the form of oxidising agents that are applied to the surface of materials.[28] For example, polystyrene was treated with sulfuric acid and chloric acid, resulting in the formation of sulfonic acid groups and hydroxyl groups, respectively, on the material surface, as confirmed by ATR IR spectroscopic analysis. Application of ozone to polystyrene has also been shown to generate a mixture of hydroxyl and carbonyl functionality, whilst a combination of chromic anhydride and sulfuric acid was used to produce OH groups on the surface of a polyurethane.[26,45] Typically, surface modification of polymers is based on the hydrolysis of bonds within the polymer by the use of acid and alkaline treatments, although other methods include reduction of surface carbonyl groups with sodium borohydride to generate hydroxyl

groups as demonstrated on poly(aryletherketones).[46] Additionally, sodium hydride was used to deprotonate a poly(tetramethylene oxide) based polyurethane, after which reaction with a lactone introduced carboxylic acid groups to the surface.[47] Harsher conditions are required for metal and inorganic substrates; a mixture of hydrogen peroxide and concentrated sulfuric acid, known as piranha solution, concentrated aqueous ammonia and nitric acid have all been used to generate hydroxyl groups at the surface of silicon, glass and metal substrates such as titanium and stainless steel.[10,23,24]

Plasma treatment, typically argon and helium plasma, generates free radical species on the outer most surface of materials; the radical species can be reacted directly with compounds of interest or they can be exposed to air or oxygen to produce hydroxyl and peroxide groups.[24] Oxygen plasma has been exposed to poly(ethylene terephthalate) and polyethylene resulting in the formation of surface peroxide, carbonyl, carboxyl and hydroxyl groups.[48,49] If amine functionality is needed, then ammonia plasma can be used, and this has been demonstrated on a wide range of polymers including polypropylene.[50] Plasma deposition is also widely used, where the plasma contains a chemical monomer which will deposit onto the surface as a thin film. Upon exposure of the surface to plasma, free radical species are produced which react with the chemical monomer initiating polymerisation to produce a thin film. An example is the creation of a polymeric thin film with aldehyde functional groups on a hydroxyethyl methacrylate contact lens by exposure to plasma containing propanal.[24] The use of free radical species in surface treatments is also observed in radiation or electron beam treatment where the surface irradiation generates free radicals, which are then exposed to the functional groups of interest.[24] For example, Hu *et al.*[51] exposed PET fibres to ^{60}Co γ-rays after which the fibres were soaked in 10 wt% *N*-vinyl formamide, and reaction of the surface radicals with *N*-vinyl formamide resulted in poly(*N*-vinylformamide) bonded to the PET film. After hydrolysis of the amide groups to amines, chitosan was bonded to the

material, as demonstrated below in Scheme 1.1. Chitosan binds to the cell walls of bacteria thus preventing metabolism of the bacteria, and consequently the chitosan terminated surface showed antibacterial activity against a range of bacteria including *S. aureus* and *P. aeruginosa*. Plasma and irradiation methods of producing and tailoring surface functionality have proved to be very efficient, but they do require sophisticated equipment whilst wet chemical surface treatments are more straightforward to perform.

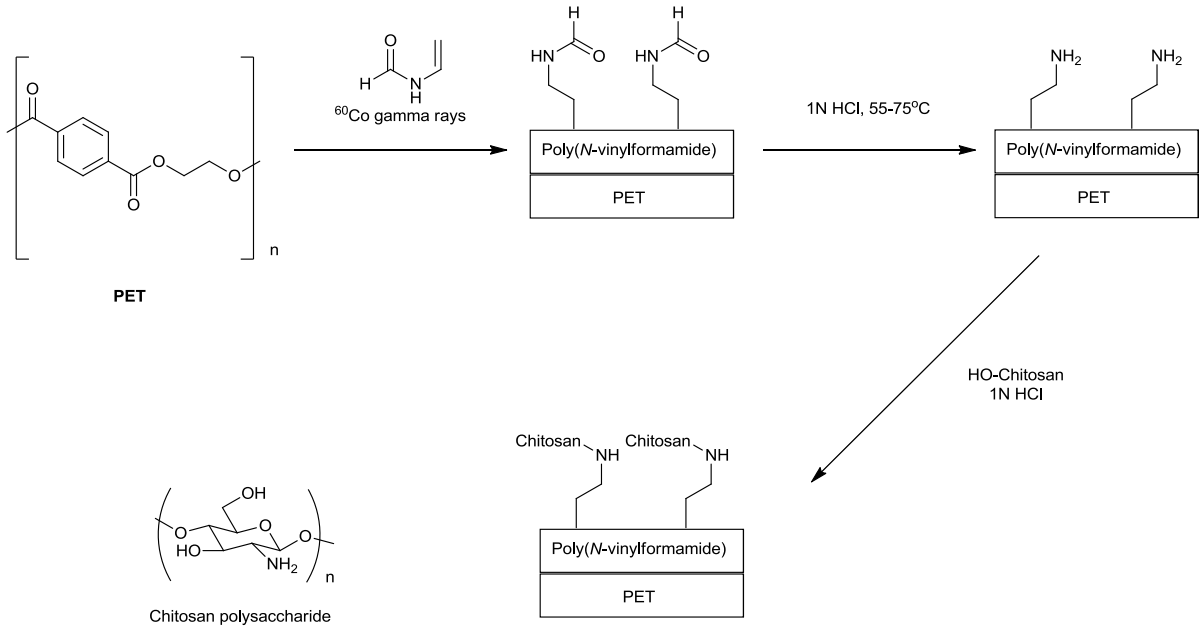

Scheme 1.1: Surface modification of PET.

1.3.2 Utilising surface functionality

Surface functionality to further modify surfaces is widely used in the preparation of antifouling and antibacterial materials, whether that surface chemistry is integral to the base material or if it is produced using one of many methods including those discussed previously. Below is a discussion of a selection of specific examples.

Alkoxysilane chemistry is widely used to attach antimicrobials, functional groups and polymers to OH groups on the surface of materials. The use of silane chemistry to bond antibacterials was inspired by the discovery, at Dow Corning's Biomedical Research Laboratory, that organosilicon-substituted quaternary ammonium salts were antibacterial in 1969, and this inspired many studies into the use of organosilanes to tether quaternary ammonium salts to materials.[24,52]

Kang *et al*.[52] demonstrated the use of alkoxysilanes in tethering hydrophilic polymers to a stainless steel substrate (Scheme 1.2) via 3-glycidoxypropyltrimethoxysilane **34**. After treatment with piranha solution, hydroxylated stainless steel **33** was reacted with silane **34** to generate epoxide terminated material **35**. Various polymers were then grafted to **35,** resulting in materials **6-9**, as previously discussed (Figure 1.2). The use of silane chemistry was also demonstrated by Yoshino *et al*.[23] on silica (Figure 1.1).

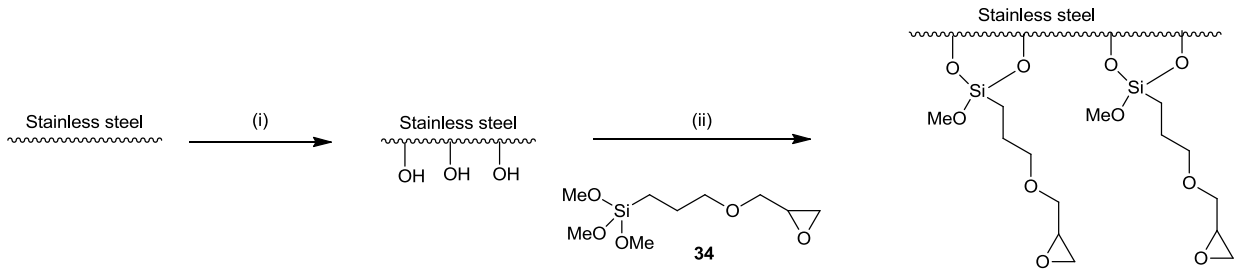

Scheme 1.2: Surface modification of stainless steel. Conditions: i) piranha solution (4:1 H_2SO_4:H_2O_2); ii) 10% **33** in toluene, 55 ˚C, 48 hours.

Carbodiimide chemistry has been used to synthesise amide and ester bonds between carboxylic acid and amine groups or hydroxyl groups.[24] A common example of this chemistry is for the attachment of peptide sequences to materials, crucial in the preparation of biomimetic substrates that control cell adhesion, since non-covalent attachment results in

poor cell adhesion. [24,28,53] Typically, attachment is via an amide bond, which can be obtained by reaction of the *N*-terminus with carboxylic acid groups on the material surface, using coupling agents such as dicyclohexyl-carbodiimide **36** or 1-ethyl-3-(3-dimethylaminopropyl)-carbo-diimide **38** (Scheme 1.3). Problems encountered with these reactions include other amino acid side chains reacting with the carboxylic acid groups and the susceptibility of the activated carboxylic acids to hydrolysis. Protection of amino acid side chains and use of anhydrous conditions have been successful methods of avoiding these problems,[53] an alternative method involves a two-step process in which the carboxylic acid is converted into ester **39** (Figure 1.8), that is less prone to hydrolysis, and then peptide coupling is conducted in a buffer at pH 8-9.[28]

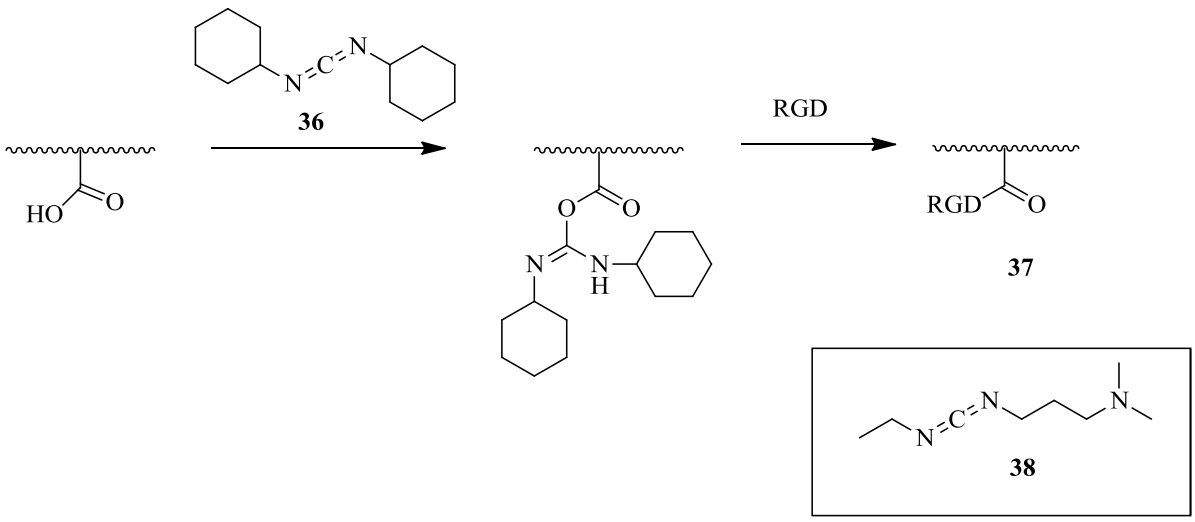

Scheme 1.3: Coupling of RGD to carboxylic acid terminated material.

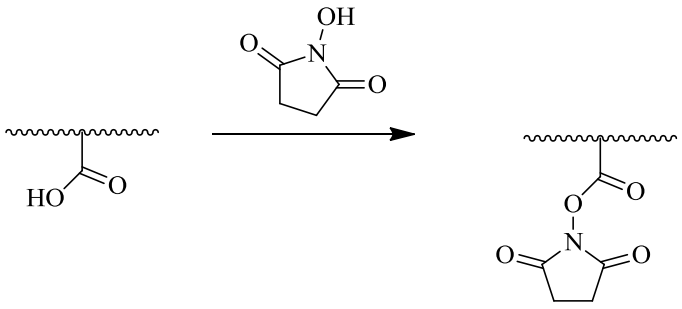

39

Figure 1.8: Activation of carboxylic acid with *N*-hydroxysuccinimde.

Carbodiimide chemistry is an example of bioconjugation, where specifically designed chemistry is used to attach bioactive compounds to the surfaces of materials. Another example of this is attachment of penicillin to PTFE by Urban *et al.*[43] (Scheme 1.4). Expanded PTFE was functionalised with maleic acid in argon plasma to give material **40** which was then hydrolysed in boiling water to expose carboxylic acid groups **41**. Reaction with thionyl chloride generated acyl chloride terminated ePTFE **42** which was reacted with polyethylene glycol (200-600 molecular weight) resulting in **43**; the PEG polymers are spacers units that serve to increase the flexibility and freedom of the penicillin units. Finally, penicillin V was reacted with the exposed end of the PEG polymers with DCC and DMAP to aid the coupling, resulting in **44**.

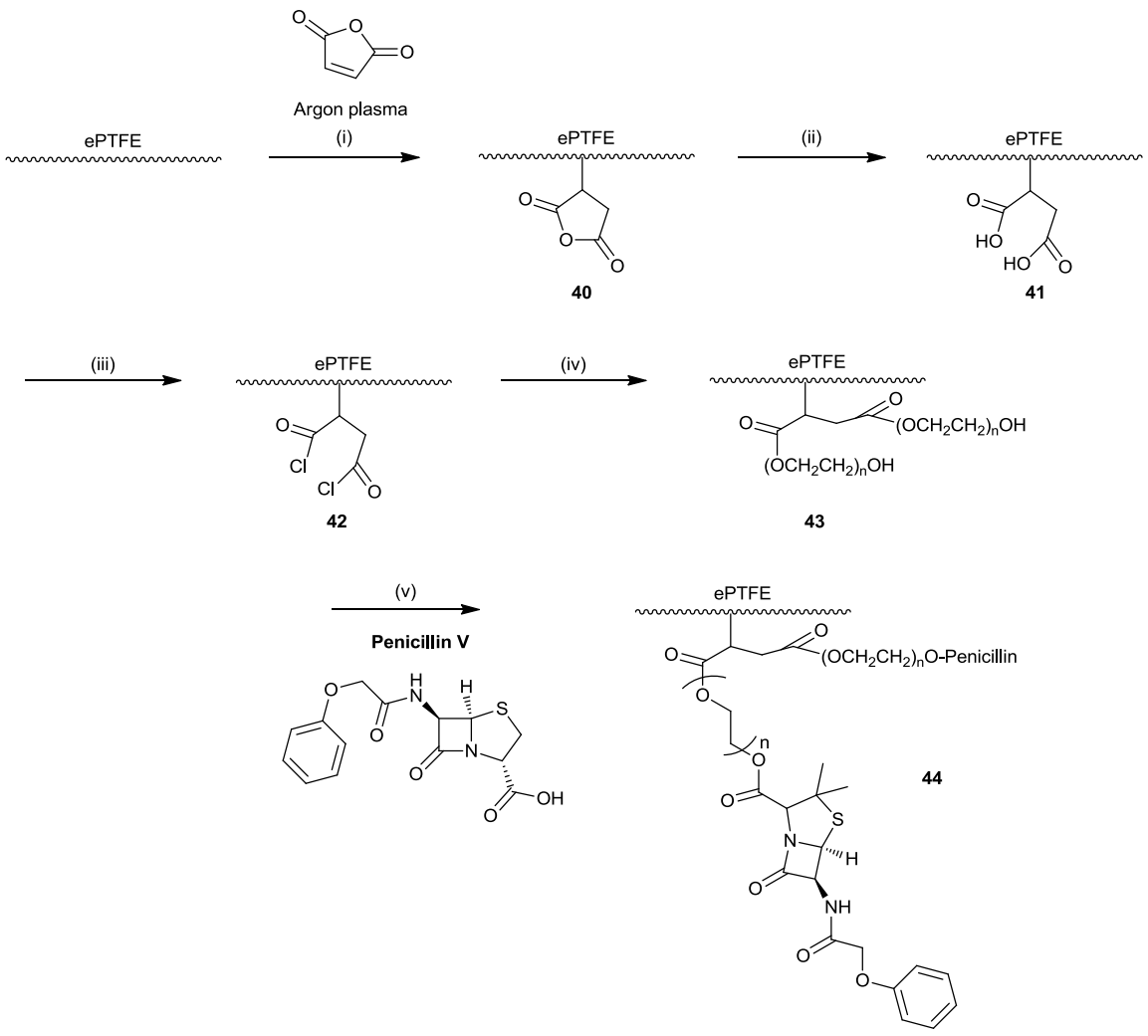

Scheme 1.4: Preparation of penicillin modified ePTFE. Conditions: i) argon plasma with maleic anhydride; ii) boiled for 30 minutes in water; iii) $SOCl_2$, reflux, 65 ˚C, 6 hours; iv) polyethylene glycol 200-600 MW in chloroform (1:1 molar mixture), 18 hours followed by neutralisation with NEt_3 then washing with water; v) DCC, DMAP, penicillin V (acidified with HCl), 4 hours.

1.3.3 Graft polymerisation

The use of polymers in antifouling coatings has been touched on briefly already; polymer spacer units are commonly used to give active molecules, for instance, antibacterials or peptides, the freedom to interact with the target species (Figure 1.9). Furthermore, hydrophilic polymers are thought to decrease protein adhesion entropically as well as from

the hydration layer surrounding them; for proteins to gain access to the surface, they must penetrate the polymers which leads to compression and loss of freedom.

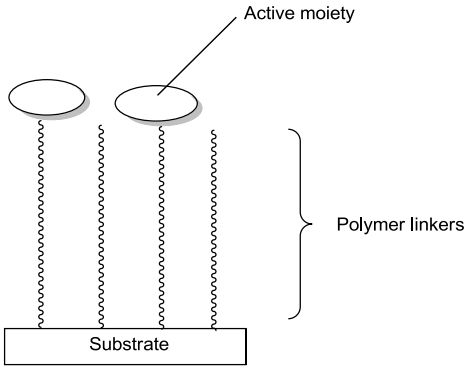

Figure 1.9: The use of polymers as linker units.

Polymer grafting is used to achieve covalent attachment of polymers to surfaces, and there are two types. 'Grafting from' involves growing a polymer from the surface, usually by creating radical species at the surface, which then react with monomers resulting in the growth of polymer chains and networks. The second method is 'grafting onto', where preformed polymers are reacted with reactive sites on the surface, as exemplified in the attachment of penicillin discussed above (Scheme 1.4, step iv).[24]

1.3.4 Modification of XAD-4

Chemical modifications of Amberlite XAD-4^{TM} have been reported in which the benzene rings in the polymer are used to covalently attach functional groups.[54,55] Friedel-Crafts acylation has been used, as exemplified in Scheme 1.5 below.[56] Friedel-Crafts acylation of XAD-4 with acetyl chloride afforded material **45**. After oxidation to the carboxylic acid **46**, reaction with thionyl chloride generated the acyl chloride terminated material **47**, which was then reacted in another Friedel-Crafts acylation resulting in functional material **48**.

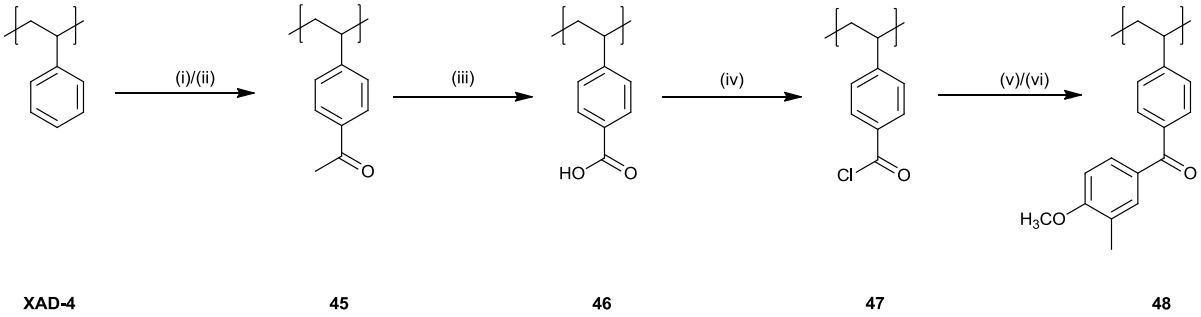

XAD-4 45 46 47 48

Scheme 1.5: Friedel-Crafts Acylation of Amberlite XAD-4. Conditions: i) $AlCl_3$, CH_3COCl, 1,2-dichloroethane, 40 ˚C; ii) H^+/H_2O; iii) $KMnO_4$, NaOH, 40 ˚C; iv) $SOCl_2$, 70 ˚C; v) $AlCl_3$, 2-methylanisole, 60 ˚C; vi) H^+/H_2O.

Two alternative methods for chemical modification of XAD-4 are featured in Scheme 1.6, both of which rely on the addition of amine functionality to the XAD-4 surface by nitration followed by reduction with tin chloride. Reaction of 2,3-dihydroxybenzaldehyde with amine terminated XAD-4 **49** under reflux furnished material **50** on which catechol was covalently bonded by an imine linkage, which could be reduced with sodium borohydride if an amine linkage is preferred.[55] Alternatively, a diazonium salt terminated polystyrene **51** was produced by exposure of the amine material **49** to sodium nitrite and hydrochloric acid. Diazonium salt terminated **51** was then reacted with salicyclic acid **52** in the presence of sodium hydroxide furnishing material **53**.[55]

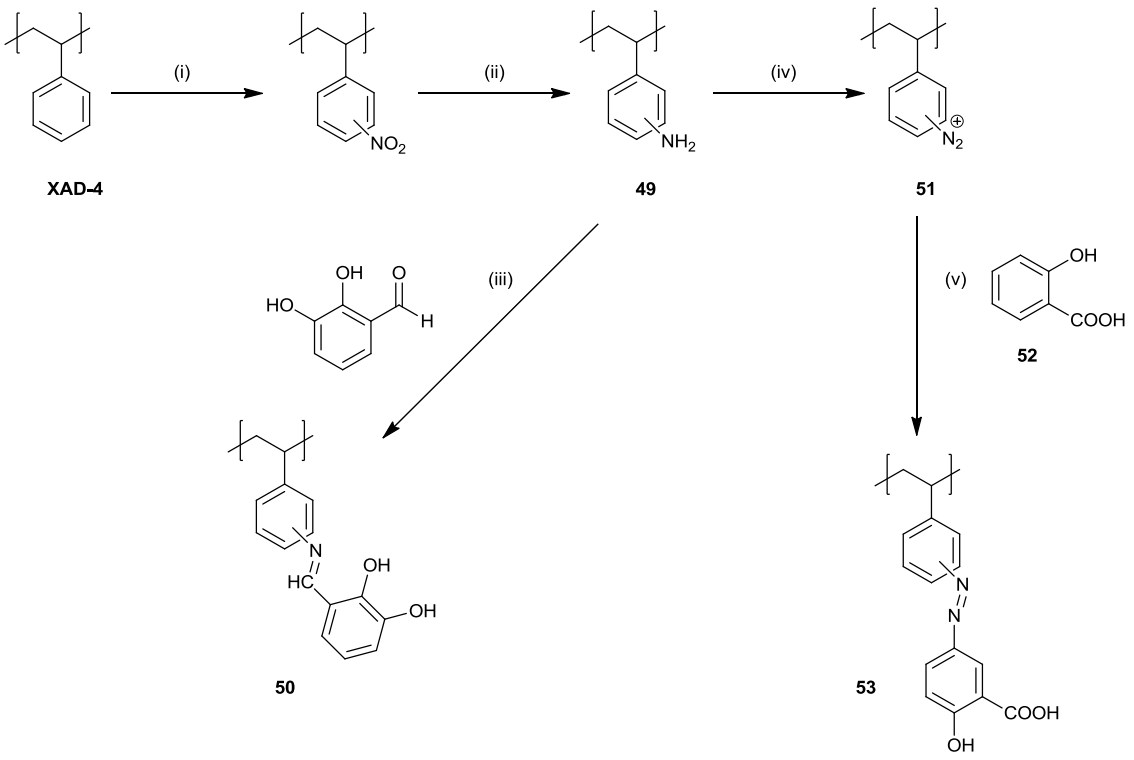

Scheme 1.6: Chemical modification of XAD-4. Conditions: (i) NHO_3, H_2SO_4, 30 min, 60 ˚C; (ii) $SnCl_2$, EtOH, 15 hrs 30 min, 90 ˚C; (iii) EtOH, 24 hrs, reflux; (iv) $NaNO_2$, HCl, 0-5 ˚C; (v) NaOH, 0-5 ˚C, 20 hrs.

1.4 Surface modification with diaryldiazo compounds

The Moloney group has made significant advances in surface modification using carbene chemistry. Diaryldiazo compounds have been used as carbene precursors that will react with the surface of materials whilst conserving the bulk properties (Scheme 1.7). The diaryldiazo is converted to a carbene upon thermal or UV exposure, which then reacts with the substrate surface resulting in covalent attachment, with the functionality of the diazo compound defining the surface properties achieved.[57]

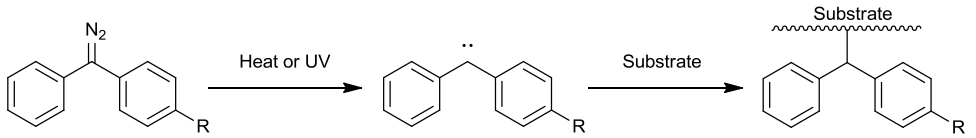

Scheme 1.7: Surface modification using diaryldiazo chemistry.

1.4.1 Preparation and reactivity of carbenes

Carbenes are highly reactive species with 6 valence electrons, including one pair of non-bonding electrons, and they can exist in the singlet and triplet states. In the singlet state, which has a bond angle of 130-150˚, the electrons are paired and are situated in an sp^2 orbital, leaving the p orbital vacant. The triplet states arise as the electrons are not spin paired and they sit in different orbitals; the bent triplet form, with a bond angle of 100-110˚, has unpaired electrons in the sp^2 and p orbitals, whereas in the linear form the unpaired electrons are in the two orthogonal p orbitals. (Figure 1.10)

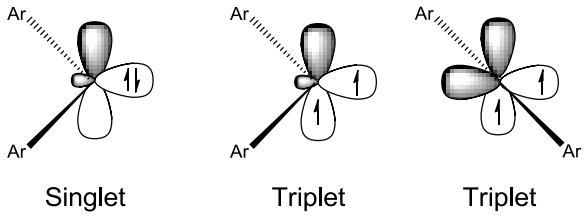

Figure 1.10: Various electronic forms of carbenes.

Typically diarylcarbenes are generated by exposing the diaryldiazo to UV irradiation or heat, as previously mentioned (Scheme 1.7). The diaryldiazo compounds are straightforward to synthesise from benzophenone **54** (Scheme 1.8); reaction with hydrazine monohydrate followed by oxidation with manganese (IV) dioxide or mercuric oxide furnishes the diaryldiazo **56** efficiently in most cases. This method is only limited by the functional groups attached to the aryl-rings. Whilst the hydrazone intermediates **55** are relatively unstable, the diaryldiazo compounds can be stored for extended periods of time at cold temperatures and most importantly in the dark, since the compounds are prone to decomposition when exposed to light. Modification of a wide range of materials has been demonstrated including glass, silica, diamond, polystyrene, cotton, polycaprolactone and PTFE.[57-60]

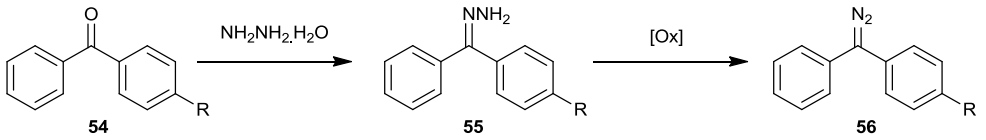

Scheme 1.8: General synthesis of diaryldiazo compounds.

Prior to this, Braybrook and Moloney used tosylhydrazones as carbene precursors, such that tosylhydrazone **57** was deprotonated to reveal a diaryldiazo that could be converted into a carbene upon UV irradiation (Scheme 1.9).[61] However, low yields of photoproducts with solvents and limitations with regards to solvents resulted in the investigation of alternative precursors.

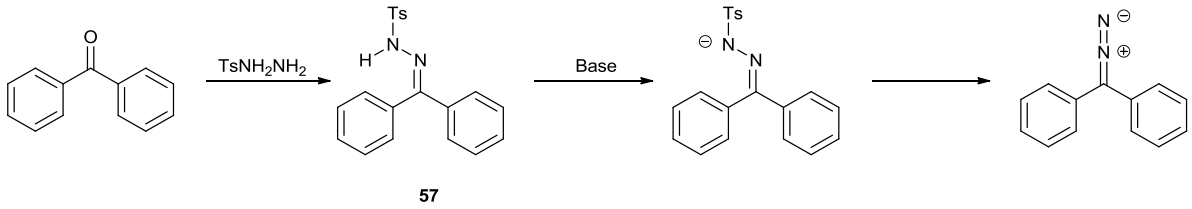

Scheme 1.9: Tosylhydrazones as carbene precursors.

Moloney and Braybrook[61] produced diazirine **58** as an alternative to the tosylhydrazone, which has a much longer synthesis sequence of 6 steps, some of which are very low yielding. When **58** was reacted with methanol the product **59** was isolated in only 15% yield. For these reasons combined Moloney abandoned the diazirine route also. However, it is notable Hayes *et al.* did have some success in using a furanone-diazirine as a carbene precursor that was used to modify the surface of nylon 6,6.[62] The diazirine route was also abandoned as the diaryl moiety proved to be difficult to manipulate in diazirine synthesis. Diaryldiazo compounds are an attractive alternative as they are reasonably stable when kept in the dark, can be easily converted to the carbene and offer a wide range of functionality options.[63]

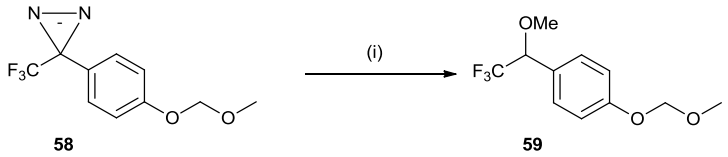

58 **59**

Scheme 1.10: Reaction of diazirine 58. Conditions: (i) Solution of **58** in MeOH was irradiated by a YAG laser at 335 nm for 10 minutes.

Diarylcarbenes are usually incredibly reactive intermediates, Scheme 1.11 displays an example of the reaction pathways followed by diarylcarbenes. When diaryldiazo compounds loose nitrogen a singlet carbene is generated after which the singlet carbene will either react with another carbene to form the azine or undergo insertion into X-H bonds, where X can be nitrogen, oxygen, hydrogen or sulfur, for example. The insertion pathway is very fast and occurs at the diffusion limit of the system, in methanol the rate constant was found to be in the order of 10^{10} $M^{-1}s^{-1}$.[64] Formation of the azine has a rate constant of 2.3×10^{10} $M^{-1}s^{-1}$.[65] Whilst reactions of the singlet carbenes occur at very fast rates, products as a result of the reactions of triplet carbenes have been detected also, in which the triplet carbenes follow a radical mechanism pathway, suggesting that intersystem crossing competes with the singlet reaction pathways.[66] Triplet carbenes can be detected by electron paramagnetic resonance.[64] Azine formation from triplet diphenylcarbene occurs at a much slower rate than the singlet system, the rate constant is 700 times slower at 3.4×10^{7} $M^{-1}s^{-1}$.[67,68] Griller *et al.*[64,68] demonstrated that triplet carbenes react with methanol and butyl amine at slower rates, with rate constants of 10^{5}-10^{7} $M^{-1}s^{-1}$.Whilst the triplet carbenes were generated using triplet sensitizers, products resulting from reaction of the singlet state were observed also. This is more evidence of intersystem crossing between the singlet and triplet carbenes, also that the carbenes exist in equilibrium with each other. Previous work suggests that the position of the equilibrium is dependent upon a range of factors including the effect of the carbenes substituents, temperature and the trapping agents present. [64,68,69,70]

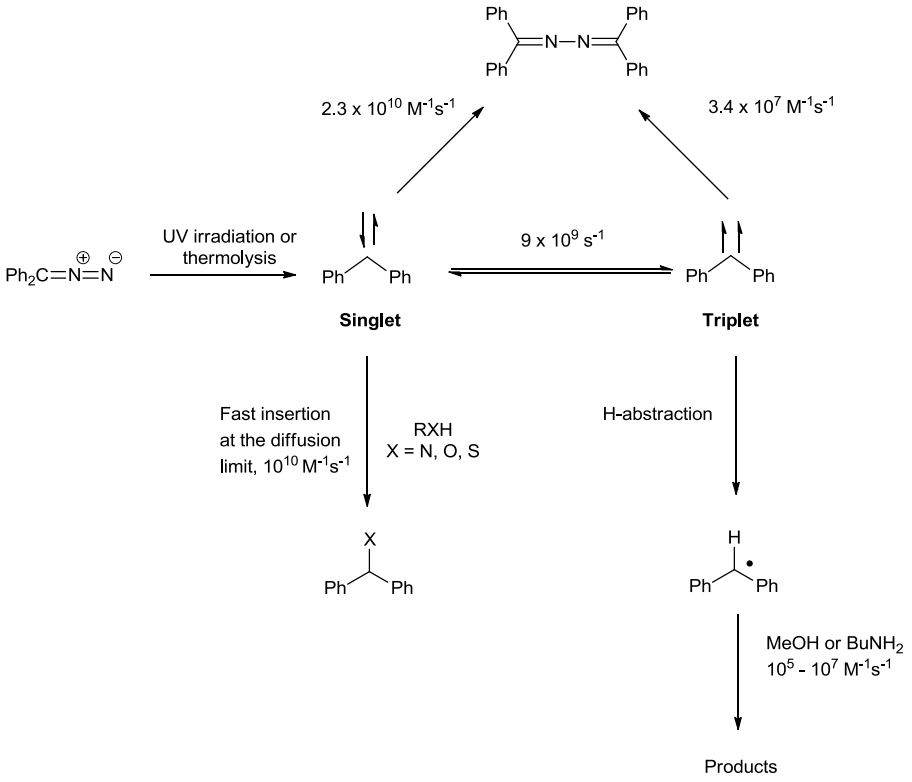

Scheme 1.11: Reactivity pathways of diaryldiazo compounds with rate constants.

Whilst for most diarylcarbenes the above pathway applies, there are significant exceptions. Recently work has been published with regards to stable triplet carbenes that have much longer lives, examples of which are in Figure 1.11.[71,72] Using laser flash photolysis it was demonstrated that **TC-1** can exist in a benzene solution for as long as 1 day whilst the presence of the triplet carbene is still detected and the half-life is estimated to be 40 minutes.[73] Another example is **TC-2** which has a half-life of 19 minutes.[74] Both triplet carbenes are stabilized by resonance of the unpaired electrons through the aromatic systems. However, it was observed that **TC-3** has a half-life of 0.5 μs in degassed benzene, demonstrating that it is necessary to block the *para* positions to prevent the carbene reacting through these centres. The reactivity is also supressed by the steric shileding of the carbene centre**.** **TC-1** and **TC-2** adopt an orthogonal geometry around the carbene centre. In **TC-1** the large bromine and trifluoro groups obstruct access to the carbene centre, whilst in **TC-2**

the four *peri*-hydrogens shield the centre. **TC-4** is in even more stable; UV absorbances indicative of the triplet carbene **TC-4** were still detected after a week of standing at room temperature, in the absence of oxygen this time was increased to 14.5 days.[75]

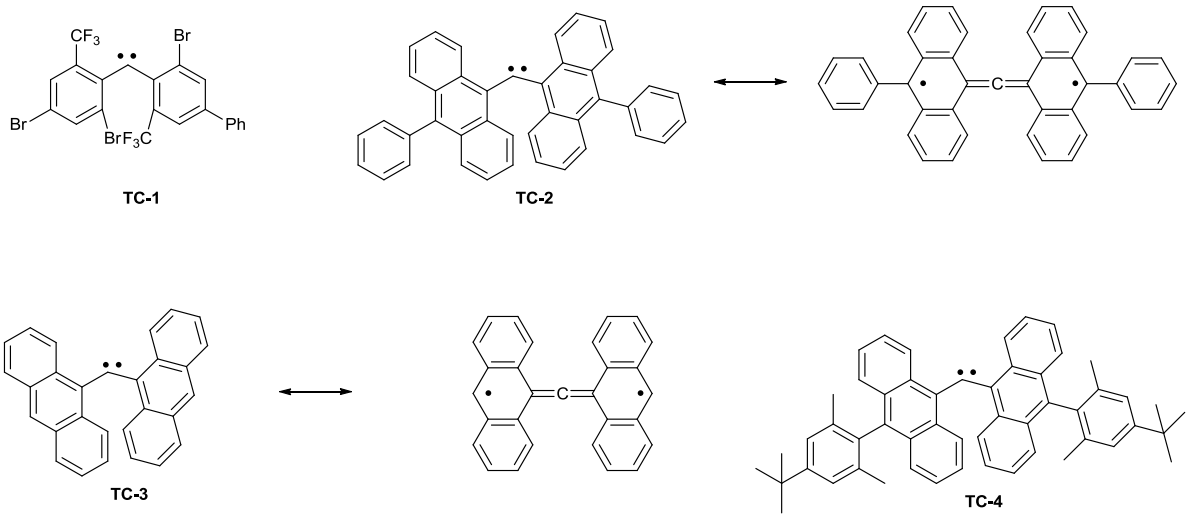

Figure 1.11: Examples of stable triplet carbenes.

The reactivity of carbenes in a solid matrix has also been a subject of investigation and it is particularly applicable to this thesis since any solvent is evaporated from the substrates prior to heating the diaryldiazo coating. Consequently, the carbene and its subsequent reactions occur in solid conditions. Tomioka *et al.*[76] have produced a review comparing the reactivity of diphenyldiazomethane and monophenyldiazomethane, after exposure to UV irradiation, at 0 ˚C and -196 ˚C; the low temperature conditions emulating the solid state matrix. Reaction with a range of alcohols, alkenes and alkanes were analysed, and the overall outcome was such that at the lower temperature the product distribution changed, with an increase in products resulting from the triplet carbene. Scheme 1.12 displays the products resulting from reaction *cis*-but-2-ene with monophenyldiazomethane. At 0 ˚C, when the reaction is still in solution, the *cis*-cylopropane product **60a** dominates, with 93% yield. Singlet carbenes are known to react with alkenes in a concerted mechanism such that the stereochemistry of the

alkene is conserved. Whereas, triplet alkenes are known to react via a radical mechanism such that rotation can occur, resulting in the *cis* and *trans* cyclopropanes.[77] At -196 ˚C the yield of the *cis*-cylcopropane **60a** decreases to 44%. There is a marginable increase in the *trans*-cylopropane **60b** from 2 to 3 %, however, there is a greater increase in products **60c**-**60e**, achieved by hydrogen abstraction by the triplet carbene.

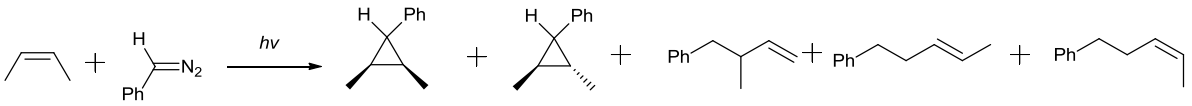

Temerapture (°C)	**60a**	**60b**	**60c**	**60d**	**60e**
0	93	2	1	1	4
-196	44	3	19	5	29

Scheme 1.12: Products observed after reaction of monophenyldiazomethane at two different temperatures.

Furthermore, reactions of diphenyldiazomethane with alcohols at -196 ˚C proceeded with larger yields of products resulting from C-H insertion or abstraction as opposed O-H insertions and abstractions. ^{13}C labelling and kinetic isotope effects with deuterium imply that the increase in C-H reaction products is a result of an increase in the concentration of triplet carbene in the matrix system. Electron paramagnetic resonance and laser flash photolysis corroborate with these observations. The work presented in Tomioka's publication[76] is extensive and suggests that in the matrix system there is an increase in the rate of intersystem crossing from the singlet to the triplet carbene. When applied to the surface modification work presented in this thesis, it does not change the outcome of the results since the modifications rely on the non-specificity of the reaction pathways of diarylcarbenes, such that a wide range of polymers can be accessed. However, it does suggest that the singlet carbene, once formed, is more likely to convert to the triplet carbene and that there will be an increase in triplet carbene reaction pathways compared to solution based reactions.

1.4.2 Surface analysis and characterisation

X-ray Photoelectron Spectroscopy (XPS), combustion analysis, fluorescence and diazonium coupling have all been used to demonstrate successful surface modification. After modification of diamond with bis(4-iodophenyl)diazomethane **61** (Figure 1.12), XPS analysis of the surface **62** detected carbon and oxygen at ~284 and 530 eV respectively, as well significant peaks representing iodine at ~622 and 634 eV (I 3d5/2 and I 3d3/2); weaker photoemissions due to iodine were also detected at 50 eV (I 4d) and 877 eV (I 3p3/2) .[59] Amine modified diamond **63** was exposed to fluoresceinNCS to generate **64**, and using fluorescence microscopy, it was possible to observe the fluorescent moieties, indicating the success of amine modifications; careful washing after every step was conducted to remove any chemistry that was not attached to the diamond.[57,59]

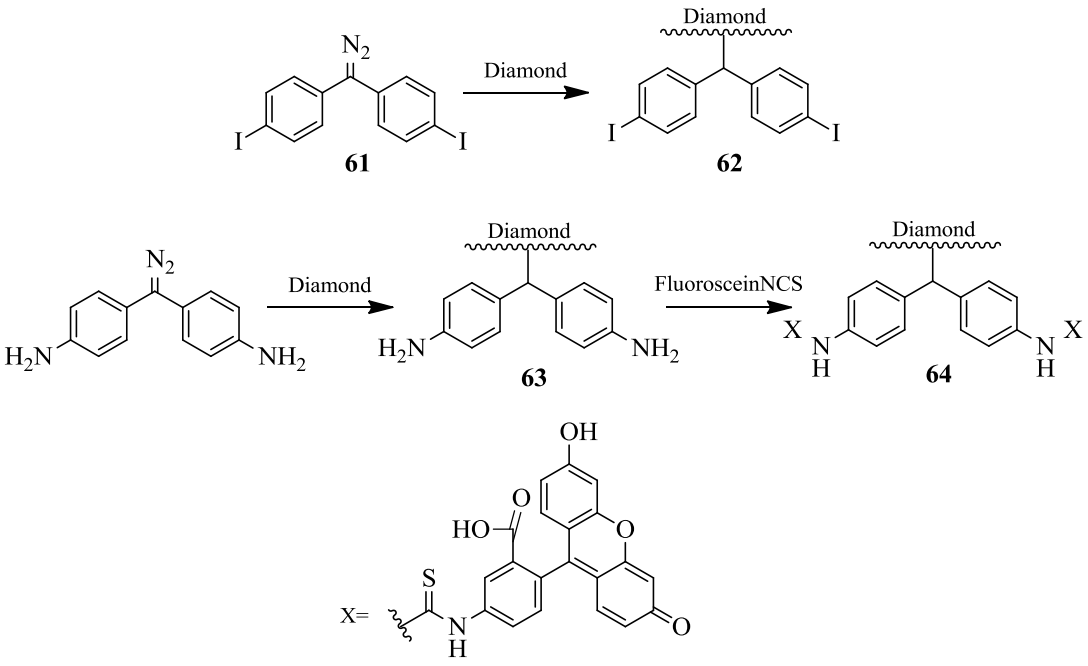

Figure 1.12: Surface modification of diamond.

Diazonium coupling to carbene modified surfaces proved to be a straightforward method to determine if surface modification had occurred. This was first investigated using chemistry

exemplified in Scheme 1.13; a range of materials including Hybond nylon membrane, polystyrene (Amberlite XAD-4), cotton and silica were coated with diazo **65**, heating to generate the carbene which could react with material surface and washing with acetone resulted in modified materials **66**. No significant changes in appearance occurred so coupling with diazonium salt **67** to the nucleophilic aniline on the surface was carried out producing **68**. The azo linkage is known to be a highly coloured chromophore so intense colouring was expected. The nylon, polystyrene and silica substrates all exhibited strong colouration after the diazonium coupling reaction, but the colour of the cotton was less intense. By comparison, unmodified materials were also exposed to diazonium salt **67**, but maximum colouration required diazo modification first. Extensive washing of cotton, nylon and polystyrene dyed substrates **68** with Soxhlet extraction in acetone and water at pH 1 and 15, resulted in a high retention of colour.[60]

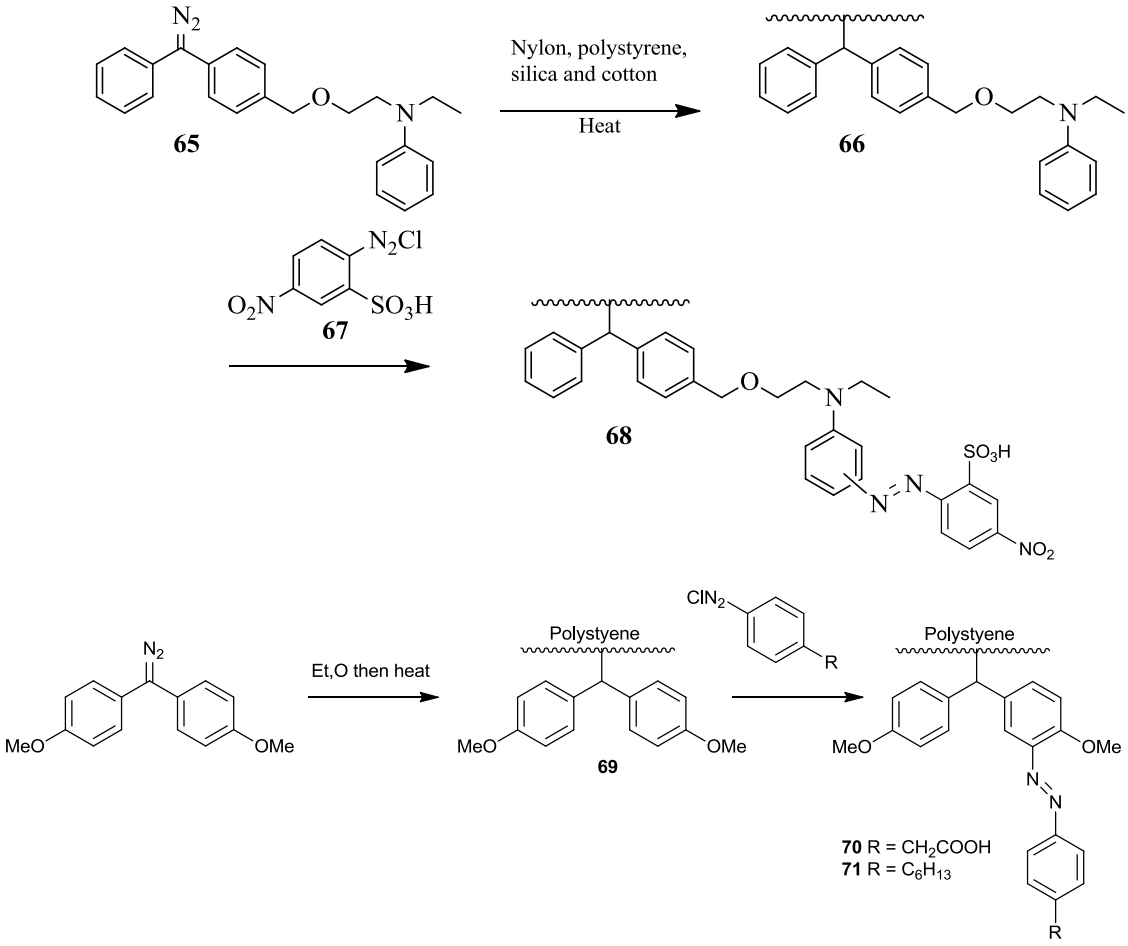

Scheme 1.13: Diazonium coupling to diazo modified surfaces.

Further work using diazonium coupling was also carried out using the dimethoxy diazo modified polystyrene (Amberlite XAD-4) **69** (Scheme 1.14), to which diazonium salts synthesised from 4-hexyl aniline and 4-aminophenyl acetic acid were coupled, furnishing acid terminated **70** as dark purple and hexyl functionalised **71** as yellow-coloured**.** IR (ATR IR) spectroscopic analysis of the materials revealed significant stretches at 1275-1220 (ether aryl-O), 1075-1020 (ether alkyl-O) and 1600-1585 cm^{-1} (aromatic C-C) and material **70** had a broad absorbance at 1710 cm^{-1} due to the carboxylate group. Combustion analysis and XPS were used to successfully confirm the presence of nitrogen after the modifications. XPS analysis detected nitrogen with a collection of signals at 399.7, 400.5, 401.7, 403.5 and 404.6 eV which were attributed to the azo linkage. Combustion analysis of hexyl and amine

functionalised materials **70** and **71** detected nitrogen, and this amount was used to calculated the surface loading of the chemistry. Acid terminated polystyrene **70** had a loading of 0.18 mmol/g and a surface coverage of 9%, whereas hexyl terminated **71** had a loading of 0.036 mmol/g which equates to a surface loading of 1.8%.[58]

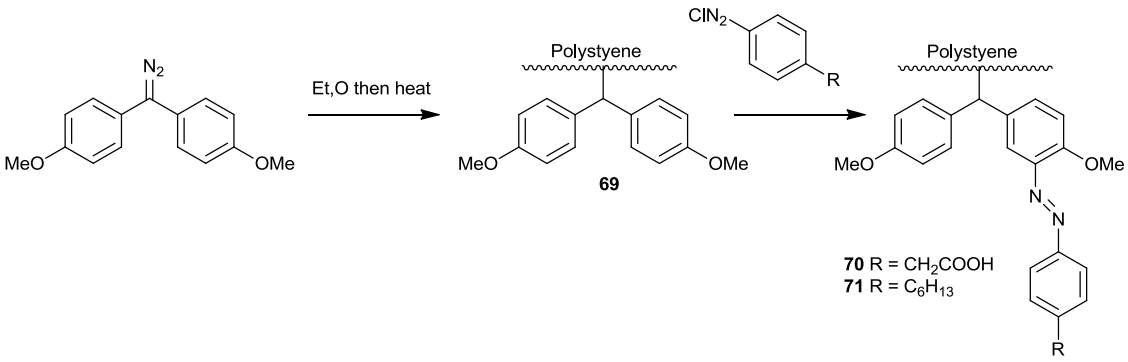

Scheme 1.14: Modification of polystyrene.

The ability to alter surface wettability with surface chemical modification has been demonstrated on PTFE, polystyrene, polyethylene (PE), silicon, glass and PET using the synthetic strategy in Scheme 1.14. Figure 1.13 features the surfaces functional surfaces produced whilst Table 1.3 displays the relevant contact angle measurements. Although the effect of the hexyl functionality **72a** is small, the effect of the carboxylate and ammonium groups is more significant, with all the materials exhibiting a decrease in contact angle compare with the untreated materials.[78]

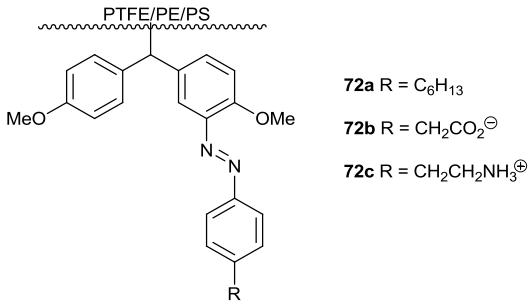

Figure 1.13: Chemically modified polymers.

Table 1.3: Contact angle of chemically modified polymers.

Material	Water contact angle (degrees)			
	Untreated	**72a**	**71**	**72**
PTFE	102.9 ± 1.4	104.0 ± 2.7	92.1 ± 4.2	104.2 ± 1.9
PE	91.1 ± 1.9	88.0 ± 1.2	86.8 ± 1.6	89.1 ± 3.0
PS	110.8 ± 3.2	114.6 ± 1.0	68.8 ± 3.7	85.3 ± 1.8

1.4.3 Biological applications

The use of surface modifications in biological applications is the overall aim of the work in this thesis. Prior to this study, the Moloney group produced biocompatible and biocidal surfaces using diazo surface modifications. Diazo **77** (Scheme 1.15) was synthesised from 4-methyl benzophenone **73** which was brominated with *N*-bromosuccinimide to form **74** then reacted with triethyl phosphite to generate **75**, and conversion into diazo **77** proceeded via hydrazone **76**. Polystyrene and Hybond-nylon were coated with diazo **77** then heated to 100 ˚C to generate the carbene, resulting in insertion into the material surfaces. Washing materials **78-H** and **78-P** with 1 molar aqueous HCl hydrolysed the phosphonate diester groups resulting in phosphonic acid terminated materials **79-H** and **79-P**, after which washing with aqueous calcium hydroxide generated the calcium phosphonate terminated materials **80-H** and **80-P**. The calcium phosphonate materials were of particular interest

since calcium phosphonate containing materials such as hydroxyapatite are used to promote cell growth, specifically in the application of bone growth.[79]

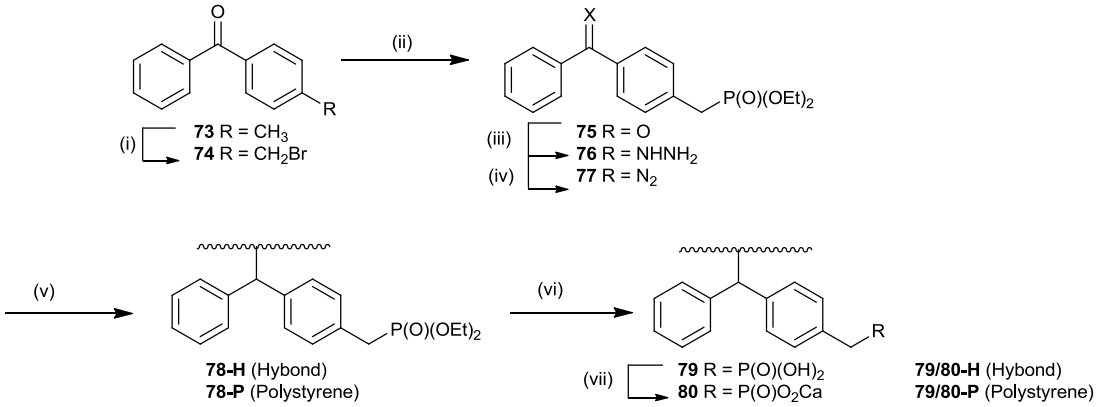

Scheme 1.15: Synthesis of phosphonate diazo and surface modification of Hybond and polystyrene. Conditions: i) *N*-bromosuccinimide, $CHCl_3$, 60 ˚C, hν (72%); ii) triethyl phosphite, 160 ˚C (86%); iii) hydrazine hydrate, MeOH (100%), 65 ˚C; iv) mercury (II) oxide, Na_2SO_4, KOH, EtOH, THF (89%); v) Hybond/polystyrene, 100 ˚C; vi) 1M aq. HCl; vii) $Ca(OH)_2$, H_2O.

The Hybond and polystyrene based materials **79-H/P** and **80-H/P** were seeded with MG63 human osteosarcoma cells and the cell proliferations over 13 days measured using an Alamar Blue assay to determine the cell count. The phosphonic acid terminated Hybond **79-H** showed lower cell proliferation than the unmodified Hybond at 5 and 8 days, 40 and 55%, respectively. However, by day 13 the cell proliferation was at a similar level to untreated Hybond with a cell count of 108% times that observed on the unmodified material**.** The cell proliferation was greater on calcium phosphonate terminated Hybond **80-H**, at 5 days the cell proliferation was 45% of that of the unmodified Hybond, by day 8 99% cell proliferation indicated that both materials were equivalent and by day 13 the calcium phosphonate terminated Hybond had a higher level of cell proliferation than umodified Hybond at 128% relative to unmodified Hybond. The assays of the polystyrene based materials **79-P** and **80-P** revealed that by day 13, the cell proliferations relative to unmodified polystyrene were at 287% and 328% for the phosphonic acid and calcium

phosphonate terminated materials. The increased cell proliferation on the polystyrene based materials is attributed to the much higher surface area of the beads (725 m^2/g) but it is notable that the polystyrene assays were less reproducible due to the static nature of the polystyrene beads. All of the materials have shown themselves to be biocompatible, with the calcium phosphonate surface demonstrating a prominent ability in propagating cell growth.[80]

Antibacterial polymers are also of interest for the reasons outlined above. Antibodies release hydrogen peroxide when irradiated with oxygen, imparting antibacterial activity, and it was proposed that a hydrogen peroxide releasing polymer would mimic this effect. Urea terminated polystyrene **82** was prepared (Scheme 1.16) which was then exposed to hydrogen peroxide under the premise that the urea would form hydrogen bonds with the hydrogen peroxide, resulting in material **83**. A loading of 8.42 x 10^{-5} mol/g of hydrogen peroxide was determined by iodometric titration. The loading was measured daily and after 96 hours, the loading had decreased to 4.13 x 10^{-5} mol/g demonstrating that only about 50% of the hydrogen peroxide had been released. Strong antibacterial activity against *S. Aureus* was observed demonstrating success in the preparation of an antibacterial material.[57]

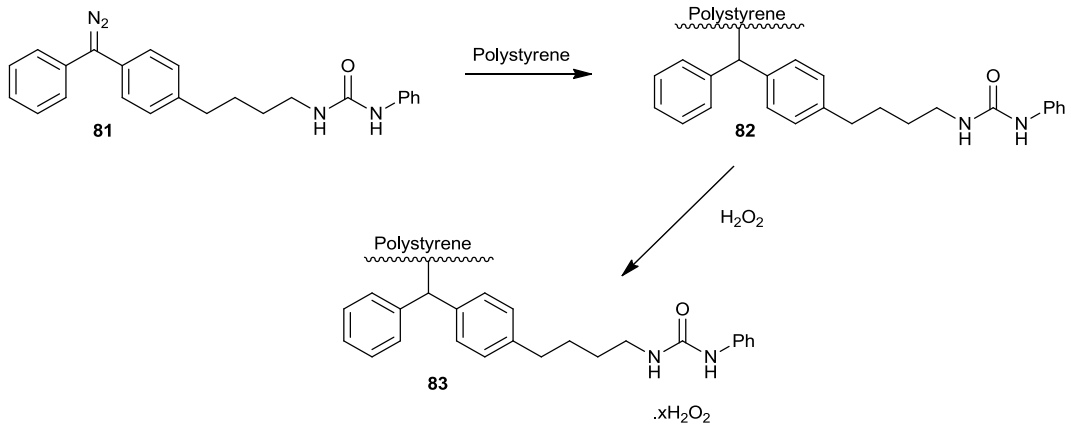

Scheme 1.16: Preparation of an antibacterial polymer.

1.5 Thesis outline

The aim of this work was to further investigate the control of biofouling with surface chemistry as well as to carry out more extensive characterisation of the materials than had been conducted previously. Diazo **65** (Scheme 1.17) was reacted with the surface of polystyrenes providing a linker to which diazonium coupling could occur; the diazonium coupling strategy was chosen as it is a straightforward, flexible strategy that produces highly coloured materials and opens the polymer surfaces to a wide range of functionalities.

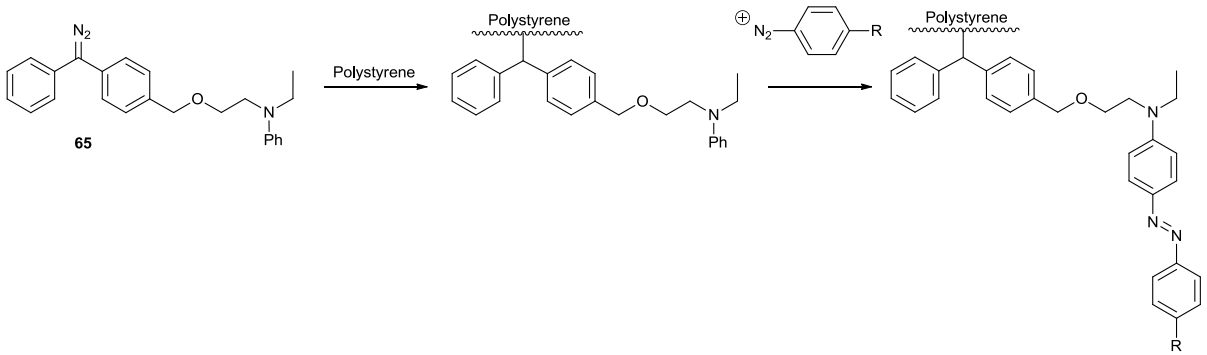

Scheme 1.17: Strategy to control of surface chemistry by chemical modifications.

Polystyrene was chosen due to its ease of availability, low-costs and for the fact that it is relatively simple to work with. However, as mentioned previously, the diazo chemistry has been used on a wide range of materials and polymers already so the work could be transferred to materials of greater interest and use. The synthesis of the organic compounds is discussed in Chapter 2, where a solution based investigation into diazonium coupling is also featured.

The first polystyrene substrate, discussed in Chapter 3, is a polymer film applied to a gold coated quartz crystal to be used in Quartz Crystal Microbalance-Dissipation (QCM-D) monitoring of protein adsorption. This technique allows real-time observation of the mass

change on the crystal as well as its viscoelastic properties, thus giving information concerning surface adsorption of protein. A selection of functional surfaces were investigated and the characterisation of these surfaces was not as extensive as that conducted on the polystyrene beads, since this work was only intended to give preliminary information concerning the effect of the surface modifications.

The second polystyrene substrate which was modified was Amberlite XAD-4 beads. Chapter 4 discusses the preparation of the broad library of materials produced as well as the extensive characterisation of these materials; the density of information gained in the characterisation is much greater than any that has been obtained of substrates previously functionalised within the Moloney group, with the intention of gaining a fuller insight into the macroscopic and microscopic effects of diaryldiazo surface modifications. These materials were exposed to bovine serum albumin and their ability to adsorb protein correlated with contact angle and other calculated molecular parameters. There has been a wealth of investigation into the effect of surface hydrophilicity on protein adsorption, however, the effect of the specific surface chemistry on protein adsorption was also of interest.

Finally, the use of the polystyrene materials as an antibacterial was of interest since antibacterial materials and coatings are used in a wide range of applications *in vivo* and otherwise. More specifically, the ability to support antibiotics on the material surface was investigated using penicillin V.

Chapter 2: Synthesis of organic coatings and solution phase investigations

The Scheme outlined previously (Scheme1.16) demonstrates the chemical modification of polystyrene surfaces using carbene intermediates. This approach proceeds with modification with diazo **65** followed by diazonium coupling to control the terminal surface functionality. The chemicals needed for the surface modifications are not all available commercially so further synthesis was required, as discussed in this Chapter. Furthermore, an investigation into the efficiency of the diazonium coupling reaction was carried out in solution to gain insight into the coupling chemistry. Initially, benzophenone **87** (Scheme 2.1) was reacted with a selection of the diazonium salts after which diazonium coupling to *N*,*N*-dimethyl aniline was explored.

2.1 Preparation of organic compounds for material modifications

2.1.1 Synthesis of diaryldiazo for surface modification

The synthetic process followed to afford diazo **65** is detailed below (Scheme 2.1); 4-bromomethyl benzophenone **86** was provided by Oxford Advanced Surfaces Ltd where it was synthesised following literature methods.[81]

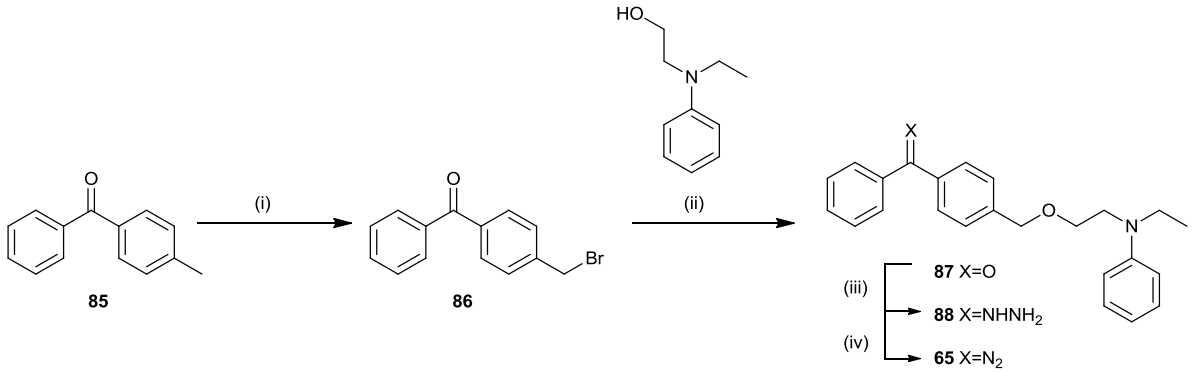

Scheme 2.1: Synthesis of diaryldiazo 65. Conditions: (i) *N*-bromosuccinimide, $CHCl_3$; (ii) NaH, THF, -78 ˚C-RT (65-77%); (iii) $NH_2NH_2.H_2O$, EtOH, reflux (51-100%).

Deprotonation of 2-ethylanilinoethanol with sodium hydride followed by reaction with bromide **86** provided benzophenone **87** reliably in good yield (65-77%).[81] Hydrazone **88** was prepared as a 1:1 mixture of the *cis* and *trans* isomers as shown by NMR spectroscopic analysis, with two singlets at 4.53 and 4.62 ppm indicating the Ar$C\underline{H}_2O$ protons of each isomer. In some cases, alcohol **89** (Scheme 2.2) was formed as a by-product of the hydrazine reaction; this was signified by extra NMR signals comprising of doublets at 2.33 ppm and 5.87 ppm representing the O-H proton and adjacent C-H proton, respectively, and a singlet at 4.54 representing the Ar$C\underline{H}_2O$ protons.

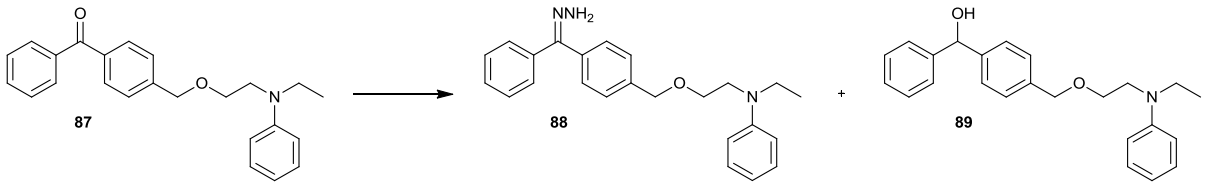

Scheme 2.2: Products afforded in the reaction of 87 with hydrazine monohydrate. Conditions: $NH_2NH_2.H_2O$, EtOH, reflux.

Usually by-product alcohol **89** was generated in small amounts, but it was observed that as the hydrazine monohydrate reagent aged, the quantity increased to up to 79% of the product mixture. Hydrazone **88** is acid sensitive, so could not be purified by silica column

chromatography; when a small amount of alcohol **89** was produced, as shown by NMR spectroscopic analysis, the product mixture was nonetheless taken forward to the diazo intermediate, in the knowledge that **89** could not insert into the polystyrene surface and should wash out. However care was taken to use relatively fresh hydrazine monohydrate wherever possible. It is known that ketones can be reduced to an alcohol by diimide;[82, 83] and as the bottle of hydrazine monohydrate aged, oxidation to diimide seems to become more likely, leading ultimately to formation of more of the alcohol (Figure 1.2).

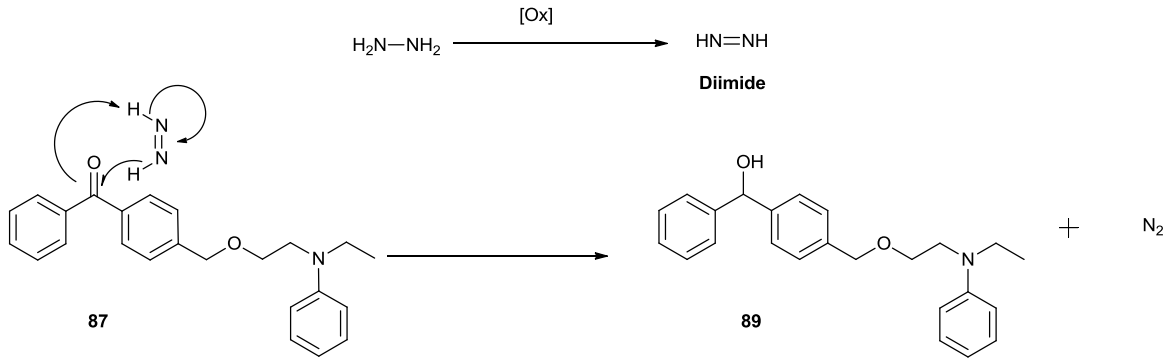

Figure 2.1: Proposed mechanism for the formation of by-product 89.

The final step of the synthetic route (Scheme 2.1) was oxidation of hydrazone **87** with manganese dioxide, providing target diazo **65** as a distinctive dark pink oil, in 79-96% yield. The yield depended upon how extensively the manganese residue was washed during the celite filtration, as the product was found stick to the manganese residue in the flask and larger scale reactions (2 – 5 g) were at times prone to lower yields. IR spectroscopic analysis of diazo **65** revealed a distinctive sharp peak at 2038 cm^{-1} which is indicative of N=N=C diazo stretch. Alcohol **89**, formed during the hydrazine step, was not oxidised back to the benzophenone during the manganese oxidation as the relevant NMR ^{1}H resonances were still observed.

2.1.2 Synthesis of diazonium salts and amine precursors

A range of diazonium salts **91a-c**, **e-j** were prepared by reaction of the amines **90a-c**, **e-j** with isopentyl nitrite and tetrafluoroboric acid in ethanol (Scheme 2.3)[55] at -5 – 0 ˚C; the resulting brightly coloured solutions were used to tailor the surface chemistry of the polystyrene.

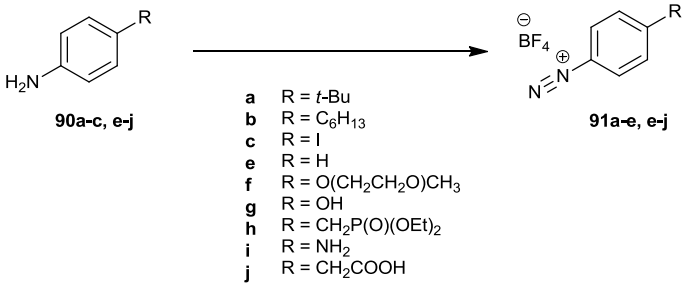

Scheme 2.3: Preparation of diazonium salts. Conditions: Isopentyl nitrite, HBF_4, EtOH, -5-0 ˚C (General Procedure 1).

Diazonium salts are known to be unstable above 0 ˚C[84] and can be explosive when dry so the salts were not isolated and used directly after preparation. Thanks to the strong colour of the salts, their formation could be easily observed over time; when the solution was no longer increasing in colour intensity completion of the reaction was assumed, with up to 1 hour being needed. A colourimetric H-acid test was also used to confirm the formation of the diazonium salts;[85] a sample of the salt solution was extracted then its pH adjusted to pH 4 using sodium acetate, and 4-amino-5-hydroxy-2,7-napthalene disulfonic acid, also known as H-acid, was added and the presence of the salt indicated by the solution turning dark purple (Scheme 2.4).

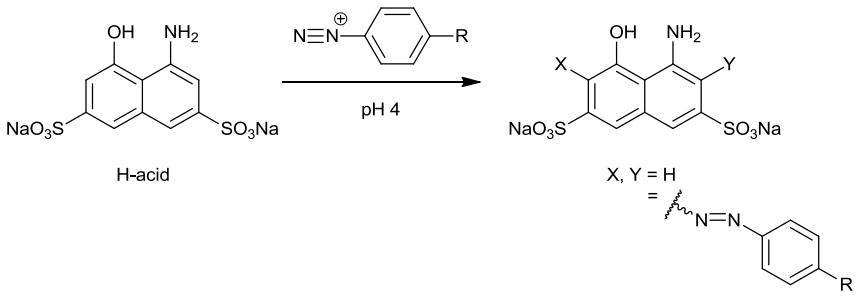

Scheme 2.4: H-acid test confirming the presence of diazonium salts.

All of the amines are commercially available apart from glycol and phosphonate diester amines **90f** and **90h** which required synthesis. Preparation of 4-(2-(2-(2-methoxyethoxy)ethoxy)ethoxy)aniline **90f** (Scheme 2.5) began with protection of 4-hydroxyaniline **92** with di-*tert*-butyl dicarbonate[86] followed by reaction with 2-(2-(2-methoxyethoxy)ethoxy)ethyl 4-methylbenzenesulfonate **96**,[87] itself produced by tosylation of triethylene glycol monomethyl ether **95**[88] affording **96** (83-95% yield), with purification not necessary. The low yielding tosylation step was due to material being retained in the aqueous layer which could not be avoided due to the highly aqueous soluble triethylene glycol chain. Removal of the BOC protecting group[87] proved to be more difficult since the product amine **90f** tended to be retained on the column, thus reducing the yield, at times significantly, with yields in the range of 44-78%.

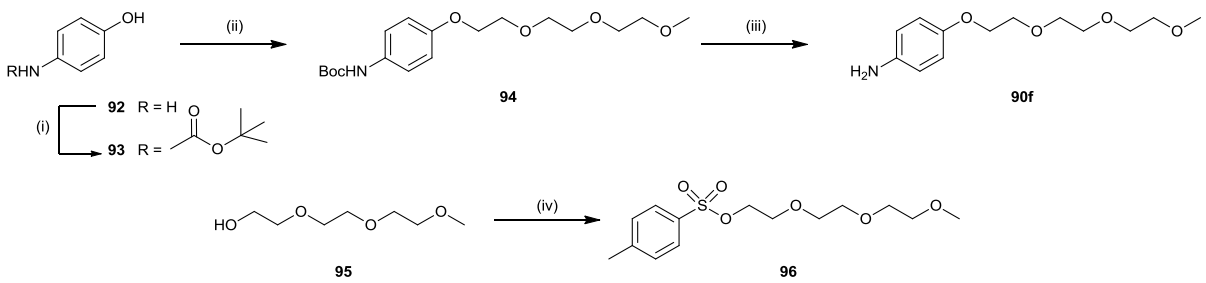

Scheme 2.5: Synthesis of 4-(2-(2-(2-methoxyethoxy)ethoxy)ethoxy)aniline 90f. Conditions: (i) Na_2CO_3, di-tert-butyl dicarbonate, THF, RT, (90%); (ii) **96**, K_2CO_3, acetonitrile, reflux (83-95%); (iii) 6:1 TFA:water 6:1 mixture, RT, 4 hrs (44-78%); (iv) NaOH, *p*-toluenesulfonyl chloride, THF:water 4:1 mixture, 0 ˚C, 4 hrs (27-52%).

Synthesis of **90h** (Scheme 2.6) began with a Michaelis-Arbuzov conversion of 4-nitrobenzyl bromide to the corresponding phosphonate **98**[89] in good yield (78%), after which **98** was reduced to the desired amine **90h**.[90]

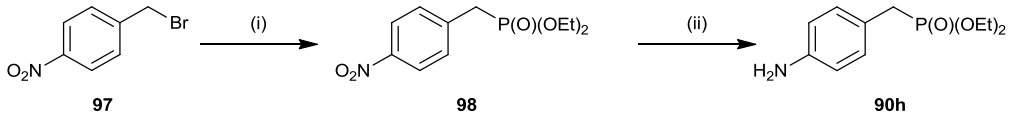

Scheme 2.6: Synthesis of Diethyl 4-aminobenzylphosphonate. Conditions: (i) triethyl phosphite, BuN_4I, 120 ˚C, 4.5 hrs. (78%); (ii) $SnCl_2$, HCl, EtOH, reflux 3 hrs. (72%).

2.2 Solution study of diazonium coupling

2.2.1 Diazonium coupling to benozophenone 87

The hexyl diazonium salt **99b** was produced using sodium nitrite in a mixture of water and diethyl ether as a pink solution at 0 ˚C.[91] Benzophenone **87** was added to the mixture then reacted for 5 hours at 0 ˚C then room temperature for 18 hours (Scheme 2.7, Procedure 2). It was anticipated that the coupling reaction should proceed quickly in high yield at 0 ˚C, however, regular analysis by TLC showed that benzophenone **87** was not consumed completely and **100b** was isolated in only 37% yield and starting material **87** had not completely reacted. An alternative solvent system of water and THF was trialled to improve the miscibility of the reaction since two phases were observed previously. After stirring at 0 ˚C for 6 hours and room temperature for 18 hours, diazonium coupled product **100b** (Scheme 2.7) was isolated in 64% yield (General Procedure 4); when this synthesis was also carried out with stirring at 0 ˚C, **100b** was obtained in 64% yield (Procedure 3).

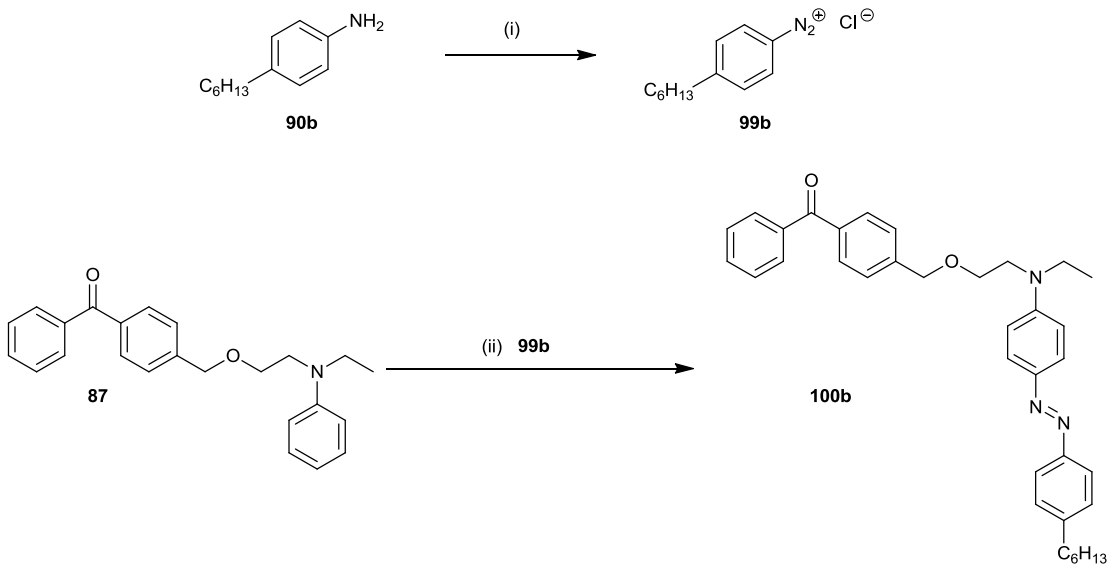

Scheme 2.7: Diazonium coupling of 4-hexylbenzenediazonium chloride with 87. Conditions: **Procedure 2** (i) $NaNO_2$, HCl, Et_2O, water, 0 ˚C; (ii) **87** (1 eq), 5 hrs at 0 ˚C then 18 hrs at RT (37%); **Procedure 3** (i) $NaNO_2$, HCl, THF, water, 0 ˚C; (ii) **87** (0.5 eq), 6 hrs at 0 ˚C (64%); **General Procedure 4** (i) $NaNO_2$, HCl, THF, water. 0 ˚C; (ii) **87** (0.5 eq), 6 hrs at 0 ˚C then RT for 18 hours (64%).

Acid **100j** (Scheme 2.8) was prepared using General Procedure 4, as discussed above, but with a disappointing yield of 10%. The crude mixture was comprised of the product and starting material **87**; separation by silica column chromatography proved to be difficult, since the mixture streaked on the column. Amine **100i** was furnished in 19% yield; again purification using a silica column proved difficult and the product was contaminated with starting material **87**. In addition, enough of **87** was isolated to account for 74% of the material put into the reaction. In both of these reactions neither of the starting materials amines **90i** and **90j**, their salts or the side-products associated with other reactions of the diazonium salts were recovered, and it was assumed that the products which were formed must be water soluble.

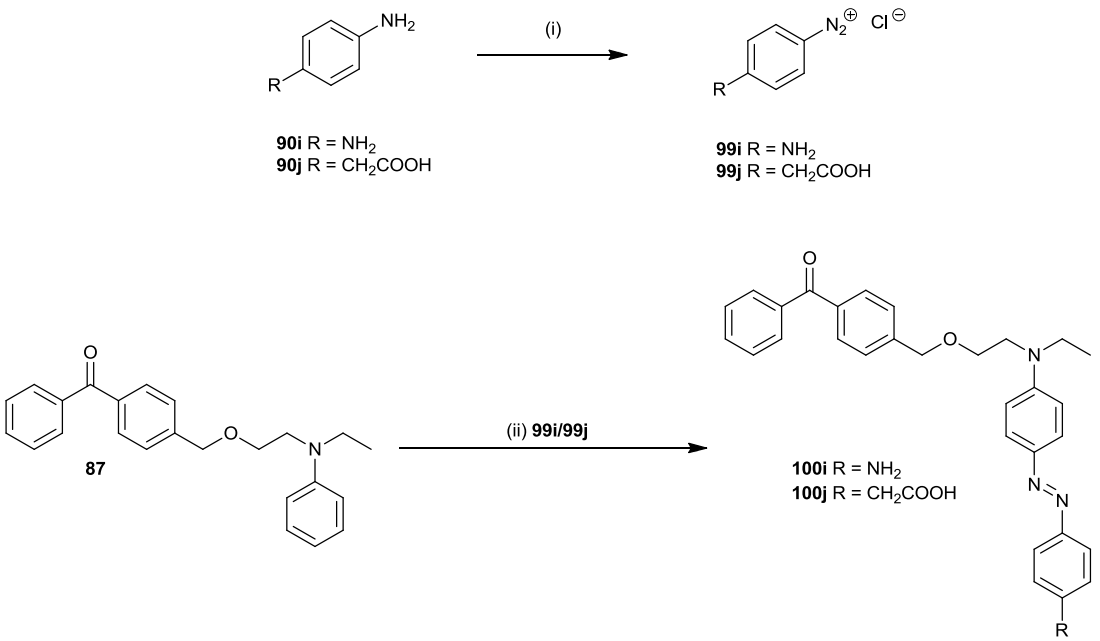

Scheme 2.8: Diazonium coupling using General Procedure 4. Conditions: i) $NaNO_2$, HCl, THF, water, 0 ˚C; ii) **87** (0.5 eq) was added and the mixture stirred for 6 hours at 0 ˚C and RT for 18 hours. **100i** (19%), **100j** (10%).

Diazonium salts **91h-j** were synthesised with isopentyl nitrite and tetrafluoroboric acid in ethanol after which benzophenone **87** was added to the salt solutions and the mixtures stirred at -5-0 ˚C then room temperature (Scheme 2.9, General Procedure 5). Reaction of **87** with acid diazonium salt **91j** followed by aqueous extraction resulted in starting material **87** only, but curiously, prior to work-up, benzophenone **87** did not dominate the NMR spectrum; the NMR spectrum was more similar to that observed for **101h** and **101i**. Synthesis of amine coupled product **101i** followed by an aqueous work up proceeded in 61% yield; the ^{1}H NMR spectroscopy data suggests that the product is the salt rather than the neutral product as discussed below. This reaction was repeated but only stirred at 0 ˚C for 1 hour, warmed to room temperature then exposed to aqueous work up (Procedure 6), and the same product amine product **101i** was furnished in 81% yield. Amine **101i** was washed with aqueous potassium carbonate in an effort to isolate the neutral product, however, this proceeded with complete conversion back to benzophenone **87** with the amine residue lost to the aqueous

phase. Furthermore, exposure of amine **101i** to methanol and acetonitrile also resulted in decomposition to **87**. Phosphonate **101h** was produced as the salt but the mixture was contaminated with amine **90h**.

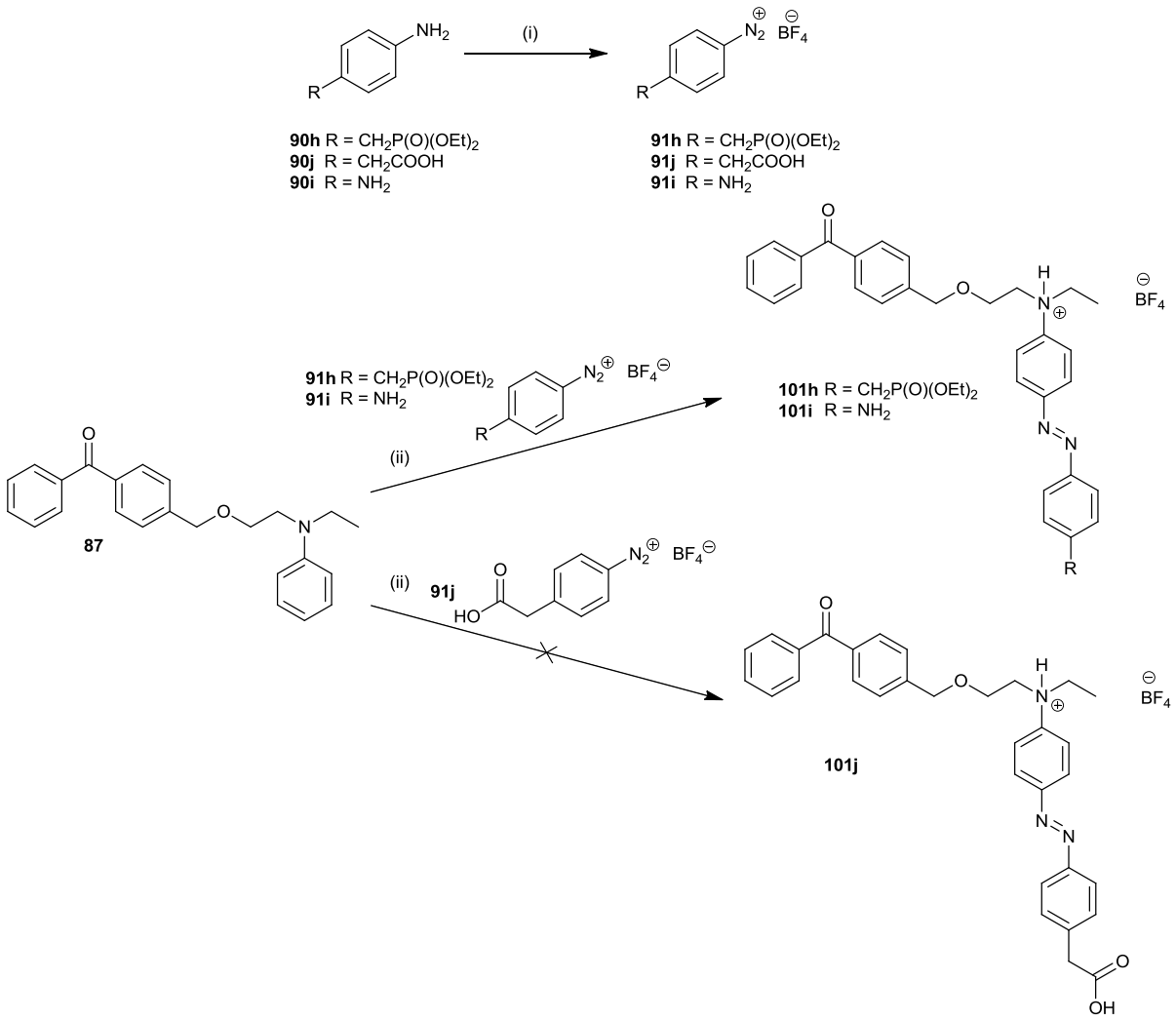

Scheme 2.9: Diazonium coupling. Conditions: (i) isopentyl nitrite and tetrafluoroboric acid in EtOH at – 5 ˚C; (ii) **General Procedure 5** after addition of **87** (1 eq) the mixture was stirred at -5-0 ˚C for 4 hours and RT for 18 hours. **101h** (100%), **101i** (61%), **101j** (0%); **Procedure 6** after addition of **87** (1 eq) the mixture was stirred at -5-0 ˚C for 1 hour. **101i** (81%).

Generation of the salts **101h**,**i** as opposed to their neutral forms can be explained by considering the number of equivalents of acid used in their synthesis. General Procedure 4 used one equivalent of hydrochloric acid to generate the highly reactive NO_2^+ cation leading

to the formation of the diazonium salt, whereas General Procedure 5 and Procedure 6 used two equivalents of tetrafluoroboric acid in the mixture, when only one is in fact needed to synthesise the diazonium salts, leaving the second equivalent available to protonate the product.

2.2.1.1 Characterisation of products

The structure of **100b** (Scheme 2.7) was determined using NMR and UV spectroscopy (Figure 2.2). The protons *ortho* to NEt have a distinctive ^{1}H resonance of an apparent doublet at 6.77 ppm of integration 2. AA'XX' coupling would be expected here, however, there is not enough fine structure in the NMR to identify the two coupling constants. This resonance couples clearly to another apparent doublet at 7.85 ppm, confirming the *para* substitution. The NMR spectra of benzophenone **87** is below in Figure 2.3 as a comparison; the protons *ortho* and *para* to NEt resonate as a doublet at 6.75 and triplet at 6.70, respectively. Since the ^{1}H NMR resonances and splitting patterns of the other aromatic rings did not change it can be assumed that diazonium coupling has not occurred on these rings UV spectrometry revealed an absorbance at 415 nm, indicative of the n→π* transition of the molecule containing an azo functionality.[92] The *trans* orientation is known to be the dominant state of an azo bond unless the *cis* isomer is particularly stabilised, for example, by hydrogen bonding. The *cis* orientation can be accessed by exposure to UV light, however this is reversible upon exposure to visible light.[93] Compounds **100i** and **100j** followed similar patterns with UV absorptions at 419 and 421nm and ^{1}H resonances at 6.78 and 6.77 ppm respectively.

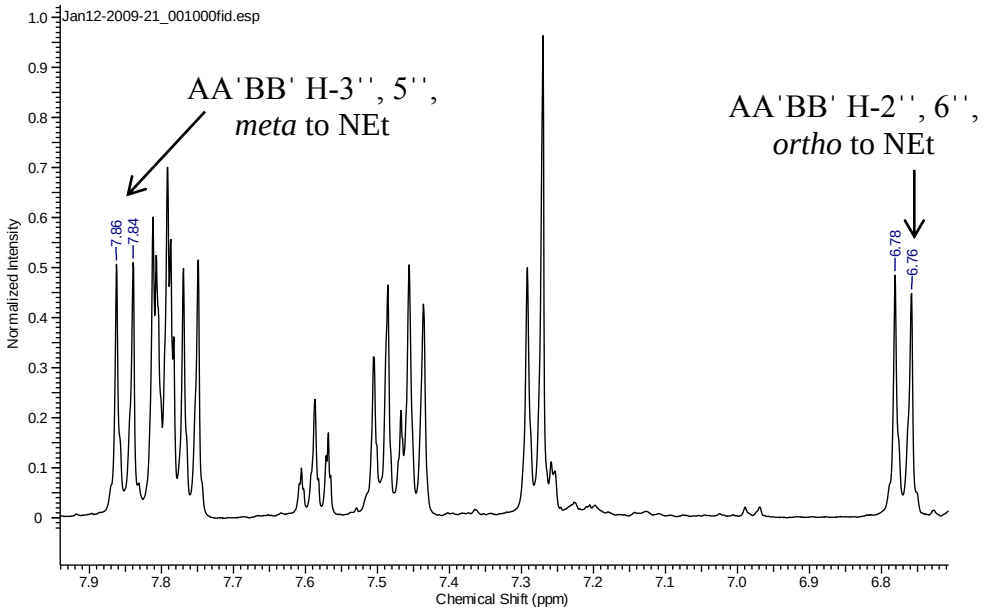

Figure 2.2: Proton NMR spectrum of 100b in deuterated chloroform.

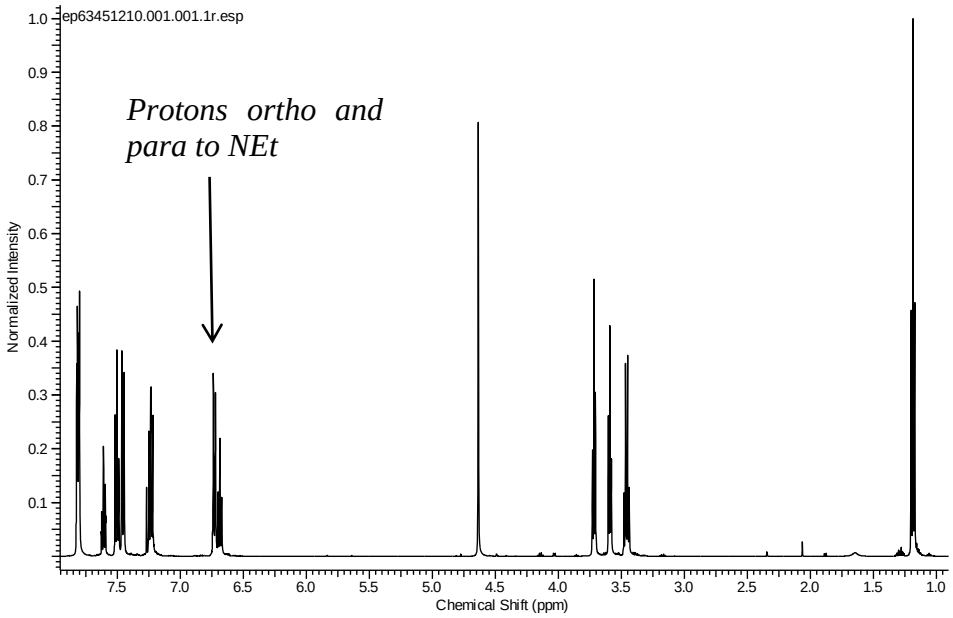

Figure 2.3: Proton NMR spectrum of benzophenone 87 in deuterated chloroform.

NMR spectroscopic analysis of the phosphonate and amine salt coupled products **101h** and **101i** proved to be difficult as the aromatic protons resonate in the 7-8 ppm region and there are no distinguishing protons (Figure 2.4). However, in both cases the absence of an apparent doublet of integration 2 at 6.8 ppm suggests that the neutral *para* coupled products

were not formed. NMR spectroscopy of amine **101i** was performed in deuterated methanol whereas the rest of the compounds were analysed in deuterated chloroform. When analysed in deuterated methanol, benzophenone **87** has resonances in the form of a triplet at 6.55 and a doublet 6.8 ppm representing the *ortho* and *para* protons of the ring in question. It is thought that the products were protonated at the ammonium (NEt) position, literature reports equivalent protons at 7.8 ppm.[94] The instability of acid **101j** to aqueous work up and of amine **101i** and phosphonate **101h** to aqueous potassium carbonate suggests that change in NMR spectrum is not simply a result of *ortho* diazonium coupling. Consequently, the assignment of *para* coupling is based upon the neutral coupled products **100b, i** and **j**.

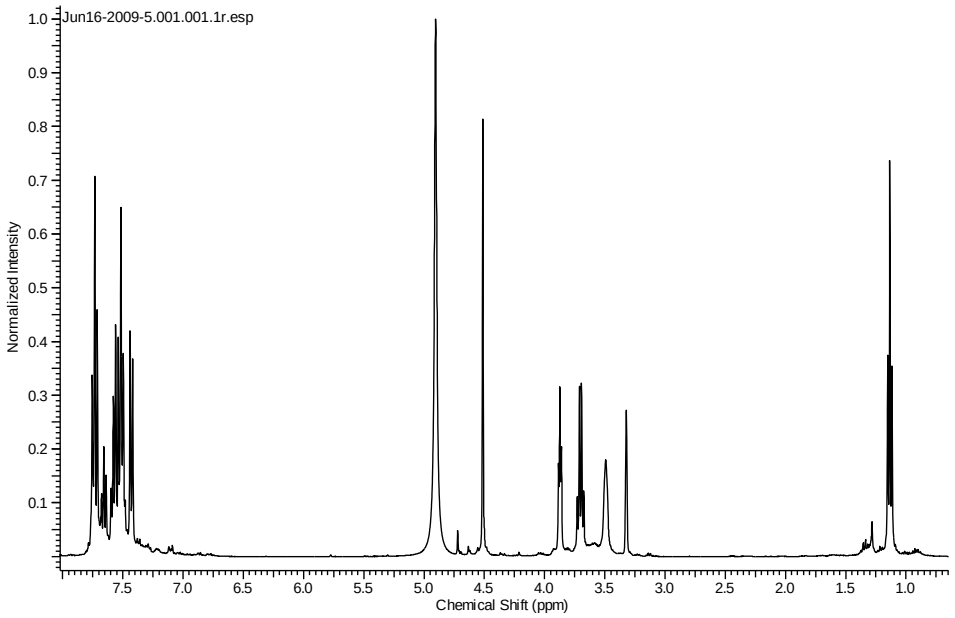

Figure 2.4: NMR spectrum of amine 101i in deuterated methanol.

High resolution mass spectrometry supports the assignment of the phosphonate coupled salt **101h**, but the presence of amine analogue **101i** was not determined by mass spectrometry, and only the benzophenone starting material **87** was detected; addition of solvent to the brown oil of **101i** resulted in a colour change to bright yellow which presumably signifies conversion of **101i** back to its starting materials. More information was gained from the UV

spectra of **101i**; it has been reported that (*E*)-4-dimethylaminoazobenzene absorbs UV light at 420 nm (in EtOH) whilst the ammonium cation absorbs UV light in the region of 320 nm and the azonium cation absorbs light at 520 nm (in EtOH).[95] UV analysis of amine coupled salt **101i** revealed a weak absorbance at 419 nm with an extinction coefficient of 4212 $mol^{-1}dm^3cm^{-1}$, also a group of absorbances in the region of 250-320 nm including a shoulder peak at 320 nm and finally a very weak absorbance at 550 nm. The shoulder peak arises from the ammonium isomer which dominates the mixture, as confirmed by NMR spectroscopic analysis, whilst the absorbance at 419 nm and 550 nm may be due to the neutral product and the azonium cation. However, these could not be identified by NMR spectroscopic analysis. From the NMR spectroscopic and mass spectrometry data it is proposed that amine and phosphonate **101i** and **101h** are in fact the ammonium cation salts. UV spectroscopy of amine **101i** corroborates this, however, absorbances indicative of the azonium cation and the neutral product were also observed suggesting that a mixture is a possibility.

2.2.2 Diazonium coupling to N,N-dimethyl aniline

Diazonium salts **91a-c**, **h-j** were prepared using isopentyl nitrite and tetrafluoroboric acid, and then were reacted with *N,N*-dimethyl aniline **102** at room temperature with and without sodium acetate (Scheme 2.10). General Procedure 7, without sodium acetate, required a basic extraction to obtain the neutral products but where sodium acetate was used (General Procedure 8), a basic extraction was not necessary. Addition of sodium acetate has been shown to improve the yields of diazonium coupling reactions by increasing the pH of the diazonium salt solution prior to addition of the nucleophile.[96] The yields and reaction times of the couplings can be found below in Table 2.1. The *t*-butyl, hexyl, iodo and amine derivatives **103a, b, c, i** all showed improvements in yield when sodium acetate was used,

whilst the addition of sodium acetate caused a decrease in yield for the phosphonate and acid derivatives **103h** and **103i**.

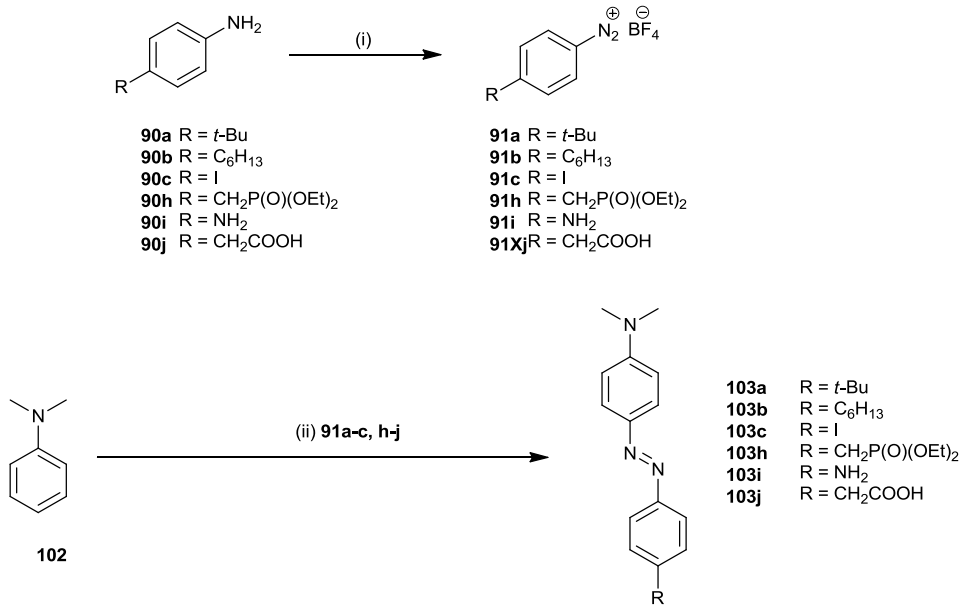

Scheme 2.10: Diazonium coupling to *N,N*-dimethyl aniline. Conditions: i) isopentyl nitrite, HBF_4, EtOH, -5 ˚C; ii) **General Procedure 7 102a-c**, **h-j** were added then the mixture warmed to room temperature and stirred; **General Procedure 8** NaOAc then **102a-c**, **h-j** were added and the mixture stirred at room temperature.

Table 2.1: Yields and reaction times of *N,N*-dimethyl aniline diazonium coupling products.

Compound[a/b]	**R**	**Reaction time at room temperature (hours)**	**% Yield**	**λ_{max} (nm)**
(*E*)-4-dimethyl aminoazobenzene	-	-	-	411[d]
103a[a]	*t*-Bu	18	72	412
103a[b]	*t*-Bu	4	91	
103b[a]	C_6H_{13}	18	20	410
103b[b]	C_6H_{13}	20	73	
103c[a]	I	0.5	47	425
103c[b]	I	0.5	57	
103h[a]	$CH_2P(O)(OEt)_2$	1	96	416
103h[b]	$CH_2P(O)(OEt)_2$	1	46	
103i[a]	NH_2	18	0	413
103i[b]	NH_2	18	12[c]	
103j[a]	CH_2COOH	20	95	415
103j[b]	CH_2COOH	18	34	

[a]Reaction completed in absence of sodium acetate; [b]reaction completed in presence of sodium acetate; [c]product is impure so exact yield unknown; [d]literature value.[97]

In all of the coupling reactions, aniline **102** and unreacted amine **90a-c**, **h-j** were recovered, with the amounts reflecting the yields above, indicating that the diazonium salt synthesis was not going to completion. Furthermore, evidence of decomposition of the hexyl diazonium salt was observed by the detection of 4-hexylphenol by mass spectrometry. Noteworthy is the reaction to generate iodide **103c**, with sodium acetate present (General Procedure 8) returned the product **103c** along with starting materials **102** and **90c** along with 1,3-bis(4-iodophenyl)triaz-1-ene **104** (Figure 2.5), as shown by NMR and mass spectrometry analysis. By-product **104** was formed by reaction of the iodo diazonium salt **91c** with 4-iodoaniline **90c**.

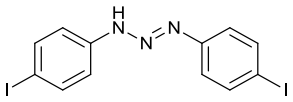

104

Figure 2.5

Reaction of aniline **102** with amine diazonium salt **91i** by both procedures proceeded with low yields. When the pH of the mixture was not adjusted by sodium acetate, the desired product was not generated and only *N*,*N*-dimethyl aniline **102** was recovered. Addition of sodium acetate improved the yield to 12% but aniline **102** was recovered as the major product.

The reaction times after addition of *N*,*N*-dimethyl aniline **102** vary, as can be seen in Table 2.1. Thin layer chromatography (TLC) was used to follow the reactions, but in most cases aniline **102** was not completely consumed, and unreacted amines **90a-c, h-j** were recovered in the crude mixtures, indicating that the diazonium salt formation was not going to

completion. The H-acid test confirms the presence of this salt, but does not indicate extent of reaction, and TLC and mass spectrometry could not be used to follow progress as the diazonium salts all decomposed when these techniques were applied. The coupling step was usually left for 18 hours to allow for maximum reaction time, but some were taken off after a shorter amount of time; similar problems were encountered earlier in coupling of benzophenone **87**. That the coupling reaction could proceed rapidly was indicated by the high yield of **103a** after only 4 hours and **103h** after only 1 hour.

As expected, these coupling reactions with *N*,*N*-dimethyl aniline **102** generated the *para* – product, as signified by four apparent doublets in the aromatic region of the ^{1}H NMR spectra. Again AA'XX' coupling is expected however the NMR spectra do not reveal enough structure to quantify it. The *trans* geometry of the azo- link was separately confirmed by UV spectroscopy. Table 2.1 shows the wavelength of adsorption signifying the n→π* transition; the values are in the same region as that quoted for (*E*)-4-dimethyl aminoazobenzene at 411 nm.[97] The bathochromic shift observed for iodide **103c** has been observed previously; the analogous chloride diazene has an adsorption at 422 nm.[98]

2.3 Conclusions

The first part of this chapter discusses the methods followed in order to synthesise diaryldiazo **65** needed for the modification of polystyrene. Also, the amines needed to prepare the diazonium salts used to prepare the necessary library of materials. The syntheses generally proved to be dependable and relatively efficient.

Investigations into diazonium coupling in solution were hindered by the lack of dependability of the diazonium salt synthesis, and incomplete synthesis of the salts was indicated by the recovery of the starting material amines. Furthermore, evidence of the

decomposition and side reactions of the diazonium salts was detected. Coupling to benzophenone **87** resulted in two groups of compounds, the neutral products **100b**, **i**, **j** and their salts **101h**, **i**, **j**, whereas coupling to *N*,*N*-dimethyl aniline **102** generated only the neutral products since a base-wash was included in the reaction work up. Generally, diazonium coupling to *N*,*N*-dimethylaniline **102** was more successful than coupling to benzophenone **87**; acid **103j** was isolated in good yield after coupling with aniline **102** but the acid benzophenone coupled product **100j** was isolated in low yield and the salt **17j** could not be isolated at all. Coupling of the amino diazonium salts **91i** and **99i** proved to be low yielding in all cases apart from when the salt **101i** was generated by coupling to benzophenone **87**, but even this was unstable in the presence of base.

The common reaction time of 18 hours that was adopted, before the root of the problem was known, was shown to be far too long and possibly too warm, after some reactions repeated at cooler temperatures and for shorter time periods were found to be superior. In hindsight, this work would benefit from more investigation into the increasing the number of equivalents of the diazonium salt as well as reducing the reaction times.

Chapter 3: 2-D Model Study

The chemistry discussed in Chapter 2 was applied to polystyrene films coated on various base substrates (Figure 3.1 and Scheme 3.1) to generate a selection of functionalised polystyrene surfaces with a range of surface chemistry. A characterisation study was performed to determine the effects of the surface modifications on the chemical composition of the surfaces and their surface properties. The aim of the work recorded in this thesis is to determine the effect of these chemical modifications on biofouling, and with that in mind, the effect of protein adsorption was investigated. Quartz crystal microbalance-dissipation (QCM-D) is a technique that monitors the change in mass, layer thickness and viscoelastic properties of a piezoelectric crystal and the layers applied to it in real time. A quartz-gold crystal was coated with polystyrene then chemically functionalised. The different functional surfaces were exposed to the protein bovine serum albumin and the change in mass was determined with QCM-D analysis.

This work was completed in collaboration with Geoffrey Nelson who is under supervision of Professor John Foord, University of Oxford. Geoffrey developed the polystyrene film, carried out the XPS experiments and also completed modelling of the QCM-D data.

3.1 Preparation of materials

Three different substrates were modified in this work, namely UV-crosslinked polystyrene on glass **105**, divinylbenzene-crosslinked polystyrene on gold on silicon wafers **106** and divinylbenzene-crosslinked polystyrene on a gold coated quartz crystal **107** that was required for the QCM-D experiments (Figure 3.1). The crystal was sourced from Q-sense and the silicon-gold substrate prepared by metal vapour deposition, carried out by Dr Robert Jacobs from the University of Oxford.

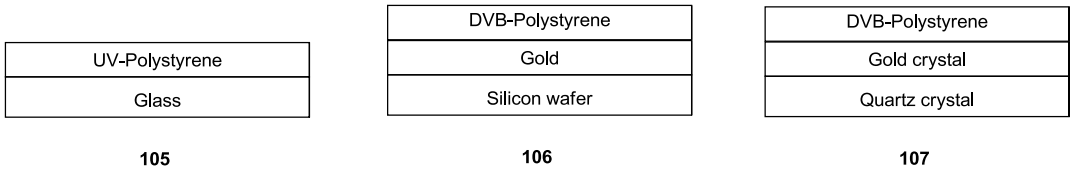

Figure 3.1: Substrates used in chemical modifications.

The polystyrene films were prepared using the protocols outlined in Chapter 6, pages 170-171. The polystyrene film on glass substrate **105** was crosslinked by exposing the film to UV light for 30 minutes, while the polystyrene films on gold **106-107** were crosslinked with divinyl-benzene (DVB) with benzoyl peroxide as an initiator. UV crosslinking is known to crosslink the surface of a polymer whereas DVB with an initiator will crosslink throughout the polymer film, resulting in a polymer more resistant to damage by solvents and the chemical treatments to follow. Consequently the DVB crosslinking method was used for the QCM-D experiments.[99]

In order to determine the most efficient temperature to use for decomposition of the diazo coating to the carbene, bis(4-iodophenyl)diazomethane **61** (Scheme 3.1) was coated onto three glass-polystyrene substrates **105** and each was heated at 93, 120 and 180 ˚C for; heating was terminated when the bright pink diazo coating had turned colourless.

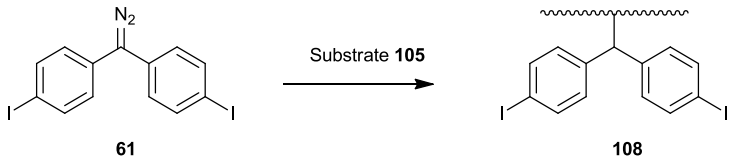

Scheme 3.1: Surface modification with bis(4-iodophenyl)diazomethane 61. Conditions: DCM, heating to 93, 120 or 180 ˚C.

XPS analysis detected iodine on each of the samples **108** at ~620 eV (I 3d5/2) and ~630 eV (I 3d3/2); the iodine 3d5/2 to carbon ratio was calculated to be 0.005, 0.011 and 0.0177 for

heating at 93, 120 and 180 ˚C, respectively. Since the amount of iodine detected, and presumably the amount of compound inserted, increased as the temperature increased, samples were subsequently all heated at 180 ˚C for the carbene activation and insertion step. However, when the glass-polystyrene substrate was modified, the samples were heated to only 120 ˚C during the carbene insertion step.

To prepare the samples for characterisation and QCM-D analysis, the different substrates were treated under the conditions detailed in Scheme 3.2.

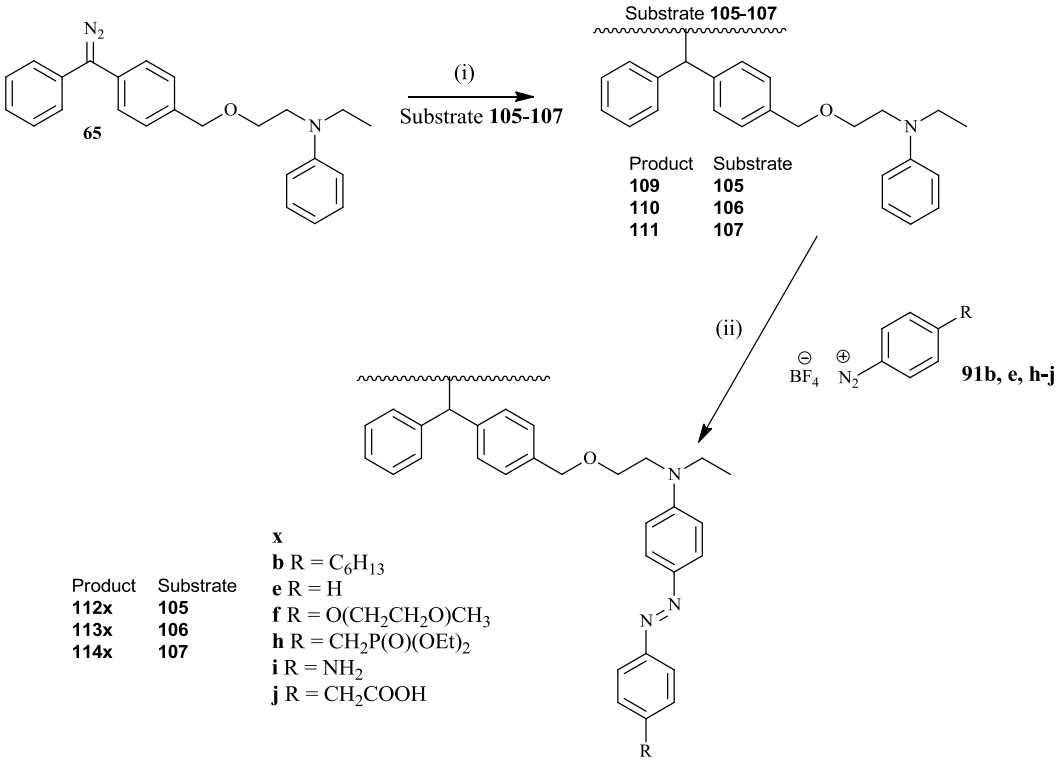

Scheme 3.2: Chemical modification of polystyrene film on gold. Conditions: i) **65** in DCM (1 w/v%), polystyrene substrate, 180 ˚C; ii) diazonium salt synthesis using General Procedure 1 (Scheme 2.3), samples soaked in salt solutions for 18 hours, 5 ˚C.

The substrate was first coated with a pink coloured solution of diazo **65** in DCM (1 w/v%) such that the substrate was completely covered (~0.2 ml per 1 cm^2 substrate was applied). Once the DCM had evaporated, the sample was heated to 180 ˚C for 2 minutes until the pink

colour was completely diminished. After washing with DCM and drying under nitrogen linker-terminated materials **109-111** were obtained. These were then soaked in the relevant diazonium salt solution in ethanol for 18 hours at 5 ˚C, washed with EtOH and DCM and then dried under nitrogen. Six diazonium salt solutions **91b**, **e**, **h-j** were prepared thus giving access to six materials of varying functionality on each of the substrates **105-107**.

3.2 Characterisation of surfaces

3.2.1 Optical microscopy

Optical microscopy of the silicon-gold based substrate **106** was used to determine if the chemistry was destroying the polystyrene film. Figure 3.2 (overleaf), a and b, are images of the gold-coated silicon wafers prior to any treatment. The details on the surface are due to dust and small gaps in the gold coating, and image b displays the edge of the sample; the large black area is silicon that was not coated. Images c and d are of the unmodified polystyrene film, substrate **106**, which was crosslinked with 1% DVB. The pale mottling detail, most pronounced in image d, is presumed to be a result of excess polymerisation resulting in clusters within the polymer. Whilst optimising the polystyrene layer, a mixture with a larger percentage of DVB was trialled, 5% instead of 1%. The images of the 5% crosslinked film, g and h, show evidence of the mottling effect at a greater concentration. After chemical modification, there was no change in the appearance of the surfaces by optical microscopy, as seen in images e and f. The mottling effect, resulting from aggregates in the polymer, is still apparent and the larger grey detail in image e is due to damage of the entire surface such that the silica base was revealed, possibly by scratching. This work does not give in-depth information concerning the structure and the effects of the chemistry on the polystyrene film; however it does demonstrate that the polystyrene was not removed during the chemical treatment with diazo **65**.

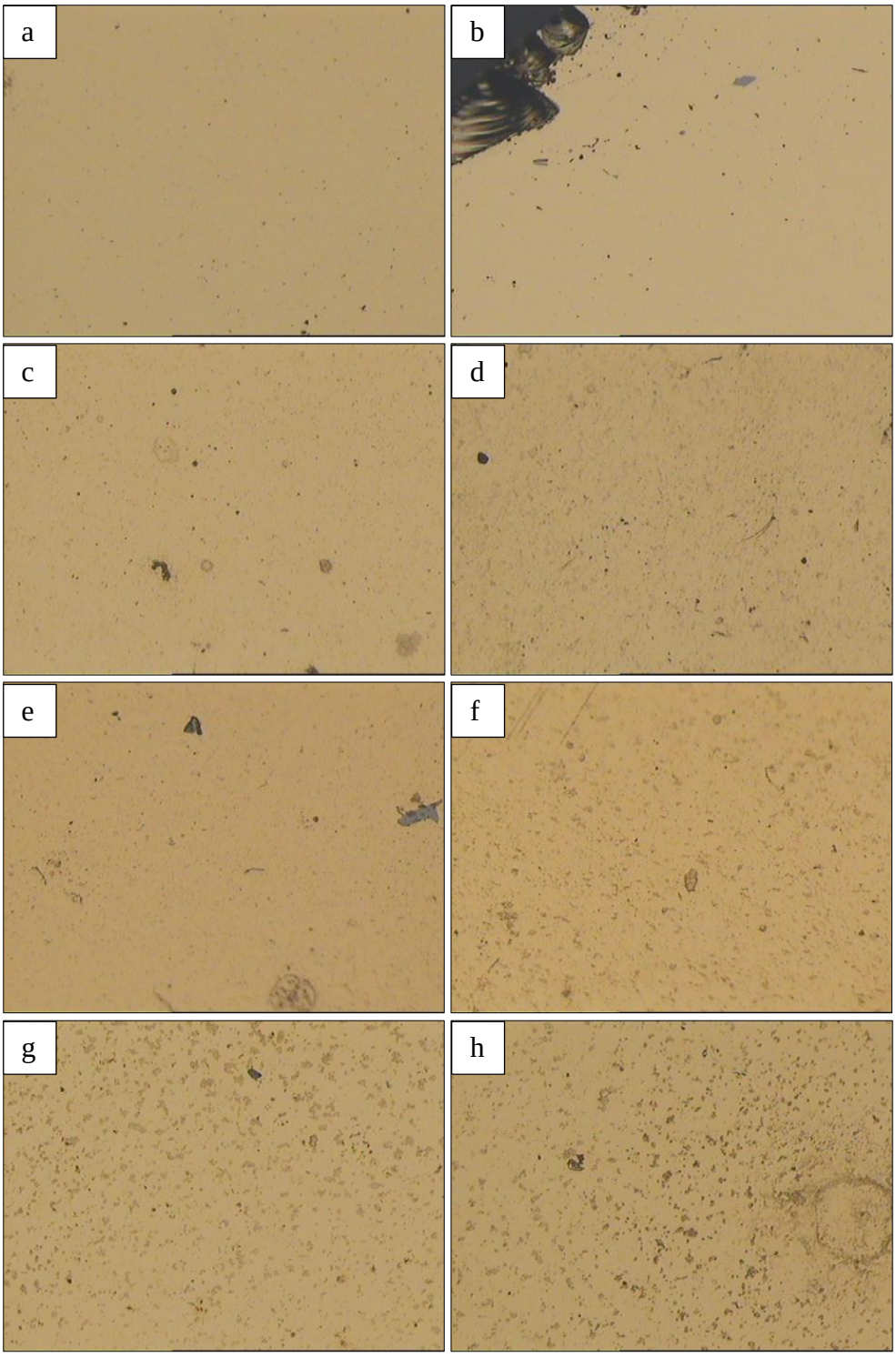

Figure 3.2: Images of the substrates before and after modification. a and b: untreated gold on silicon wafer; c and d: polystyrene film (substrate **106)**; e and f: linker terminated surface **113**; g and h: polystyrene film with 5% DVB.

3.2.2 XPS

X-ray photoelectron spectroscopy (XPS) of the chemically modified materials on substrate **105**, glass coated with a UV-crosslinked polymer film, was conducted to detect nitrogen and other significant elements after modification; nitrogen was found to have been added consistently in both modification steps. Surface **109**, which had only been modified by the linker molecule, had a nitrogen (N1s) emission at 407 eV. The diazonium coupled substrates all had nitrogen emissions (N1s) in the region of 400-401 eV and the nitrogen carbon (N1s/C1s) ratios are displayed in Table 3.1.

Table 3.1: N/C ratios calculated using XPS data for modified glass-polystyrene surfaces.

Material	R	N/C ratio found	N/C ratio expected
109	-	0.012	0.040
112b	C_6H_{13}	0.046	0.081
112f	$O(CH_2CH_2O)CH_3$	0.061	0.079
112h	$CH_2P(O)(OEt)_2$	0.058	0.083
112i	NH_2	0.036	0.129
112j	CH_2COOH	0.035	0.091

All of the materials have a lower N/C ratio than would be expected; amine-terminated substrate **112i** is especially low, so XPS analysis was repeated for this substrate, giving a second analysis giving a ratio of 0.022. However, in both cases, two peaks at ~400 and ~396 eV were seen in this region, only one peak at ~400-410 eV was observed for the other surfaces; the second peak is conformation of the presence of a different environment of nitrogen which may be NH_3^+. As expected, oxygen and carbon were detected in all of the materials as was silicon, presumably as a residue from glass pipettes and laboratory equipment; O1s was detected between 532-533 eV, and there were multiple C1s peaks

between 285-288 eV. Finally, phosphorus (2p) was detected on phosphonate-terminated substrate **112h** at 126 eV (2p).

3.2.3 Contact angle

The angle at which a droplet of solvent settles on a surface can be used to measure the wettability of a surface with a solvent of choice; water contact angles give an indication of the degree of hydrophilicity of the surface, and by altering surface chemical functionality of the polystyrene beads, it was expected that there would be a change in wettability. The water contact angles of silicon-gold based surfaces **106**, **110**, **113b**, **e**, **g**, **h-j** were measured to gain insight into the hydrophilic nature of the surfaces and to determine if the wettability was altered by the chemical modifications (Table 3.2).

Table 3.2: Contact angle analysis.

Substrate	R	Contact angle (degrees)[a]	Standard deviation
106	Unmodified	87.2	6.3
110	-	83.6	4.8
113b	C_6H_{13}	94.3	4.4
113e	H	89.8	2.9
113f	$O(CH_2CH_2O)_3CH_3$	92.9	3.8
113h	$CH_2P(O)(OEt)_2$	82.6	7.9
113i	NH_2	99.0	6.9
113j	CH_2COOH	91.1	3.2

[a]Average of six values.

Prior to chemical modification, the polystyrene film **106** has a contact angle of 82.7˚ and conversion to linker-modified substrate **110** has a very small effect on the contact angle. Hexyl and phenyl terminated surfaces **113b** and **113e** both became more hydrophobic as expected, however, the glycol, amine and acid terminated surfaces **113f**, **113i** and **113j** also revealed an increase in hydrophobicity, which is opposite to the expected. The standard

deviations are large, suggesting that the polymer surface is not homogeneous and with no closer imaging of the surfaces after chemical modification, it is not possible to see how uniform the modified surfaces have become. The mottling observed by optical microscopy has been accounted for by aggregates within the polymer, and these may disrupt the surface uniformity.

It is notable that the contact angles are in a relatively small range of 83.6-99.0˚ with large standard deviations, which may signify that the surfaces are all relatively similar. The π-π stacking interactions between the polystyrene film and the surface chemistry may result in the modification chemistry adopting a horizontal structure instead of a vertical structure (Figure 3.3). Consequently, the functional end-groups may be less exposed, and so will not have a significant effect on the surface wettability.

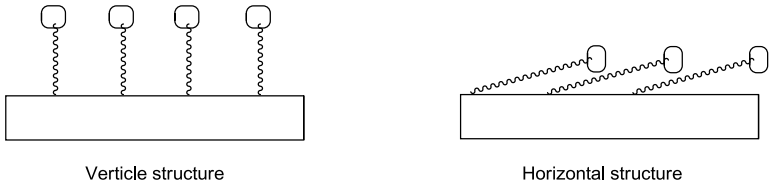

Figure 3.3: Possible surface structure of chemical modifications.

3.2.4 Ellipsometry

This technique was used to determine the thickness of the polystyrene film and the layer of chemical modification, and the results are displayed below (Table 3.3). The base substrate was silicon-gold with DVB crosslinked polystyrene, **106**. The polystyrene film thickness is 82 nm, but this is based on one measurement only; multiple measurements were taken but only one could be successfully fitted as the laser beam did not have a smooth path through sample, which is itself a further indication of an inhomogeneous film. This problem was not

encountered after chemical modification, suggesting that the film may have contained air pockets that were filled with solvent or the chemistry during the modification steps.

Table 3.3: Thickness of chemical modification layers.

Sample	R	Thickness (nm)	Standard deviation	XPS thickness (nm)
106	Unmodified	82[a]	-	-
110	-	6.5[b]	1.5	6.6
113b	C_6H_{13}	12[b]	2.1	8.9
113f	$O(CH_2CH_2O)CH_3$	7.8[b]	3.4	16.6
113h	$CH_2P(O)(OEt)_2$	9.3[b]	2.1	10.3
113i	NH_2	11[b]	6.9	-
113j	CH_2COOH	13[b]	0.0005	-

[a]One measurement only; [b]average of three measurements.

The thickness of the chemical modifications ranges from 6.5 nm for linker-terminated surface **110** to 12 nm for acid-terminated surface **113j**. The linker-terminated surface has the thinnest layer, but the surfaces terminated with longer chains are notable in their greater thicknesses; the glycol-terminated chain has one of the thinner measurements but also one of the larger standard deviations. Notably, the acid terminated surface **113j** has the thickest chemical layer with the smallest standard deviation. If an error of +/- 1 standard deviation is assumed for the ellipsometry data, then the difference in thickness between the surfaces is not especially significant. The layer thicknesses estimated by XPS[100] are also featured in Table 3.3; it is evident that these values are of the same magnitude as those obtained using ellipsometry. However, there are some significant differences, such as the measurements obtained for glycol terminated **113f**. It is notable that the substrate and polymer crosslinking method differ for the two experiments. Also, XPS is carried out under vacuum; the surface structure may have changed during vaporisation of excess solvents under vacuum which could change the polystyrene and modification layer thicknesses.

3.3 QCM-D analysis

Quartz crystal microbalance-dissipation (QCM-D) is used to detect incremental changes of mass in real time experienced by an oscillating piezoelectric crystal. When a voltage is applied the crystal it will resonate, however, the mass of the crystal will alter the frequency of vibration. The change in frequency Δf is directly proportional to the change in mass Δm as described by the Sauerbrey equation:

$$\Delta m = -(C\Delta f/n)$$

where C is the mass sensitivity constant (17.7 ng/cm^2 for a 5 MHz crystal) and n is the overtone number. This relationship can be applied to rigid, thin adsorbed layers that couple directly to the crystal surface. In contrast, layers that are soft, have viscoelastic properties, or do not couple directly to the crystal, are not best analysed with this relationship since it underestimates the mass adsorbed onto the crystal. Soft layers can be better analysed by simultaneously recording the change in frequency and dissipation of the crystal. Dissipation D is defined as:

$$D = E(lost)/2\pi E(stored)$$

E(stored) refers to the energy stored in the oscillator and *E(lost)* is the energy lost when the voltage connected to the oscillating crystal is switched off. Adsorbed layers that are not tightly bound and have more freedom will have a higher dissipation. Using the Voigt model, the change in frequency and dissipation can be used to calculate the mass, thickness, elastic shear modulus and the viscosity of adsorbed layers that are 'soft' with viscoelastic properties.[101-105]

This technique has been widely used to monitor protein adsorption, with the reversibility of protein adsorption being demonstrated by water and phosphate-buffered saline washing sequences.[102,106,107] The $\Delta D/\Delta f$ relationship has been used to gain information concerning the rigidity of adsorbed layers as well as water content; as the protein films become stiffer the $\Delta D/\Delta f$ term decreases which can be indicative of protein rearrangement to enhance binding to the crystal surface, on the other hand, as the water content of the adsorbed layer increases $\Delta D/\Delta f$ increases.[102]

Gold coated quartz crystals were coated with polystyrene resulting in substrate **107**. Chemical treatment of **107** furnished linker terminated **111** and surfaces **114b**, **e**, **f**, **h**-**j**, as discussed above. The crystals were loaded into the cell then exposed to phosphate buffered saline (PBS), usually for ~16 hours, until the crystal had equilibrated. Bovine serum albumin (BSA) in PBS (80 mg/L) was pumped across the crystal until the frequency change plateaued. A PBS rinse was used to remove unbound protein, after which the surfaces were exposed to Hellmanex solution (2% in water) to clean the crystal (Figure 3.4).

Figure 3.4, over the page, displays the QCM-D trace for hexyl-terminated surface **114b**. After addition of the BSA/PBS solution the frequency decreases as the modified polystyrene film adsorbed BSA, whilst the dissipation increased. Rinsing with PBS was accompanied by a small gain in frequency signifying loss of some of the protein from the surface. Each of the surfaces **114b**, **e**, **f**, **h-j**, linker-terminated surface **111**, unmodified polystyrene **107** and bare gold were all exposed to the same procedure although the timings differed, as the rate and amount of protein adsorbed and desorbed differed between the surfaces.

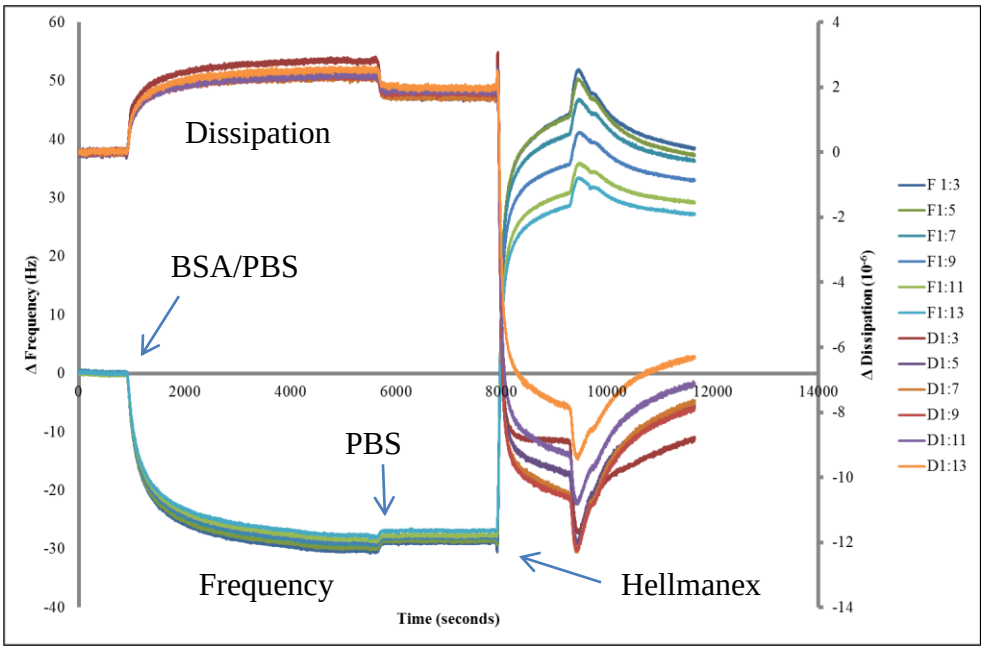

Figure 3.4: Example QCM-D trace of hexyl terminated surface 114b.

Below is a discussion concerning the change in mass of the modified crystals after exposure of BSA/PBS and after the PBS rinse using the Sauerbrey and Voigt models. The 5th, 7th and 9th overtones were used for the calculations, with higher overtones being more sensitive to changes of the surfaces applied to the crystal; the 3rd overtone is not very sensitive to changes at the surface, it is more affected by changes to the crystal, whilst the 11th and 13th overtones are more sensitive to the periphery of the adsorbed layers. For the purpose of modelling the zero-point was taken to be the time at which the BSA/PBS solution was added. All of the data associated with this work can be found in Chapter 6, Tables 6.5-6.7, pages 173-174.

3.3.1 BSA deposition

Since the surfaces were exposed to the protein solution for different times, the change in mass was calculated at 20, 36 and 53 minutes, as well as just before the PBS rinse, this mass has been termed the total mass. Figures 3.5 and 3.6 display the mass adsorbed using the

Saurebrey and Voigt models for calculation, for some of the surfaces the later times have no data since the PBS rinse was started at different times.

Using the Sauerbrey relationship to calculate the mass change after exposure to BSA (Figure 3.5), it was revealed that the phenyl- **114e** and phosphonate diester- **114h** terminated surfaces have the smallest mass uptake at 20 minutes with 174.6 and 220.5 ng/cm^2, respectively. They continue to have a low mass uptake through the other time intervals. Phosphonate diester terminated surface **114h** actually loses mass throughout across all of the time intervals, this suggests that the adsorbents are easily taken back into the bulk solution and that the binding interactions are disrupted by the flow of the protein solution across the sample. This is surprising as the phosphonate diester is capable of forming hydrogen bonds with water and the protein as are other terminal groups that have a much higher mass increase, the acid terminated surface **114j** for instance. The hexyl, amine and acid terminated surfaces **114b**, **114i** and **114j** all continued to increase in mass throughout the time intervals, with the total deposition time being 77.1, 43.6 and 60.3 minutes for these experiments, respectively. This could be indicative of a number of things: increase in water adsorption, increase in protein adsorption, and the reorganisation of the proteins on the surface to achieve stronger binding and increase surface protein contact. The Sauerbrey relationship is sensitive to surface contact so as protein surface contact increases so will the apparent mass. After 20 minutes, the surface with the largest mass is glycol terminated **114f** with 468.5 ng/cm^2 and hexyl **114b** has a similar mass 445.1 ng/cm^2, the second highest mass. Polyethylene glycol functionalised materials are known to decrease protein adsorption through highly hydrated surfaces,[2] the high mass uptake observed may be due to water rather than BSA. The hexyl surface **114b** was designed to be hydrophobic and encourage protein adsorption; van der Waals forces of interaction are expected to be the dominant

interaction force of this surface which lends itself to protein adsorption and reorganisation rather than hydration.

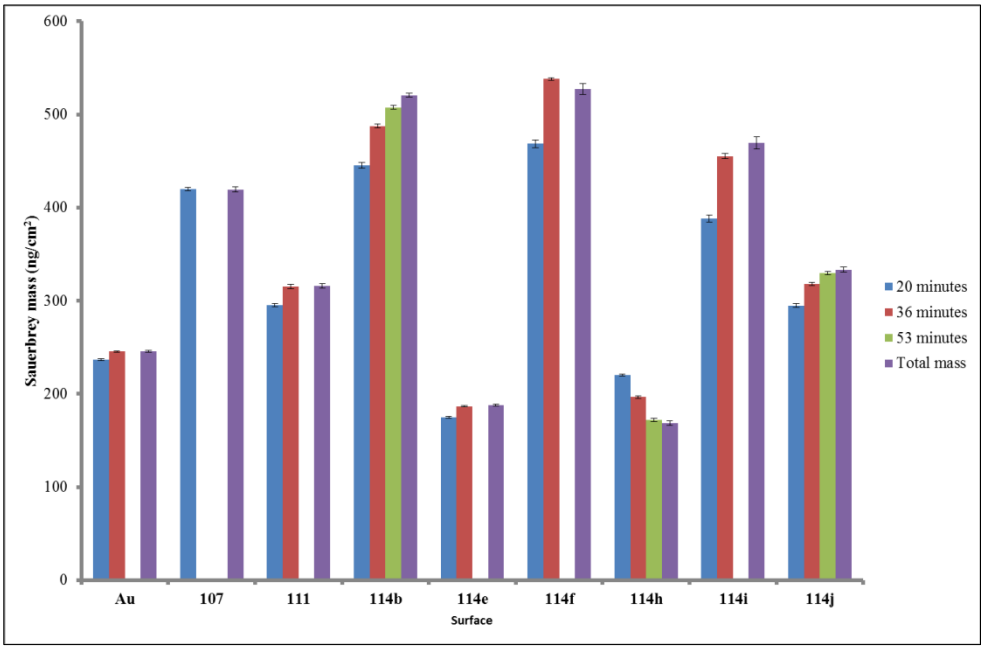

Figure 3.5: Sauerbrey mass increase after exposure to BSA/PBS solution.

The masses calculated using the Voigt model (Figure 3.6) were generally greater than those observed with the Sauerbrey model, after 20 minutes the Voigt range is 180.8-1401.7 ng/cm^2 where the Saurebrey range is 174.6-468.5 ng/cm^2.This is to be expected, since the Voigt model will take into account species not directly bonded to the crystal, even though they still form part of the adsorption layer. The phenyl and phosphonate surfaces **114e** and **114h** have the smallest masses again, with the hexyl and amine terminated surfaces **114b** and **114i** having the largest masses; after 20 minutes **114b** has adsorbed 1817.3 and **114i** 1401.7 ng/cm^2. The most significant difference between the two models, apart from a general mass increase with Voigt, is the placement of glycol terminated surface **114f**; the Sauerbrey model shows this surface to have the largest mass after 20 minutes, however the Voigt model determines that this surface adsorbs 660.5 ng/cm^2 in the same time period, 64% less than the absorbed by hexyl terminated **114b**.

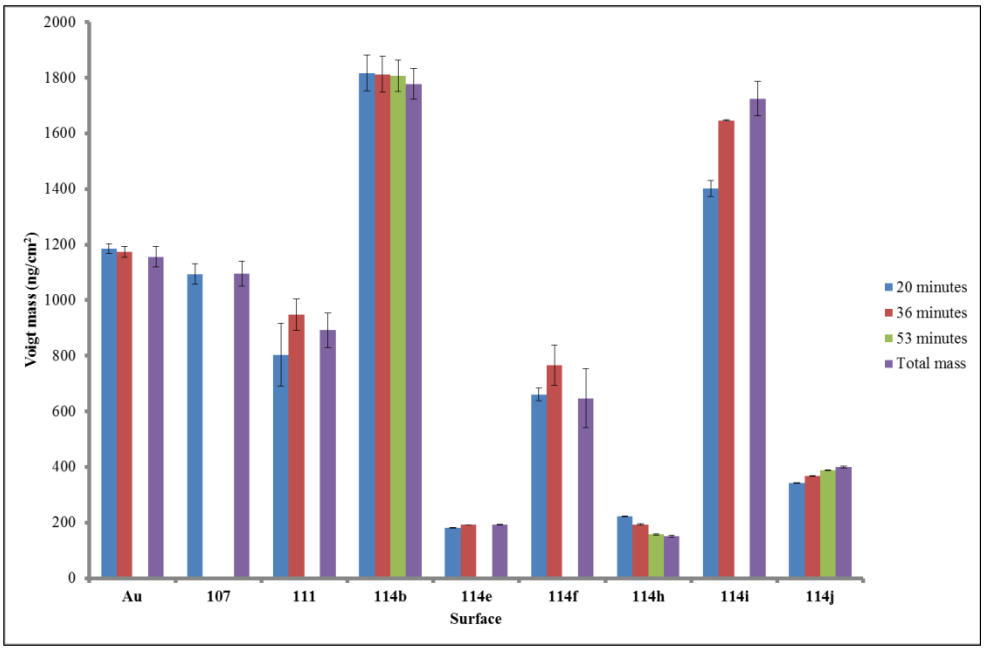

Figure 3.6: Mass increase calculated using the Voigt model.

A direct comparison of the mass calculated using both methods after 20 minutes (Figure 3.7) reveals that both models calculated similar masses for the phenyl, phosphonate diester and acid terminated materials **114e**, **114h**, **114j**, suggesting that the layers adsorbed on the surfaces are rigid and that they have strong contact with the polystyrene film/crystal. The glycol terminated surface **114f** has a relatively small difference of 192 ng/cm^2. The difference in mass calculated using the two models for the rest of the surfaces is appreciable, suggesting that the layers adsorbed are not rigid and that they are made up of extended multilayers with reasonable flexibility and viscoelasticity.

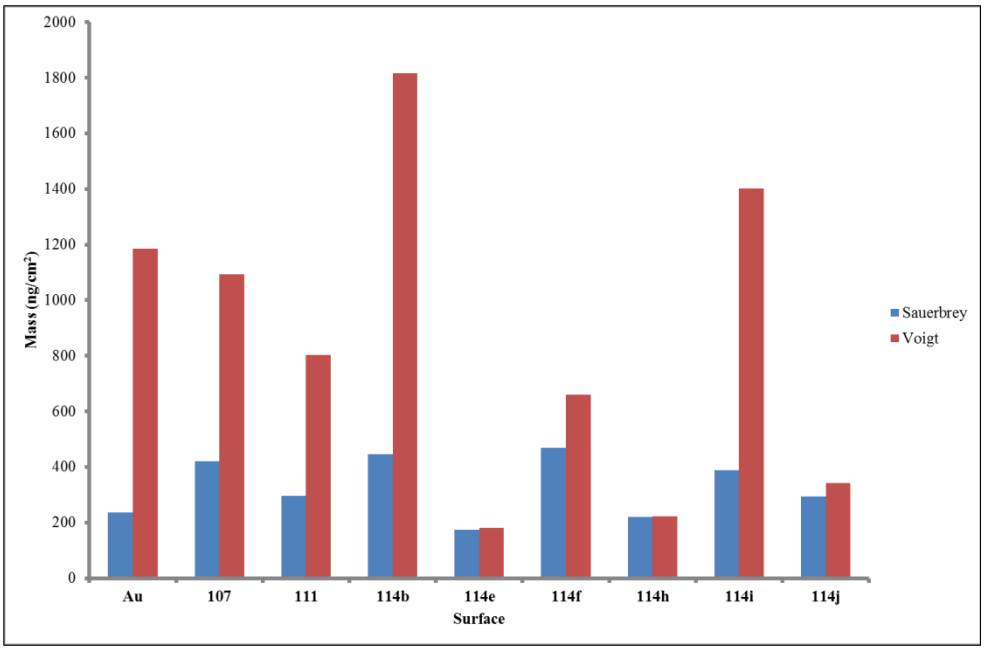

Figure 3.7: Comparison of mass uptake of surfaces after 20 minutes of exposure to BSA/PBS.

Comparison of mass with contact angle was carried out in order to determine the effect of surface hydrophilicity on adsorption, with its effect on protein adsorption being of particular interest (Figure 3.8). The Sauerbrey masses do not reveal a correlation with contact angle. It could be said that there are two groups in the Voigt correlation, both of which have increasing adsorption with increasing contact angle, as the surfaces become more hydrophilic. One of the groups is made up of **107**, **111**, **114b** and **114h** (unmodified polystyrene, linker, hexyl and phosphonate diester terminated) and the other is made up **114e**, **114f**, **114i** and **114j**, which are terminated with the phenyl, acid, glycol and amine functionalities. However, no common themes connect the surfaces in the groups, implying that the two groups may be coincidence rather than a trend. It is notable that the measured contact angles do not reflect the terminal functional groups, for example, the glycol surface **114f** has a more hydrophobic contact angle (92.9˚) than unmodified polystyrene **107** (87.2˚) and a similar contact angle to the hexyl terminated surface **114b** (94.3˚), even though glycol functionality has produced highly hydrophilic surfaces previously, as discussed in Chapter

1.[25] These contact angles were taken under open conditions, however, the closed aqueous conditions of the QCM-D cell may result in rearrangement of the surface chemistry to expose the more hydrophilic distinguishing functional groups.

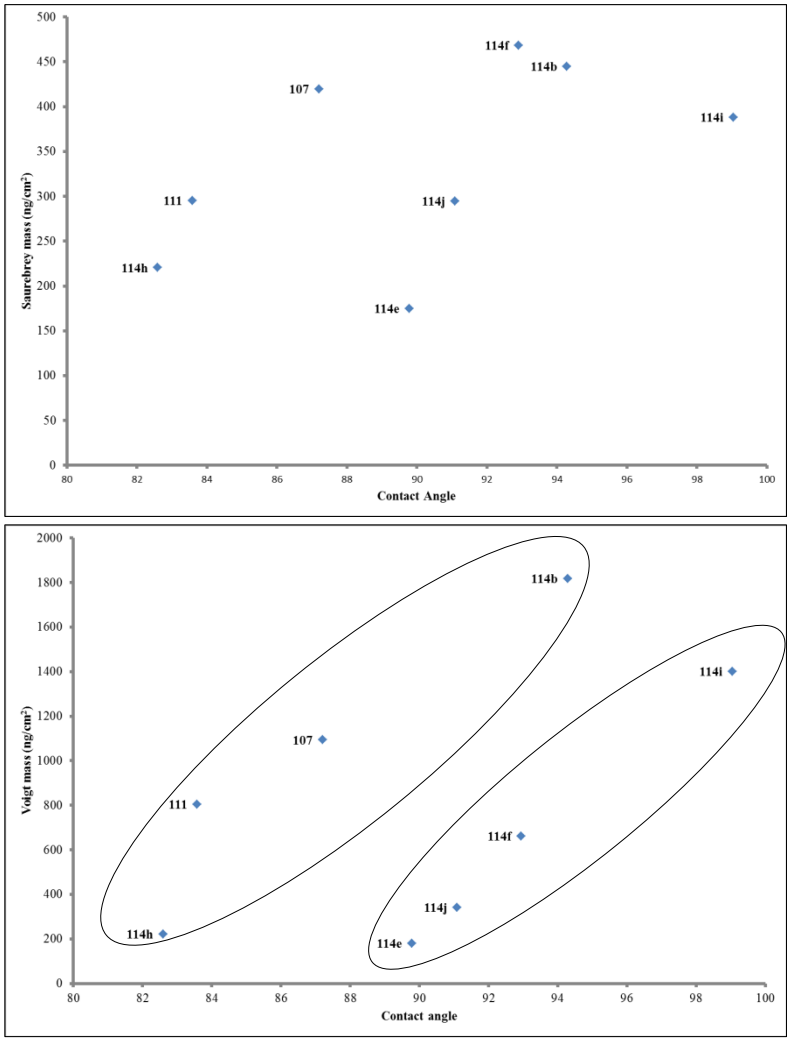

Figure 3.8: Correlation of Sauerbrey and Voigt mass uptakes after 20 minutes exposure to BSA/PBS with contact angle.

3.3.2 PBS rinse

The surfaces were exposed to PBS, pH 7.4, in order to remove any BSA not bonded to the modified polystyrene surfaces. The resulting mass was calculated after 29, 35 and 41 minutes using the Sauerbrey and Voigt models (Table 3.4); the mass at 29 minutes proved to

be most useful since not all of the samples were rinsed for as long as 35 and 41 minutes. The mass lost is based in the difference between the mass after 29 minutes of the PBS rinse relative to the mass of the sample just prior to the PBS rinse, the total mass. According to the Sauerbrey calculations, the gold and amine **114i** surfaces increase in mass during the PBS rinse, whilst the Voigt calculations reveal an increase in mass for the hexyl surface **114b** only (Figure 3.9). The increase in mass may be due to the following: the adsorption of water and ions from the PBS, reorganisation of the protein to strengthen the binding with the surface, and irreversible protein binding to the surface.[107] The mass increase due to protein reorganisation is more applicable to the Sauerbrey results due to those masses being more influenced by contact of the layer with the crystal.

Table 3.4: Change mass after PBS rinse. All masses reported in ng/cm^2.

Surface	Sauerbrey			Voigt		
	Total mass[a]	**Rinse mass (standard deviation)**	**Mass lost in rinse**	**Total mass[a]**	**Rinse mass (standard deviation)**	**Mass lost in rinse**
Au	245	358 (1.3)	-113	1156	699 (21.2)	456
107	419	367 (1.8)	53	1096	761 (9.4)	334
111	316	140 (1.3)	176	892	150 (0.3)	743
114b	520	502 (1.9)	19	1777	1974 (27.2)	-196
114e	188	188 (0.9)	0	193	189 (0.5)	4
114f	527	398 (1.3)	129	647	407 (1.0)	240
114h	169	123 (1.5)	45	151	109 (1.0)	43
114i	469	714 (3.9)	-244	1725	710 (3.6)	1015
114j	333	316 (1.6)	17	399	191 (0.1)	209

[a]Total mass is the mass adsorbed prior to the PBS rinse.

Figure 3.9 below displays a graph comparing the mass lost during the PBS rinse as calculated using both methods. All of the surfaces except the hexyl and phosphonate diester terminated materials **114b**, **114h** exhibit greater loss of mass by the Voigt calculations. In

the case of amine terminated **114i** this is very significant, where a loss of 710 ng/cm^2 as calculated by the Voigt model and a gain of 244 ng/cm^2 of mass was calculated by the Sauerbrey model. This suggests that during the PBS rinse loosely bound species that are not in direct contact with the surface are lost, thus decreasing the Voigt mass. However, the increase in Sauerbrey mass suggests that the contact of the polymer surface with adsorbents is increasing; this is in indicative of protein rearrangement to increase surface-protein interactions. The opposite trend was observed by hexyl terminated **114b** in that the Sauerbrey mass deceased by as 19 ng/cm^2 whilst the Voigt mass increased by 196 ng/cm^2. Protein interactions with the hexyl terminated surface will be via the non-polar regions of the protein, thus leaving the polar regions exposed to adsorb water and other ions during the PBS rinse. This has been shown by the Voigt mass since these ions and water will not be directly bound to the polymer surface.

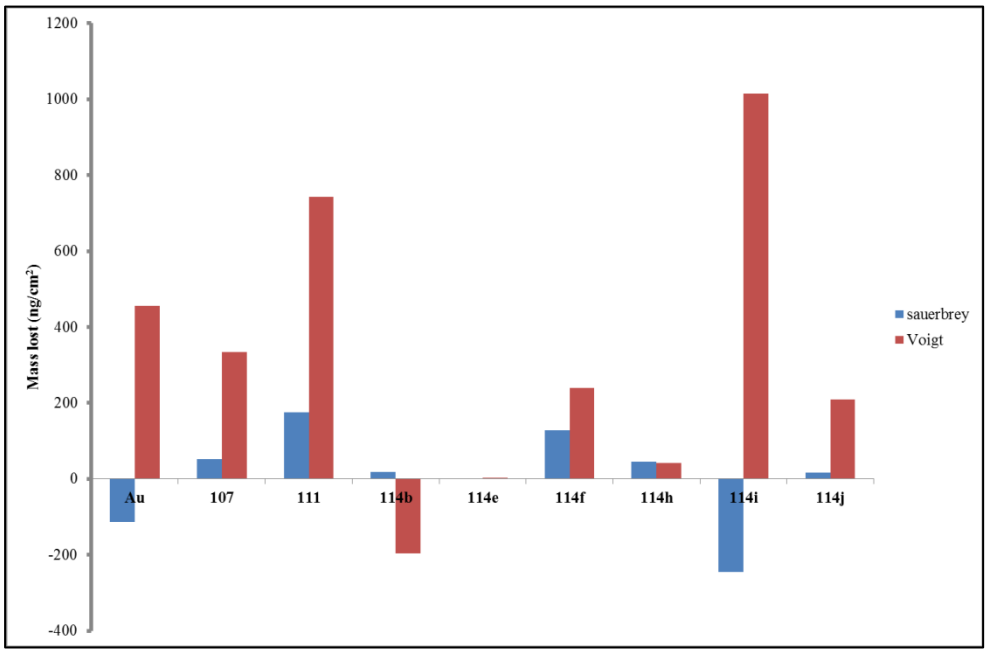

Figure 3.9: Graph displaying the mass lost during the PBS rinse.

Phenyl-terminated surface **114e** is of particular interest, since very little mass was lost, the Sauerbrey calculation showed no change in mass whilst the Voigt calculation resulted in a

loss of 4 ng/cm^2. In addition, phosphonate diester surface **114h** lost 45 ng/cm^2 and 43 ng/cm^2 by the Sauerbrey and Voigt calculations. This may be further evidence supporting the hypothesis that these surfaces adsorb thin rigid layers, which are not altered significantly during the rinse process. However this could also be a result of the surfaces having a low affinity for the protein so the characteristics of the polystyrene film are dominating.

Figure 3.10 displays a graphical representation of the masses of the crystals after the PBS rinse, termed the rinse mass in Table 3.4. It is of interest that the resulting Sauerbrey masses, for **111**, **114e**, **114f**, **114h** and **114j** (linker, phenyl, glycol, phosphonate diester and acid terminated) are all similar or the same as their Voigt counterparts; the PBS rinse has removed the loosely bound proteins to leave rigid layers that are tightly bound to the surface.

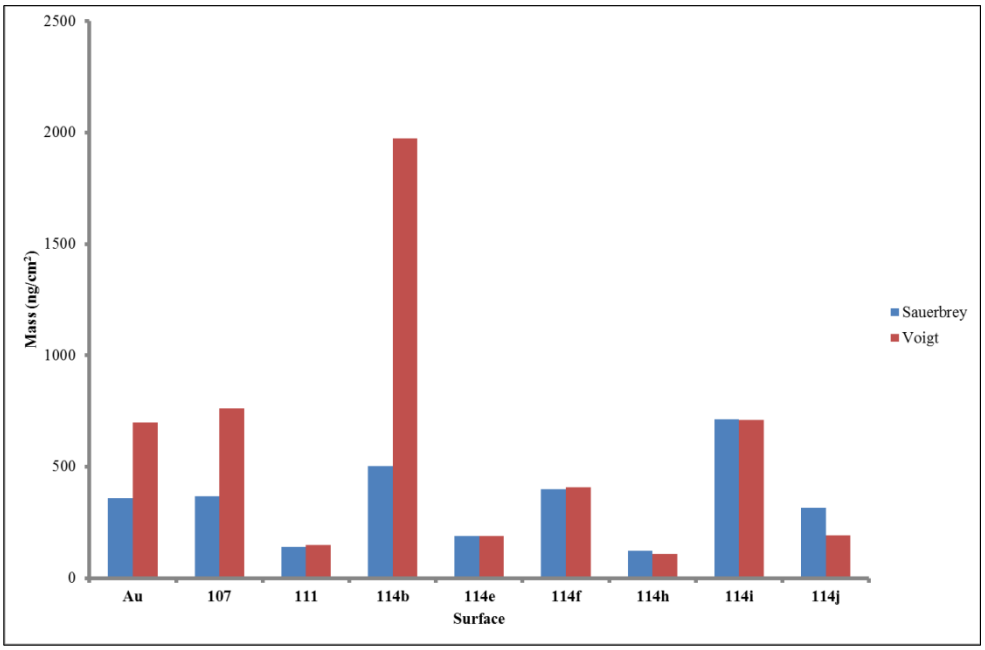

Figure 3.10: Sauerbrey and Voigt masses after the PBS rinse.

As mentioned above, the change in the $\Delta D/\Delta f$ value can give an indication as to the change in rigidity of the adsorbed layer as well as the change in water content, where an increase in

ΔD/Δf is indicative of a more viscoelastic layer with a greater a water content. Figure 3.11 displays these values after 20 minutes exposure to BSA, at the total mass (before the PBS rinse) and after the PBS rinse.

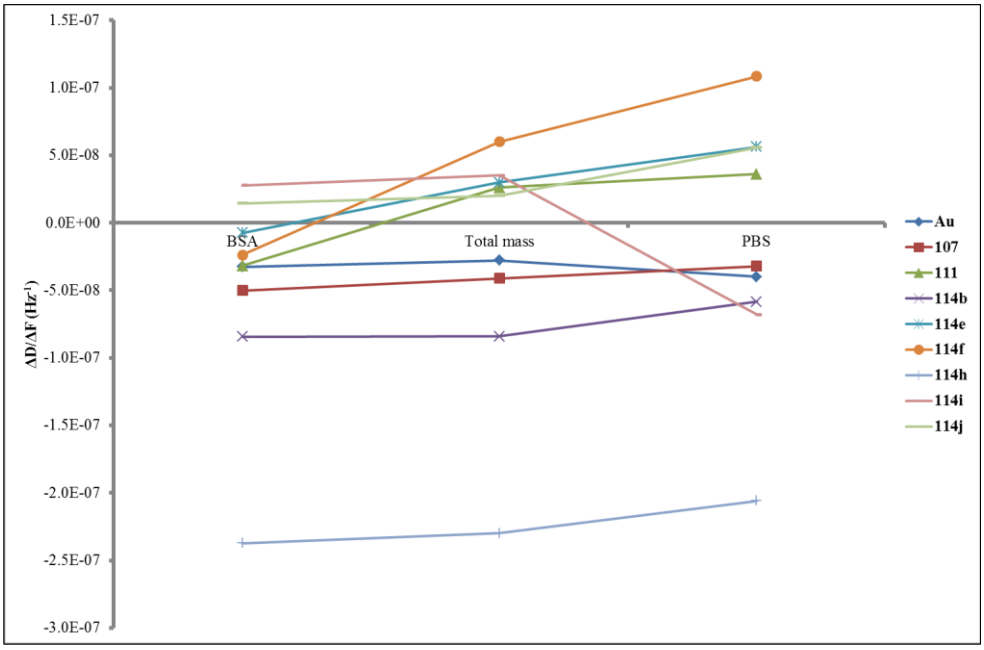

Figure 3.11: Plot of *ΔD/Δf* after 20 minutes exposure to BSA (BSA), the end of the BSA exposure (total mass) and after a PBS rinse for 29 minutes (PBS).

It is immediately obvious that the phosphonate-terminated surface **114h** generally exhibits lower *ΔD/Δf* values at all three times, indicating that the surface has a much lower water content and that the adsorbed layer is the most rigid of all the surfaces. Between the BSA and total mass points, the linker, phenyl and glycol terminated surfaces **111**, **114e**, **114f** exhibit the largest increases in *ΔD/Δf,* with the glycol surface showing the largest increase. The other surfaces exhibit very little change in *ΔD/Δf* up to the total mass. During the PBS rinse, all of the surfaces except **Au** and **114i** exhibit an increase in *ΔD/Δf* with the glycol surface **114f** having the largest increase; this is presumably a result of water uptake during the rinse step. The decrease in *ΔD/Δf* by the untreated gold surface is small, however, amine surface **114i** experiences the largest decrease in *ΔD/Δf* of all the observed changes. This is

thought to be a consequence of reorganisation of the protein on the surface resulting in a more rigid layer.

3.3.3 QCM-D conclusions

Determining the effect of the surface chemistry on protein adsorption has proved difficult using the QCM-D technique as it does not differentiate between protein and water adsorption. Hook *et al*. carried out a study into the adsorption of various proteins onto titanium oxide using QCM-D, ellipsometry and optical waveguide light spectroscopy (OWLS).[108] Consistently across all six proteins investigated, QCM-D exhibited larger masses than the other two techniques; ellipsometry and OWLS both use the change in refractive index of different layers to determine the mass of protein adsorbed and so the mass measured can be described as the 'dry mass', since water is excluded. QCM-D, however, only measures the change in frequency due to mass and structure, therefore the difference in mass between QCM-D and the 'dry mass techniques' is due to water bound by the surface or the proteins. In an earlier publication, Hook presented an investigation into adsorption of the mussel adhesive protein Mefp-1 onto methyl-terminated SAMs using QCM-D and ellipsometry. Hook reported that the Sauerbrey mass was composed of 91% water whilst the Voigt mass was composed of 94% water.[109] In an effort to estimate the amount of water contained in each of the adsorption layers after exposure to BSA/PBS silicon-gold-polystyrene based surfaces **106**, **113b**, **e**, **f, h-i** were soaked in BSA/PBS and then ellipsometry was used to determine the amount of BSA on each of the surfaces. The thicknesses of the surface-BSA layers were smaller than the polystyrene and surface chemistry layers measured in Table 3.3, so modelling of the surface-BSA layers was unsuccessful. This could be attributed to discrepancies in the polystyrene and chemical modification layer thicknesses between samples. Consequently, whilst the surfaces do

perform differently, their performance in relation to protein adsorption only cannot be rationalised. The discussion below attempts to explain the performance of the chemistry in relation to water and protein adsorption.

When trying to understand the adsorption patterns after 20 minutes of BSA exposure, it is important to remember that the Sauerbrey mass accounts predominantly for species bonded directly to the crystal but may include multilayers as long as they are rigidly attached to the preliminary layer. The Voigt mass takes into account extended multilayers that are not rigidly attached, especially water. Although the untreated gold surface will bind protein by formation of S-Au bonds, its capability to hydrogen bond is minimal. Consequently, the Sauerbrey mass will be dominated by protein adsorption, but the Voigt mass will take into account multilayers of proteins that are not bound directly to the crystal as well as water contained within the protein layers. The $\Delta D/\Delta f$ values of Au do not exhibit much variation between the different points, however, the values are generally smaller than most of the other surfaces, this also lends itself to the protein dominating the adsorption layer. Unmodified polystyrene **107** can bind protein by hydrophobic van der Waals interactions. The surface again has comparatively small $\Delta D/\Delta f$ values indicating that protein adsorption dominates relative to the other surfaces. The masses calculated differ greatly between all of the functionalised surfaces indicating that the end groups are exposed and influencing adsorption. When the Sauerbrey mass after 20 minutes of BSA exposure is considered for the linker and phenyl-terminated materials **111** and **114e** (175 and 295 ng/cm^2), the masses are relatively small, indicating that water and protein adsorption at the surface is minimal. This implies that the linker molecule does not coordinate water or protein significantly. Addition of the azo linkage only giving **114e** leads to a minor increase in adsorption directly to the surface. As discussed in Chapter 1, PEG terminated surfaces are known to decrease protein adsorption via extensive hydration of the surface; glycol surface **114f** has a high

Sauerbrey mass, relative to the other surfaces, which may be a result of hydrogen bonding water to the surface rather than protein adsorption. The Voigt mass of **114f** after 20 minutes is only 192 ng/cm^2 more than the Sauerbrey mass, which is a very small difference compared with those for some of the other surfaces, suggesting that protein adsorption is minimal as a result of the hydration layer at the surface. Furthermore, the $\Delta D/\Delta f$ values increase significantly throughout, which correlates to an increase in water content within the adsorption layer. The hexyl-terminated surface **114b** exhibits high adsorption behaviour with both models, and the difference between this surface and the linker-terminated surface **111** is an azo-bonded 4-hexylaniline group which will not have a high affinity to water, so that the mass determined by the Saurbrey method is most likely as a result of BSA bonded by van der Waals forces. Protein adsorption may dominate with Voigt mass as well, however, it is likely that water will be trapped in the protein layer. There is little change in $\Delta D/\Delta f$ during BSA exposure, however, a small increase during the PBS rinse may signify more water being adsorbed into the protein layer. Carboxylic acids are known to have a high affinity to the basic binding sites in BSA,[110-114] and this, combined with the similarity between the Sauerbrey and Voigt masses of acid terminated **114j** after 20 minutes, 295 and 342 ng/cm^2, respectively, suggests that the proteins are forming strong bonds with the surface, generating a compact layer and that any water adsorption is within the proteins. The mass lost during the PBS rinse was calculated to be 17 and 206 ng/cm^2 by the Sauerbrey and Voigt models, respectively. The Saurebrey mass loss suggests that the proteins are bound very strongly to the modified polymer surface and the Voigt mass corroborates with this and suggests that the extended multilayers are also bound relatively strongly, especially when the surface is compared to the linker and hexyl-terminated surfaces **111** and **114b** which lose significantly more mass during the rinse. It has been mentioned already that phosphonate diester **114h** exhibits similar levels of adsorption by the Voigt and Saurbrey models with

low levels of adsorption, and it is noteworthy that phosphonate terminated materials have been found to be biocompatible as a result of their ability to absorb water.[30] This surface, **114h**, has the lowest values of $\Delta D/\Delta f$ suggesting that the adsorbed layer is more rigid than the other materials. The amine-terminated surface **114i** has the ability to bond water by hydrogen bonding and could also bind protein by deprotonation of the aniline resulting in electrostatic effects. The significant decrease in $\Delta D/\Delta f$ during the PBS rinse suggests that protein adsorption may dominate since the decrease is indicative of protein reorganisation.

3.4 Conclusions

Chemical modification of the surfaces proved successful, as confirmed by XPS which detected iodine, nitrogen and phosphorous on the relevant samples. Contact angle analysis was used to observe the effect of the surface chemistry on surface wettability since this property has proved to have a large impact on protein adsorption. In fact, the different terminal functional groups did not appear to influence the contact angles as would be expected, with the surface designed to be hydrophilic such as glycol **113f** actually having a more hydrophobic contact angle than unmodified polystyrene. However, it is notable that the range of contact angles was relatively small with large standard deviations. These two points promoted the question as to how the chemistry was aligned on the surface and whether the end functional groups, attached by diazonium coupling, were actually exposed. Also, the large standard deviations suggest that the polystyrene film or the surface modifications are not homogenous. Ellipsometry and XPS were used to determine the thickness of the surface modification layers, which was in the order of 10 nm. This is comparable to the thickness of modification performed by Leonard and Moloney featured in Scheme 1.9 (Chapter 1), where 6.3 nm was measured. It was assumed that a monolayer of the modification chemistry had a height of 0.75 nm, consequently the thickness measured

was thought to be equivalent to approximately 9 monolayers. The chemistry used by Leonard *et al.* was slightly different to that described in this chapter but the methods and molecular compositions are similar.[58] Ellipsometry of the unmodified polystyrene proved to be problematic due to inhomogeneity within the polystyrene layer; this suggests that the contact angle data was affected by the bulk polystyrene layer rather than the chemical layers.

The QCM-D investigations revealed that all of the surfaces affected water and protein adsorption differently. It was hypothesised that the end functional groups were not exposed to influence the water contact angles, but the QCM-D results contradict this; if the end groups were not exposed, the surfaces would be expected to exhibit similar adsorption traits. The two techniques exposed the surfaces to different environments, during contact angle analysis the surfaces were open to the atmosphere and exposed to only one drop of water, whilst the surfaces were in a closed cell for QCM-D under a constant flow of aqueous based solutions. It is possible that the effect of the aqueous system alters the conformation of the chemistry on the surface, exposing the end functionalities more effectively. To determine the effect of the surface chemistry on protein adsorption, an alternative technique is needed since water and protein adsorption cannot be distinguished by QCM-D; ellipsometry has been used in the literature but attempts to replicate this were hindered by inhomogeneity of the polystyrene film. Nonetheless, the work described in this Chapter confirmed that surface modification was occurring and that the surface chemistry did alter the adsorption properties of the surfaces in a biological environment.

Chapter 4: Preparation and Characterisation of XAD-4 Based Materials

Following the interesting results discussed in Chapter 3, an investigation of a library of materials with more diverse surface chemistry was made. This Chapter describes the preparation and extensive characterisation of materials based on XAD-4 polystyrene beads; characterisation was carried out in order to obtain evidence for surface modification, as well elucidation of the surface structure and properties, both of which would be expected to affect protein adsorption. Two groups of materials were prepared; the first group were prepared by diazo modification, creating a linker to which diazonium coupling was carried out **116a-m**, the second group were prepared by diazonium coupling directly to the polystyrene surface **117a-m**. The first group will be described as 'linker coupled' and the second group as 'directly coupled' (Figure 4.1).

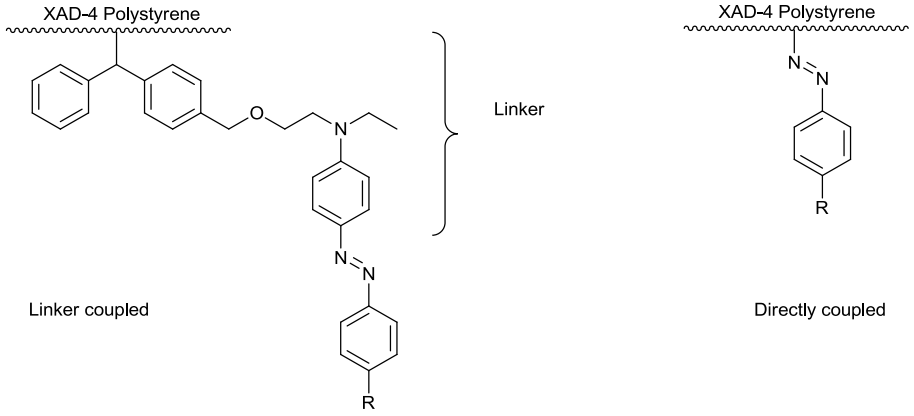

Figure 4.1

The use of the newly applied surface chemistry to bind penicillin V producing an antibacterial material was of interest also. The preparation and characterisation of these penicillin-loaded materials is also discussed.

4.1 Choice of base material and target surface functionalities

Amberlite™ XAD-4™ polystyrene beads were chosen as the base material as they are easily available, economical, safe to work with and solvent resistant due to crosslinking. XAD-4 polymer beads are one of a range of highly porous adsorbents developed by Rohm and Haas; having been designed to adsorb hydrophobic molecules and surfactants,[115] with a surface area of 725 m^2/g, a pore size of 40 Å and particle size of 0.3-1.2 mm.[116]

For the surface modification work, thirteen terminal functionalities were chosen (Scheme 4.1) in order to generate a wide range of functionally modified materials for detailed investigation. Alkyl terminated materials **116a** and **116b** were designed to generate hydrophobic surfaces. The iodine terminated material **116c** was prepared as a useful characterisation tool, since iodine was expected to be useful marker in XPS and combustion analysis, as had been earlier demonstrated with bis(4-iodophenyl) terminated surface **108** (Chapter 3). As discussed in Chapter 1, hydrophilic materials are known to minimise protein adhesion, as extensive investigation of glycol-terminated surfaces has shown, and for this reason glycol and hydroxyl-terminated materials **116f** and **116g** were prepared. Amine-terminated surfaces have previously proved to produce more hydrophilic surfaces and primary amine **116i** could be easily converted to the dimethylamine **116d**.[78] Carboxylic acid groups are known to have a high affinity for the protein bovine serum albumin;[113, 114] since adsorption of this protein would be a key focus in this work, the known affinity of this functional group on surface **116j** would provide a useful reference in the modified materials. Phosphonate and calcium phosphonate surfaces have previously been shown to enhance cell adhesion and growth; conversion of **116h** to the phosphonate monoester **116k**, phosphonic acid **116l** and the calcium phosphonate **116m** materials was straightforward thus widening

the library of functional materials. The materials were numbered in order of increasing % polar surface area as calculated in Chapter 5.1, page 124.

4.2 Preparation of biopassive materials

Amberlite^{TM} XAD-4^{TM} polystyrene beads are supplied wet with aqueous sodium chloride and sodium carbonate salts to prevent bacterial growth.[116] Prior to use, these beads were washed extensively with water and acetone, then dried on a sinter funnel under vacuum, although in this state, the beads were brittle and required careful handling.

4.2.1 Preparation of linker coupled materials.

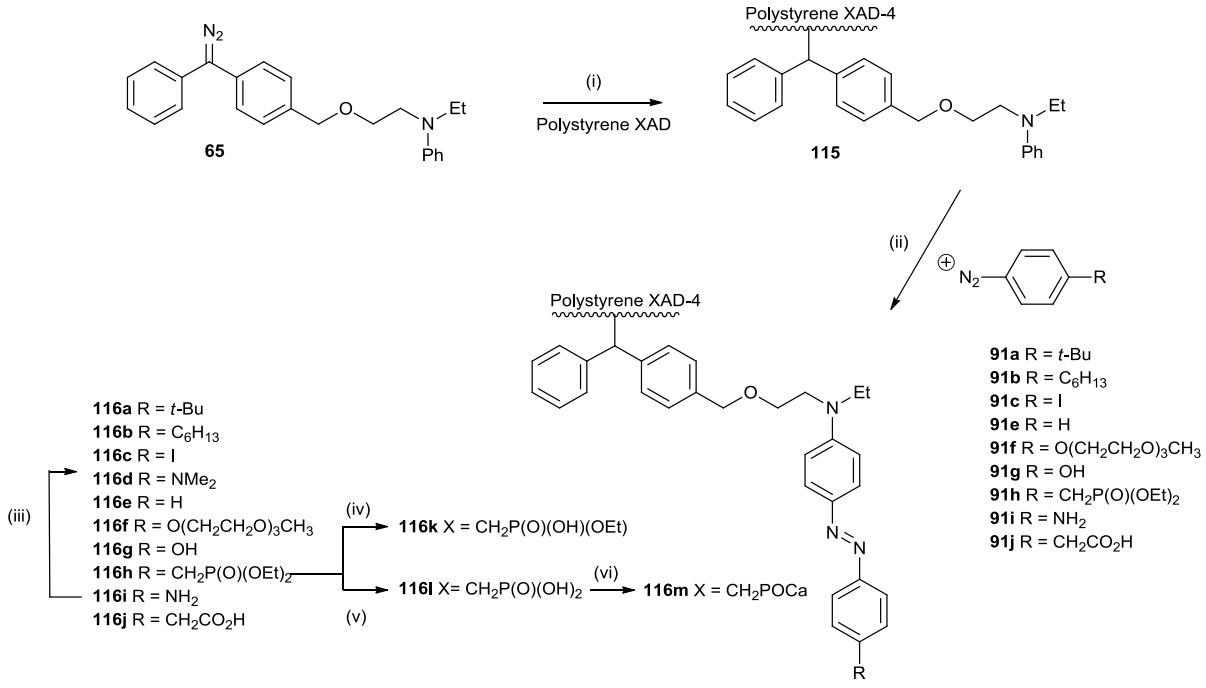

Scheme 4.1: Preparation of materials. Conditions: i) 120 ˚C; ii) diazonium salt solution in EtOH, 18 hrs, 5 ˚C; iii) MeI, EtOH, 18 hrs; iv) 5% aq. NaOH, 18 hrs; v) 1M aq. HCl, 18 hrs ; vi) 10% aq. CaOH.

Scheme 4.1 outlines the modification process used to manipulate the surface chemistry of the beads. The beads were first immersed in a dark pink solution of the diazo **65** (5% w/v) in

diethyl ether such that the beads were completely covered and the solvent was then removed *in vacuo*, giving intensely coloured pink beads on which the diazo compound **62** was physisorbed; the rotary motion ensured that all of the beads were coated. These beads were heated to 120 ˚C, giving an off white/pale yellow colour, consistent with conversion of the diazo function to the carbene by loss of nitrogen. Washing with acetone and then drying on a sinter over vacuum resulted in linker-terminated polymer **115**; the aniline group on the polystyrene surface acts as a linker molecule to facilitate diazonium coupling. Material **115** was soaked in ethanol-diazonium salt solutions **91a-c**, **e-i** at 5 ˚C; this was done to stop the diazonium salts decomposing before they had reacted with the surface of **115**. In each case, the salt solution had deepened or changed colour and the beads had done so also, images of the resulting materials that can be found in Figure 4.2.

The phosphonate diester terminated surface **116h** could be manipulated further by hydrolysis in acidic and basic conditions[80,117] resulting in phosphonic acid **116k** and phosphonate monoester **116l**. Material **116h** was washed with 10% aqueous calcium hydroxide affording **116m** and a dimethyl terminated surface **116i** was made by stirring **116d** in methyl iodide. For these modifications, agitation was avoided since the beads were brittle and broke up very easily and when required, only gentle stirring was used.

4.2.2 Preparation of directly coupled materials

Directly coupled materials **117a-c, e-i**, in which the diazonium salts **91a-c, e-i** were reacted with the polystyrene, without the use of a linker, were prepared also (Scheme 4.2). The washed beads were soaked in the diazonium salt solutions whilst standing at 5 ˚C in a direct replication of the conditions used to prepare materials the linker-coupled materials discussed above. Further manipulation of the surface chemistry was attempted in steps ii-vi (Scheme

4.2) using the same conditions as those for used for preparation of materials **116d** and **116k-m** as discussed in section 4.2.1.

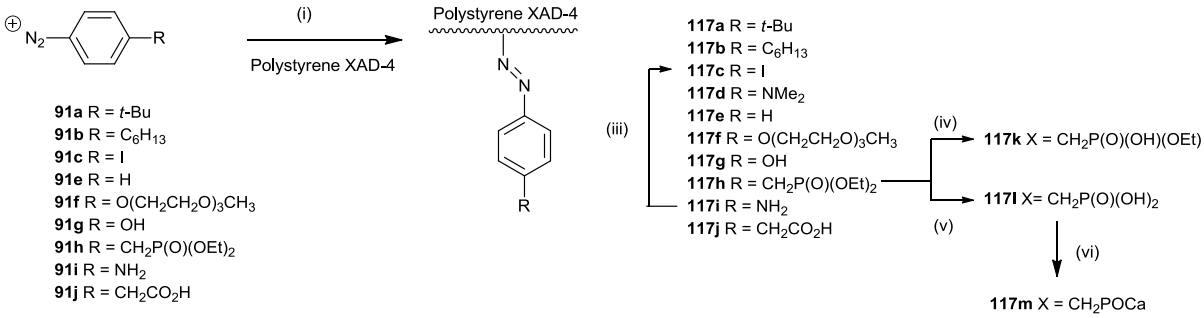

Scheme 4.2: Preparation of materials. Conditions: Conditions: i) 120 ˚C; ii) diazonium salt solution in EtOH, 18 hrs, 5 ˚C; iii) MeI, EtOH, 18 hrs; iv) 5% aq. NaOH, 18 hrs; v) 1M aq. HCl, 18 hrs ; vi) 10% aq. CaOH.

The directly coupled materials **117a-m** were prepared to determine if the aniline linker mediated and improved the diazonium coupling step, as well as determining if the diazonium salt would couple directly with the polystyrene. The presence of the azo linkage was expected to lead to highly coloured materials if coupling to the polymer occurred. Furthermore, since XAD-4 is a highly absorbent material, it is possible that instead of reacting with the materials, the salts would merely be physisorbed onto the beads. If this occurred, then the diazonium salt might be expected to decompose and the colour due to the N=N chromophore would not be observed.

4.3 Visual indication of diazonium coupling

Figure 4.2 below show images of all of the materials produced using the modification techniques discussed above. Unmodified polystyrene is white and there is no distinctive colour change after modification with the diazo **65** to generate **115**. Linker coupled materials **116a-m** are strongly coloured in shades of dark red, purple, brown, orange and yellow; in contrast the directly coupled materials **117a-m** are generally much paler in colour.

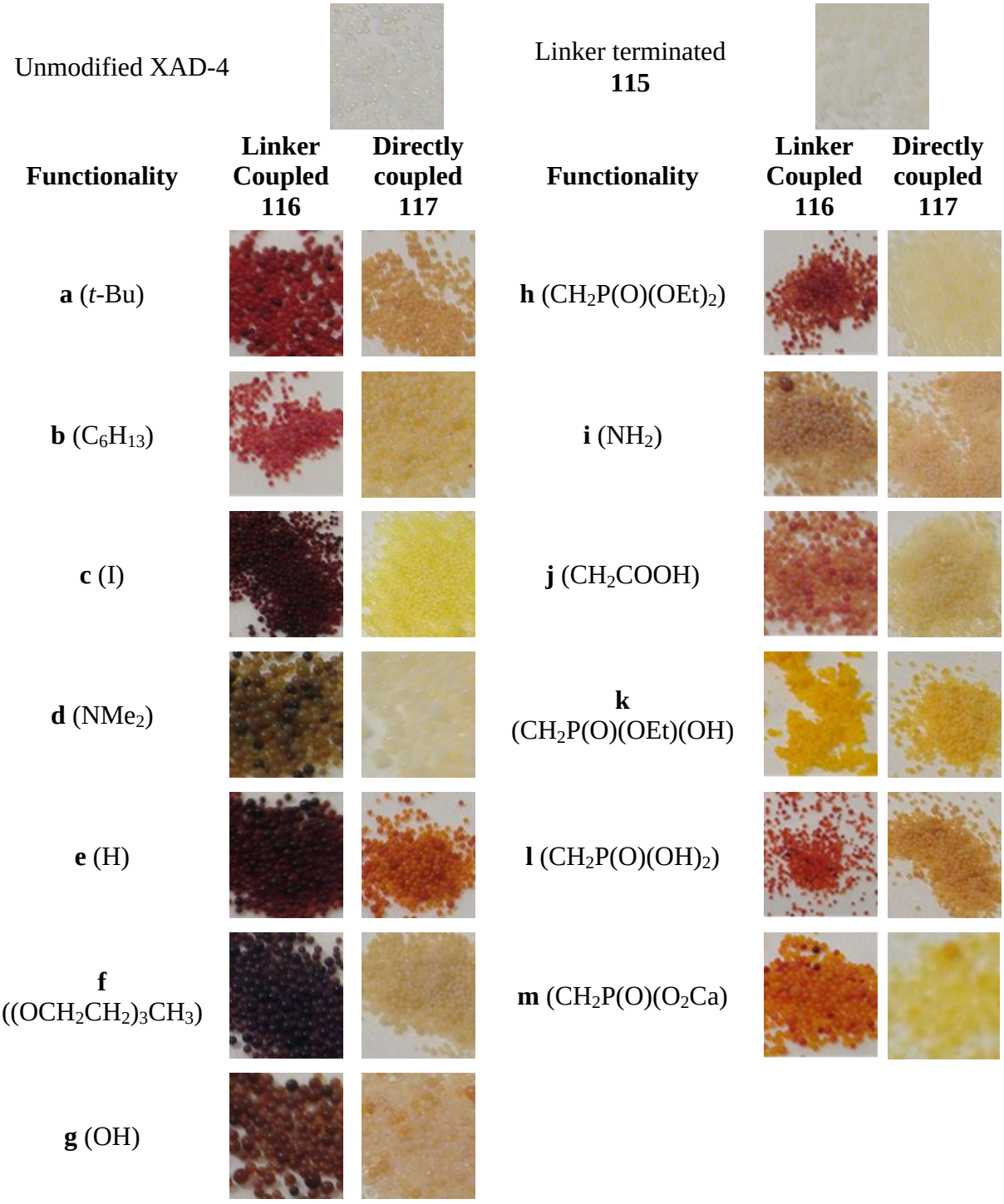

Figure 4.2: Library of functionalised materials.

Coloured species are observed when the wavelength of light they absorb falls in the visible region of the electromagnetic spectrum. Azo bonds are known to be highly coloured chromophores and as such are commonly used in dyes.[92] As previously mentioned, the linker molecule was expected to react with the diazonium salts in the standard coupling

mechanism, resulting in the azo linkage that would generate highly coloured materials; the aromatic ring was made nucleophilic by the presence of the electron donating nitrogen. By contrast, the aromatic rings on unmodified polystyrene are not particularly nucleophilic and have no electron donating groups to promote diazonium coupling to the salts. The relative colours of the materials corroborate with these hypotheses, with the linker-coupled materials being much stronger coloured than their directly coupled material counterparts.

4.4 Characterisation of biopassive materials

The characterisation of the modified materials was done in collaboration with Professor Cleo Choong and Meghali Bora from NTU in Singapore; the XPS, contact angle, SEM, DCS and TGA experiments were carried out by Choong and Bora.

4.4.1 XPS

To determine the change in surface elemental composition of the materials after modification, X-ray photoelectron spectroscopy (XPS) was employed. The technique relies on the characteristic binding energies of electrons of different atoms and their electronic environments to identify specific elements. XPS is typically sensitive to a depth of 10 nm; previous work has shown that diazo modification results in a layer of 6.3 nm thick where 4,4'-(diazomethylene)bis(methoxybenzene) was used to modify silicon (Scheme 1.9), which is in the same range of XPS penetration.[58]

XPS was carried out on the linker coupled materials only. Carbon, oxygen and nitrogen were observed on all materials with typical binding energies of 282 (C1s), 531 (O2s) and 398 (N1s) eV. Calcium was observed at 439 eV on the calcium phosphonate terminated material **116m**, however, the additional elements of phosphorous and iodine were not observed on materials **116c, h, k** and **l** (iodide, phosphonate diester, phosphonate monoester

and calcium phosphonate terminated). Finally, sodium (Na1s) was detected on unmodified polystyrene at 1069 eV, which may be due to residual sodium chloride and sodium carbonate left from the aqueous medium that the beads were transported in.

Reaction of amine terminated **116i** with methyl iodide could have produced a number of possible products or a mixture of these products, and monomethylamine, dimethyl amine or the quaternary ammonium salt terminated polystyrene are all possible. Ochoa *et al*. found that corrosion inhibition layers on carbon steel containing a nitrogen-based quaternary ammonium salt have a N1s peak at 402 eV whereas layers containing the amine revealed the N1s peak at 400 eV.[118] The dimethyl amine and amine-terminated materials **116d** and **116i** do not exhibit vast differences in their N binding energies, 397 and 398 eV, respectively, but other methods of surface analysis along with how they interacted with the proteins (Chapter 5) show the materials to be different so for the purpose of this work **116d** has been defined as dimethyl amine terminated.

Table 4.1 displays the N1s/C1s ratios calculated using the % atomic concentrations determined by XPS and those expected; the expected values are based on the coatings only and do not include the polystyrene. Prior to any modification, nitrogen is detected in a small amount on the polystyrene which is assumed to be due to contamination. The ratio observed for linker-terminated material **115** is 0.056, and when compared with the expected value of 0.04, the discrepancy is not that large. All of the ratios of the diazonium-coupled materials are smaller than the expected, some significantly; **116b, d, g, i** and **k** (hexyl, dimethyl amine, hydroxyl, amine and phosphonate terminated) are all under half of the expected value. The calculated ratios are based upon 1:1 coupling of the diazonium salts to the linker on the polystyrene surface, the small ratios may be evidence of the coupling step not being

very efficient, which may be expected due since the porous nature of the materials and the steric restrictions of the surfaces may restrict the diazonium coupling step.

Table 4.1: Comparison of N1s/C1s ratios found with those expected.

Material	R	N/C ratio expected	N1s/C1s ratio found[a]
XAD-4	-	0	0.010
115	-	0.04	0.056
116a	*t*-Butyl	0.086	0.048
116b	C_6H_{13}	0.081	0.020
116c	I	0.097	0.041
116d	NMe_2	0.117	0.042
116e	H	0.097	0.074
116f	$O(CH_2CH_2O)_3CH_3$	0.079	0.044
116g	OH	0.097	0.031
116h	$CH_2P(O)(OEt)_2$	0.083	0.038
116i	NH_2	0.129	0.026
116j	CH_2COOH	0.091	0.041
116k	$CH_2P(O)(OH)(OEt)$	0.088	0.033
116l	$CH_2P(O)(OH)_2$	0.094	0.050
116m	$CH_2P(O)O_2Ca$	0.094	0.039

[a]Ratios calculated using the % atomic concentrations of the surfaces and are an average of two experiments.

4.4.2 Attenuated total internal reflectance infra-red analysis (ATR-IR)

ATR-IR spectroscopy allows for direct IR analysis on solids without the need for dispersion in an inert medium. The sample is loaded onto a diamond crystal, through which the IR beam is emitted, and a sample depth ranging from 0.5 and 5 μm is analysed.[119] ATR IR spectroscopy relies on close contact between the sample and the crystal, and this is often achieved by clamping the substrate onto the diamond platform. For the modified polymers, this inevitably crushed the beads and in so doing exposed more of the unmodified areas. In addition, contact of these powders is confined to small areas; consequently weak spectra were obtained for some of the materials.[120] In an attempt to observe absorption bands that were weakly or not at all observed in the raw spectra, the base material spectrum was subtracted; unmodified polystyrene was subtracted from linker-terminated material **115** and

the directly coupled materials **116a-m**, whilst the spectra of linker-terminated material **115** was subtracted from the linker-coupled materials **117a-m**.

The significant stretches of the materials are displayed below in Tables 4.2 and 4.3 (a complete record of the data is in Chapter 6, Tables 6.10-6.12). Notably, absorbances were not observed for the azo bond resulting from diazonium coupling in any of the materials; the pseudo symmetrical nature of the diphenyl azo linkage makes this group relatively inactive to IR. In all spectra, a set of two broad peaks in the region of 2160-1980 cm^{-1} were observed and these are due to the diamond on which the materials were supported. Literature records XAD-4 with significant peaks at 2931, 1657, 1604, 1446, 1220, 990, 902 cm^{-1};[54] these were observed on the modified materials as well as other peaks as shown in Tables 4.2 and 4.3.

4.4.2.1 Linker coupled materials

Linker-terminated material **115** shows the significant groups resulting from the first step of modification. As expected, alkyl C-H stretches were observed as one broad peak at 2960-2931 and a strong single peak at 2859, but of course the polystyrene base material also contributes in this region. The ether group in the linker was signified by the aryl-O and alkyl-O stretches at 1252 and 1084 cm^{-1}, whilst there are two stretches due to C-N vibration, the aromatic stretch at 1535 and the aliphatic stretch at 1169 cm^{-1}. Finally, a stretch at 1601 cm^{-1} due to the vibration of the aromatic C=C bonds was observed also, although this is observed in the blank material at 1603 cm^{-1} as well. After diazonium coupling, the peaks resulting from the linker were still generally observed. Notable diagnostic peaks are a hydroxyl stretch at 3400 in hydroxyl terminated **116g**, N-H stretches at 3404 and 3280 cm^{-1} on the amine terminated material **116i** and a peak at 1723 cm^{-1} as a result of the carbonyl bond on the acid functionalised material **116j**. The phosphonate diester material **116h** displayed peaks at 1217 and 1017 for the P=O and P-OEt groups respectively, whilst the

phosphonate monoester **116k** presented peaks at 1298 and 1040 cm^{-1} for the P=O and P-OH groups. The phosphonic acid functionalised material gave the P=O stretch at 1298 as well as a P-OH stretch at 1040 with a peak at 2601 due to the OH groups,ao P-OEt band at 1017 cm^{-1} was not observed indicating complete hydrolysis. The final material in this group **116m** is terminated with a phosphonic calcium salt; ATR IR spectroscopic analysis of this material indicated the stretches due to the linker as discussed above, but the only other absorbance observed was of $P(O)\text{-}O^-$ group at 2617 cm^{-1}.

Table 4.2: Significant stretches observed by ATR IR spectroscopy.

Material	R	ATR IR (cm^{-1})
XAD-4	-	2931, 1657, 1604, 1446, 1220, 990, 902
115	-	1601, 1511, 1252, 1169, 1090
116a	*t*-Butyl	1603, 1513, 1354, 1252, 1178, 1085
116b	C_6H_{13}	1326, 1602, 1080
116c	I	1601, 1377, 1286, 1075, 547
116d	NMe_2	1601, 1511, 1351, 1170, 1086
116e	H	1602, 1511, 1316, 1195, 1092
116f	$O(CH_2CH_2O)_3CH_3$	1603, 1511, 1362, 1252, 1085
116g	OH	3400, 1603, 1512, 1252, 1169, 1086
116h	$CH_2P(O)(OEt)_2$	1602, 1276, 1217, 1191, 1062
116i	NH_2	3404, 3280, 1602, 1328, 1217, 1062
116j	CH_2COOH	3020, 1793, 1723, 1602, 1329, 1085
116k	$CH_2P(O)(OH)(OEt)$	2606, 1602, 1298, 1081, 1071
116l	$CH_2P(O)(OH)_2$	2601, 1602, 1352, 1276, 1251, 1170, 1083, 1018
116m	$CH_2P(O)O_2Ca$	2625, 1601, 1511, 1252, 1170, 1084

Glycol and iodide materials **116f** and **116c** have additional distinctive absorbances at 1240 and 541 cm^{-1}, respectively, the former being due to an aromatic C-O bond and the latter, a C-I bond; in both materials the aromatic C-H stretches were concealed by strong broad peaks at 3247 and 3215 cm^{-1}, respectively, and this is due to excess moisture in the samples or in the atmosphere. The *t*-butyl, hexyl, dimethyl amine and hydrogen modified materials **116a**, **b**, **d** and **e** do not have any other distinctive absorbances other than those for the linker

molecule described above; for the first three, this is to be expected since the R groups add no additional bonds.

4.4.2.2 Directly coupled materials

Table 4.3 below displays the diagnostic IR absorbances. In each material, C-H stretches are observed in the region of 3000-2700 cm^{-1}. Materials **117f, h-m** (glycol, the phosphonate material and its derivatives, acid and amine terminated) display broad absorbances of prominent intensity in the region of 3200 cm^{-1} which is attributed to excess water on the samples. The terminal groups all have the ability to bind water so removing excess water from the samples would be expected to be more difficult with these materials. This broad absorbance unfortunately would obscure any spectral detail from introduced N-H and O-H groups.

Table 4.3: Significant absorbance bands observed on directly coupled materials.

Material	R	ATR-IR (cm^{-1})
117a	*t*-Butyl	2967-2940, 1603
117b	C_6H_{13}	2929, 2856
117c	I	2930, 2859
117d	NMe_2	2973-2910, 1604
117e	H	2963, 2691, 1602
117f	$O(CH_2CH_2O)_3CH_3$	2957, 2858
117g	OH	3020, 2974-2883, 1603
117h	$CH_2P(O)(OEt)_2$	2932, 2903, 2857
117i	NH_2	2930, 2858
117j	CH_2COOH	2929, 2858
117k	$CH_2P(O)(OH)(OEt)$	2923, 2853, 1277
117l	$CH_2P(O)(OH)_2$	2926, 2855, 1276
117m	$CH_2P(O)O_2Ca$	2930, 2165

In materials **117a**, **d**, **e**, and **g**, with *t*-butyl, dimethylamine, phenyl and hydroxyl functionalised surfaces, the aromatic C=C stretch is observed in the region of 1603 cm^{-1},

although this is seen in blank polystyrene also so does signify additional functionality. P=O stretches at 1277 cm^{-1} and 1276 cm^{-1} in phosphonate monoester terminated **117k** and phosphonic acid terminated **117l** are observed, but these are the only two materials that display any significant absorbances resulting from chemical modification.

4.4.3 Combustion Analysis

Addition of nitrogen during both of the modification steps meant that the percentage of nitrogen in each material could be used to calculate the surface loading of the chemical modification. From the % N value, nitrogen loading in mmol/g was calculated, and from this the loading of surface modification chemistry in mmol/g was deduced; in the case of the linker modified materials 1:1 diazonium coupling of the salts to the linker molecules was assumed with 100% efficiency. With the knowledge of the bead surface area at 725 m^2/g (manufacturer's data), the number of molecules per cm^2 could be calculated. To estimate the % surface coverage, a limiting factor (Ao) was used, this being an estimate of the area that each molecule of surface modification occupies along the polystyrene surface. A film made up of *para* benzene derivatives has been found to have a limiting factor of 0.24 nm^2/molecule and films based on anthracene derivatives have limiting factors of 0.45-0.48 nm^2/molecule.[121] The limiting factor of the directly coupled materials was assumed to be 0.24 nm^2/molecule whilst the limiting factor of the linker coupled materials was 1.17 nm^2/molecule, as determined by the average cross sectional area of the linker and linker coupled molecules, calculated using Chemicalize (Table 5.1, Chapter 5, page 125).[122] It was possible to calculate the diazonium coupling efficiency of the materials that were modified with the diazo linker first. Finally, the value N representing the ratio of unmodified to modified sites was calculated; for the purpose of the calculation, a site is assumed to be equivalent to a styrene monomer and only one reaction per monomer can occur due to space

restrictions. Below is a discussion of the combustion analysis of the linker coupled and directly coupled materials. The raw data can be found in Chapter 6, Table 6.13-6.14 and Appendix II contains example calculations.

The surface loading of the chemistry, based on the percentage of nitrogen, was found to range from 0.038 mmol/g (**116d**) to 0.357 mmol/g (**116c**) which results in a surface coverage range of 5-51%, and Table 4.4 displays the full range of data. The diazonium coupling efficiency was calculated for materials **116a-m** using the number of mmol/g of nitrogen on linker-terminated polymer **115**, 0.179 mmol/g, producing a wide range of values, 21-200%.

Table 4.4: Combustion analysis of linker coupled materials.

Material	R	mmol surface modification / g polymer (%N)	Molecules / cm^{2} [a]	Surface coverage (%)[b]	Coupling efficiency (%)[c]	N[d]
115	-	0.179 (0.25)	1.48×10^{13}	25	n/a	50
116a	*t*-Butyl	0.062 (0.26)	5.14×10^{12}	9	35	149
116b	C_6H_{13}	0.067 (0.28)	5.54×10^{12}	9	37	138
116c	I	0.357 (1.50)	2.97×10^{13}	51	200	20
116d	NMe_2	0.038 (0.21)	3.11×10^{12}	5	21	251
116e	H	0.167 (0.70)	1.38×10^{13}	24	93	52
116f	$O(CH_2CH_2O)_3CH_3$	0.124 (0.52)	1.03×10^{13}	18	69	71
116g	OH	0.057 (0.24)	4.75×10^{12}	8	32	163
116h	$CH_2P(O)(OEt)_2$	0.121 (0.34)	1.01×10^{13}	17	68	72
116i	NH_2	0.046 (0.26)	3.86×10^{12}	7	26	202
116j	CH_2COOH	0.052 (0.22)	4.35×10^{12}	7	29	178
116k	$CH_2P(O)(OH)(OEt)$	0.150 (0.63)	1.25×10^{13}	21	84	58
116l	$CH_2P(O)(OH)_2$	0.145 (0.61)	1.21×10^{13}	21	81	60
116m	$CH_2P(O)O_2Ca$	0.076 (0.32)	6.33×10^{12}	11	43	120

[a]Calculated on the basis of $725 m^2/g$ surface area for XAD-4; [b]limiting area of 1.71 nm^2/molecule is assumed as calculated using Chemicalize (www.chemicalize.com); [c]diazonium coupling efficiency = expected N/actual N in mmol/g where expected N = 0.179 mmol × number of N in the molecule; [d]N is the ratio of unmodified sites to modified sites calculated using the combustion analysis.

Iodo and phenyl-terminated materials **114c** and **114e** exhibited the highest efficiencies, 200% and 93%, respectively; the 200% efficiency suggests that that multiple reactions with the surface linker may be occurring. The terminal groups on both materials are the smallest of all the terminal functionalities, so the space occupied by these groups will be much less. This allows for greater amounts of the diazonium salt to pack into the pores of the material and around the visible surface which lends itself to increased efficiency.

Combustion analysis also detected phosphorous on phosphonate and phosphonic acid materials **116h, l, m** and iodine on iodide-terminated **116c** (Table 4.5). The coupling efficiencies were calculated using the expected ratio of N:P and N:I being 1:3, with the iodo-terminated material **116c** having a very large coupling efficiency of 1383%. The calcium phosphonate material **116m** exhibited a coupling efficiency of 38%, significantly smaller than phosphonic acid material **116l** from which it was made; this may be result of reaction conditions eroding the surface of the beads.

Table 4.5: Combustion analysis of selected materials.

Material	Functionality	Observed data	Expected % I or P[a]	Expected (Observed) mmol/g I or P	% Efficiency[b]
116c	I	%I: 1.66 %N: 0.35	0.12	0.009 (0.131)	1383
116k	$CH_2P(O)(OH)(OEt)$	%P: 0.11 %N: 0.63	0.21	0.068 (0.036)	52
116l	$CH_2P(O)(OH)_2$	%P: 0.17 %N: 0.61	0.20	0.066 (0.055)	83
116m	$CH_2P(O)O_2Ca$	%P: 0.06 %N 0.59	0.16	0.053 (0.019)	38

[a]Expected % of P or I = % N/3; [b]efficiency = actual/expected in mmol/g.

Two different methods of estimating the diazonium coupling efficiency have been presented. The method based on the percentage of nitrogen only (Table 4.4) is dependent

upon the loading of the linker being the same for all the materials, whereas the second method (Table 4.5) does not depend upon this, so it may give a more reliable value for the coupling efficiencies. However, the efficiency of coupling of the iodo material **116c**, calculated using the second method, is extremely large, which leads to questioning of the validity of the values, unless this is accounted for by physisorption of the diazonium salt occurring also.

Table 4.6: Combustion analysis of directly coupled materials.

Material	R	mmol surface modification / g polymer (%N)	Molecules / cm^{2} [a]	Surface coverage (%)[b]	N[c]
117a	*t*-Butyl	<0.036 (<0.1)	$<2.97 \times 10^{12}$	<0.7	64
117b	C_6H_{13}	<0.036 (<0.1)	$<2.9 \times 10^{12}$	<0.7	65
117c	I	0.318 (0.89)	$<2.6 \times 10^{13}$	6.2	4
117d	NMe_2	<0.024 (<0.1)	$<1.9 \times 10^{12}$	<0.5	42
117e	H	0.121 (0.34)	1.0×10^{13}	2.4	18
117f	$O(CH_2CH_2O)_3CH_3$	0.154 (0.43)	1.28×10^{13}	3.0	12
117g	OH	<0.036 (<0.1)	$<2.97 \times 10^{12}$	<0.7	65
117h	$CH_2P(O)(OEt)_2$	0.054 (0.15)	4.45×10^{12}	1.0	41
117i	NH_2	0.010 (0.04)	7.91×10^{11}	0.2	110
117j	CH_2COOH	0.011 (0.03)	8.90×10^{11}	0.2	222
117k	$CH_2P(O)(OH)(OEt)$	0.139 (0.39)	1.16×10^{13}	2.7	14
117l	$CH_2P(O)(OH)_2$	0.164 (0.46)	1.36×10^{13}	3.2	12
117m	$CH_2P(O)O_2Ca$	<0.036 (<0.1)	$<2.97 \times 10^{12}$	<0.7	64

[a]Calculated on the basis of $725 m^2/g$ surface area for XAD-4; [b]limiting area of 1.71 nm^2/molecule is assumed as calculated using Chemicalize (www.chemicalize.com); [c]N is the ratio of unmodified sites to modified sites calculated using combustion analysis.

Nitrogen was detected on all of the directly coupled materials but in significantly lower quantities than the linker-coupled analogues (Table 4.6). The loadings and surface coverage calculated for materials that have <0.1% N are the upper limit values, since the amount of nitrogen on the surface was below the measurable detection limit. The loading of the chemistry ranges from 0.024 (**117d**) to 0.318 (**117c**), thus giving a surface coverage range of 0.2 – 6.2%. Notably, iodo-terminated material **117c** demonstrates the highest loading and surface coverage by far, indication again of the small terminal group allowing for tighter

packing of the diazonium salt and its residues in the pores of the materials; the iodo-linker coupled material **116c** also had the highest loading of the linker coupled materials. Combustion analysis detected phosphorous on the phosphonate diester, monoester, phosphonic acid and calcium phosphate materials **117h**, **k**, **l** and **m** with % P of 0.04, 0.06, 0.09 and 0.10, respectively. Again, the percentage of phosphorous detected is much smaller than that for the corresponding linker-coupled materials.

Comparison of the loadings of the linker-coupled materials with those made previously in the group is very positive. Leonard used 4,4'-(diazomethylene)bis(methoxybenzene) (Scheme 1.14, Chapter 1) to modify the same polystyrene beads and diazonium coupling with two salts to obtain materials loaded with 1.5×10^{13} and 2.99×10^{12} molecules/cm^2 corresponding to surface coverage of 9 and 1.8%, respectively.[58] The number of molecules/cm^2 observed in this thesis are in the same region as those obtained by Leonard, although there is an improvement in surface coverage with some diazonium salts. Commercially available functionalised polystyrene resins have loadings ranging between 1.5-3 mmol/g for an amine modified resin **118** (Figure 4.3), 0.6 - 1.7 mmol/g for hydroxyl resin **119** and lower loadings of 0.6 - 1.2 mmol/g for resins modified with longer chain groups such as **120**.[116,123] The loading of linker terminated material **115** has a loading at the lower end of the range of the resins commercially available and these loadings decrease after diazonium coupling. However, the commercial loadings result from a bespoke method finally tuned for the specific groups applied to the surface and the method in this thesis offers a simple process that may be applied to a wide range of base materials. The benefit of this generality was considered to be more important for the purpose of this thesis than further optimising the loadings.

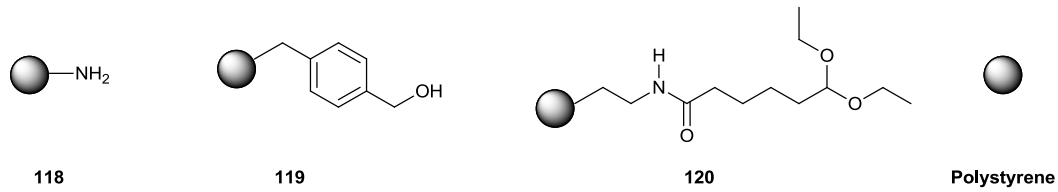

Figure 4.3: Examples of commercially available resins.

4.4.4 Contact Angle

Since the base material was spherical polystyrene beads, standard methods of contact angle measurement were not possible since usually a flat surface is required to support the droplet. A flotation method (Figure 4.4) was used in which a bead of each material was floated on a water droplet resting on a glass slide and the angle θ analysed using contact angle software and video imaging[124] with θ decreasing as hydrophilicity increases. The data presented below is an average of 5 measurements carried out on 5 different beads.

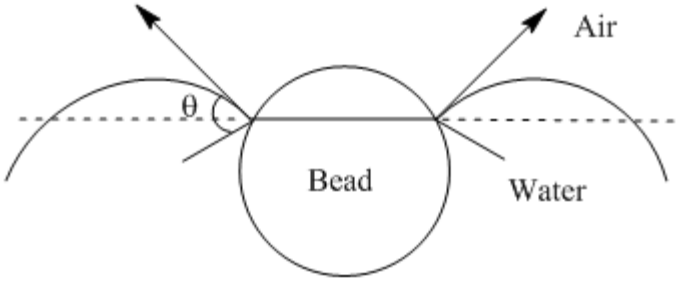

Figure 4.4: Flotation method of contact angle measurement.[124]

Prior to any chemical treatment, the contact angle of XAD-4 polystyrene was 53˚, after reaction with the diazo the contact angle was reduced to 37˚; linker-terminated material **115** is the most hydrophilic of all the materials which may be a consequence of residual sodium chloride or sodium carbonate left behind after transportation in an aqueous medium. The materials generated after diazonium coupled **116a-m** exhibited a range of surface wettability with contact angles of 43-73˚. Phenyl-terminated material **116e** demonstrates the effect of

diazonium coupling without a significant terminal group (R=H) and has a contact angle of 64˚. Materials that are more hydrophilic than phenyl-terminated **116e** include **116f-k**, these materials are terminated with glycol, hydroxyl, phosphonate diester, amine, acid and phosphonate monoester groups, all of which are capable of hydrogen bonding with water. Materials **116a-d** are the more hydrophobic with contact angles ranging from 55-60˚. Interestingly, the two most hydrophobic materials are **116l** and **116m** which are terminated with phosphonic acid groups and calcium phosphonate.

Table 4.7: Contact angle analysis of linker coupled materials.

Material	R	Contact angle (degrees)[a]	Standard deviation
XAD-4	-	53	9
115	-	37	7
116a	*t*-Butyl	59	7
116b	C_6H_{13}	55	7
116c	I	59	6
116d	NMe_2	60	10
116e	H	64	5
116f	$O(CH_2CH_2O)_3CH_3$	43	5
116g	OH	53	11
116h	$CH_2P(O)(OEt)_2$	49	5
116i	NH_2	51	6
116j	CH_2COOH	50	10
116k	$CH_2P(O)(OH)(OEt)$	50	3
116l	$CH_2P(O)(OH)_2$	73	8
116m	$CH_2P(O)O_2Ca$	73	7

[a]Values averaged from five measurements.

The standard deviations are significant and if an error of ± standard deviation is assumed, then the diazonium coupled materials all overlap with each other to some degree. A more pronounced effect with smaller standard deviation may have been seen on a material that is more homogenous; Amberlite XAD-4 beads are porous with an extensive rough surface structure which is not ideal for contact angle analysis as the pores will disrupt the alignment of the water to the bead. Furthermore, a different bead was used for each measurement, and

although all spherical, they were not identical in size and morphology, and this will have a significant effect on the standard deviations. Advancing and receding contact angles would give more accurate information for the inhomogeneous bead surface, however, it would not have eliminated the variations between individual beads and their sizes.[125] Nonetheless, noteworthy correlations were observed between protein adsorption and contact angle as will be discussed in Chapter 5.

4.4.5 Imaging of beads with SEM

Scanning electron microscopy (SEM) was necessary to observe the microscopic surface structure of the beads and how it was affected by the chemical modifications; the materials were all coated in gold before the imaging was conducted.

Images a and b in Figure 4.5 are of the polystyrene beads before modification, however, the beads had been washed with acetone and dried. Image a shows the beads to be spherical but with rough surface structure; clusters of pores are observed as well as some areas in which sections of the beads have flaked away; the beads are brittle when dry and abrasion during transportation seems likely to lead to surface erosion. A closer image of the bead, 4.5.b, shows that there are crystals on the surface which are thought to be sodium carbonate or sodium chloride, since sodium was also observed by XPS analysis. Since chloride ions were not detected by XPS, sodium carbonate is more likely. After modification with the diazo generating linker-modified material **115**, the spherical structure of the beads was maintained (Figure 4.5.c). However, the outer surface of the bead is covered irregularly with raised globular structures (Figure 4.5.d) which are large enough to give the beads an uneven morphology (Figure 4.5.c). The globular structures are likely to be a result of aggregation of diazo **65** in solution or during coating. Some of the structures appear to be raised from the surface, indicating that washing did not remove all of the material that did not react with the

bead surface. Since the globular structures are not observed on any of the diazonium coupled materials except glycol **116f**, it is assumed that they did not react with the polystyrene and were removed during the diazonium coupling reaction.

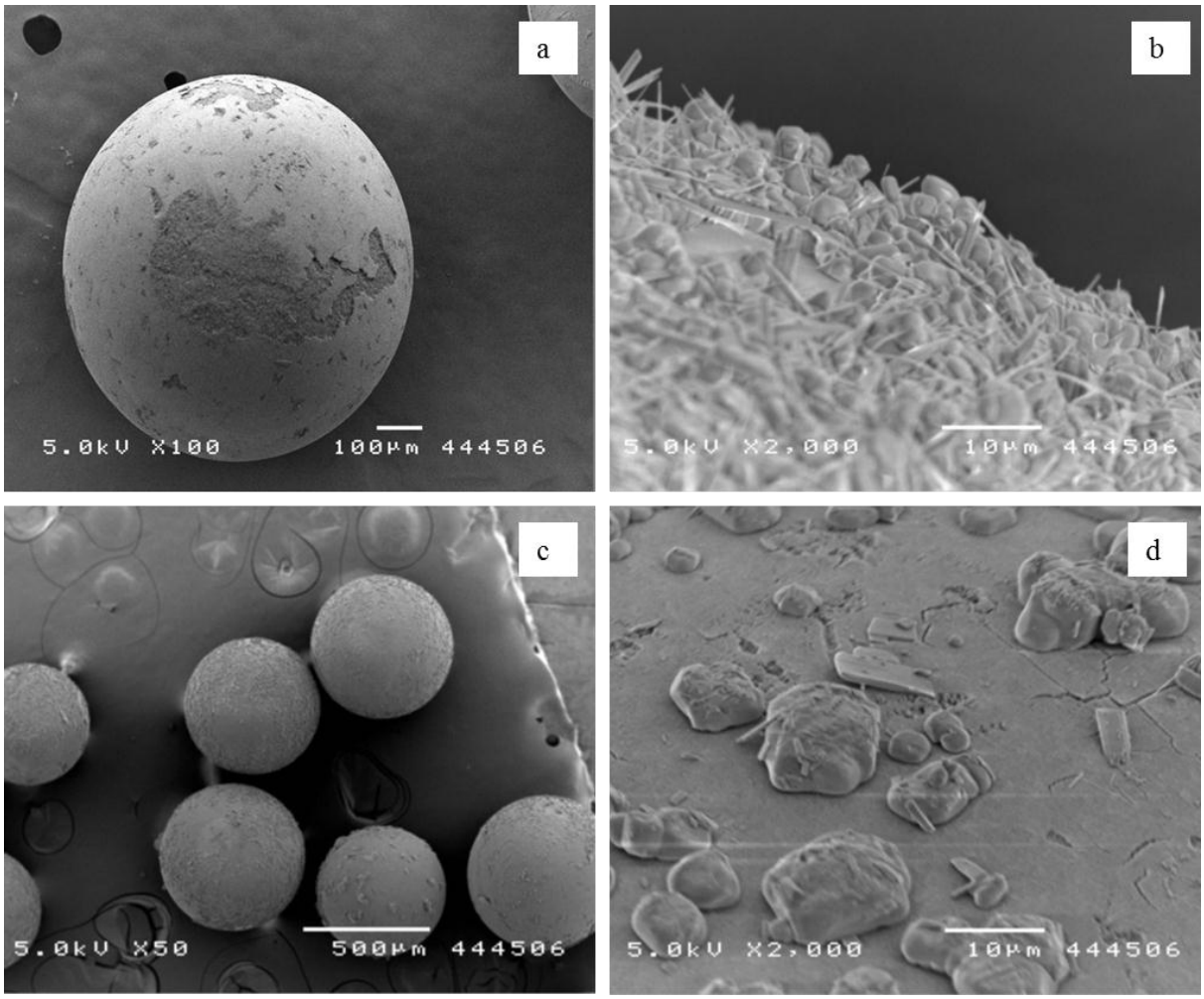

Figure 4.5: SEM images. a and b are images of unmodified XAD-4 whilst c and d are images of linker terminated **115**.

SEM images of a selection of linker-modified materials that have undergone diazonium coupling can be found in Figure 4.6. The fragile nature of the beads is illustrated in image 4.6.b where large sections of the beads have broken off and one of the beads shows a section flaking away; the cleanliness and shape of the damaged areas suggests a physical force such as abrasion as the cause rather than the chemistry. Image 4.6.a is of a bead that has not succumbed to the same fate. Images 4.6.c and 4.6.d exhibit the rough surface morphology that results from the porous structure of the beads and that there are localised clusters of pores, but these clusters are thought to be too large to have been created by chemical modification since they are in the order of 10 μm in length. The surface structure attributed to excess sodium chloride and sodium carbonate was not detected on any of the diazonium coupled materials suggesting that the diazonium coupling step helps to clean the sample, and soaking of the beads in EtOH or water for a prolonged time period may have been a more effective method of cleaning them after the first modification step.

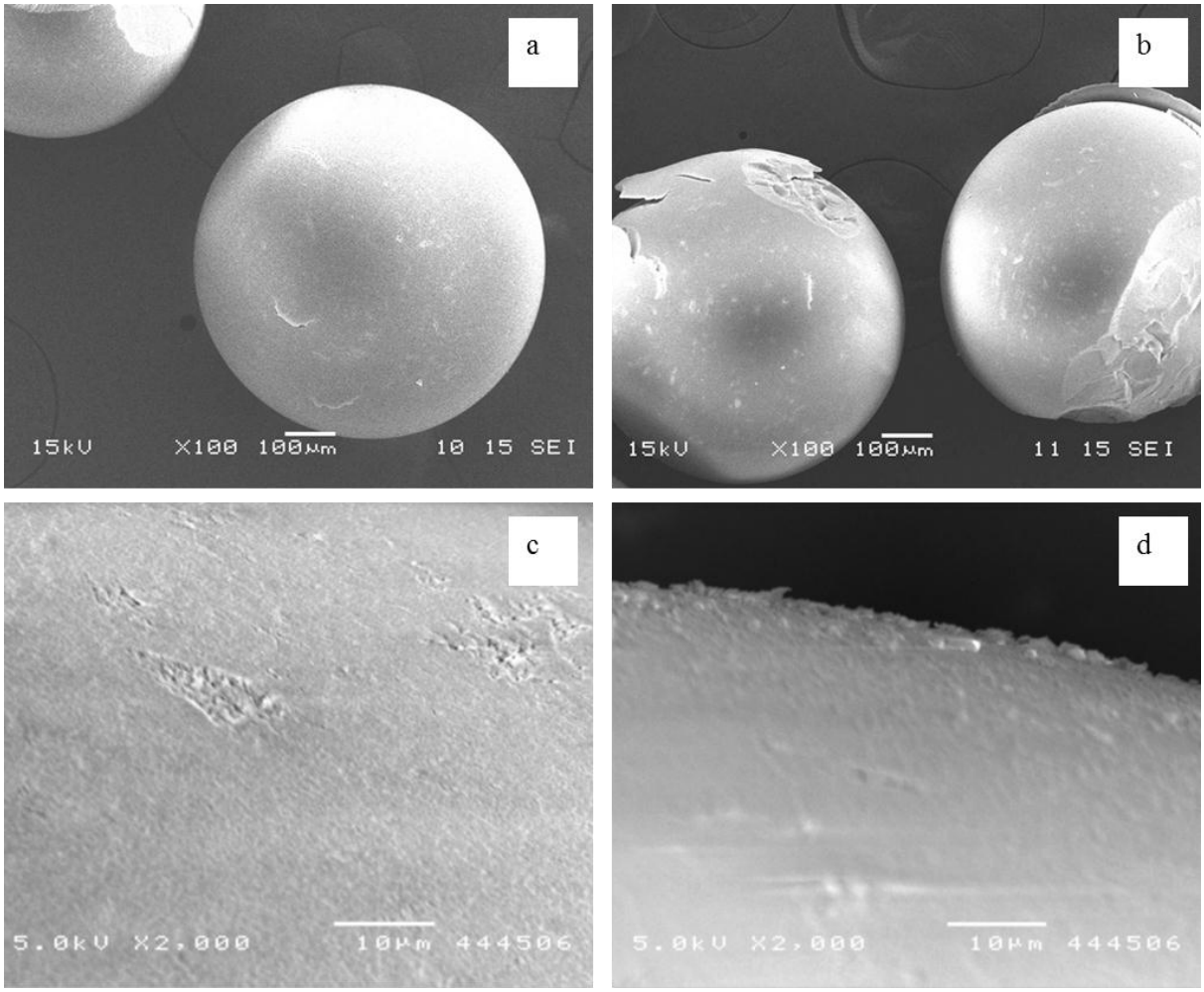

Figure 4.6: SEM images. a and b are images of hydroxyl terminated material **116g**, c is amine terminated material **116i** and d is diester phosphonate material **116h**.

Globular deposits were observed on the glycol modified material **116f** as seen in images 4.7.a and 4.7.b (Figure 4.7), and this is the only diazonium coupled material that showed this type of deposit. In solution, the glycol chains can interact with each other; either the chains will align via van der Waals interactions, or hydrogen bonding mediated by EtOH and water will cause the salt molecules to aggregate. If diazonium salt **116f** aggregated in solution and deposited on the surface, this sort of structure could be expected. Furthermore, if the salt synthesis did not go to completion, the unreacted amines could also aggregate and then deposit on the surface. These images are evidence of the need to wash the samples more

effectively and that an alternative way of coating is needed for the glycol diazonium salt such that aggregation of the salt does not occur.

Images c-f in Figure 4.7 feature the surfaces of the beads were modified using methods that extend beyond diazonium coupling. Phosphonate diester material **116h** was stirred in an aqueous solution 1 M HCl to give phosphonic acid **116l** (Figure 4.7.c); track marks can be seen on the surface bead, probably a result of stirring with a stirrer bar. Hydrolysis of **116h** in aqueous sodium hydroxide resulted in phosphonate monoester **116k** and SEM analysis of the outer surface (Figure 4.7.d) showed needle-shaped crystals which could be sodium hydroxide. Also, there are right angle and linear shaped fractures in the surface of the bead which appear to be fractures in a crystalline surface; since the beads are amorphous, this suggests that there is a crystalline coating on the outer surface of the bead, since an amorphous structure would not result in such ordered deformation. However, XPS analysis does not show any sodium on the surface; the only explanation can be that these crystalline regions are localised rather than covering the whole surface and the XPS and SEM observed different areas. The linear fractures are also observed in the calcium phosphonate-terminated material **116m** (Figure 4.7.e) and it is possible that there is residual calcium hydroxide on the surface. Image 4.7.e displays regions of indentation where the pores are more localised, this will disrupt any inorganic film which may lead to fractures being more irregular. Finally, image 4.7.f shows dimethylamine-terminated material **116d**, as an example of the beads maintaining the spherical structure even after three modification steps.

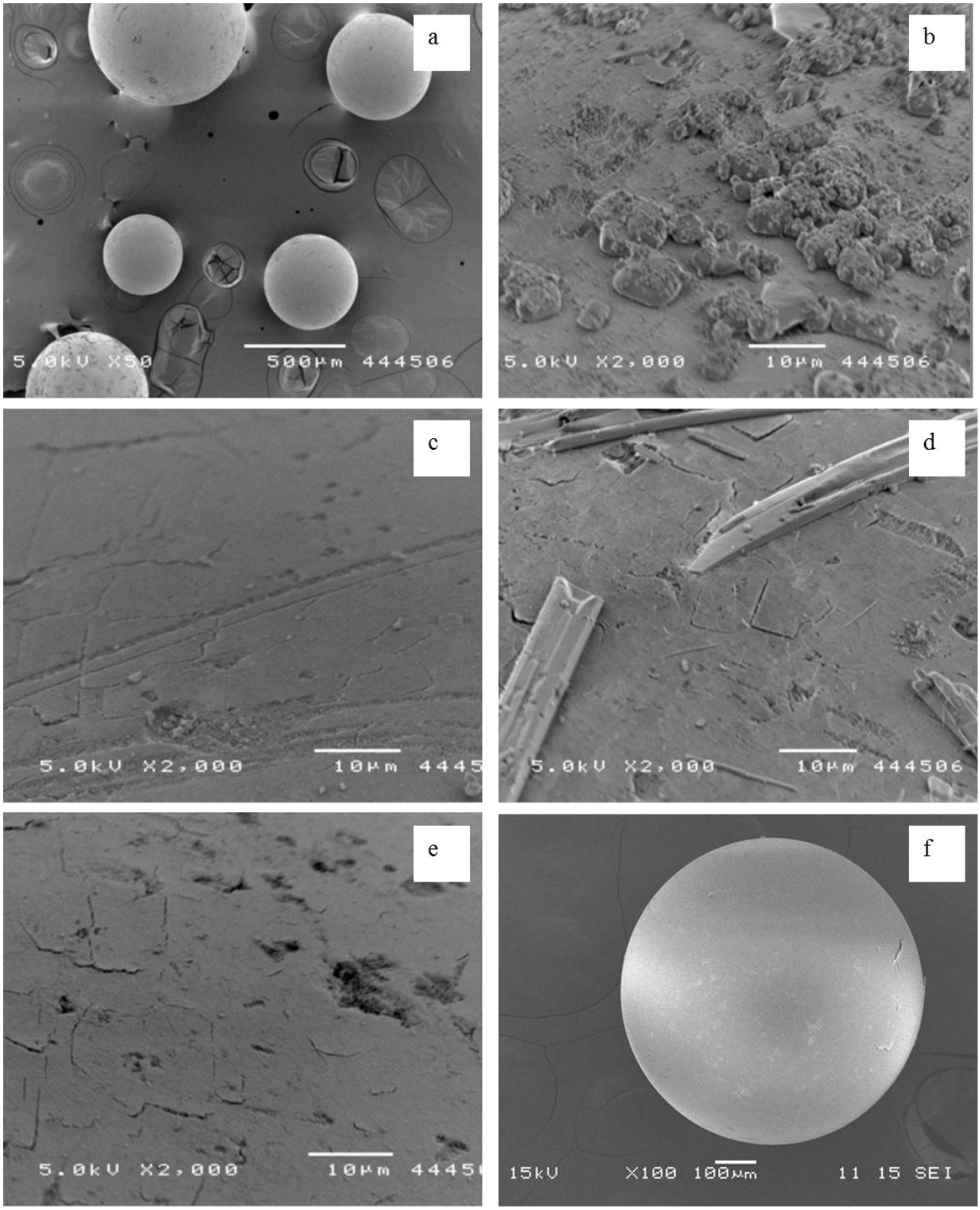

Figure 4.7: SEM images. Images a and b feature the glycol material **116f**, c is phosphonic acid terminated material **116l**, d displays the surface of material **116k** which is terminated with a phosphonate mono-ester group image e shows the calcium phosphonate terminated material **116m**, and f is the dimethyl amine terminated bead **116d**.

4.4.6 Thermal analysis

Thermal gravitational analysis (TGA) was used to measure the change in mass, whilst the samples were heated a rate of 10 ˚C per minute up to 600 ˚C, and from this the decomposition temperature of the materials was calculated. Unmodified XAD-4 decomposed at 475˚C whilst linker-terminated **115** decomposed at 473˚C and the decomposition temperature of coupled materials **116a-m** ranged from 473 to 477 ˚C for phosphonic acid and phosphonate diester materials **116l** and **116h,** respectively. These temperatures are comparable to data reported by Bernard *et al.* who described the decomposition of catechol modified XAD-4 due to degradation of the aromatic groups to be at 490 ˚C.[55]

Table 4.8: Table to show the decomposition temperature measured by TGA analysis and the thermal event as measured by DSC between 25 ˚C and 260 ˚C.

Material	R	TGA Decomposition temperature (˚C)[a]	DSC Thermal event (˚C)[a]
XAD-4	-	475	101
115	-	473	105
116a	*t*-Butyl	473	98
116b	C_6H_{13}	474	94
116c	I	476	98
116d	NMe_2	476	97
116e	H	474	98
116f	$O(CH_2CH_2O)_3CH_3$	474	98
116g	OH	476	96
116h	$CH_2P(O)(OEt)_2$	477	97
116i	NH_2	475	94
116j	CH_2COOH	471	98
116k	$CH_2P(O)(OH)(OEt)$	477	99
116l	$CH_2P(O)(OH)_2$	473	96
116m	$CH_2P(O)O_2Ca$	474	96

[a]Average temperatures.

The thermal activity of the materials was further analysed using differential scanning calorimetry (DSC) which allows measurement of thermophysical properties such as the glass transition, melting and crystallisation temperatures. Since the polystyrene is amorphous, the glass transition temperature was of particular interest, specifically if it was altered by the chemical modifications. The materials were heated at from 25 to 260 ˚C and the temperatures at which there was a thermal event can be found above in Table 4.8. An event at 101 was observed for XAD-4, 105 for **115** and a range of 94 to 99 ˚C for the diazonium coupled materials. The glass transition temperature for non-crosslinked polystyrene has been measured to be in the range of 96.9 - 99.8 ˚C and also at 107 ˚C.[126-129] The thermal events in Table 4.8 are thought to be the glass transition temperatures of residual non-crosslinked polystyrene within the beads and that the glass transition temperature of crosslinked polystyrene exists out of the range measured. Branger *et. al.*[55] conducted DSC analysis of XAD-4 up to 800 ˚C and observed further events such as depolymerisation at 343 ˚C and degradation of the aromatic groups at 627 ˚C. The data obtained by TGA and DSC do not demonstrate significant changes between the modified and unmodified materials signifying that the thermal properties of the materials have been conserved during the modification processes.

4.5 Preparation and characterisation of antibacterial materials

Amine-terminated material **116i** was soaked in a solution of penicillin V in PBS (phosphate buffered saline) to produce material **121** (Scheme 4.3), in which it was assumed that the penicillin would be bound to the surface *via* electrostatic interaction between the carboxylate group on the penicillin and the protonated aniline on the bead surface. After diazonium coupling in acidic conditions, the material was not washed with base so that the protonated

aniline would be present on some or all of the surface. Unmodified XAD-4 was exposed to penicillin V using the same protocol (Scheme 4.3) giving material **122** for comparison.

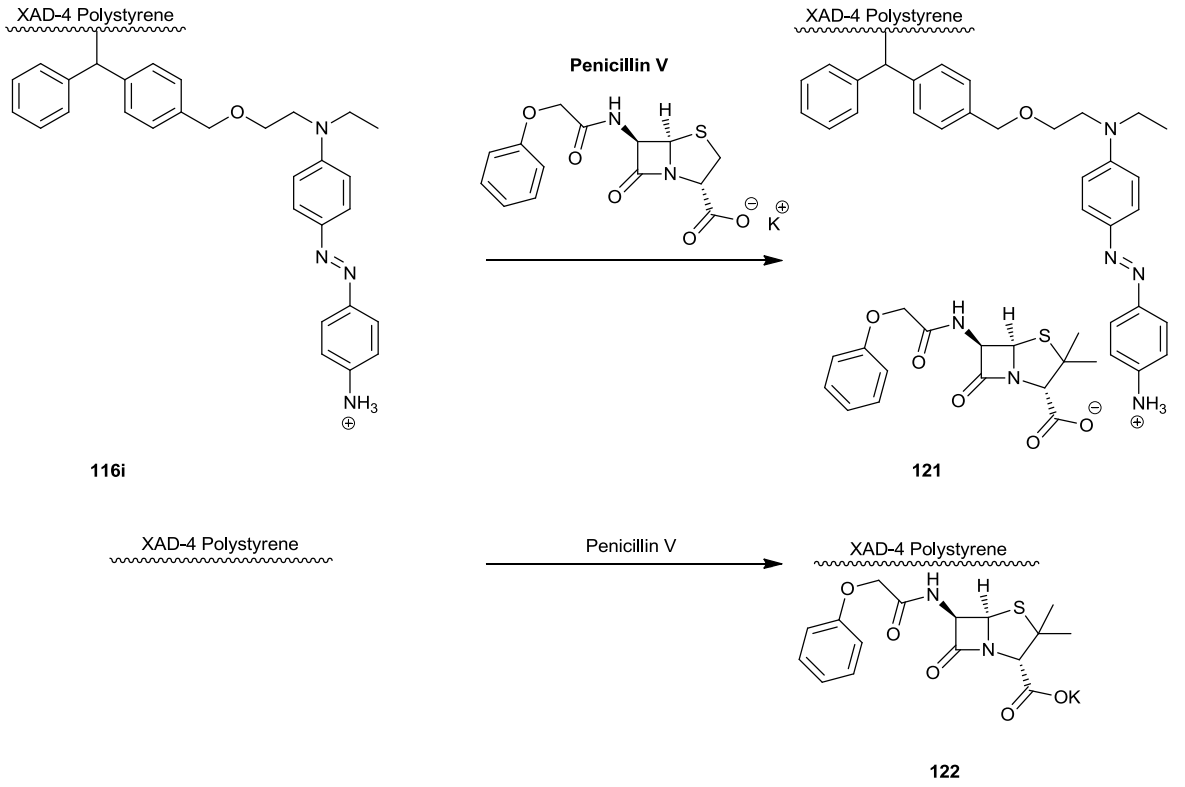

Scheme 4.3: Preparation of penicillin loaded materials. Conditions: materials soaked in a solution of penicillin V in PBS (5 μmol/ml) followed by thorough washing with water.

XPS and combustion analysis were used to determine if penicillin V was present on the materials after washing. XPS analysis detected oxygen, carbon, nitrogen, silicon and sodium in both cases, but no sulfur was observed. Silicon was observed due to contamination of the materials in the lab environment and from glassware used during the chemical treatments. However, combustion analysis did detect sulfur, and from the percentage of sulfur the loading of penicillin V could be calculated; 0.14 mmol/g of penicillin V was detected on amine-modified material **121**, whilst material **122** has a loading of 0.18 mmol/g. Although both materials have very similar loading levels, this gave no information for the binding behaviour of penicillin. Amberlite XAD-4 is a polystyrene based resin designed for the

adsorption of small molecules, usually from polar solvents; this appears to function on the basis of pore entrapment, and the materials prepared herein were washed with water which was not successful in removing absorbed penicillin V. [115]

4.6 Conclusions

Successful modification of XAD-4 polystyrene has been demonstrated with XPS and ATR-IR confirming the presence of significant elements and functional groups that were are expected by the chemical treatments. Combustion analysis provided further evidence, with confirmation of nitrogen after each of the modification steps as well as detection of phosphorous and iodine on a selection of the linker-coupled materials that had been functionalised with these elements. The loadings of the chemistry exhibited by the linker-coupled materials are significantly higher than those of the directly coupled counterparts, suggesting that the mechanism of retention of the diazonium salts differs between the two groups of materials. Furthermore, the linker-coupled materials are more intensely coloured than the corresponding directly coupled materials. This evidence suggests that the linker coupled materials were modified by covalent attachment of the diazonium salts via an azo linkage, whereas the directly coupled materials retain the decomposed diazonium salt residues by physisorption. The effect of the chemical modifications on surface contact angle was investigated; variations in the contact angles were observed and typically the chemistry influenced the hydrophilicity of the polystyrene, with materials that have the ability to hydrogen bond water being generally more hydrophilic and the materials terminated with alkyl groups more hydrophobic. However, the effect of the surface chemistry on the contact angle was not strongly pronounced and the angles were accompanied by significant standard deviations for reason already discussed.

SEM, DSC and TGA analysis were carried out determine the effect of the chemical modifications on the structure and physical properties of the beads. SEM analysis demonstrated that the overall structure of the beads was left intact but interesting surface structure was observed in the form of globular and crystalline deposits on the surface of the beads. Where macroscopic destruction of the beads was observed, the fracture lines were clean and looked to be a result of abrasion; this confirmed the need to take care when handling the dry materials since they are brittle. The thermal events observed on modified and unmodified polystyrene are all very similar suggesting that the chemistry is not altering the thermal properties of the beads and the glass transition temperatures measured by DSC is that of residual non-crosslinked polystyrene. Notably, the glass transition temperature for linker terminated **115** is 105 ˚C, where the other materials range between 94 - 100 ˚C. The globular deposits left behind after carbene modification, thought to be unreacted carbene residue, may have affected increased the Tg of the non-crosslinked polystyrene.

The presence of penicillin V on antibacterial materials **121** and **122** was confirmed by detection of sulfur by combustion analysis, however both materials were revealed to have similar loadings; **121** and **122** are based in amine-terminated material **116i** and XAD-4 respectively. The absorbent properties of XAD-4 makes it difficult to establish if amine modified **121** is supporting the penicillin by electrostatic interaction rather than adsorption into the pores as occurs in XAD-4 based material **122**. In order to gain more information regarding the mechanism by which penicillin V is supported on an amine-modified substrate, an alternative polymer that is less porous and can be washed more thoroughly will need to be investigated; a flat polymer may prove to be more successful.

Chapter 5: Assessment of Biological Properties

Biomaterials that can control biofouling and reduce infection are of great interest, for applications ranging from implants to wound dressings and clothing; the library of materials discussed in Chapter 4 provided a wide range of functionality suitable for investigation of biological properties. This Chapter initially reports an investigation of how chemical surface functionality can control protein adsorption (Figure 5.1), and reports preliminary results which make use of such modified polymers as antibacterial materials and drug delivery vehicles, using penicillin V as the prototype.

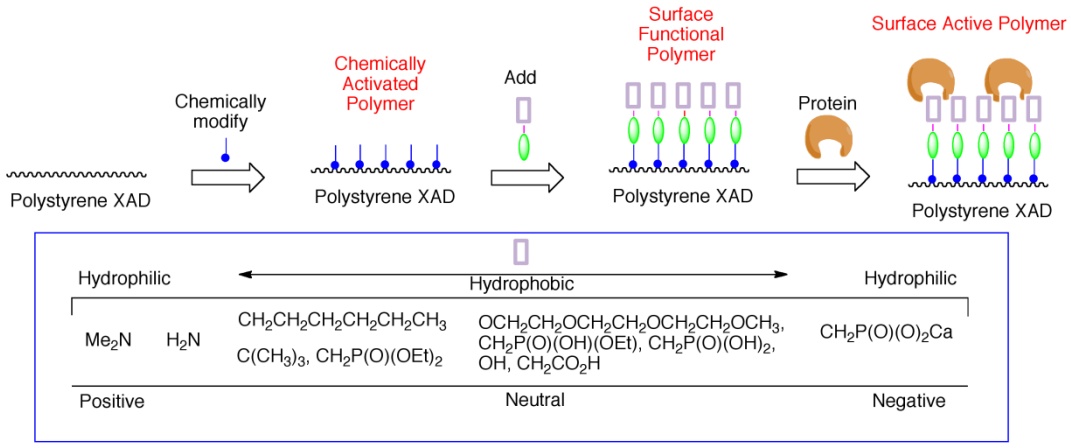

Figure 5.1: Surface modification strategy to control protein adsorption.

5.1 Protein Adsorption

Protein adsorption has implications for understanding the biocompatibility of a surface, since upon implantation of any foreign body, the first bio-response is non-specific protein adsorption on the implant surface. Non-specific protein adhesion on biomaterials can result in a range of undesirable or unexpected events,[2] for instance, when plasma proteins such as fibrinogen interact with synthetic surfaces, their conformation can be significantly altered,[8] resulting in enhanced platelet and erythrocyte adhesion as well as induced coagulation; these

reactions are invariably detrimental to the acceptance and function of the device. The control of non-specific protein adhesion is therefore an important task in the design of new biomaterials.

The effect of surface functionality on protein adsorption was investigated using materials **115** and **116a-m** (Figure 5.2), whose preparation and characterisation was fully described in Chapter 4. The protein adsorption experiments were kindly carried out under the supervision of Professor Cleo Choong, NTU Singapore.

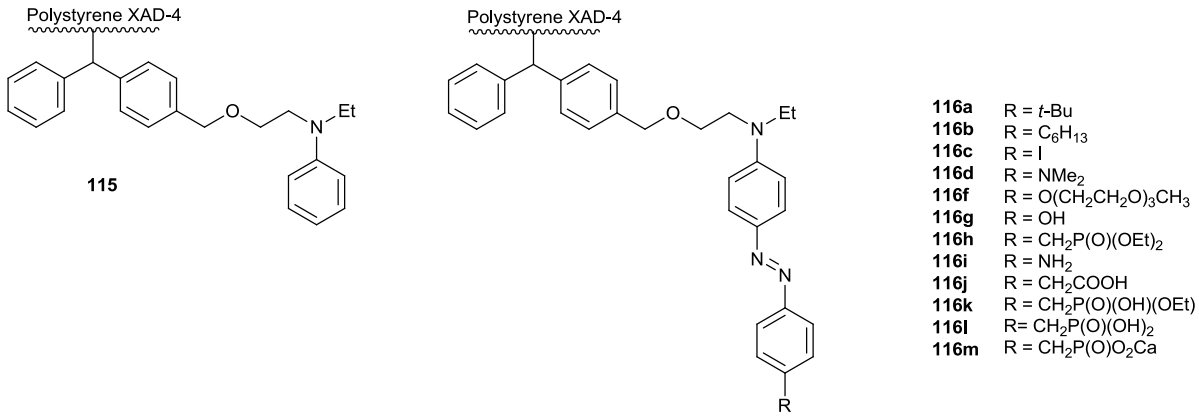

Figure 5.2: Materials used for protein adsorption studies.

5.1.1 Protein adsorption after three hours

Following sterilisation, the materials **115, 116a-d, f-m** were incubated in a solution of the protein, bovine serum albumin (BSA), in phosphate-buffered saline (PBS) at physiological pH. The beads were filtered to remove the supernatent solution and then soaked in sodium dodecyl sulfate (SDS), a surfactant which removes the adsorbed protein from the material; the optical density of the resulting solution was measured and from this the amount of protein adsorbed onto the beads was calculated by comparison to an appropriate calibration curve, and the data are presented in bar chart form (Figure 5.3).

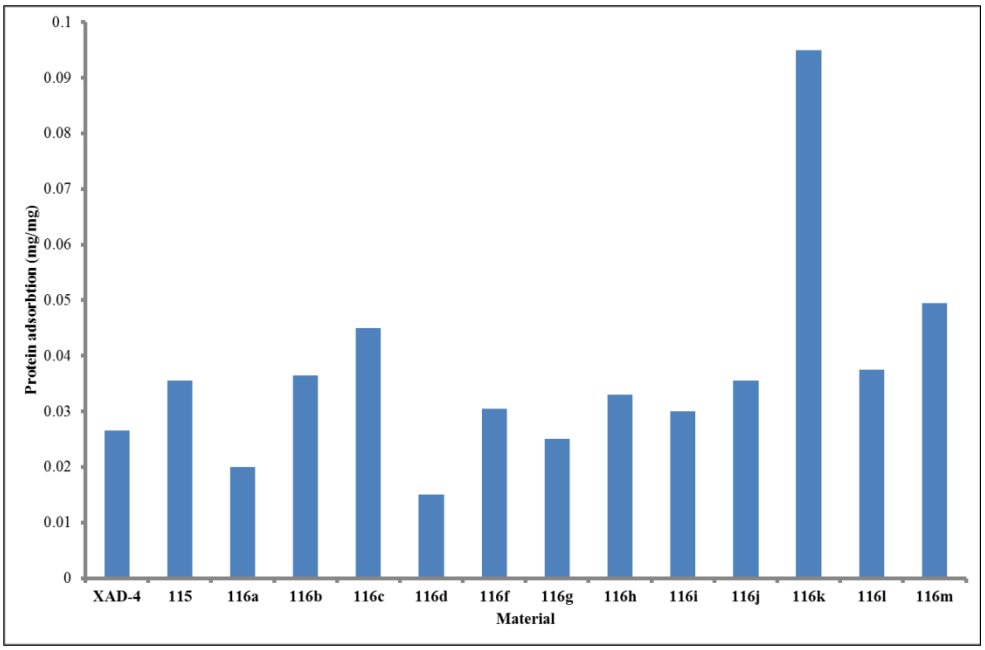

Figure 5.3: The amount of protein adsorbed on the variously modified beads and unmodified XAD-4 after a three hour incubation time. Data presented is of one measurement of protein adsorption per material.

The majority of the materials show increased protein adsorption relative to unmodified XAD-4, and in particular the phosphonate monoester-terminated material **116k** adsorbed the greatest amount of protein of all materials. On the other hand, the *t*-butyl, dimethyl amine and hydroxyl terminated materials **116a**, **d** and **g** show a lower level of BSA adsorption, whilst the glycol-modified material **116f** has a comparable level of adsorption to that of XAD-4. Since the loadings of the introduced chemical surface functionality do vary, as calculated using combustion analysis (Table 4.4, Chapter 4), these initial binding data were adjusted to grams of protein adsorbed per mmol of surface modification, termed the adjusted protein adsorption, the results of which are displayed in Figure 5.4. The protein adsorptions range from 0.126 to 0.667 g/mmol, with the iodide terminated material **116c** having the lowest adsorption. Phosphonate monoester terminated material **116k** remains as a material with high adsorption, and is similar to **116b**, **i**, **j** and **m** (iodo, amine, acid and calcium

phosphonate terminated), with acid terminated **116j** having the highest adjusted adsorption at 0.03 g/mmol of surface modification.

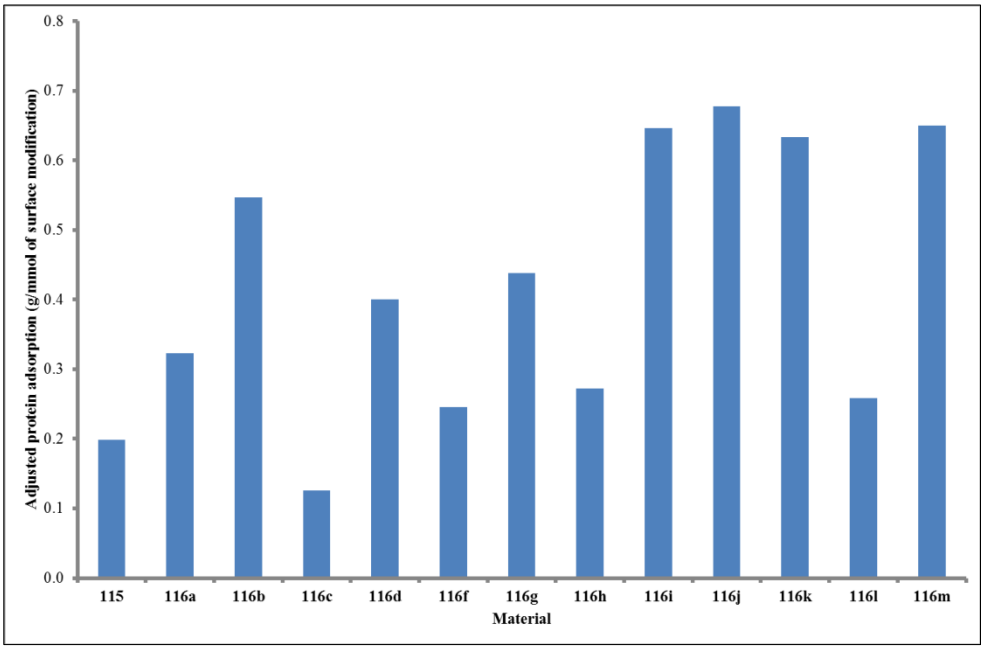

Figure 5.4: Protein adsorption adjusted to allow for the surface chemical functionality loading. Data presented is of one measurement of protein adsorption per material.

The effect of the hydrophilicity on the capability of a surface to absorb proteins has been extensively discussed with the conclusion that protein adsorption is hindered by hydrophilic surfaces. That being the case, it was expected that a correlation of water contact angle with protein binding be observed. Comparison of the adjusted protein adsorption with the average measured contact angle of the materials (Figure 5.5; contact angle data taken from Table 4.7, Chapter 4) shows a general trend; a broad linear correlation is observed in the central region from **115** to **116m,** although materials **116c**, **l**, **k**, **j**, **i** and **b** (iodo, phosphonic acid, phosphonate monoester, acid and amine terminated) in particular deviate from the trend, suggesting that the ability of the materials to adsorb protein is affected by other factors.

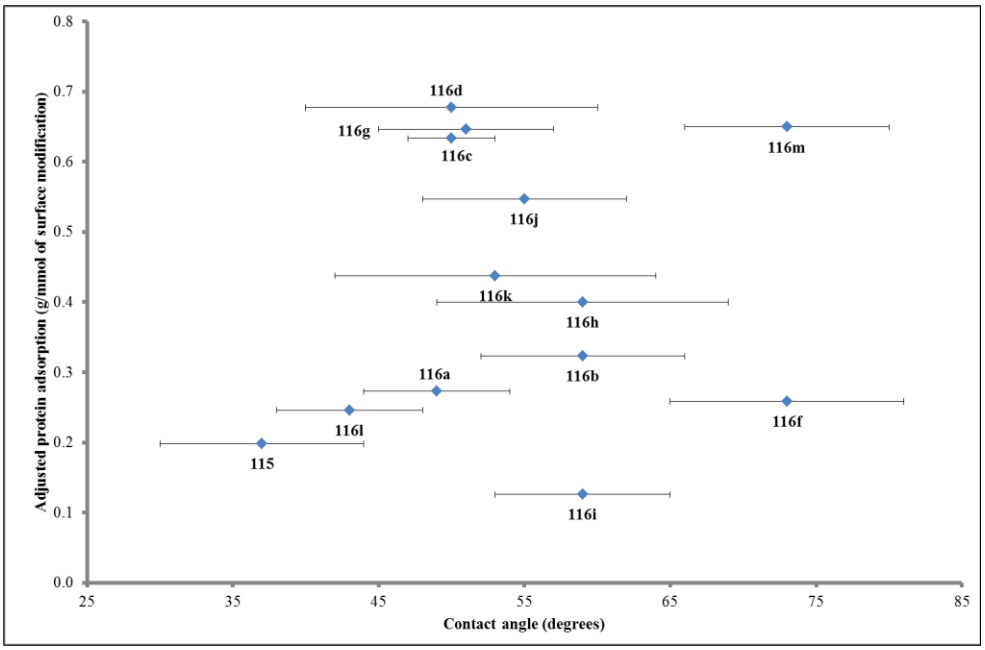

Figure 5.5: Correlation of adjusted protein adsorption with contact angle. Errors of plus and minus one standard deviation are displayed.

Chemicalize (www.chemaxon.org) was used to calculate cheminformatic molecular descriptors often used in the design of drug candidates.[130] Although this software is designed for molecules in solution, considering the length of the linker molecule to which the functional groups of interest are joined, a high degree of freedom is possible; thus it was proposed that the calculable parameters may provide insight into the surface properties and therefore the behaviour of the materials when exposed to BSA. Table 5.1, contains the results of the cheminformatic analysis. The structures used to calculate the parameters are displayed in Figure 5.6.

Table 5.1: Parameters calculated using Chemicalize (www.chemaxon.org).

Material	R	ClogP	Polarisability	Molecular refractivity	Polar surface area ($Å^2$)	Molecular surface area ($Å^2$)	% Polar surface area	Volume ($Å^3$)	Minimum area ($Å^2$)	Maximum area ($Å^2$)
123	-	8.6	55.7	114.9	12.5	743.6	1.7	453.0	85.6	120.0
124a	*t*-Bu	12.6	74.2	197.9	37.2	1009.5	3.7	610.4	111.4	170.6
124b	C_6H_{13}	13.8	77.9	207.3	37.2	1006.0	3.7	643.7	113.3	182.8
124c	I	12.0	71.6	192.6	37.2	906.2	4.1	565.5	105.6	161.0
124d	NMe_2	11.1	73.8	193.7	40.4	965.8	4.2	587.7	107.9	168.6
124e	H	11.0	66.9	179.2	37.2	870.1	4.3	540.8	104.0	152.8
124f	$O(CH_2CH_2O)_3OCH_3$	10.8	82.4	218.8	74.1	1164.6	6.4	697.5	119.5	200.2
124g	OH	10.7	67.4	181.2	57.4	892.2	6.4	549.9	104.4	157.2
124h	$CH_2P(O)(OEt)_2$	11.4	80.6	213.6	72.7	1119.1	6.5	672.5	113.9	192.5
124i	NH_2	10.2	68.0	183.9	63.2	896.3	7.1	551.9	103.8	159.2
124j	CH_2COOH	10.4	71.0	190.5	74.5	950.9	7.8	586.7	111.5	165.7
124k	$CH_2P(O)(OEt)(OH)$	9.5	76.7	204.3	83.7	1049.0	8.0	636.2	113.3	179.7
124l	$CH_2P(O)(OH)_2$	8.5	72.7	195.1	94.7	980.1	9.7	601.3	112.1	167.3
124m	$CH_2P(O)(O_2Ca)$	8.5	72.5	192.8	100.4	975.6	10.3	596.5	114.6	166.0
						Average areas of **124a-m**			110.5	171.2

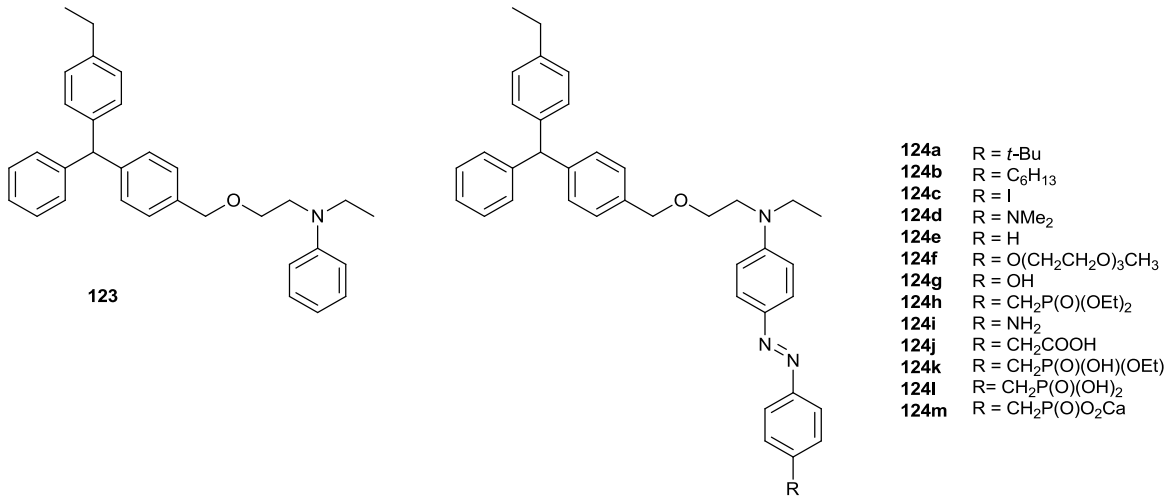

Figure 5.6: Structures used for cheminformatic parameter calculations.

ClogP is the partition coefficient between water and octanol and it gives a measure of lipophilicity; as expected the alkyl terminated **124a** and **b** species show the most preference for octanol with the highest values of 12.6 and 13.8, respectively, as a result of the terminal groups interacting with the octanol carbon chain by van der Waals interactions. The phosphonic acid **124l** and calcium phosphonate **124m** terminated molecules have the lowest value of 8.5. Polarisability is a measure of the tendency of the electronic distribution of the molecule to be distorted by an external electric field; species that have more polarisable bonds will be prone to distortion. This is observed by the glycol system possessing the highest polarisability at 82.4 whilst the linker system **123** has the lowest at 55.7. Calculated molecular refractivity (CMR), a parameter representing the effect of the volume and dispersive interactions that influence ligand receptor interactions was also calculated; linker **123**, with the smallest volume, has the smallest CMR of 114.9 and phenyl terminated **124e** has the smallest value out of the diazonium coupled species. The latter is an indication of that the terminal groups, added by diazonium coupling, enhance the ability of the species to interact with the protein receptors. The molecular surface area (MSA) measures the area of the molecule accessible to solvent whilst the polar surface area (PSA) represents the area of

the molecule made up of polar atoms, a parameter that has shown good correlation with the ability of drugs to move through cell membranes and the % polar surface area (%PSA) is the polar surface area relative to the molecular surface area. The PSA and %PSA values follow similar trends as would be expected, where the alkyl and iodo terminated species **124a**, **b** and **c** have the smallest values and an increase is observed with an increase in polar bonds and atoms. Finally, the volume and the minimum and maximum area of the molecules has also been calculated.[122,130-132]

The adjusted protein adsorption was correlated with each of the parameters listed, and a full set of the results can be found in Appendix II, the correlations with PSA and %PSA showed the most interesting trends (Figure 5.7).

Three groups follow the pattern of increasing protein adsorption with increasing PSA and %PSA (Figure 5.7); at the higher adsorption level, this includes **116b**, **i** and **j** (hexyl, amine, and acid terminated), at the medium adsorption level, **115**, **116a**, **d**, **g**, **k** and **m** (linker only, *t*-butyl, dimethyl amine, hydroxyl, phosphonate monoester and calcium phosphonate terminated) at the low adsorbing level, **116c**, **f**, **h** and **l** (iodo, glycol, phosphonate diester and phosphonic acid terminated). This is perhaps not surprising, since the increase in polar bonds, indicated by increasing PSA, the possibility of surface-protein electrostatic interactions will be increased, thus increasing the likelihood and strength of the binding interaction.

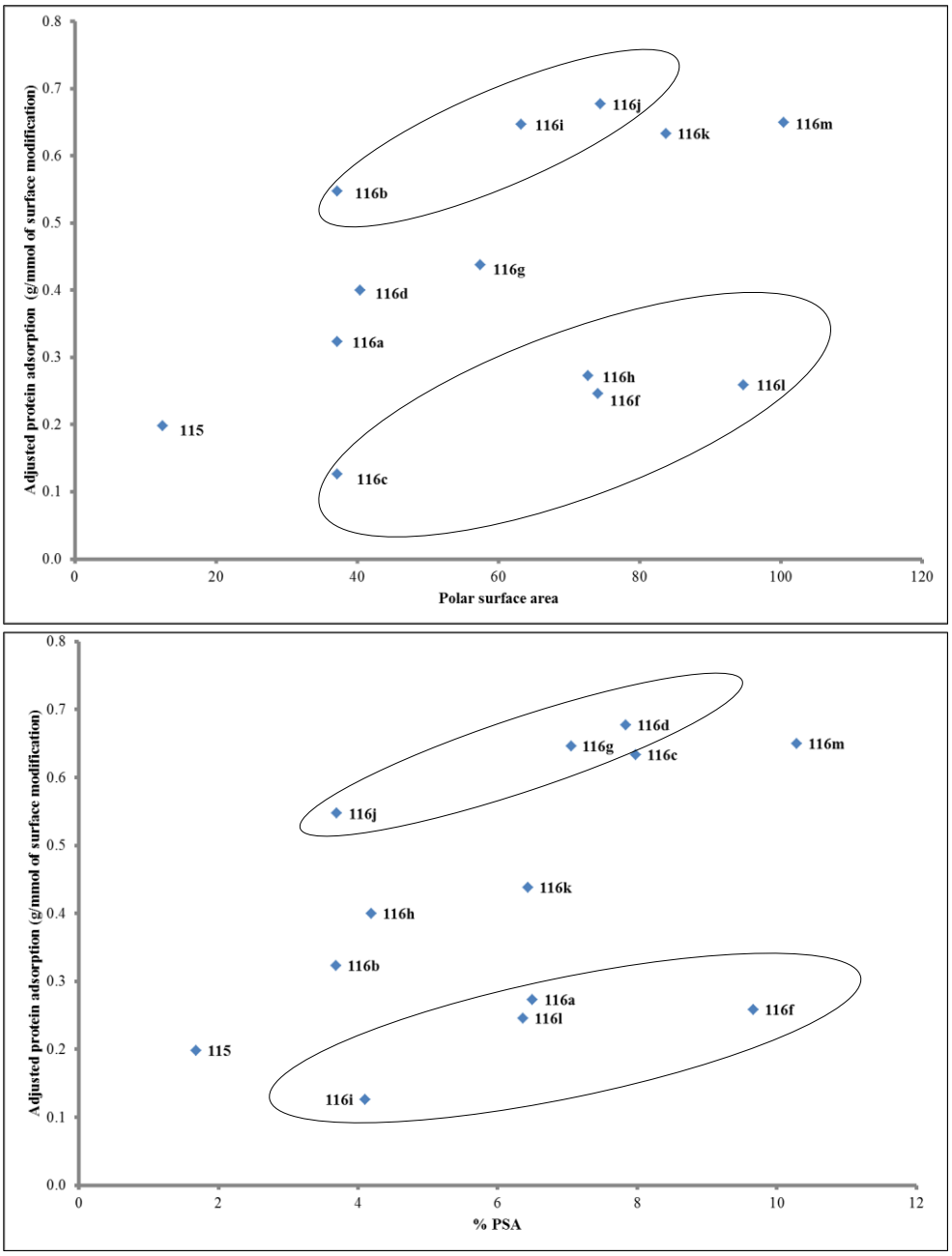

Figure 5.7: Correlation of PSA and %PSA with adjusted protein adsorption.

5.1.2 Time-course protein adsorption

In order to develop understanding into the adsorption of BSA over a period of time, a selection of the materials were exposed to a known concentration of BSA in PBS for 1, 3, 6, 12, and 24 hours; the amount of protein adsorbed after the different times was calculated from the change in optical density of the protein solution, and quantified by calibration using

standard curve. The experiments were carried out in triplicate, resulting in the protein adsorption data presented in Figure 5.8 and in Table 6.18 in Chapter 6.

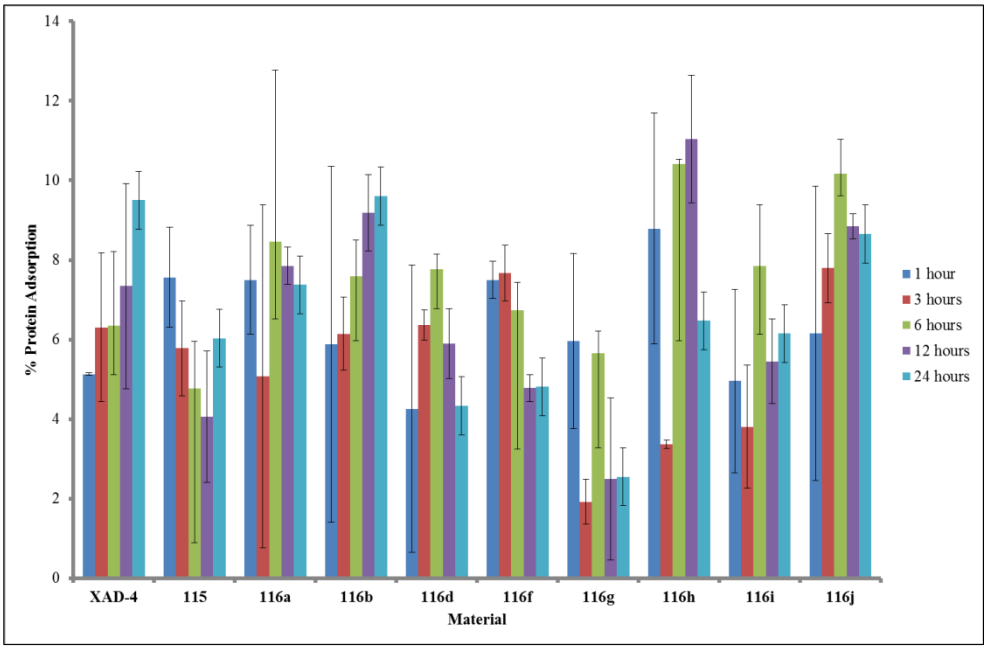

Figure 5.8: Average % protein adsorption generated from three measurements, with error of plus and minus one standard deviation assumed.

The % protein adsorption was adjusted to account for the surface loading of the chemistry, as presented in Figure 5.9. The adjusted protein adsorption gave more information concerning the effect of the applied surface chemistry. It is apparent that variability of BSA adsorption over time is observed over a 24 hour time period (Figures 5.8 and 5.9); hexyl-functionalised material **116b** is the only substrate which continued to adsorb protein over the full assay time period, while the rest have the maximum adsorption point before 24 hours. This signifies that protein adsorption is initially rapid but reversible and tends to a steady-state value, which is possibly influenced by protein displacement by water. Protein adsorption has been described to occur in two steps: the first step is reversible adsorption, while the second requires a change of protein conformation resulting in irreversible adsorption.[133] Water adsorption will most likely compete with the proteins until the water-

surface and protein-surface equilibriums are at a steady state. Once adjusted to account for surface loading of the chemistry (Figure 5.9), materials **116a**, **b**, **d**, **i** and **j** (*t*-butyl, hexyl, dimethyl amine, amine and acid terminated) exhibit high levels of adsorption, while the lower binding materials are terminated with oxygen rich units, such as glycol, hydroxyl and phosphonate diester functionalities **115**, **116f**, **116g** and **116h.**

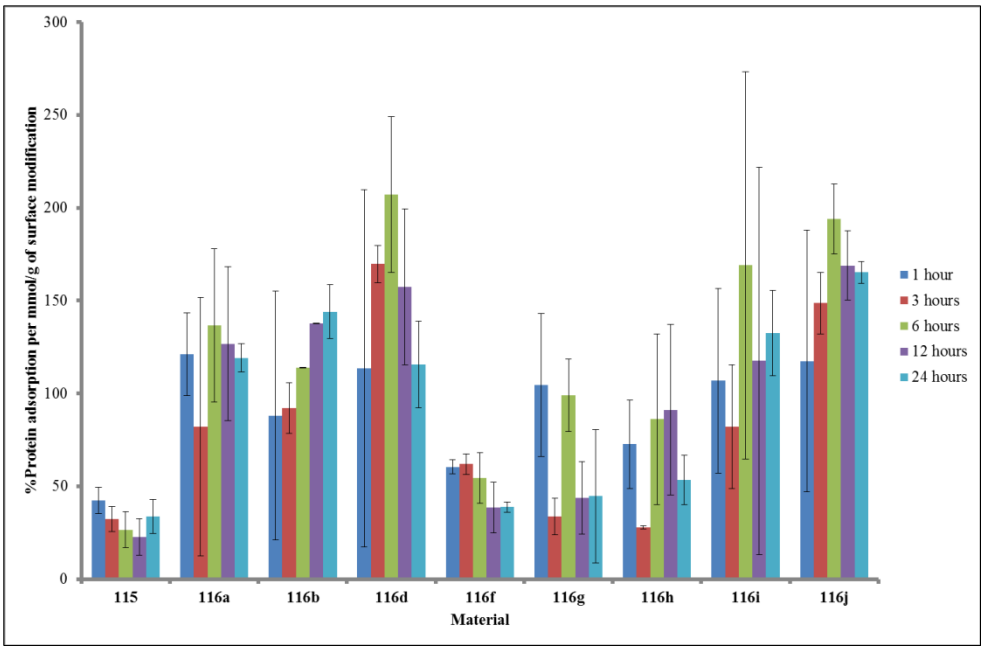

Figure 5.9: Adjusted percentage protein adsorption. Three replicates per material was performed and an error plus or minus one standard deviation is displayed.

The average adjusted % protein adsorption data at 1, 12 and 24 hours was compared with the contact angle data which revealed interesting time-course behaviour (Figure 5.10). When the average contact angles and protein adsorption quantities are considered, after one hour, adsorption has a broad linear correlation with contact angle with an R^2 value of 0.7542 indicating that generally increasing the hydrophobicity of a surface leads to increased protein adsorption. Notably, however, acid and amine terminated materials **116i** and **j** deviate from the trend, giving higher levels of protein adsorption than their surface contact angles would predict. By 12 hours, this linear trend is preserved only weakly, with an R^2

value of 0.5168, for which the glycol and acid functionalised materials **116g** and **j** deviate significantly. Between 1 and 12 hours, materials **115**, **116f** and **g** (linker modified, glycol and hydroxyl terminated materials) have lost protein rather than continued to adsorb it, presumably due to the hydration layer surrounding the surface that restricts adsorption and displacement behaviour of the protein by water. The hydrophobicity correlation is completely lost at 24 hours, with two distinct groups of materials observed. The lower adsorbing materials are terminated with the linker molecule, glycol, hydroxyl and phosphonate diester groups **115**, **116f**, **g** and **h**. The higher adsorbing materials are **116a**, **b**, **d**, **i** and **j** (*t*-butyl, hexyl, dimethyl amine, amine and acid terminated), all of which have contact angles at the higher end of the range, with the exception of the acid and amine terminated materials **116i** and **j**.

Vogler *et al.*[134] describe the Gibb's energy of adsorption (ΔG) as being the sum the following three parameters: ΔG (hydrophobic effect), the energy gained in the protein coming out of solution and water hydrogen bonding with itself, this can be assumed to be constant for purified proteins; ΔG (dehydration), the energy required to displace water contained within the hydration layer on the surface of the material; ΔG (interaction) which considers the affinity of the protein for the surface functionality and the bonding interactions that are formed.

$$\Delta G = \Delta G(hydrophobic) + \Delta G(dehydration) + \Delta G(interaction)$$

With Vogler's hypothesis in mind, the linear correlation of contact angle with adsorption at 1 hour suggests that initially the ΔG (dehydration) term dominates. For the materials that do not gain or retain significant amounts of protein after 1 hour, such as **115**, **116f** and **g** (linker, glycol and hydroxyl terminated), this term continues to dominate, with the hydration layers

becoming more extended and thus requiring more energy to displace. However, when materials continue to adsorb more protein, the ΔG (interaction) term competes and eventually dominates. The phosphonate diester terminated material **116h** is interesting in that the amount of protein it adsorbs generally increases throughout the experiment, albeit slowly, but then decreases after 12 hours; this implies that the phosphonate diester group will interact with binding sites of BSA, but the interaction is not strong enough to compete with water, suggesting that the phosphonate diester does not compliment the BSA binding sites. Finally, the acid and amine terminated materials **116i** and **116j** show high affinity for BSA from the outset with their adsorption levels being consistently higher than those expected based in their surface contact angles, suggesting that the ΔG (interaction) term dominates in Vogler's equation. This is consistent with the known binding sites of BSA that bind acidic functional groups, in particular carboxylic acids as discussed below.

Correlation of average protein adsorption at 1, 12 and 24 hours with % PSA (Figure 5.11) revealed interesting patterns across the three time points. After 1 and 12 hours, two groups follow a linear trend of increasing adsorption with increasing % PSA. The first group is composed of materials terminated with the linker, *t*-butyl, hexyl and dimethyl amine groups **115**, **116a**, **b** and **d** which will bind BSA through van der Waals interactions. The other is made up of materials **116f**, **g**, **h**, **i** and **j**, terminated with glycol, hydroxyl, phosphonate diester, amine and acid groups, these groups bind BSA with electrostatic hydrogen bonding.

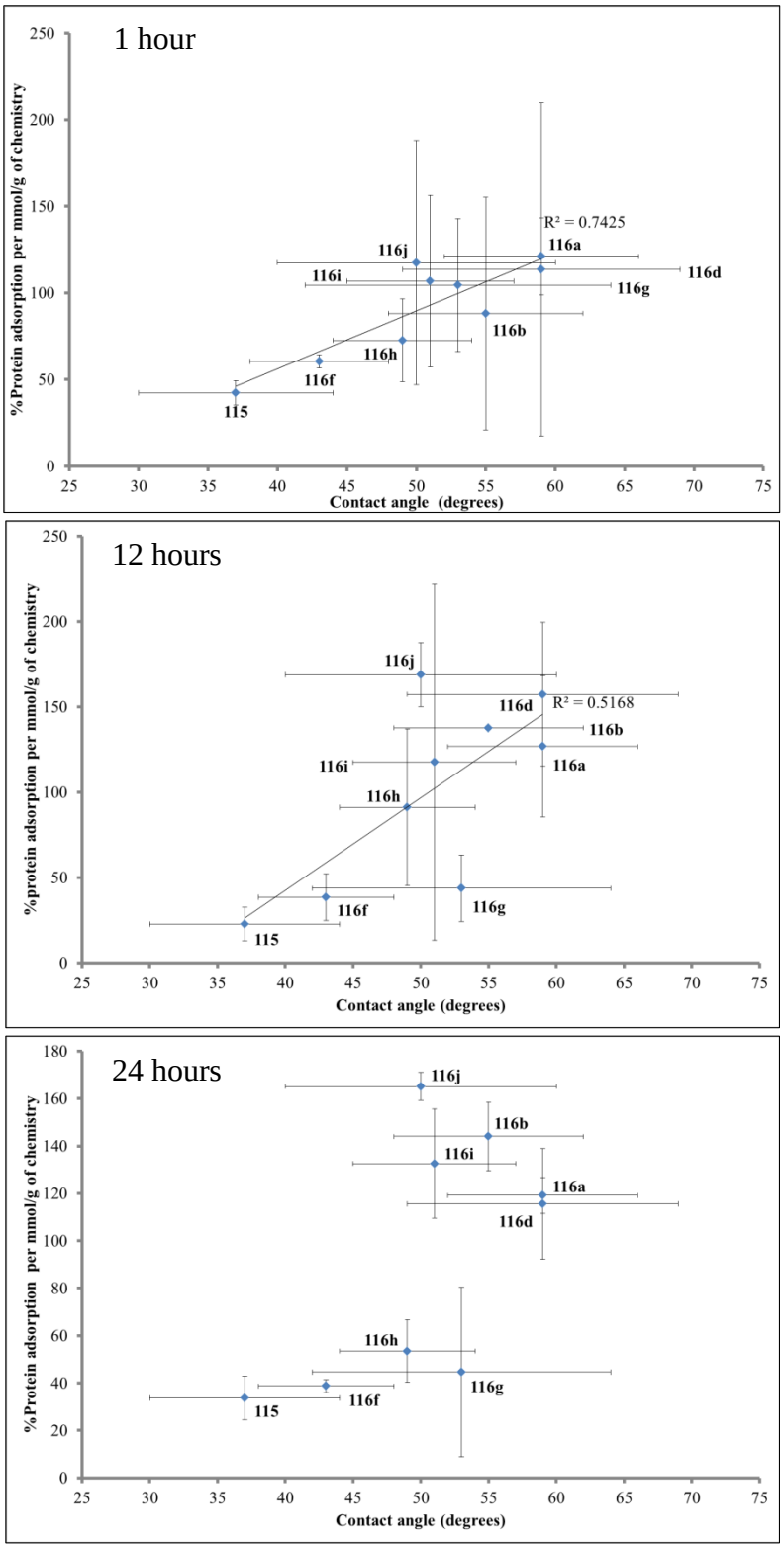

Figure 5.10: Correlation of contact angle with adjusted percentage protein adsorption at 1, 12 and 24 hours.

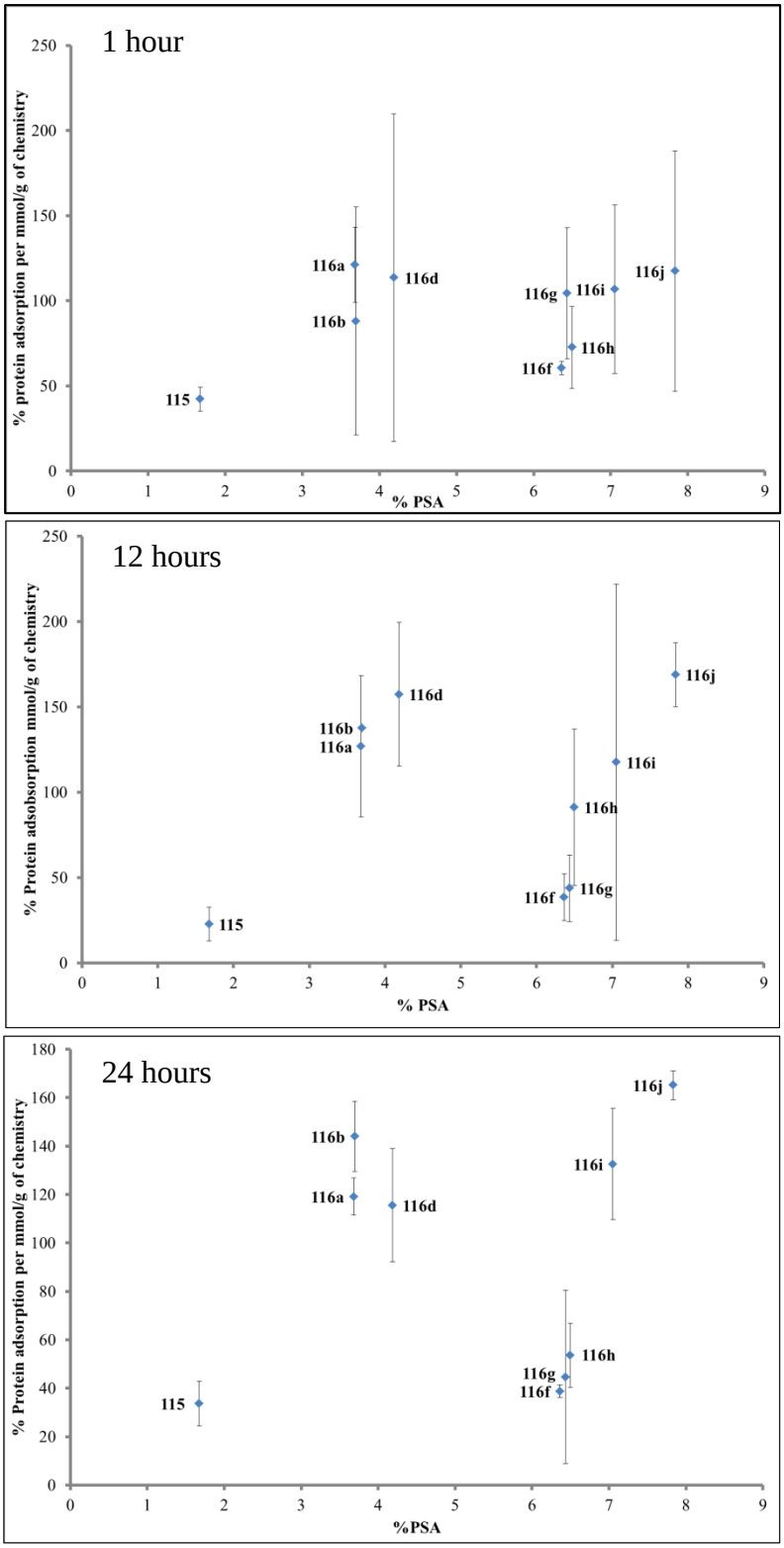

Figure 5.11: Correlation of %PSA with adjusted % protein adsorption at 1, 12 and 24 hours.

Investigations into human serum albumin (HSA) have revealed that the protein has two dominant binding sites both of which are generally hydrophobic, but with polar regions as well.[110] The sites differ in their size and location of the polar cavities; one site is larger and has two polar regions, one close to the entrance and one further into the cavity, whereas the other binding site has one small polar region located close to the entrance.[111] Two of the binding sites observed on BSA have proved to have similar binding affinities to that of HAS.[112] The two groups observed in the % PSA correlations may be due to interactions with the two dominant binding sites of BSA, one group for each site. Furthermore, acidic groups and specifically aromatic carboxylic acids have a high affinity for both protein binding sites as a result of the basic residues found in the cavities[113,114] which accounts for the consistently high % protein adsorption exhibited by acid terminated **116j**, relative to the measured contact angle, from the outset. By 24 hours, three groups of materials are observed in the correlation; the first, **116f**, **g** and **h** (glycol, hydroxyl and phosphonate diester terminated) all of which have low protein adsorption and bind water preferentially; the second, **116a**, **b** and **d** (*t*-butyl, hexyl and dimethyl amine), all of which bind the protein with van der Waals interactions; finally the third, **116i** and **j**, which interact with the protein via hydrogen bonding. Material **115** does not fit into any of these groups; surface analysis revealed that sodium salts were present of the surface of this material which will influence the surface properties and protein adsorption abilities. BSA has an isoelectric point of 4.7 so at pH 7.4 will possess a significant negative charge[135] which will result in repulsion of any negative ions on the material surface, such as Cl^- or CO_3^- from residual sodium chloride and sodium carbonate. BSA deposition on a cellulosic membrane was reduced when the negative charge character of the membrane was increased by γ-irradiation, resulting in an increase in surface hydroxyl groups,[136] although whether this was a result of increased surface

hydrophilicity also is not commented on. Furthermore, the repulsion between surface ions and solution ions contained in the PBS buffer will also reduce protein adsorption.[137]

5.1.3 Conclusions

The protein adsorption experiments indicate that whilst surface hydrophilicity is important for reducing protein adsorption, it is not the only factor to be considered. Correlations with contact angle data indicate that materials terminated with functionality that has a high affinity for the protein will adsorb protein, regardless of the hydrophilicity of the surface, and acid terminated material **116j** is good example of this. Furthermore, the time course adsorption investigation showed that whilst hydrophilicity is initially important, over time surface functionality becomes more dominant, with Vogler's expression for the Gibbs energy of adsorption providing a useful tool for the discussion of the various factors. The correlations with cheminformatic parameters PSA and % PSA demonstrated some interesting trends, especially in the time course analysis; notably these parameters do not take into account the natural affinity of functional groups for protein receptors and water hydration effects so the correlations have limitations. However, correlation of protein adsorption with % PSA at 1 and 12 hours revealed two distinct groups of materials that that interact with the protein by different mechanisms and it is proposed that during initial binding the groups interact with the two known binding sites on BSA, but by 24 hours, this correlation is no longer observed, at which point the limitation of using the molecular parameters to explain patterns in protein adsorption is observed.

This work has shown that chemical surface modification can produce a set of materials that will interact with BSA to different degrees thus allowing for the control of protein adsorption on surfaces.

5.2 Antibacterial materials

As discussed in Chapter 1, tethering antimicrobial agents onto surfaces can lead to a decrease in biofilm formation as a result of contact killing of bacteria. Urban *et al.* showed that tethering penicillin to ePTFE (expanded polytetrafluoroethylene) via a polyethylene glycol spacer resulted in a surface that was resistant to bacteria and biofouling, however, the length of the linker was essential for the bioactivity.[43] As a preliminary investigation into the use of the functional materials to deliver antibiotics, amine-based material **121** was prepared, as described in Chapter 4. XAD-4 control **122** was also prepared using the same conditions so that the effect of the amine surface functionality could be observed (Figure 5.12).

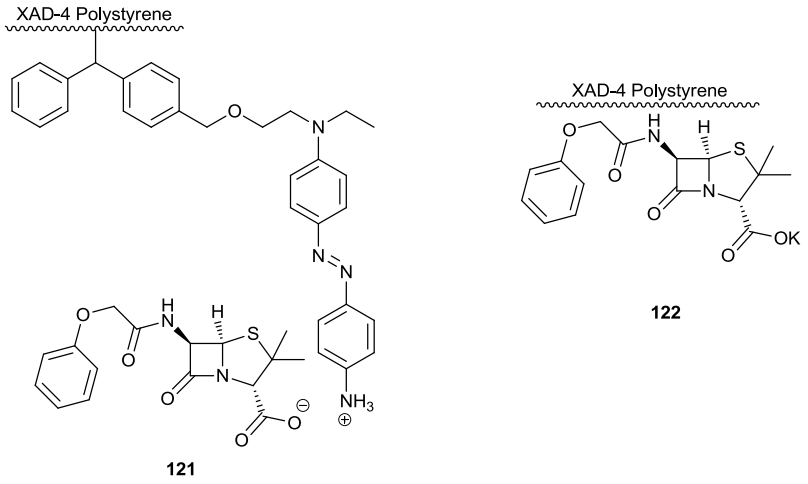

Figure 5.12: Antibacterial materials.

Materials **121** and **122** were tested for their activity against Gram negative bacterium *E. coli* and Gram positive bacterium *S. aureus* using cephalosporin C as a standard with a hole plate assay. Both materials proved to be active against *E. coli*, with the % relative potencies of the materials being in the following ranges: 0.028-0.124% for amine-modified material **121** and 0.134-0.427% for **122**. The % relative potency compares the amount of penicillin with the amount of cephalosporin C required for the same level activity, thus giving a further

indication as to the activity of the antibacterial in comparison with a known antibacterial (% relative potency = (moles of penicillin V/moles of cephalosporin C)×100). Figure 5.13 below demonstrates the change in % relative potency with mass of modified polymer per incubation well. It was expected that the % relative potency should be relatively constant across the different sample masses, but the amine-modified material **121** exhibits some variation, with the majority of points localised around 0.1%. XAD-4 material **122** demonstrates much wider variation, indicating that the release of penicillin is less controlled, this contrasts with more controlled behaviour of the amine modified material **121**.

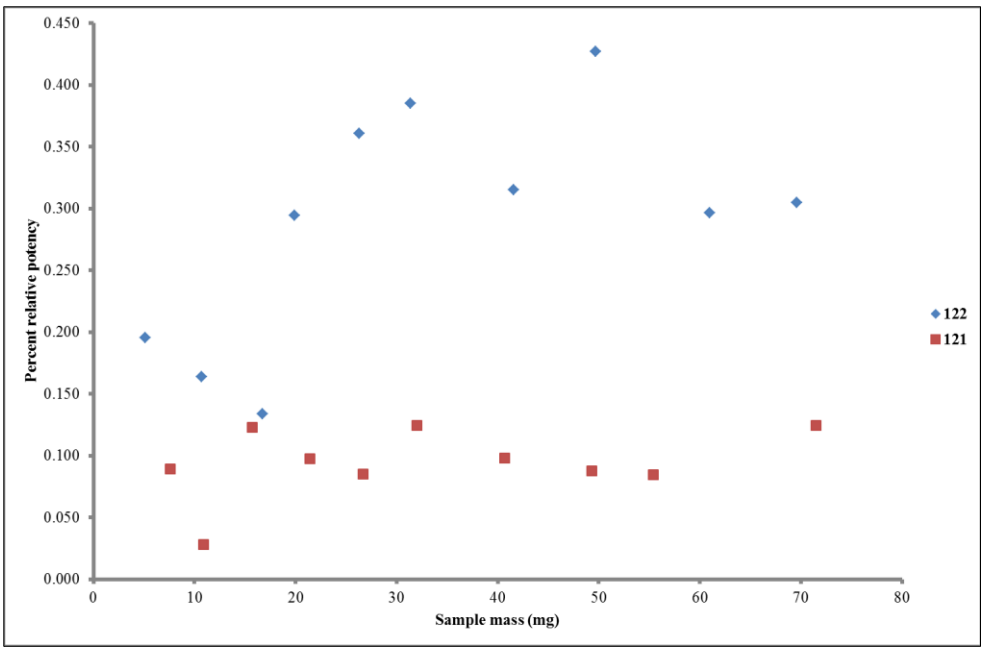

Figure 5.13: Variation in % relative potency as it changes with sample mass. One replication of antibacterial activity per material was performed with each type of bacteria.

Penicillin V is a highly active antibiotic with percentage relative potency values in the region of 250% relative to cephalosporin C (Appendix III); this, coupled with the wide variation of the data stated above, prompted the question as to how much of the penicillin was being released from the materials. A hole plate assay of the activity of penicillin V in solution against *E. Coli* was performed by Apichat Aphaiwong (Appendix III), and from this

data, the moles of penicillin V released from the materials could be calculated (Table 5.2). The range of % relative potency based on the amount of penicillin V released was found to be 140-480% for **121** and 139-1201% for **122**. Interestingly, the moles of penicillin V released over the time course of the assay is actually only a small fraction of the number of moles loaded onto the materials. It is notable that, for both materials, the percentage of penicillin V released decreases exponentially as the sample mass increases (Figure 5.14), and this accounts for the observed trend of increasing % relative potency.

Table 5.2: Table displaying the calculated available amount of penicillin V compared with that released.

Mass of 121 (mg)	Total amount of penicillin V (µmoles)	Penicillin V released (nmoles)	% Penicillin released	Mass of 122 (mg)	Total amount of Penicillin V (µmoles)	Penicillin V released (nmoles)	% Penicillin released
7.6	1.06	0.90	0.085	5.1	0.92	1.30	0.141
10.9	1.53	0.40	0.026	10.7	1.94	1.65	0.085
15.7	2.20	1.55	0.071	16.7	3.02	1.80	0.060
21.4	3.00	1.60	0.053	19.9	3.60	2.40	0.067
26.7	3.74	1.65	0.044	26.3	4.76	2.70	0.057
32	4.48	2.00	0.045	31.4	5.68	2.85	0.050
40.7	5.70	2.00	0.035	41.6	7.53	2.90	0.039
49.3	6.90	2.05	0.030	49.7	9.00	3.20	0.036
55.4	7.76	2.10	0.027	61	11.0	3.10	0.028
71.5	10.0	2.50	0.025	69.6	12.6	3.20	0.025

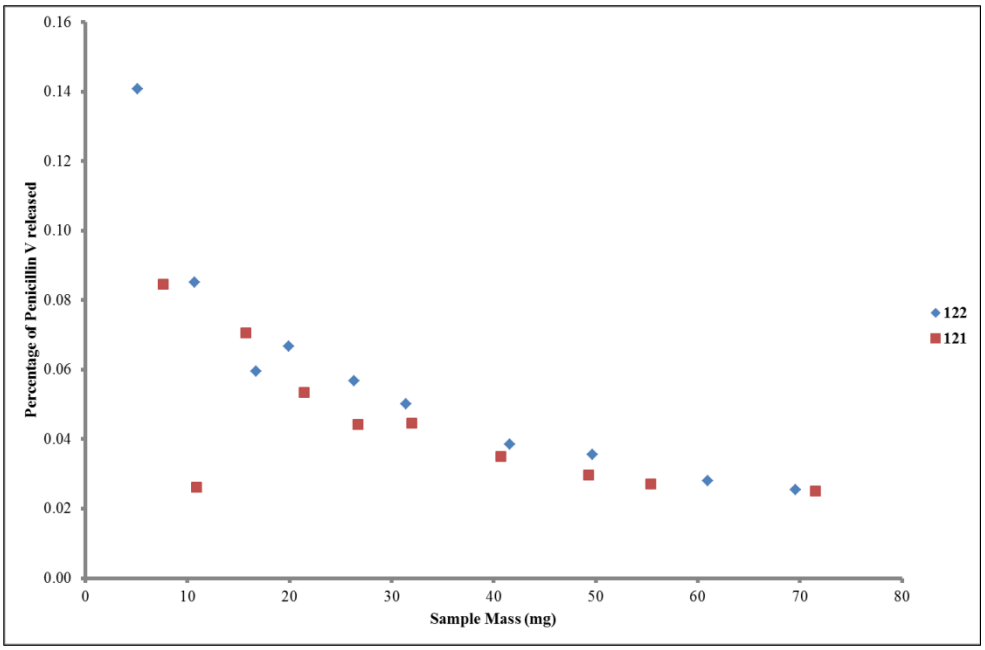

Figure 5.14: Release of penicillin from materials 121 and 122.

When the activity of the materials against *S. aureus* was tested, it was found that both materials had extremely potent activity and that the zone sizes observed far exceeded that of the standard calibration. Material **122** generated zone sizes all of which are approximately 41 mm, whilst amine-modified material **121** had slightly smaller zone sizes in the range of 31-41 mm. The complete data can be found in Table 6.20, Chapter 6, page 196. The range of % relative potencies based on the total amount of penicillin V present are 140-480 % and 149-640% for **121** and **122**, respectively (Figure 5.15). The variation in values is wide, with amine **121** showing generally lower relative potencies and less variation with the exception of one data point. The amount of penicillin V released could not be determined since the penicillin V in solution proved to be too potent to obtain the necessary results.

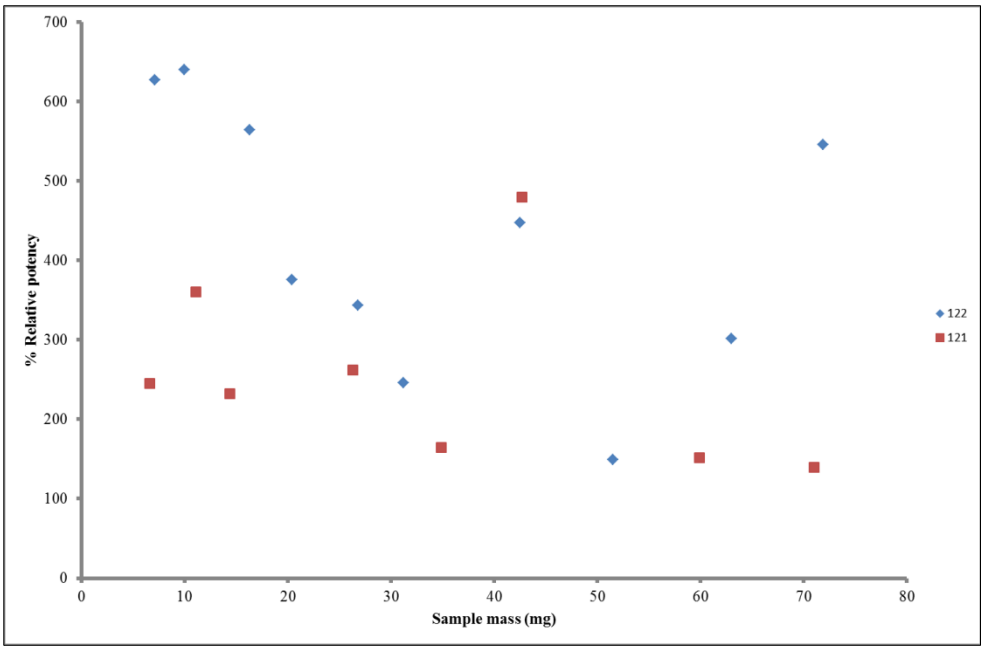

Figure 5.15: Variation of % relative potency with sample mass.

5.2.1 Conclusions

The bioassay experiments revealed that both materials are active against *E. coli* and *S. aureus*, with **122** which was based on unmodified XAD-4, showing slightly increased activity against both strains of bacteria; this may be a consequence of the higher loading of penicillin on **122** or it may be due to the different method by which the penicillin was being bound, with the electrostatic binding of amine polymer **121** leading to a slower and more controlled release. Comparison of the activity against *E. coli* with that of penicillin V in solution showed that the amount of penicillin needed to generate the activity by the materials was far less than the amount loaded onto the surface. In addition, a trend of decreasing relative potency and percentage of penicillin V released with increasing sample mass was observed in both materials. This trend may be due to surface exposure of the beads to the agar-bacteria gel. Different masses of beads were all placed in wells of the same size (1 cm diameter) so that as the sample mass increased the contact area decreased, consequently the core of the beads are not in such efficient contact with the agar. This

preliminary work was successful in showing that penicillin V is still active when absorbed into XAD-4 based materials.

5.3 Summary

This thesis has demonstrated surface modification of polystyrenes by carbene insertion, followed by diazonium coupling, is a simple and successful method to prepare a collection of materials that share bulk properties and yet differ in their surface chemistry. Further reaction of a selection of the functional surfaces were carried out, including hydrolysis of the phosphonate diester group and conversion of amine-terminated surface **116i** to dimethyl amine **116d**. It has also been shown that the surface chemistry influences protein adsorption on two different polystyrene substrates.

TGA, DSC and SEM analysis of modified XAD-4 materials confirmed that the polymers shared the same thermal properties as untreated XAD-4, within the temperature ranges analysed, and that the physical nature of the beads was maintained during the chemical modifications. XPS and ATR-IR spectroscopic analysis provided conformation of the presence of the functional groups and elements expected after modification. However, it is notable that iodine could not be detected by XPS on the XAD-4 based material **116c**; conversely, combustion analysis successfully detected iodine at high percentage and the strong dark purple colour of the linker coupled material was indicative of successful modification. A similar occurrence was observed on penicillin-loaded materials **121** and **122**, where sulphur was detected by combustion analysis but not by XPS. Combustion analysis of the linker-coupled XAD-4 materials **115** and **116a-m** also confirmed successful modification of XAD-4 by the detection of nitrogen after the carbene insertion and diazonium coupling, and phosphorous analysis was similarly effective when applicable. This also provided information concerning the loadings of the surface chemistry, which ranged

from 0.038 mmol/g to 0.357 mmol/g. When these loadings were compared to those of their directly coupled counterparts, that were prepared without the electrophilic linker, they were found to be consistently larger. This combined with the intense colouration of the linker coupled materials indicates that the linker facilitates diazonium coupling resulting in the highly coloured azo linkage. When the linker molecule it is not used, as in materials **117a-m**, physisorption of the diazonium salts is probably operating. Chemical modification of spun polystyrene films on gold and glass was also conducted and XPS was used to show that addition of the requisite functional groups was successful.

QCM-D was employed to monitor BSA adsorption of the different functional surfaces based on polystyrene films. The experiments revealed that all of the surfaces performed differently, suggesting that chemical surface functionality does influence adsorption, however, the adsorption of BSA could not be differentiated from the adsorption of water and ions from the PBS solution. The protein assay, based on changes in optical density of BSA/PBS solutions, performed on the XAD-4 materials **115** and **116a-m** proved to be more conclusive, since the change in optical density corresponded directly to the amount of protein adsorbed. Again, the materials all performed differently with interesting time-course behaviour and relationships with contact angle and % polar surface area (PSA) of the functional groups were established. It was concluded that surface hydrophilicity influenced protein adsorption initially, with a general trend of increasing protein adsorption with increasing surface contact angle and so hydrophobicity. However, over time the strength of the interactions between the protein binding sites and the surface functional groups became more dominant and any correlation with contact angle was lost. Comparison of protein adsorption with % PSA demonstrated that in the first 12 hours increasing % PSA resulted in increased protein adsorption in two groups of materials relating to two different binding sites on BSA, however by 24 hours the correlation was lost.

Preliminary investigations into the use of the functional materials for drug delivery and antibacterial materials was carried out, where amine-terminated material **116i** and untreated XAD-4 were exposed to penicillin V. The resulting materials **121** and **122** were assayed using the hole plate method and exhibited activity against *E. coli* and *S. aureus*, Gram-negative and Gram-positive bacterium respectively. Future work in this will aim to determine the role of the amine functionality in binding the penicillin as well as controlling its release. Furthermore, an alternative assay such as a broth assay may give more conclusive results quantifying the materials' activity.

Chapter 6: Experimental

Protocols not carried out by Emily Parker have been indicated by †, but these protocols have been included for information since Emily Parker conducted all the analysis and the results are discussed in detail in this thesis.

6.1 General procedures and equipment

Reactions were carried out in oven dried flasks open to the atmosphere using standard solvents, petrol refers to petroleum ether with boiling point 40-60 ˚C; dry solvents and inert nitrogen atmosphere were only used when indicated in the experimental procedures. Dry THF was obtained by passage through a dry alumina column. Water refers to the use of de-ionised water. Where necessary, temperatures below room temperature were achieved using cooling baths; ice/NaCl/water (-5 ˚C) ice/water (0 ˚C) and acetone/CO_2(s) (-78 ˚C). When possible, reactions were followed with thin layer chromatography (TLC) with Merck aluminium foil backed sheets pre-coated with 0.2 mm Kieselgel 60 F_{254} silica gel, product spots were visualised with UV fluorescence (λ_{max} 254 nm). Column chromatography was performed with Merck Geduran Si 60 silica gel (0.040-0.063 mm). Solvents were evaporated under reduced pressure at 40 ˚C on a Buchi Rotavapor R-210 with a Vacuubrand CVC2 pump and pressure control system.

Characterisation of compounds was done using the following equipment and settings. Melting points were measured with a Stuart Scientific SMP1 melting point apparatus. UV-visible spectra were obtained with a Perkin-Elmer UV Lamda 14P spectrometer with solutions in DCM; the path length is 1 cm and the data is reported in nanometers (nm) with the molar extinction coefficients ($dm^3mol^{-1}cm^{-1}$). Infrared (IR) spectra were recorded on a Bruker Tensor 27 FT-IR spectrometers; selected absorption maxima are reported in

wavenumbers (cm^{-1}). ^{1}H NMR were recorded on Bruker DPX200 (200 MHz), DPX400 (400 MHz), DQX400 (400 MHz) and AVC500 (500 MHz) spectrometers and COSY were obtained on a Bruker DQX400 and AVC500. ^{13}C NMR were recorded on DQX400 (100 MHz) and AVC500 (125 MHz) spectrometers, HMBC, HSQC HMQC and DEPT spectra were obtained with these instruments also. Chemical shifts (δ_H, δ_C) are reported in parts per million (ppm), coupling constants (*J*) are in hertz (Hz) and the following abbreviations are used: s (singlet), br s (broad singlet), d (doublet), dd (doublet doublet), t (triplet), q (quartet), m (multiplet), app. (apparent). Low resolution mass spectra (*m/z)* were obtained with a Fisons Platform spectrometer with electrospray ionisation (ESI) and a Fisons AutoSpec-oaTpf spectrometer with field ionisation (FI). A Bruker microTOF was used to obtain high resolution mass spectra; *m/z* values are reported in Daltons and their intensities are a function of the base peak.

Surface characterisation discussed in Chapter 3 was carried out with the following equipment: XPS was performed on a lab built spectrometers at 10^{-9} – 10^{-10} Torr, with an Al K-α X-ray source (1486.6 eV); contact angle analysis was conducted with an IT concepts Tracker Drop Shape Analysis and the angles presented are an average of the two sides of the droplet; a Picometer Ellipsometer, Beaghole Instruments and Igor Pro software were used to carry out ellipsometry analysis, three measurements per sample were conducted over a range of 30 to 80˚, and a Mitutoyo microscope with Nplan Apolo magnification accessory was used to capture images of the substrates, images are 460 μm wide. QCM-D was performed with an E1 QCM-D instrument with Q-soft software, and Q-tools software was used to process the data.

Characterisation of the materials described in Chapter 4 was performed with following instruments; XPS spectroscopy was carried out on a Kratos Axis Ultra Spectrometer with a

monochromatic Al–Kα (1486.71 eV) X-ray source, the surface wide scans were recorded with a pass energy of 160 eV and elemental narrow scans were obtained with 40 eV; Bio-Rad FTS-6000 was used to conduct ATR-IR analysis of the materials with a diamond screw tip accessory; a JSM6360A JEOL scanning electron microscope was used to image the surfaces of the XAD-4 beads and TA Instruments Q2950, Q500 and DSC Q10 were used to carry out the thermal analysis of the materials with the Q2950 and Q500 instruments being used for TGA analysis. XPS spectroscopy of penicillin materials **121** and **122** was performed by Cardiff Catalysis Institute and all combustion analysis of all the materials was provided by MEDAC Ltd. (www.medacltd.com).

6.2 Chapter 2

6.2.1 Organic coatings and amines used for diazonium salt synthesis

The numbering system that has been used in the NMR data description of some compounds differs to that used for their names, the numbering system is displayed in Figure 6.1. Other compounds have been assigned according to their compound names.

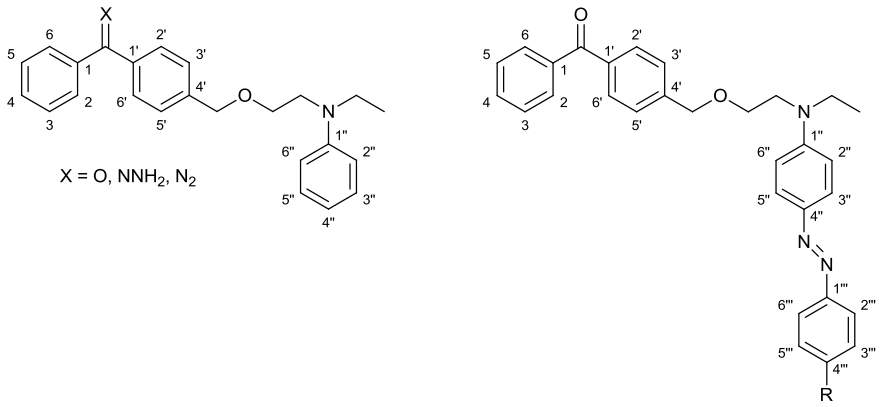

Figure 6.1

In the case of *para* substituted benzene moieties, the resonances have been described as apparent (app.) doublets. AA'XX' coupling is expected but there is not enough fine structure

in the NMR spectra, however the broad base of the doublet suggests that the resonances are not just straightforward doublets.

(4-((2′-(Ethyl(phenyl)amino)ethoxy)methyl)phenyl)(phenyl)methanone 87[81]

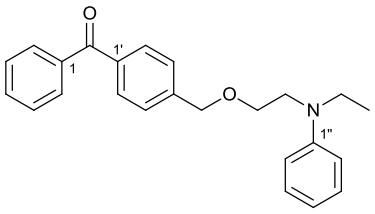

This procedure was carried out under an nitrogen inert atmosphere using dry THF. A solution of 2-(*N*-ethylanilino)ethanol) (3.32 g, 20.0 mmol) in THF (20 ml) was added to sodium hydride (0.74 g, 31.0 mmol) in THF (10 ml) at – 78 ˚C. The mixture was warmed to room temperature then stirred for 30 minutes after which it was re-cooled to 0 ˚C. A solution of 4-methylbromobenzophenone[60] (4.95 g, 17.8 mmol) in THF (20 ml) was added through a cannula, the mixture warmed to room temperature and then stirred for 72 hours. The THF was removed *in vacuo* then the reaction was quenched with sat. aq. $NaHCO_3$ (20 ml). The resulting mixture was extracted with DCM (15 ml), after which the organic phase was washed with water (2 x 20 ml), dried over $MgSO_4$ then filtered and concentrated to a dark green oil (8.32 g). Purification via column chromatography (eluent 9:1 petrol:EtOAc) gave **87** as a yellow oil (4.59 g, 72%). R_f 0.45 in 6:1 petrol:EtOAc; ν_{max}/cm^{-1} 2970 (C-H), 1926, 1818, 1652 (C=O), 1505; δ_H (400 MHz, $CDCl_3$) 1.21 (3H, t *J* 7.1, $NCH_2C\underline{H}_3$), 3.48 (2H, q *J* 7.1, $NC\underline{H}_2CH_3$), 3.61 (2H, t *J* 6.2, $OCH_2C\underline{H}_2N$), 3.73 (2H, t *J* 6.2, $OC\underline{H}_2CH_2N$), 4.65 (2H, s, $ArC\underline{H}_2O$), 6.70 (1H, t *J* 7.2, H-4′′), 6.75 (2H, d *J* 8.3, H-2′′, 6′′), 7.26 (2H, app. t *J* 7.8, H-3′′, 5′′), 7.46-7.53 (4H, m, H-3′, 5′, 3, 5), 7.62 (1H, t *J* 7.4, H-4), 7.83 (4H, app. d *J* 7.3, H-2′, 6′, 2, 6); δ_C (100 MHz, $CDCl_3$) 12.2 ($NCH_2\underline{C}H_3$), 45.5 ($N\underline{C}H_2CH_3$), 50.1 ($OCH_2\underline{C}H_2N$), 68.5 ($O\underline{C}H_2CH_2N$), 72.7 ($Ar\underline{C}H_2O$), 111.8 (C-2′′, 6′′), 115.8 (C-4), 127.1, 128.3, 129.4, 130.1 and 130.3 (C-3′′, 5′′, 2′, 3′, 5′, 6′, 2, 3, 5, 6), 132.4 (C-4), 136.8 and 137.8 (C-1′, 1),

143.2 (C-4'), 147.7 (C-1''), 196.4 (C=O); *m/z* (ESI^+) 382 ($[M+Na]^+$, 40%), 360 ($[M+H]^+$, 100%.

(4-((2'-(Ethyl(phenyl)amino)ethoxy)methyl)phenyl)(phenyl)hydrazone 88[81]

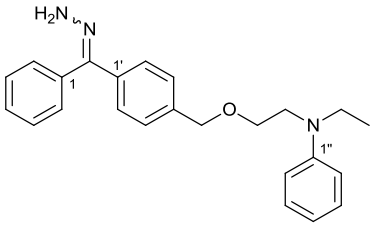

Hydrazine monohydrate (2 ml, 4.2 mmol) was added to a solution of **87** (3.10 g, 8.36 mmol) in EtOH (15 ml) and the mixture was heated to reflux. Analysis by mass spectrometry after 16 hours showed complete consumption of **87** so the reaction mixture was cooled to room temperature. Water (5 ml) was added then the EtOH was removed *in vacuo*. DCM (10 ml) was added to the residue and the solution was washed with water (3 x 10 ml), then dried over $MgSO_4$ and filtered. Concentration *in vacuo* gave a 1:1 mixture of two diastereoisomers in the form of a colourless oil (3.12g, 91%). ν_{max}(film)/cm^{-1} 3406 (N-H), 3026 (N-H), 2866 (C-H), 1598 (C=N); δ_H (400 MHz, $CDCl_3$) 1.41-1.22 (3H, m, NCH_2CH_3), 3.40-3.50, 3.52-3.55, 3.59-3.67 and 3.73-3.76 (6H, 4 x m, NCH_2CH_3 and OCH_2CH_2N), 4.53 (1H, s, 0.5 x $ArCH_2O$), 4.62 (1H, s, 0.5 x $ArCH_2O$), 6.65-6.75 (3H, m, H-2'', 4'', 6''), 7.20-7.32 (7H, m, H-3'', 5'', 2', 6', 2, 4, 6), 7.46-7.57 (4H, m, H-3', 5', 3, 5); δ_C (100 MHz, $CDCl_3$) 12.2 (NCH_2CH_3), 45.5 (NCH_2CH_3), 50.1, 68.0 and 68.4 (OCH_2CH_2N and OCH_2CH_3N), 73.0 and 73.1 ($ArCH_2O$), 111.7 and 111.8 (C-2'', 6''), 115.7 and 115.8 (C-4''), 126.5, 126.5, 127.4, 128.1, 128.5, 128.8, 128.9, 129.3, 129.3 and 129.4 (C-2, 3, 5, 6, 2', 3', 5', 6', 3'' and 5''), 132.2, 132.9, 137.9, 138.2, 138.4, 139.2 and 147.7 (C-1, 1', 4', 1''), 149.0 and 149.1 ($C=NNH_2$); *m/z* (ESI^+) 374 ($[M+H]^+$, 100%).

(4-((2ˈ-(Ethyl(phenyl)amino)ethoxy)methyl)phenyl)(phenyl)methanol 89

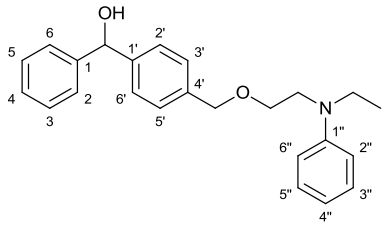

Alcohol **89** was generated as a by-product in the conversion of benzophenone **87** to hydrazone **88**. **89** could not be isolated, it was only observed in the product mixture. δ_H (400 MHz, $CDCl_3$) 1.16-1.22 (3H, m, $NCH_2C\underline{H}_3$), 2.33 (1H, d *J* 3.4, $Ar_2CHO\underline{H}$), 3.41-3.49, 3.54-3.62 and 3.65-3.75 (3 x m, 6H, $N\underline{C}H_2CH_3$, $OC\underline{H}_2C\underline{H}_2N$), 4.54 (2H, s, $ArC\underline{H}_2O$), 5.87 (1H, d *J* 3.4, $C\underline{H}OH$), 6.67-6.76 (3H, m, H-2ˈˈ, 4ˈˈ, 5ˈˈ), 7.21-7.27, 7.30-7.34 and 7.37-7.44 (3 x m, H-3ˈˈ, 6ˈˈ, 2ˈ, 3ˈ, 5ˈ, 6ˈ, 2, 3, 4, 5, 6); δ_C (100 MHz, $CDCl_3$) 12.2 ($NCH_2\underline{C}H_3$), 45.5 ($N\underline{C}H_2CH_3$), 50.1, 68.0 and 68.4 ($OCH_2\underline{C}H_2N$ and $OCH_2\underline{C}H_3N$), 73.0 and 73.1 ($Ar\underline{C}H_2O$), 111.7 and 111.8 (C-2ˈˈ, 6ˈˈ), 76.1 $Ar_2\underline{C}HOH$, 115.7 and 115.8 (C-4ˈˈ), 126.5, 126.5, 127.4, 128.1, 128.5, 128.8, 128.9, 129.3, 129.3 and 129.4 (C-2, 3, 5, 6, 2ˈ, 3ˈ, 5ˈ, 6ˈ, 3ˈˈ and 5ˈˈ), 132.2, 132.9, 137.9, 138.2, 138.4, 139.2 and 147.7 (C-1, 1ˈ, 4ˈ, 1ˈˈ), 149.0 and 149.1 ($\underline{C}$=NNH_2); *m/z* (ESI^+) 362 ($[M+H]^+$, 100%).

(4-((2ˈ-(Ethyl(phenyl)amino)ethoxy)methyl)phenyl)(phenyl)diazo 65[138]

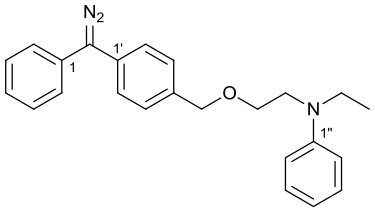

Manganese (IV) oxide (activated 98%) (1.38 g, 15.6 mmol), potassium hydroxide (0.361 g, 6.43 mmol) and sodium sulphate (1.24 g, 8.73 mmol) were added to a stirring solution of hydrazone **88** (2.25 g, 6.00 mmol) in MeOH (30 ml). The mixture was stirred in the dark for

3 hours after which analysis by mass spectrometry showed complete consumption of starting material **88**. The methanol was removed *in vacuo* and then DCM was added (30 ml). The mixture was filtered through a celite plug and the filtrate was washed with water (20 ml), dried over $MgSO_4$, filtered and concentrated to give the product **65** as a dark pink oil (2.13 g, 96%). ν_{max}(neat)/cm^{-1} 2866 (C-H), 2038 (N=N=N); δ_H (400 MHz, $CDCl_3$) 1.18 (3H, t *J* 7.0, $NCH_2C\underline{H}_3$), 3.45 (2H, q *J* 7.0, $NC\underline{H}_2CH_3$), 3.57 (2H, t *J* 6.4, $OCH_2C\underline{H}_2N$), 3.69 (2H, t *J* 6.4, $OC\underline{H}_2CH_2N$), 4.55 (2H, s, $ArC\underline{H}_2O$), 6.66-6.73 (3H, m, H-2'', 4'', 6''), 7.19-7.25, 7.27-7.32 and 7.36-7.43 (11H, 3 x m, C-2', 3', 5', 6', 2, 3, 4, 5, 6, 3'', 5''); δ_C (100 MHz, $CDCl_3$) 12.1 ($NCH_2\underline{C}H_3$), 45.4 ($N\underline{C}H_2CH_3$), 50.1 ($OCH_2\underline{C}H_2N$), 68.0 ($O\underline{C}H_2CH_2N$), 68.0 ($Ar\underline{C}H_2O$), 111.7 (C-2'', 6''), 115.7 (C-4''), 125.2, 125.6, 128.6, 129.1 and 129.3 (C-2, 3, 4, 5, 6, 2' 3', 5', 6', 3'' and 5''), 128.9 ($\underline{C}(N_2)$), 129.6 (C-1', 1), 135.7 (C-4'') and 147.7 (C-1''); *m/z* (ESI^+) 372 ($[M+H]^+$, 100%).

***tert*-Butyl(4-hydroxyphenyl)carbamate 93**[86]

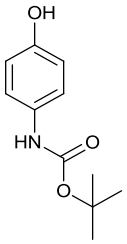

A solution of di-*tert*-butyl dicarbonate (1.10 g, 5.04 mmol) in THF (10 ml) was added portion wise to a stirring solution of 4-aminophenol **92** (5.06 g, 4.58 mmol) and Na_2CO_3 (4.85 g, 13.7 mmol) in THF (50 ml) at 0 ˚C. The mixture was warmed to room temperature then stirred for 17 hours. The THF was removed *in vacuo* then the resulting solid dissolved in DCM (20 ml) and washed with water (4 x 20 ml). The organic phase was dried over $MgSO_4$, filtered and concentrated to **93** as a white/brown solid (8.61 g, 90%). mp 139-141 ˚C {lit. [139] mp 144-145 ˚C}; ν_{max}(neat)/cm^{-1} 3360 (N-H/O-H), 1697 (C=O); δ_H (400 MHz,

$CDCl_3$) 1.52 (9H, s, C(C<u>H</u>$_3$)$_3$), 5.18 and 6.34 (2H, 2 x br s, O<u>H</u> and N<u>H</u>), 6.75 (2H, app. d *J* 8.5, H-3, 5) 7.18 (2H, app. d *J 8.5*, H-2, 6); δ_C (100 MHz, $CDCl_3$) 28.3 (C(<u>C</u>H$_3$)$_3$), 80.8 (<u>C</u>(CH$_3$)$_3$), 115.7 (C-3, 5), 121.2 (C-2, 6), 131.0 (C-1), 151.9 (C-4), 153.4 (<u>C</u>=O); *m/z* (ESI^-) 208 ($[M-H]^-$, 100%).

***tert*-Butyl(4-(2-(2-(2-methoxyethoxy)ethoxy)ethoxy)phenyl)carbamate 94**[87]

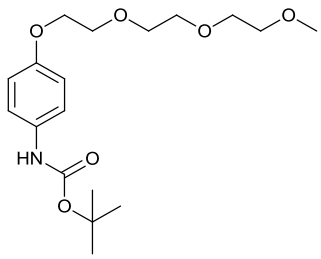

Portions of *tert*-butyl(4-hydroxyphenyl)carbamate **93** (202 mg, 0.97 mmol), 2-(2-(2-methoxyethoxy)ethoxy)ethyl 4-methylbenzenesulfonate **96** (307 mg, 0.97 mmol) and potassium carbonate (283 mg, 1.94 mmol) were combined in acetonitrile (15 ml) then heated to reflux for 21 hours. The reaction mixture was cooled to room temperature then filtered and the filtrate concentrated *in vacuo* to a brown liquid (363 mg, 95%). ν_{max}(neat)/cm^{-1} 3325 (N-H), 2875 (C-H), 1715 (C=O); δ_H (400 MHz, $CDCl_3$) 1.50 (9H, s, C(C<u>H</u>)$_3$)$_3$, 3.38 (3H, s, OC<u>H</u>$_3$), 3.54-3.56, 3.64-3.69 and 3.72-3.74 (8H, 3 x m, 2 x H-1'', 2'', 1''', 2'''), 3.83 (2H, t *J* 4.8, 2 x H-2'), 4.09 (2H, t *J* 4.8, 2 x H-1'), 6.43 (1H, br s, N<u>H</u>), 6.84 (2H, app. d *J* 8.5, H-3, 5), 7.25 (2H, app. d *J* 8.5, H-2, 6); δ_C (100 MHz, $CDCl_3$) 28.4 (C(<u>C</u>H$_3$)$_3$), 59.0 (O-<u>C</u>H$_3$), 67.7 (C-1'), 69.8 (C-2'), 70.5, 70.6, 70.8, 71.9 and 76.7 (C-1'', 2'', 1''', 2'''), 80.2 (<u>C</u>(CH$_3$)$_3$), 115.0 (C-3, 5), 120.4 (C-2, 6), 131.6 (C-1), 153.1 (C-4), 154.8 (<u>C</u>=O); *m/z* (ESI^+) 378 ($[M+Na]^+$, 100%); HRMS (ESI^+) $C_{18}H_{29}NNaO_6^+$, ($[M+Na]^+$) requires 378.1887 where found 378.1889.

4-(2-(2-(2-Methoxyethoxy)ethoxy)ethoxy)aniline 90f[87]

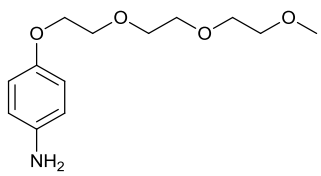

A mixture of *tert*-butyl (4-(2-(2-(2-methoxyethoxy)ethoxy)ethoxy)phenyl)carbamate **94** (2.84 g, 8 mmol) in 6:1 TFA:DCM (18 ml) was stirred at room temperature for 4 hours. The reaction was quenched with 5% aq. NaOH and the organic phase extracted. The aqueous layer was washed with DCM (2 x 10 ml) and the combined organic fractions were dried over $MgSO_4$, filtered and concentrated *in vacuo* to a brown oil (1.66 g). Purification *via* silica column chromatography (eluent EtOAc) gave **90f** as a brown liquid (1.32 g, 65%). R_f 0.16 (2:1 petrol:EtOAc); ν_{max}(neat)/cm^{-1} 3355 (N-H), 2875 (C-H), 1350 (ArC-N), 1235 (ArC-O), 1107 (C-O); δ_H (400 MHz, $CDCl_3$) 3.38 (3H, s, OC<u>H</u>$_3$), 3.54-3.56, 3.64-3.69 and 3.72-3.74 (8H, 3 x m, 2 x H-1'', 2'', 1''', 2'''), 3.81 (2H, t *J* 5.0, 2 x H-2'), 4.05 (2H, t *J* 5.0, 2 x H-1'), 6.62 (2H, app. d *J* 8.6, H-2, 6), 6.75 (2H, app. d *J* 8.6, H-3, 5); δ_C ($CDCl_3$, 100 MHz) 59.0 (O<u>C</u>H$_3$), 68.1 (C-1'), 69.9 (C-2'), 70.5, 70.6, 70.8 and 71.9 (C-1'', 2'', 1''', 2'''), 115.6 and 116.3 (C-2, 3, 5, 6); 140.2 (C-1), 151.9 (C-4); *m/z* (ESI^+) 511 ($[2M+H]^+$, 100%), 278 ($[M+Na]^+$, 100%) and 256 ($[M+H]^+$, 50%).

2-(2-(2-Methoxyethoxy)ethoxy)ethyl 4-methylbenzenesulfonate 96[88]

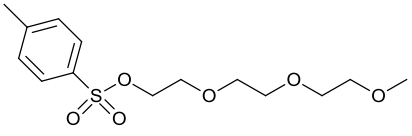

A portion of NaOH (2.14 g, 53.5 mmol) was added to a stirring mixture of triethylene glycol monomethyl ether (5.8 ml, 36.0 mmol), THF (40 ml) and water (20 ml). The mixture was cooled to 0 ˚C then *p*-toluenesulfonyl chloride (7.41 g, 38.9 mmol) was added slowly after

which the mixture was stirred at 0˚C for 4 hours. Water was added to the mixture then the organic phase separated and the aqueous layer extracted with DCM (3 x 15 ml). The combined organic fractions were washed with 1 M HCl (15 ml) then brine (15 ml) after which the organic fraction was dried over $MgSO_4$, filtered and concentrated to a mixture of a white solid and yellow oil (7.12 g, 62 %). The crude product mixture was purified *via* silica column chromatography (eluent 3:1 petrol:EtOAc then EtOAc) to afford **96** as a colourless liquid (3.62 g, 31%). R_f 0.85 (2:1 petrol:EtOAc); ν_{max}(neat)/cm^{-1} 2879 (C-H), 1356 (S=O), 1247 (C-O), 1177 (S=O), 1018(C-O); δ_H (400 MHz, $CDCl_3$) 2.39 (3H, s, Ar-C$\underline{H}_3$), 3.31 (3H, s, OCH_3), 3.46-3.48 and 3.53-3.57 (8H, 2 x m, 2 x H-1'', 2'', 1''', 2'''), 3.63 (2H, t *J* 4.9, 2 x H-2'), 4.10 (2H, t *J* 4.9, 2 x H-1'), 7.29 (2H, app. d *J* 8.1, H-3, 5), 7.74 (2H, app. d *J* 8.1, H-2, 6); δ_C (100 MHz, $CDCl_3$) 21.6 (Ar-CH_3), 58.9 (OCH_3), 68.6, 29.3, 70.5, 70.5, 70.6, 71.8 (C-1', 2'. 1'', 2'', 1''', 2'''); 127.9 (C-2, 6), 129.8 (C-3, 5), 132.9 (C-4), 144.8 (C-1); m/z (ESI+)341 ($[M+Na]^+$, 75%).

Diethyl 4-nitrobenzylphosphonate 98[89]

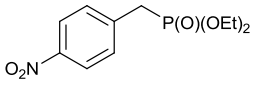

Triethyl phosphite (2 ml, 11.7 mmol), tetrabutyl ammonium iodide (132 mg, 0.36 mmol) and 4-nitrobenzyl bromide (1.09 g, 5.05 mmol) were combined and stirred at 120 ˚C for 4.5 hours. The mixture was cooled to room temperature then purified *via* silica column chromatography (eluent 4:1 petrol:EtOAc) to yield **98** as a yellow liquid (1.07 g, 78%). R_f 0.27 4:1 petrol:EtOAc; ν_{max}(neat)/cm^{-1} 2985 (C-H), 1520 (N-O asym.), 1348 (N-O sym.), 1249 (P=O), 967 (P-O); δ_H (400 MHz, $CDCl_3$) 1.20 (6H, t J_{HH} 7.1, 2 x OCH_2CH_3), 3.20 (2H, d J_{HP} 22.4, $ArCH_2P$), 3.96-4.03 (4H, m, 2 x OCH_2CH_3), 7.42 (2H, app. dd J_{HH} 8.7 J_{HP} 2.3, H-2, 6), 8.11 (2H, app. d J_{HH} 8.7, H-3, 5); δ_C (100 MHz, $CDCl_3$) 16.3 (d J_{CP} 6.0, 2 x

OCH_2CH_3), 33.8 (d J_{CP} 136.1, $ArCH_2P$), 62.4 (d J_{CP} 7.0, 2 x OCH_2CH_3), 123.6 (d J_{CP} 3.0, C-2, 6), 130.6 (d J_{CP}, 6.0, C-3, 5), 139.7 (d J_{CP} 9.1, C-1), 146.9 (d J_{CP} 4.0, C-4); m/z (ESI^-) 272 ($[M-H]^-$, 100%).

Diethyl 4-aminobenzylphosphonate 90h[90]

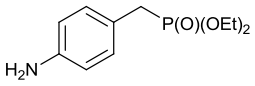

Tin (II) chloride di-hydrate (333 mg, 1.48 mmol) and conc. HCl (0.2 ml, 6.58 mmol) were added to a stirring solution of diethyl 4-nitrobenzylphophonate **98** (140 mg, 0.513 mmol) in EtOH (15 ml). The mixture was heated to reflux for 3 hours then cooled to room temperature before the pH was adjusted to 8-9 using 5% aq. NaOH. The mixture was extracted with $CHCl_3$ (3 x 20 ml) and the combined organic fractions washed with water (40 ml) then brine (40 ml). The resulting organic solution was dried over $MgSO_4$, filtered and concentrated *in vacuo* to give **90h** as a yellow solid (67.1 mg, 74%). R_f 0.39 (EtOAc); mp 84-85 ˚C{lit. mp[90] 93-95 ˚C}; ν_{max}(neat)/cm^{-1} 3430 (N-H), 2980 (C-H), 1615, 1225 (P=O), 1050 (P-O), 965, 850; δ_H (400 MHz, $CDCl_3$) 1.24 (6H, t J_{HH} 7.1, $P(O)(OCH_2C\underline{H}_3)_2$), 3.1 (2H, d J_{HP} 20.9, $ArC\underline{H}_2P$), 3.95-4.05 (4H, m $P(O)(OC\underline{H}_2CH_3)_2$), 6.64 (2H, app. d J_{HH} 8.4, H-3, 5), 7.08 (2H, app. dd J_{HH} 8.4 J_{HP} 2.4, H-2, 6); δ_C ($CDCl_3$, 100 MHz) 16.4 (d J_{CP} 6.0, $P(O)(OCH_2\underline{C}H_3)_2$, 32.7 (d J_{CP} 138.8, $Ar\underline{C}H_2P$), 62.0 (d J_{CP} 7.0, $P(O)(O\underline{C}H_2CH_3)_2$), 115.3 (d J_{CP} 3.0, C-3, 5), 121.0 (d J_{CP} 10.1, C-1), 130.6 (d J_{CP} 7.0, C-2, 6), 145.2 (C-4); m/z(ESI^-) 242 ($[M-H]^-$, 100%).

H-acid test

A sample of the diazonium salt solution (1 ml) was removed and the pH adjusted to pH 4 with sodium acetate. H-acid, (4-amino-5-hydroxy-2,7-napthalene disulfonic acid) (1 mg) was added to the pH adjusted salt solution resulting in a suspension. After thorough mixing

the suspension was left to stand at room temperature for 15 minutes. In the presence of the diazonium salt the suspension turned from pale brown to dark purple.

General Procedure 1: Preparation of diazonium salts 91a-c, e-j[140]

a	R = *t*-Bu
b	R = C_6H_{13}
c	R = I
e	R = H
f	R = $O(CH_2CH_2O)CH_3$
g	R = OH
h	R = $CH_2P(O)(OEt)_2$
i	R = NH_2
j	R = CH_2COOH

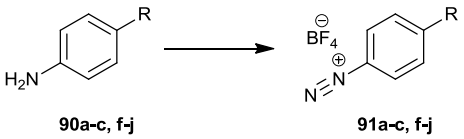

90a-c, f-j **91a-c, f-j**

a	R = *t*-Bu
b	R = C_6H_{13}
c	R = I
e	R = H
f	R = $O(CH_2CH_2O)CH_3$
g	R = OH
h	R = $CH_2P(O)(OEt)_2$
i	R = NH_2
j	R = CH_2COOH

A stirring solution of the amine (1 eq) in EtOH was cooled to -5 ˚C then isopentyl nitrite (1 eq) and tetrafluoroboric acid (2 eq) were added an the mixture was stirred for up to 1 hour until the colour change was complete and the colour had reached a constant level of intensity. H-acid test confirmed presence of the diazonium salt. The diazonium salts were used immediately

6.2.2 Diazonium coupling in solution

(*E*)-(4-((2'-(ethyl(4''-((4'''-hexylphenyl)diazenyl)phenyl)amino)ethoxy)methyl)phenyl)(phenyl)methanone 100b

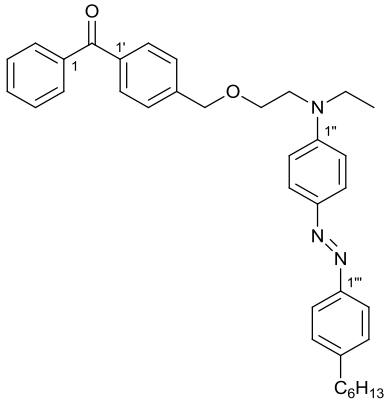

Procedure 2

A mixture of sodium nitrite (73 mg, 1.05 mmol) and conc. HCl (0.03 ml, 1 mmol) in Et_2O (2 ml) and water (4 ml) was stirred at 0 ˚C. 4-Hexyl aniline (0.15 ml, 1 mmol) was added and the solution was stirred at 0 ˚C for 1 hour. The H-acid test was used carried out to confirm presence of the diazonium salt. A solution of (4-((2'-(ethyl(phenyl)amino)ethoxy)methyl)phenyl)(phenyl)methanone **87** (358 mg, 1 mmol) in minimal Et_2O was added and the mixture stirred for 5 hours at 0 ˚C then at room temperature for 18 hours. The mixture was washed with water, dried over $MgSO_4$, filtered and concentrated. Purification by silica column chromatography (eluent 6:1 petrol:EtOAc) was carried to produce **100b** (200 mg, 37 %).

Procedure 3

A mixture of sodium nitrite (40 mg, 0.58 mmol) and conc. HCl (0.02 ml, 0.66 mmol) in water (1 ml) was stirred at 0 ˚C. A solution of 4-hexyl aniline (0.08 ml, 0.54 mmol) in THF (1 ml) was added to the sodium nitrite mixture and the solution was stirred at 0 ˚C for 1 hour then the H-acid test performed. **87** (109 mg, 0.30 mmol) in THF (1 ml) was added and the mixture stirred for 6 hours at 0 ˚C. The mixture was washed with water, dried over MgSO4, filtered and concentrated. Purification by silica column chromatography (eluent 5:1 petrol:EtOAc) produced **100b** in 64% yield.

Following Procedures 2-3 and General Procedure 4, **100b** was isolated as an orange oil. R_f 0.23 (6:1 petrol: EtOAc); $\lambda_{max}(CH_2Cl_2)$/nm 415 (34000 $mol^{-1}dm^3cm^{-1}$); ν_{max}/cm^{-1} 2928, 2856 (C-H), 1737, 1660 (C=O), 1600 (N=N), 1516, 1448, 1373, 1244, 1157, 1139, 1047; δ_H (400 MHz, $CDCl_3$) 0.90 (3H, t *J* 6.9, $C\underline{H}_3C_7H_{10}Ar$), 1.24 (3H, t *J* 7.1, $C\underline{H}_3CH_2N$), 1.31-1.68 (6H, m, $CH_3C\underline{H}_2C\underline{H}_2C\underline{H}_2C_2H_2Ar$), 1.61-1.69 (2H, m, $C_4H_9C\underline{H}_2CH_2Ar$), 2.67 (2H, t *J* 7.7, $C_5H_{11}C\underline{H}_2Ar$), 3.55 (2H, q *J* 7.1, $CH_3C\underline{H}_2N$), 3.66-3.69 (2H, m, $OCH_2C\underline{H}_2N$), 3.74-3.77

(2H, m, OC<u>H</u>$_2$CH$_2$N); 4.64 (2H, s, ArC<u>H</u>$_2$O), 6.77 (2H, app. d *J* 9.3, H-2'', 6''), 7.25-7.29 (2H, m, H-3''', 5'''), 7.44-7.50 (4H, m, H-3', 5', 3, 5), 7.59 (1H, t *J* 6.8, H-4), 7.76 (2H, app. d *J* 8.3, H-2''', 6'''), 7.78-7.81 (4H, m, H-2', 6', 2'', 6''), 7.85 (2H, app. d *J* 9.3, H-3'', 5''); δ_C (100 MHz, $CDCl_3$) 12.6 (<u>C</u>H$_3$C$_5$H$_{10}$Ar), 14.1 (CH$_3$<u>C</u>H$_2$C$_4$H$_8$Ar), 22.6 (CH$_3$CH$_2$<u>C</u>H$_2$C$_3$H$_6$Ar), 29.0 (C$_3$H$_7$<u>C</u>H$_2$C$_2$H$_4$Ar), 31.4 (C$_4$H$_9$<u>C</u>H$_2$CH$_2$Ar), 35.8 (C$_5$H$_{11}$<u>C</u>H$_2$Ar), 45.9 (<u>C</u>H$_3$CH$_2$N), 50.2 (OCH$_2$<u>C</u>H$_2$N), 68.3 (O<u>C</u>H$_2$CH$_2$N), 72.8 (O<u>C</u>H$_2$Ar), 111.2 (C-2'', 6''), 122.1 (2''', 6'''), 125.0 (3'', 5''), 127.0 (C-3', 5'), 128.3 (3''', 5'''), 129.0 (C-3, 5), 130.0 (C-4), 130.3 (C-2', 6'), 132.4 (C-2, 6), 136.9 (C-1, 1'), 142.9 (C-4'), 143.5 (C-1''), 144.7 (C-4'''), 150.0 (C-4''), 151.4 (C-1'''), 196.4 (<u>C</u>=O); *m/z* (ESI$^+$) 548.3 ([M+H]$^+$, 100%); HRMS (ESI$^+$) 548.3669 found, 548.3272 expected.

General Procedure 4: Diazonium coupling to benzophenone 87.

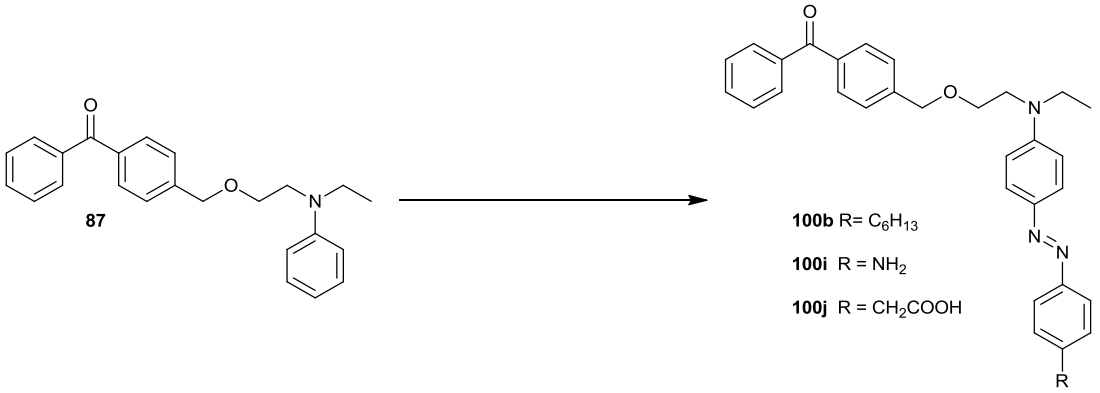

A mixture of sodium nitrite (1.1 eq) and conc. HCl (1.2 eq) in water (1 ml per mmol of amine) was stirred at 0 ˚C. A solution of amine (1 eq) in THF was added to the sodium nitrite mixture and the solution was stirred at 0 ˚C for 1 hour after which the H-acid test performed. Benzophenone **87** (0.5 eq) in THF was added and the mixture stirred for 6 hours at 0 ˚C and at room temperature for 18 hours. The mixture was washed with water, dried over $MgSO_4$, filtered and concentrated. Purification by silica column chromatography was performed furnishing the products **100b, i**, **j**, the yields are in Table 6.1 below.

Table 6.1: Table of yields resulting in diazonium coupling to 87.

Product	mmol of 87	% Yield
100b	0.303	64
100i	0.270	19
100j	0.290	10

(*E*)-(4-((2'-(ethyl(4''-((4'''-aminophenyl)diazenyl)phenyl)amino)ethoxy)methyl)phenyl)(phenyl)methanone 100i

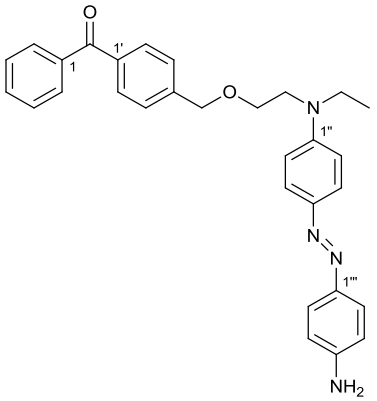

100i was isolated as a brown oil using General Procedure 4 and was purified by silica column chromatography (eluent 2:1 petrol:EtOAc). R_f 0.77 (2:1 petrol:EtOAc); λ_{max} (CH_2Cl_2)/nm 419 (1809 $mol^{-1}dm^3cm^{-1}$); ν_{max} (neat)/cm^{-1} 3200 (N-H), 2923 (C-H), 1656 (C=O), 1597 (N=N), 1513, 1447, 1393, 1352 (C-N), 1313, 1136, 768; δ_H (500 MHz, $CDCl_3$) 1.25 (3H, t *J* 7.1, $NCH_2C\underline{H}_3$), 3.53-3.61 (2H, m, $NC\underline{H}_2CH_3$), 3.67-3.72 (2H, m, $OCH_2C\underline{H}_2N$), 3.75-3.77 (2H, m, $OC\underline{H}_2CH_2N$), 4.64 (2H, $OC\underline{H}_2Ar$), 6.78 (2H, app. d *J* 9.4, H-2'', 6''), 6.78 (6H, m, H-3, 5, 3', 5', 2''', 6'''), 7.59 (1H, app. t *J* 6.8, H-4), 7.79-7.88 (8H, m, H-2, 6, 2', 6', 3'', 5'', 3''', 5'''); δ_C (125 MHz, $CDCl_3$) 12.2 ($NCH_2\underline{C}H_3$), 45.9 ($N\underline{C}H_2CH_3$), 50.1 ($OCH_2\underline{C}H_2N$), 68.5 ($O\underline{C}H_2CH_2N$), 72.8 ($O\underline{C}H_2Ar$), 111.2 (C-2'', 6''), 122.1-132.4 (14 x Ar$\underline{C}$H), 136.8-153.2 (7 x Ar$\underline{C}$), 196.4 ($\underline{C}$=O).

(*E*)-(4-((2′-(ethyl(4′′-((4′′′-phenyl acetic acid)diazenyl)phenyl)amino)ethoxy)methyl)phenyl)(phenyl)methanone 100j

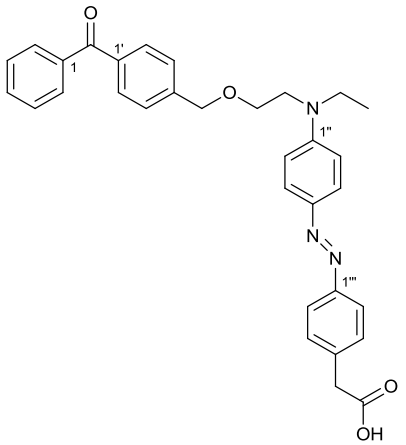

100j was prepared using General Procedure 4 and was purified using silica column chromatography (eluent 2:1 petrol:EtOAc to 10:1 EtOAc:MeOH) to give **100j** as a dark orange oil. $\lambda_{max}(CH_2Cl_2)$/nm 421 (21000 $mol^{-1}dm^3cm^{-1}$); ν_{max}(neat) /cm^{-1} 2965 (C-H), 2360, 1710 (C=O), 1656 (Ar_2C=O), 1599 (N=N), 1515, 1395 (C-N), 1278, 1138 (C-O), 1017, 925; δ_H (500 MHz, $CDCl_3$) 1.24 (3H, t *J* 7.0, C<u>H</u>$_3$CH$_2$N), 3.55 (2H, q *J* 7.0, CH$_3$C<u>H</u>$_2$N), 3.50-3.77 (6H, m, OC<u>H</u>$_2$C<u>H</u>$_2$N, ArC<u>H</u>$_2$O), 4.64 (OC<u>H</u>$_2$Ar), 6.77 (2H,app. d *J* 9.0, H-2′′, 6′′), 7.29-7.50 (6H, m, H-3, 5, 3′′, 5′′, 2′′′, 6′′′), 7.50 (1H, t *J* 7.4, H-4), 7.78-7.82 (6H, m, H-2, 6, 2′′, 6′′, 3′′′, 5′′′), 7.86 (2H, app. d *J* 9.0, H-3′′, 5′′); δ_C (125 MHz, $CDCl_3$) 12.2 (<u>C</u>H$_3$CH$_2$N), 40.8 (<u>C</u>H$_2$COOH), 45.9 (CH$_3$<u>C</u>H$_2$N), 50.2 (OCH$_2$<u>C</u>H$_2$N), 68.3 (O<u>C</u>H$_2$CH$_2$N), 72.8 (O<u>C</u>H$_2$Ar), 111.3 (C-2′′, 6′′), 122.4 (C-3′′′, 5′′′), 127.0 (C-3′′, 5′′), 128.3-130.3 (C-2, 6, 2′′, 6′′, 3, 5, 3′′, 5′′, 2′′′, 6′′′), 132.4 (C-4), 134.4 (C-4′′′), 136.9 and 137.6 (C-1, 1′), 142.8 (C-4′), 143.4 (C-1′′), 150.2 (C-4′′), 152.4 (C-1′′′), 176.3 ((CH$_2$)(OH) <u>C</u>=O); 196.4 (Ar_2<u>C</u>=O); *m/z* (ESI$^+$) 522 ([M+H]$^+$, 15%), 580 ([M+MeCN+NH$_4$]$^+$, 100%); HRMS (ESI$^+$) found 522.2382, 522.2387 expected.

General Procedure 5: Dizonium coupling to benzophenone 87 using isopentyl nitrite.

A solution of the amine (1 eq) in EtOH (0.1 mmol/ml) was set to stir at -5 ˚C. Isopentyl nitrite (1 eq) and tetrafluoroboric acid (2 eq) were added and the mixture was stirred for 1 hour. A solution of (4-((2ˈ-(ethyl(phenyl)amino)ethoxy)methyl)phenyl)(phenyl)methanone **87** (1 eq) in minimal THF was added and the mixture stirred for 6 hours at -5-0 ˚C and at room temperature for 18 hours. The mixture was washed with water, dried over $MgSO_4$, filtered and concentrated. The yields of these reactions are displayed in Table 6.2.

Table 6.2: Yields prior to K_2CO_3 wash resulting from diazonium coupling following General Procedure 5.

Product	mmol of 87	% Yield
101h	0.142	100
101i	0.284	61
101j	0.276	0

Procedure 6

A solution of *p*-phenylenediamine **90i** (61.2 mg, 0.57 mmol) in EtOH (3 ml) was set to stir at -5 ˚C. Isopentyl nitrite (0.08 ml, 0.6 mmol) and tetrafluoroboric acid (0.06 ml, 1 mmol) were added and the mixture was stirred for 1 hour. A solution of (4-((2ˈ-(ethyl(phenyl)amino)ethoxy)methyl)phenyl)(phenyl)methanone **87** (200 mg, 0.56 mmol) in THF (2 ml) was added and the mixture was stirred for 1 hour at 0 ˚C then 1 hour at room temperature. The mixture was washed with water, dried over $MgSO_4$, filtered and concentrated to give **101i** as a red/brown oil (220 mg, 81%).

(*E*)-(4-((2′-(ethyl(4′′-((4′′′-diethyl benzylphosphonate)diazenyl)phenyl)amino)ethoxy)methyl)phenyl)(phenyl)methanone tetrafluoroborate salt 101h

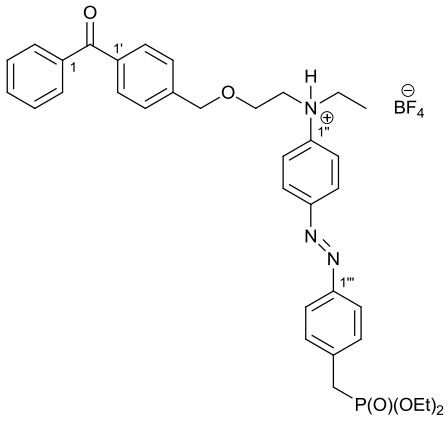

101h was prepared using General Procedure 5 and is a dark pink oil. Characterisation based on crude material which is contaminated with **87** and diethyl 4-aminobenzylphosphonate **90h**. ν_{max}/cm^{-1} (neat) 2985 (C-H), 1655 (C=O), 1600, 1545, 1385 (C-N), 1280, 1065 (C-O), 840; δ_H (400 MHz, $CDCl_3$) 1.21-1.28 and 1.13-1.16 (9H, 2 x m, C$\underline{H}_3$CH$_2$N, P(O)(OCH$_2$C$\underline{H}_3$)$_2$), 3.41-3.46 (m), 3.67 (br s), 3.80-3.84 (m) and 3.93-4.13 (m) (12H, OC$\underline{H}_2$C$\underline{H}_2$N, P(O)(OC$\underline{H}_2$CH$_3$)$_2$ and ArC$\underline{H}_2$P), 4.47 (2H, s, OC$\underline{H}_2$Ar), 7.32 (2H, app. d *J* 8.1, H-3′′, 5′′), 7.35-7.37 and 7.43-7.60 (11H, 2 x m, ArC-$\underline{H}$), 7.69 (2H, app. d *J* 8.1, H-2′′, 6′′), 7.73-7.76 (4H, m, H-2, 6, 2′, 6′); δ_C (100 MHz, $CDCl_3$) 10.2 and 16.3 (C$\underline{H}_3$CH$_2$N and P(O)(OCH$_2$C$\underline{H}_3$)$_2$, 53.4, 55.7, 58.5, 62.8 and 63.1 (OC$\underline{H}_2$C$\underline{H}_2$N, CH$_3$C$\underline{H}_2$N, P(O)(OC$\underline{H}_2$CH$_3$)$_2$, OC$\underline{H}_2$Ar), 72.6 (ArC$\underline{H}_2$O), 127.4 (C-3′′, 5′′), 122.2, 128.3-132.6, 141.5 (15 x Ar$\underline{C}$), 136.5, 137.0, 137.4 and 137.4 (C-1, 1′, 4′, 1′′, 4′′, 1′′′, 4′′′), 198.6 ($\underline{C}$=O); *m/z* (ESI$^+$) 614 ([M+H]$^+$, 61%); HRMS (ESI$^+$) 614.2779 found, 614.2778 expected.

(*E*)-(4-((2′-(ethyl(4′′-((4′′′-aniline)diazenyl)phenyl)amino)ethoxy)methyl)phenyl)(phenyl)methanone tetrafluoroborate salt 101i

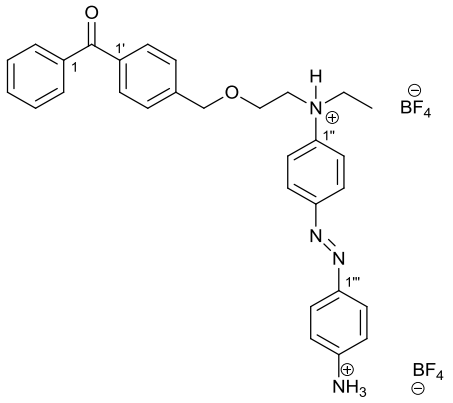

Crude product used for analysis. **101i** was prepared using General Procedure 5 and Procedure 6 and was isolated as a brown oil; $\lambda_{max}(CH_2Cl_2)$/nm 419 (1809 $mol^{-1}dm^3cm^{-1}$); ν_{max}(neat)/cm^{-1} 3600 (N-H), 3300 (N-H), 2875 (C-H), 1655 (C=O), 1600 (N=N), 1279, 1100 (C-O), 925, 790, 735, 700; δ_H (500 MHz, MeOD) 1.15 (3H, t *J* 7.2, C<u>H</u>$_3$CH$_2$N), 3.51 (3H, br s, OCH$_2$C<u>H</u>$_2$N, N-<u>H</u>), 3.72 (2H, q *J* 7.2, CH$_3$C<u>H</u>$_2$N), 4.25 (2H, s, OC<u>H</u>$_2$Ar), 7.44 (2H, app. d *J* 8.1, 2 x ArC<u>H</u>), 7.52-7.61 (8H, m, H-3, 5, 3′, 5′, 4 x ArC<u>H</u>), 7.67 (1H, t *J* 6.8, C-4), 7.73-7.76 (6H, H-2, 6, 2′, 6′, 2 x ArC<u>H</u>); δ_C (125 MHz, MeOD) 10.7 (<u>C</u>H$_3$CH$_2$N), 55.1 (CH$_3$<u>C</u>H$_2$N), 58.1 (OCH$_2$<u>C</u>H$_2$N), 65.1 (O<u>C</u>H$_2$CH$_2$N), 73.6 (O<u>C</u>H$_2$Ar), 122.9, 127.6-132.0 (15 x Ar<u>C</u>H), 133.9, 134.0, 137.6, 138.7, 138.8, 143.7 (C-1, 1′, 4′, 1′′,4′′, 1′′′, 4′′′), 198.4 (<u>C</u>=O).

General Procedure 7: Procedure for diazonium coupling to *N,N*-dimethyl aniline.

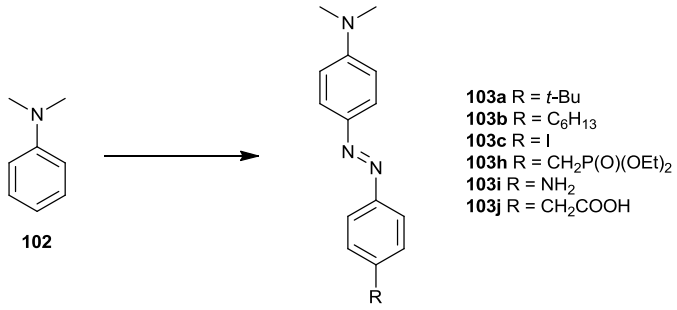

A solution of the amine (1 eq) in EtOH was stirred at -5 ˚C . Isopentyl nitrite (1 eq) and tetrafluoroboric acid (2 eq) were added and the mixture was stirred for 1 hour at -5-0 ˚C. *N,N*-dimethyl aniline (1 eq) was added and the mixture stirred at room temperature for the time period given in Table 6.3. The EtOH was removed *in vacuo* then the residue dissolved in DCM and washed with sat. aq. K_2CO_3. The aqueous phase was washed with DCM until the resulting organic phase was colourless. The organic fractions were combined, dried over $MgSO_4$, filtered and concentrated *in vacuo*. Purification by silica column chromatography was performed if necessary and the yields of the reactions are in Table 6.3.

Table 6.3: Reaction times and yields obtained using General Procedure 7.

Product	mmol of 102	% Yield	Reaction time for step 2 (hrs)
103a R=*t*-Bu	0.67	72	18
103b R=C_6H_{13}	1.13	20	18
103c R=I	0.46	47	0.5
103h R=$CH_2P(O)(OEt)_2$	0.55	46	1
103i R=NH_2	0.95	0	18
103j R=CH_2COOH	0.66	95	18

Procedure 8: Diazonium coupling to *N,N*-dimethyl aniline with adjusted pH.

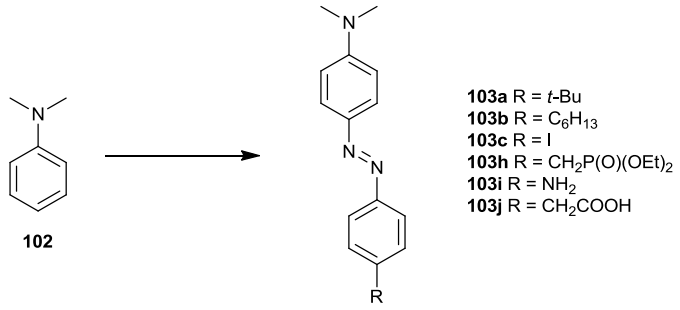

A solution of the amine (1 eq) in EtOH was set to stir at -5 ˚C. Isopentyl nitrite (1 eq) and tetrafluoroboric acid (2 eq) were added and the mixture was stirred for 1 hour at -5-0 ˚C. Sodium acetate (1 eq) followed by *N,N*-dimethyl aniline (1 eq) were added then the mixture stirred at room temperature for the time periods in Table 6.4. The EtOH was removed *in vacuo* then the residue dissolved in DCM and washed with water. The aqueous phase was washed with DCM until the resulting organic phase was colourless. All the organic fractions were combined, dried over $MgSO_4$, filtered and concentrated *in vacuo*. Purification by silica column chromatography was performed if necessary and the yields are displayed in Table 6.4.

Table 6.4: Reaction times and yields obtained using General Procedure 8.

Product	mmol of 102	% Yield	Reaction time for step 2 (hrs)
103a R=t-Bu	0.67	91	4
103b R=C_6H_{13}	1.13	73	18
103c R=I	0.46	57	0.5
103h R=$CH_2P(O)(OEt)_2$	0.56	96	1
103i R=NH_2	0.95	12	18
103j R=CH_2COOH	0.66	34	18

(*E*)-4-((4ˈ-(*tert*-butyl)phenyl)diazenyl)-*N*,*N*-dimethylaniline 103a

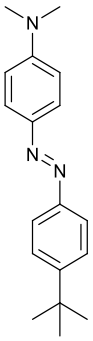

103a was purified by column chromatography (eluent 20:1 petrol:EtOAc) and isolated as a red solid. R_f 0.44, 15:1 (petrol:EtOAc); mp 156-158˚C {lit. mp[141] 137-137.5˚C}; λ_{max} (CH_2Cl_2)/nm 412 (5040 $mol^{-1}dm^3cm^{-1}$); ν_{max}(neat)/cm^{-1} 2964 (C-H), 1600 (N=N), 1515, 1442, 1520, 1362 (C-N), 1229, 1159, 1140, 945, 839, 818; δ_H (400 MHz, $CDCl_3$) 1.38 (9H, s, C(C$\underline{H}_3$)$_3$), 3.09 (6H, s, N(C$\underline{H}_3$)$_2$), 6.77 (2H, app. d *J* 9.2, H-2, 6), 7.51 (2H, app. d *J* 8.8, H-2ˈ, 6ˈ), 7.79 (2H, app. d *J* 8.8, H-3ˈ, 5ˈ), 7.88 (2H, app. d *J* 9.2, H-5, 3); δ_C (100 MHz, $CDCl_3$) 31.4 (C($\underline{C}$H$_3$)$_3$), 34.8 ($\underline{C}$(CH$_3$)$_3$), 40.3 (N($\underline{C}$H$_3$)$_2$), 111.5 (C-2, 6), 121.9 (C-3ˈ, 5ˈ), 124.7 (C-3, 5), 125.8 (C-2ˈ, 6ˈ), 143.8 (C-1), 151.1 (C-1ˈ), 152.2 (C-4), 152.7 (C-4ˈ); *m/z* (ESI^+) 282 ($[M+H]^+$, 100%); HRMS (ESI^+) 282.1969 found 282.1965 expected.

(*E*)-4-((4ˈ-hexylphenyl)diazenyl)-*N*,*N*-dimethylaniline 103b

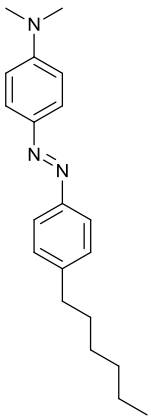

103b was purified by silica column chromatography (eluent 20:1 petrol:EtOAc) and was isolated as an orange solid. R_f 0.58 (10:1 petrol:EtOAc); m.p. 74 ˚C; $\lambda_{max}(CH_2Cl_2)$/nm 410 (24000 $mol^{-1}dm^3cm^{-1}$); ν_{max}(neat)/cm^{-1} 2925 (C-H), 2854 (C-H), 1599 (N=N), 1515, 1443, 1400, 1393 (C-N), 1230, 1154, 1139, 946, 818; δ_H (400 MHz, $CDCl_3$) 0.91-0.94 (3H, m, $C\underline{H}_3C_5H_{10}Ar$), 1.35 (6H, br s, $CH_3C\underline{H}_2C\underline{H}_2C\underline{H}_2C_2H_5Ar$), 1.64-1.72 (2H, m, $C_4H_9C\underline{H}_2CH_2Ar$), 2.96 (2H, t *J* 7.7, $C_5H_{11}C\underline{H}_2Ar$), 3.08 (6H, s, $N(C\underline{H}_3)_2$), 6.78 (2H, app. d *J* 9.1, H-2, 6), 7.32 (2H, app. d *J* 8.3, H-2', 6'), 7.80 (2H, app. d *J* 8.3, H-3', 5'), 7.90 (2H, app. d *J* 9.1, H-3, 5); δ_C (100 MHz, $CDCl_3$) 14.2 ($\underline{C}H_3C_5H_{10}Ar$), 22.6, 29.0, 31.4 and 31.7 ($CH_3\underline{C}H_2\underline{C}H_2\underline{C}H_2\underline{C}H_2CH_2Ar$), 35.8 ($C_5H_{11}\underline{C}H_2$), 40.3 ($N(\underline{C}H_3)_2$), 111.5 (C-2, 6), 122.2 (C-3, 5), 124.8 (C-3', 5'), 129.0 (C-2', 6'), 143.8 (C-1), 144.7 (C-4'), 151.5 (C-1'), 152.2 (C-4); HRMS (FI) 309.2216 [M^+] found where 309.2205 expected.

(*E*)-4-((4'-iodophenyl)diazenyl)-*N*,*N*-dimethylaniline 103c

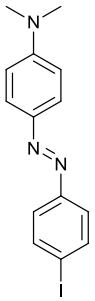

103c was purified with silica column chromatography (eluent 30:1 petrol:EtOAc) affording an orange solid. R_f 0.67 (4:1 petrol:EtOAc); mp 166-169 ˚C {lit. mp[142] 163.5-164 ˚C}; $\lambda_{max}(CH_2Cl_2)$/nm 425 (3840 $mol^{-1}dm^3cm^{-1}$); ν_{max}(neat)/cm^{-1} 2922 (C-H), 1602, 1514, 1470, 1419, 1363 (C-N), 1231, 1156, 1051, 827, 733, 700, 649; δ_H (400 MHz, $CDCl_3$) 3.10 (6H, s, $N(C\underline{H}_3)_2$), 6.76 (2H, app. d *J* 9.2, H-2, 6), 7.59 (2H, app. d *J* 8.6, H-2', 6'), 7.81 (2H, app. d *J* 8.6, H-3', 5'), 7.88 (2H, app. d *J* 9.2, H-3, 5); δ_C (100 MHz, $CDCl_3$) 40.3 ($N(\underline{C}H_3)_2$), 95.2 (C-4'), 111.5 (C-2, 6), 123.9 (C-2', 6'), 125.2 (C-3, 5), 138.1 (C-3', 5'), 143.5 (C-1), 152.6

and 152.6 (C-4, 1ˈ); *m/z* (ESI^+) 352 ($[M+H]^+$, 100%); HRMS (ESI^+) 352.0315 found, 352.0305 expected.

1,3-bis(4-iodophenyl)triaz-1-ene 104

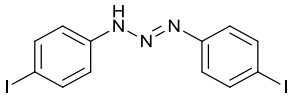

104 was generated as a pale yellow solid as a by-product in the reaction of *N,N*-dimethyl aniline with iodo diazonium salt **91c** by Procedure **8**. R_f 0.68 (10:1 petrol:EtOAc); mp 170-173 ˚C; ν_{max}(neat)/cm^{-1} 3200, 2923 (C-H), 2853 (C-H), 1586, 1501, 1476; δ_H (100 MHz, $CDCl_3$) 7.14 (4H, AAˈBBˈ d, ArH-2, 6, 2ˈ, 6ˈ), 7.69 (4H, AAˈBBˈ d, ArH-3, 5, 3ˈ, 5ˈ); δ_C (100 MHz, $CDCl_3$) 119.8 (ArC-2, 6, 2ˈ, 6ˈ), 138.3 (ArC-3, 5, 3ˈ, 5ˈ), other carbons not detectable due to contamination; *m/z* (ESI^-) 448 ($[M-H]^-$, 100%); HRMS (ESI^-) 447.8808 found, 447.8808 expected.

(*E*)-4-((4ˈ-diethyl benzylphosphonate))diazenyl)-*N,N*-dimethylaniline 103h

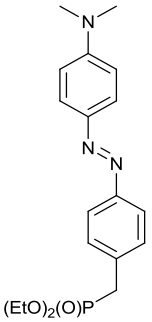

103h was purified by silica column chromatography (eluent 1:1 petrol:EtOAc) to give an orange solid. R_f 0.61 (1:1 petrol:EtOAc); m.p. 101-105 ˚C; $\lambda_{max}(CH_2Cl_2)$/nm 416 (2500 $mol^{-1}dm^3cm^{-1}$); ν_{max}(neat)/cm^{-1} 2903 (C-H), 1599 (N=N), 1518, 1442, 1401, 1363 (C-N), 1350, 1156, 1136 (P=O), 1025 (P-OEt), 956; δ_H (400 MHz, $CDCl_3$) 1.25 (6H, t *J* 7.1,

P(O)(OCH$_2$C$\underline{H}_3$)$_2$), 3.07 (6H, s, N(C$\underline{H}_3$)$_2$), 3.21 (2H, d *J* 22$_{HP}$, ArC$\underline{H}_2$P), 4.00-4.06 (4H, m, P(O)(OC$\underline{H}_2$CH$_3$)$_2$), 6.75 (2H, app. d *J* 9.1, H-2, 6), 7.40 (2H, app. dd J_{HH} 7.6 and J_{HP} 2.2, H-3', 5'), 7.80 (2H, d *J* 7.6, H-2', 6'), 7.87 (2H, d *J* 9.1, H-3, 5); δ_C (100 MHz, $CDCl_3$) 16.3 (P(O)(OCH$_2$$\underline{C}H_3$)$_2$, 33.1 (d *J* 138.2, Ar$\underline{C}H_2$P), 40.3 (N($\underline{C}H_3$)$_2$), 62.3 (P(O)(O$\underline{C}H_2CH_3$)$_2$), 111.5 (C-2, 6), 122.3 (C-2', 6'), 124.9 (C-3, 5), 130.3 (C-3', 5'), 132.9 (C-1'), 143.6 (C-1), 152.1 and 152.4 (C-4 and C-4'); *m/z* (ESI$^+$) 751 ([2M+H]$^+$, 100%), 376 ([M+H]$^+$, 40%); HRMS (ESI$^+$) 376.1786 found where 376.1785 expected.

(*E*)-4-((4'-aminophenyl))diazenyl)-*N*,*N*-dimethylaniline 103i

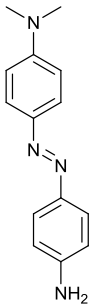

103i was purified by silica column chromatography (eluent 10:1 petrol:EtOAc to EtOAc) and was isolated as an dark brown oily solid that was contaminated with an unknown impurity. λ_{max} (CH_2Cl_2)/nm 413 (5980 mol^{-1}dm^{3}cm^{-1}); ν_{max} (neat)/cm^{-1} 3336 (N-H), 2917 (C-H), 1599, 1517, 1362 (C-N), 1149, 823; δ_H (400 MHz, $CDCl_3$) 3.08 (6H, s, N(C$\underline{H}_3$)$_2$), 6.76 (2H, app. d *J* 9.1, H-2, 6), 6.92 (2H, app. d *J* 8.8, H-3', 5'), 7.79 (2H, app. d *J* 8.8, H-2', 6'), 7.84 (2H, app. d *J* 9.1, H-3,5); δ_C (125 MHz, $CDCl_3$) 40.4 (N($\underline{C}$H$_3$)$_2$), 115.5 (C-2, 6), 116.6 (C-3', 5'), 124.0 (C-2', 6'), 124.5 (C-3', 5'), 143.6 (C-1), 147.5 (C-4'), 152.0 (C-1'), 157.2 (C-4); *m/z* (ESI$^+$) 241 ([M+H]$^+$, 25%).

(*E*)-4-((4'-phenyl acetic acid))diazenyl)-*N*,*N*-dimethylaniline 103j

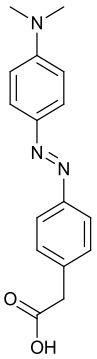

103j was purified by silica column chromatography (eluent 6:1 petrol:EtOAc to 1:5 MeOH:EtOAc) and isolated as a black solid. R_f 0.38 (1:6 petrol:EtOAc); m.p. 166-168 ˚C; $\lambda_{max}(CH_2Cl_3)$/nm 415 (10000 $mol^{-1}dm^3cm^{-1}$); ν_{max}/cm^{-1} 2918, 1709 (C=O), 1599 (N=N), 1517, 1357 (C-N), 1250, 1138, 820; δ_H (400 MHz, $CDCl_3$) 3.10 (6H, s, N(C<u>H</u>$_3$)$_2$), 3.72 (2H, s, ArC<u>H</u>$_2$COOH), 6.85 (2H, app. d *J* 9.1, H-2, 6), 7.47 (2H, app. d *J* 8.5, H-2', 6'), 7.80 (2H, app. d *J* 8.5, H-3', 5'), 7.85 (2H, app. d *J* 9.1, H-3, 5); δ_C (100 MHz, $CDCl_3$), 39.8 (N(<u>C</u>H$_3$)$_2$), 40.6 (Ar<u>C</u>H$_2$COOH), 111.9 (C-2, 6), 122.3 (C-3', 5'), 125.1 (C-3, 5), 130.4 (C-2', 6'), 137.0 (C-4'), 143.8 (C-1), 132.4 (C-1'), 153.2 (C-4), 205.8 (<u>C</u>=O); *m/z* (ESI^+) 306 ($[M+Na]^+$, 30%); HRMS (ESI^+) 306.1206 found, 306.1213 expected.

6.3 Chapter 3

The polystyrene films were prepared by Geoffrey Nelson. Prior to any modifications the base substrates were cleaned in piranha solution (3:1 H_2SO_4:H_2O_2) for 10 minutes then rinsed with de-ionized water after which the substrate was dried under a gentle stream of nitrogen gas. Special care was needed in handling the QCM-D crystals. A spin coater, Laurell Technologies Corp., Model WS-400B-6NPP/LINE, was used to spin coat the polystyrene films onto the gold and glass surfaces. The gold coated quartz crystals for QCM-D were sourced from Q-Sense.

Polymer film preparation- UV crosslinked[†]

A solution of polystyrene (20 mg/ml) powder, MW 211600, in toluene was filtered through a PTFE filter then sonicated for 15 minutes. A polystyrene film was applied to a glass slide by spin-coating 5 x 200 µl droplets for 1 minute at 2000 rpm then heated at 170 ˚C for 2 hours. Finally the substrates were then exposed to broad band UV light for 30 minutes to crosslink the polystyrene film.

Polymer film preparation- DVB crosslinked[†]

A solution of polystyrene powder, MW 211600, in toluene (20 mg/ml) was filtered through a PTFE filter then sonicated for 15 minutes. Divinyl benzene (DVB) was washed with 5% aq. sodium hydroxide to remove the stabilizers then added to the polystyrene solution (0.55 µl/ml) and the mixture sonicated for 5 minutes more. After addition of benzoyl peroxide (1 mol per mole of polystyrene monomer) the mixture was shaken by hand then spin coated onto the base substrates (silicon-gold or quartz-gold), 5 x 200 µl droplets at a rate of 2000 rpm. The samples were then heated for 8 hours at 90 ˚C under a nitrogen atmosphere.

Modification with bis(4-iodophenyl) diazomethane to give 108

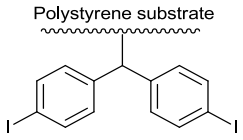

Using substrate, a solution of bis(4-iodophenyl) diazomethane **61** (1 w/v%) was applied to the glass-polystyrene substrate **105** such that the sample was completely coated in the pink solution (~0.1 ml per 1 cm^2). This was done on three separate samples which were heated at 93 ˚C, 120 ˚C and 180 ˚C until the pink colour was gone. Once the samples had cooled they were washed with DCM and dried with a stream of nitrogen gas.

Chemical modification of polystyrene substrates

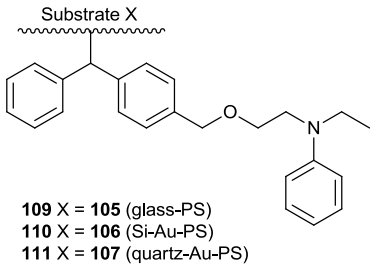

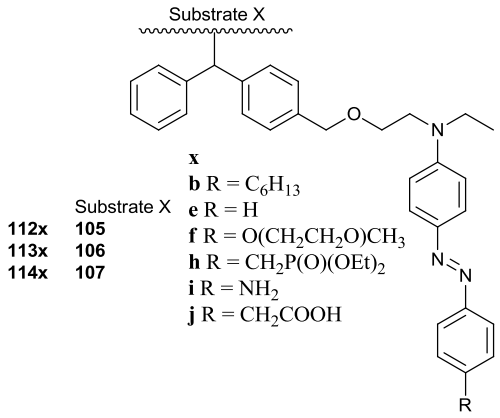

A solution of diazo **65** in DCM (1 w/v%) was prepared then applied to the polystyrene substrates **105-107** with a pipette such that they were completely covered (~0.2 ml per 1 cm^2 substrate). The DCM was allowed to evaporate naturally then the sample heated at 180 ˚C* until the coating was no longer pink, at 180 ˚C this took about 2 minutes. Once the samples had cooled they were washed with DCM then dried under a gentle stream of nitrogen, affording **109**-**111**. The samples were immersed in a solution made up of 0.1 mmol of the relevant diazonium salt, as prepared in General Procedure 1 (Chapter 6.2), for 18 hours at 5 ˚C, after which they were washed with EtOH and DCM then dried under a gentle stream of nitrogen giving **112**, **113** and **114 b**, **e**, **f**, **h-i**.

*The samples where glass was the base substrate used for XPS were heated to 120 ˚C.

Quartz-crystal microbalance-dissipation protocol

Prior to use the solutions were degassed under vacuum to prevent bubbles forming in the QCM-D run and warmed to room temperature. The unmodified, polystyrene coated (**107**), and modified crystals were loaded into the cell then the system equilibrated at 25 ˚C with phosphate buffered saline (PBS) pH 7.4, equilibration was usually carried out for ~16 hours. The BSA/PBS solution (80 mg if BSA per 1 L of PBS) was pumped through the system

until the frequency and dissipation traces had reached a steady state, then a PBS rinse was carried out until the frequency and dissipation traces were at a steady state. Finally, hellmanex solution (2% in water) was pumped through the system to clean the crystal. The Sauerbrey and Voigt masses were calculated at various time points during the BSA/PBS exposure and the PBS rinse. All of the data is presented as an average using the 5^{th}, 7^{th} and 9^{th} overtones for calculations.

Table 6.5: Mass increase during BSA/PBS exposure calculated using the Sauerbrey model.

Sample	Surface functionality	20 minutes		36 minutes		53 minutes		Total mass deposited		
		Mass (ng/cm^2)	Standard deviation	Mass (ng/cm^2)	Standard deviation	Mass (ng/cm^2)	Standard deviation	Mass (ng/cm^2)	Standard deviation	Total deposition time (minutes)
Au	Gold	236.6	1.1	245.4	0.9	-	-	245.5	0.9	38.4
107	Polystyrene	419.7	1.8	-	-	-	-	419.3	2.7	23.7
111	-	295.3	1.9	314.9	2.4	-	-	316.0	2.4	33.3
114b	C_6H_{13}	445.1	3.0	487.4	2.1	507.5	1.9	520.4	2.1	77.1
114e	H	174.6	1.1	186.6	0.8	-	-	187.8	1.1	44.1
114f	$O(CH_2CH_2O)CH_3$	468.5	4.2	537.9	1.3	-	-	527.1	5.6	37.7
114h	$CH_2P(O)(OEt)_2$	220.5	1.0	196.5	1.5	172.0	1.5	168.6	2.2	58.9
114i	NH_2	388.3	3.6	455.3	2.5	-	-	469.2	6.5	43.6
114j	CH_2COOH	294.9	1.9	318.1	1.6	329.9	1.7	333.3	2.6	60.3

Table 6.6: Mass increase during BSA/PBS exposure calculated using the Voigt model.

Sample	Surface functionality	20 minute deposition		36 minute deposition		53 minute deposition		End of Deposition		
		Mass (ng/cm^2)	Standard deviation	Mass (ng/cm^2)	Standard deviation	Mass (ng/cm^2)	Standard deviation	Mass (ng/cm^2)	Standard deviation	Total deposition time (minutes)
Au	Gold	1184	17.3	1174	19.5	-	-	1157	37.1	38.4
107	Polystyrene	1093	36.6	-	-	-	-	1096	45.3	23.7
111	-	803	113.4	948	56.3	-	-	892	62.2	33.3

114b	C_6H_{13}	1817	65.4	1812	64.4	1807	56.9	1778	55.4	77.1
114e	H	181	0.8	192	0.7	-	-	193	0.8	44.1
114f	$O(CH_2CH_2O)CH_3$	661	22.7	766	73.2	-	-	647	106.5	37.7
114h	$CH_2P(O)(OEt)_2$	222	1.6	193	1.7	157	1.6	152	3.0	58.9
114i	NH_2	1402	28.2	1646	2.0	-	-	1725	62.2	43.6
114j	CH_2COOH	342	1.5	367	1.1	389	1.6	340	4.1	60.3

Table 6.7: Masses calculated after rinsing with PBS at various time points of the rinse.

Surface	**Surface functionality**	**Sauerbrey**						**Voigt**					
		29 minute rinse		**35 minute rinse**		**41 minute rinse**		**29 minute rinse**		**35 minute rinse**		**41 minute rinse**	
		Mass	**SD**	**Mass**	**SD**	**Mass**	**SD**	**Mass**	**SD**	**Mass**	**SD**	**Mass**	**SD**
Au	Gold	358	1.3	351	1.4	344	1.4	699	21.2	675	17.9	657	17.6
107	Polystyrene	367	1.8	361	1.6	-	-	761	9.4	745	11.4	147	-
111	-	140	1.3	-	-	-	-	150	0.3	-	-	-	-
114b	C_6H_{13}	502	1.9	502	1.8	-	-	1974	27.2	1602	139.7	27	-
114e	H	188	0.9	-	-	-	-	189	0.5	-	-	-	-
114f	$O(CH_2CH_2O)CH_3$	398	1.3	390	1.1	388	1.1	407	1.0	401	0.8	396	0.8
114h	$CH_2P(O)(OEt)_2$	123	1.5	98	1.5	-	-	109	1.0	114	1.0	-	-
114i	NH_2	714	3.9	694	2.8	671	2.2	710	3.6	678	2.3	665	1.2
114j	CH_2COOH	316	1.6	339	1.6	313	1.7	191	0.1	231	0.4	187	0.3

SD= standard deviation. Masses in ng/cm^2

6.4 Chapter 4

6.4.1 Preparation of materials 116a-m, 117a-m

Modification of Polystyrene XAD-4 beads with *N*-(2-((4-(Diazo(phenyl)methyl)benzyl)oxy)ethyl)-*N*-ethylaniline 65 to give 115

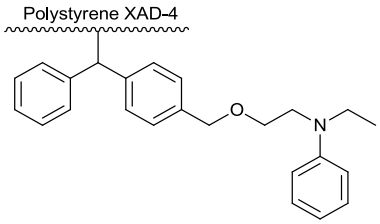

The XAD-4 beads were washed with copious amounts of water then acetone and dried under vacuum on a sinter funnel. *N*-(2-((4-(Diazo(phenyl)methyl)benzyl)oxy)ethyl)-*N*-ethylaniline **65** (5 w/w%, relative to bead weight) was dissolved in Et_2O then Amberlite XAD-4 beads were added to the solution. Et_2O was added such that the beads were completely submerged then the mixture was concentrated to dryness *in vacuo*. The beads were heated to 120 °C until they had turned from pink to off yellow/white in colour. The beads were then washed with acetone through a sinter funnel and the beads were left to dry under vacuum to give **115**.

Diazonium coupling to polystyrene surfaces

116a R = *t*-Bu
116b R = C_6H_{13}
116c R = I
116e R = H
116f R = $O(CH_2CH_2O)_3CH_3$
116g R = OH
116h R = $CH_2P(O)(OEt)_2$
116i R = NH_2
116j R = CH_2CO_2H

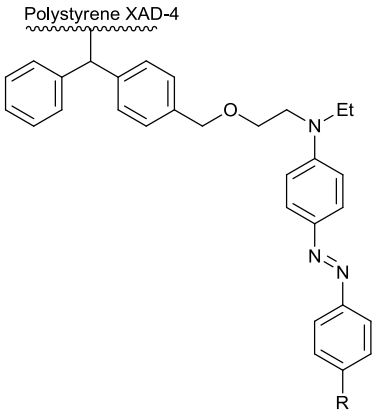

117a R = *t*-Bu
117b R = C_6H_{13}
117c R = I
117e R = H
117f R = $O(CH_2CH_2O)_3CH_3$
117g R = OH
117h R = $CH_2P(O)(OEt)_2$
117i R = NH_2
117j R = CH_2CO_2H

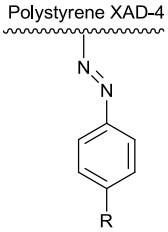

Linker coupled materials **116a-c**, **e-j** and directly coupled materials **Xa-c**, **e-j** were all prepared using this method. The relevant diazonium salt solution **91a-c**, **e-j** was prepared using General Procedure 1 (Section 6.1). A solution containing two equivalents of the diazonium salt was prepared based on the moles of diazo **65** used to modify that mass of beads. The XAD-4 or linker terminated beads **115** were immersed in the salt solution, more EtOH was added when necessary to ensure the beads were submerged, and the mixture was covered and left to stand at 5 ˚C for 18 hours. The beads were filtered through a sinter funnel under vacuum and washed with acetone until the washings were colourless then the beads dried under vacuum.

Preparation of dimethyl amine terminated materials 116d and 117d

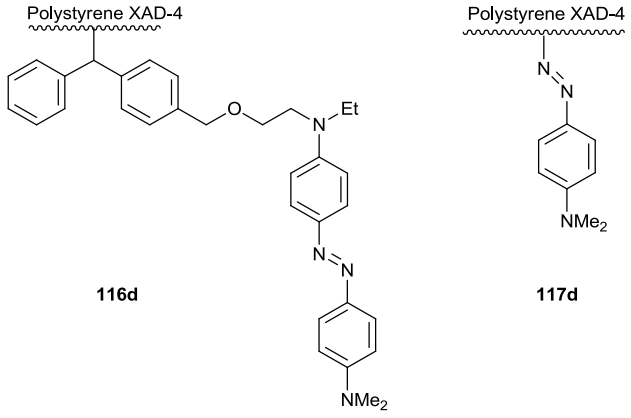

116i and **117i** were stirred in a solution of excess methyl iodide in EtOH at room temperature for 18 hours. The materials were then filtered, washed with EtOH and dried.

Preparation of phosphonate monoester terminated materials 116k and 117k

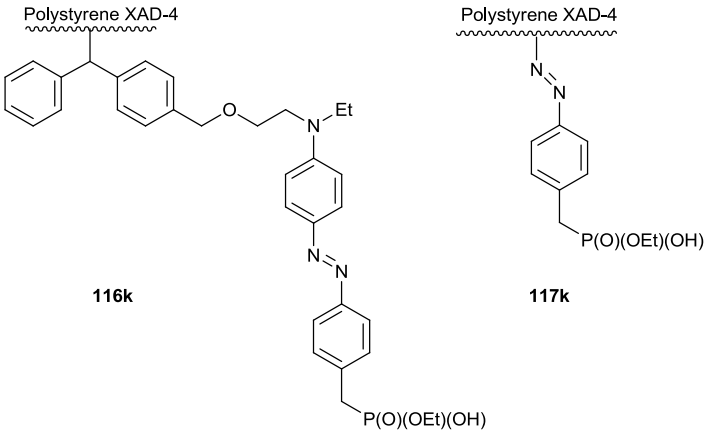

116k **117k**

Materials **116h** and **117h** were immersed in 5% aq. NaOH and left to stand for 18 hours. The mixture was then filtered and the beads washed with water then dried under vacuum.

Preparation of phosphonic acid terminated materials 116l and 117l

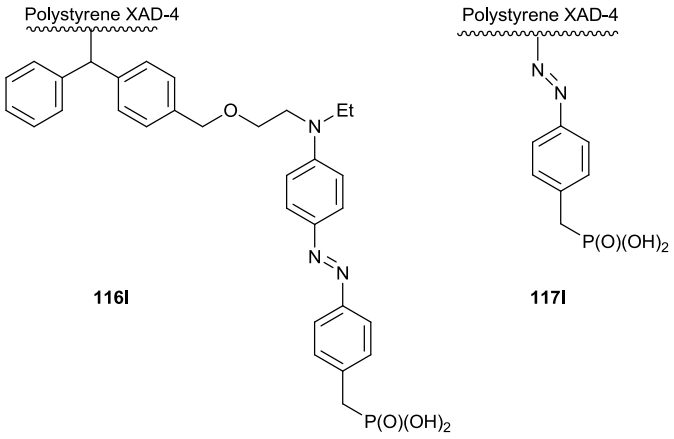

116l **117l**

Materials **116h** and **117h** were gently stirred in an aqueous 1 M solution of HCl for 18 hours. The mixture was filtered, washed with water then the beads dried under vacuum.

Preparation of calcium phosphonate terminated materials 116m and 117m

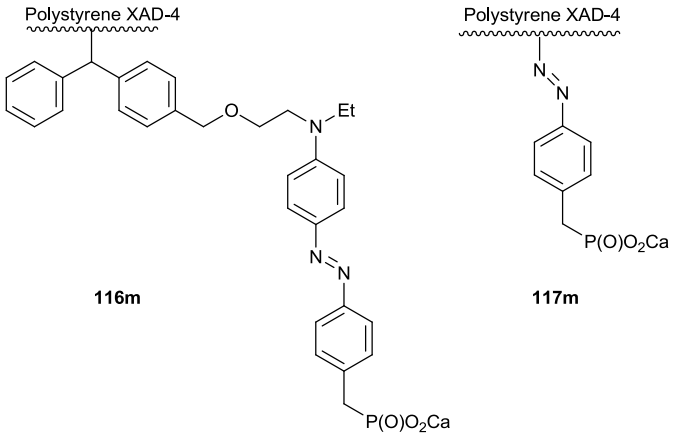

Materials **116l** and **117l** were washed with sat. aq. CaOH after which the resulting materials were washed with water to remove excess CaOH.

6.4.2 Characterisation of materials 115, 116a-m and 117a-m

6.4.2.1 Experimental protocols

ATR-IR

A Bio-Rad FTS-6000 was used to conduct ATR-IR analysis of the materials. The beads were position on the diamond accessory and fastened into place using the screw tip. The spectrum of the base material was subtracted from the measured spectra and the ATR-IR data can be found below in Tables 6.10-6.12.

Contact angle measurement[†]

For contact angle measurements, the polystyrene microspheres were randomly chosen from each sample group and placed on the surface of water droplet positioned on a clean glass slide. They were imaged and measured using a contact angle analyser (FTA32 Video 2.0, First Ten Angstroms). For each materials five measurements were taken on five different beads. The average results are presented in Table 4.7.

TGA analysis[†]

Approximately 10 mg of particles were weighed in a TGA specific platinum pan, which was placed in the high precision balance and heated at a ramp rate of 10 ˚C per minute up to 600 ˚C in an atmosphere of nitrogen (40%) and air (60%). From a temperature vs. weight% plot the decomposition temperature was calculated. Table 6.15 displays a summary of the results.

DSC analysis[†]

Approximately 5 mg of particles were weighed in an aluminium pan and heated at a ramp rate of 10 or 20 ˚C per minute over a temperature range of 25 ˚C to 260 ˚C in an atmosphere of nitrogen.

6.4.2.2 Characterisation data

Table 6.8: XPS data summary of carbon, nitrogen and oxygen peaks as provided by Professor Cleo Choong.

Material R	% Atomic concentration			Atomic ratios (N/C)			Binding energy (eV) (FWHM)			Average binding energy (eV)		
	O	N	C	Found	Expected	Average found ratio	O	N	C	O	N	C
XAD-4 Polystyrene (1)	15.47	0.82	83.71	0.010	0	0.010	530.6 (3.329)	397.7 (1.318)	282.3 (2.792)	530.6	397.7	282.3
115 (1)	11.33	5.00	83.68	0.060	0.04	0.056	529.7 (2.861)	397.4 (1.563)	281.8 (1.378)	529.6	397.3	281.8
116 (2)	8.94	4.52	86.54	0.052	0.04		529.4 (2.646)	397.2 (1.567)	281.8 (1.364)			
116a (1) *t*-Butyl	10.78	4.1	85.12	0.048	0.086	0.048	534.5 (2.668)	402.7 (4.588)	287.2 (1.342)	534.5	402.7	287.2
116b (1) C_6H_{13}	7.58	1.77	90.65	0.020	0.081	0.020	529.7 (2.847)	397.7 (1.706)	281.8 (1.601)	529.7	397.7	281.8
116c (1) I	9.57	3.47	86.96	0.040	0.097	0.041	532.1 (4.607)	397.6 (2.172)	282.7 (3.574)	532.4	399.2	283.1
116c (2) I	9.24	3.69	87.07	0.042	0.097		532.6 (3.174)	400.8 (2.141)	283.5 (3.946)			
116d (1) NMe_2	7.23	3.75	89.02	0.042	0.117	0.042	529.6 (2.598)	397.3 (1.205)	284.6 (1.327)	529.6	397.3	284.6
116e (1) H	14.67	5.88	79.44	0.074	0.097	0.074	533.6 (3.627)	402.5 (2.708)	284.6 (3.916)	533.6	402.5	284.6
116f (1) $O(CH_2CH_2O)_3CH_3$	8.63	1.56	89.82	0.017	0.079	0.044	531.1 (3.077)	398.9 (2.328)	283.4 (2.376)	530.4	398.5	283.2

116f (2) $O(CH_2CH_2O)_3CH_3$	10.75	5.95	83.31	0.071	0.079		529.7 (2.666)	398 (1.605)	282.9 (2.068)			
116g (1) OH	21.07	2.4	76.53	0.031	0.097	0.031	532.2 (2.847)	401.6 (0.494)	286.9 (1.793)	532.2	401.6	286.9
116h (1) $CH_2P(O)(OEt)_2$	8.74	2.02	89.24	0.023	0.083	0.038	529.3 (2.957)	397.1 (1.435)	281.6 (1.550)	529.3	397.1	281.7
116h (2) $CH_2P(O)(OEt)_2$	10.9	4.59	84.51	0.054	0.083		529.2 (2.713)	397.0 (1.494)	281.7 (1.419)			
116i (1) NH_2	20.53	3.11	76.36	0.041	0.129	0.026	530.6 (3.228)	397.5 (1.850)	282.8 (2.335)	530.5	397.8	282.8
116i (2) NH_2	14.33	0.91	84.76	0.011	0.129		530.3 (3.264)	398.1 (1.431)	282.7 (1.650)			
116j (1) CH_2COOH	8.46	4.61	86.93	0.053	0.091	0.041	530.5 (3.409)	397.9 (2.255)	282.6 (2.039)	531.2	398.3	282.9
116j (2) CH_2COOH	14.05	2.44	83.51	0.029	0.091		531.8 (3.922)	398.6 (1.720)	283.2 (3.513)			
116k (1) $CH_2P(O)(OH)(OEt)$	10.45	2.55	87.01	0.029	0.088	0.033	529.7 (3.288)	397.8 (1.731)	282.1 (1.802)	530.0	397.7	282.2
116k (2) $CH_2P(O)(OH)(OEt)$	10.59	3.13	86.28	0.036	0.088		530.2 (3.328)	397.5 (1.493)	282.3 (1.772)			
116l (1) $CH_2P(O)(OH)_2$	9.13	4.87	85.99	0.057	0.094	0.050	529.2 (2.705)	397.2 (1.308)	281.7 (1.359)	529.7	397.2	281.8
116l (2) $CH_2P(O)(OH)_2$	10.97	3.74	85.29	0.044	0.094		530.1 (2.998)	397.1 (1.471)	281.8 (1.424)			
116m (1) $CH_2P(O)O_2Ca$	14.12	2.84	83.04	0.034	0.094	0.039	531 (3.356)	398.4 (2.138)	283.9 (2.965)	531.2	398.9	284.0
116m (2) $CH_2P(O)O_2Ca$	11.85	3.65	84.49	0.043	0.094		531.3 (4.663)	399.4 (2.792)	284.0 (3.334)			

Table 6.9: ATR-IR data for materials prior to diazonium coupling.

Material	Raw data (cm^{-1})	Subtracted data (cm^{-1})	Significant peaks (cm^{-1})
XAD-4	3437, 2961, 2932, 1714, 1602, 1487, 1511, 1444, 1360, 1220, 1090, 990, 902, 833, 795	-	3437 (ar. C-H); 2961, 2932 (C-H) 1602 (ar. C=C)
115	3341, 2960, 2931, 2859, 2726, 2650, 2291, 2121, 2109, 1666, 1603, 1512, 1487, 1444, 1285, 1252, 1169, 1086, 989, 838, 795	3337, 2929, 2858, 2398, 2159, 1967, 1745, 1511, 1480, 1447, 1353, 1084, 902, 836, 795, 708	3341 (ar. C-H); 2960, 2931 (C-H) 1601 (ar. C=C); 1353 (ar. C-N) 1252 (aryl-O); 1169 (C-N) 1084 (alkyl-O)

Table 6.10: ATR-IR data for linker coupled materials.

Material	R	Raw data (cm^{-1})	Subtracted data (cm^{-1})[a]	Significant peaks (cm^{-1})
116a	*t*-Butyl	2960, 2933, 2762, 2695, 2456, 2362, 2325, 2236, 2210, 2116, 2066, 1894, 1712, 1603, 1513, 1488, 1444, 1354, 1286, 1252, 1228, 1178, 1085, 990, 902, 830, 795	2974, 2942, 2881, 2653, 2360, 2325, 2115, 1982, 1711, 1604, 1515, 1491, 1445m 1360, 1226, 1175, 1087, 993, 900, 835, 795	2960-2762 (C-H); 1603 (ar. C=C) 1354 (ar. C-N); 1252 (aryl-O) 1085 (alkyl-O)
116b	C_6H_{13}	3385, 2959, 2873, 2775, 2654, 2437, 2324, 1979, 1803, 1602, 1488, 1326, 1080, 989, 899, 830, 792, 708	2972, 2877, 2651, 2438, 2323, 1979, 1604, 1489, 1337, 1080, 988, 799, 792, 702	3385 (ar. C-H); 2959, 2873 (C-H) 1602 (ar. C=C); 1326 (ar. C-N) 1080 (alkyl-O)
116c	I	3215, 2923, 2854, 2536, 2450, 2276, 2203, 2132, 2886, 1999, 1942, 1929, 1740, 1462, 1377, 1286, 1138, 1075, 988, 905, 787,	3246, 2930, 3858, 2162, 1980, 1739, 1252, 1180, 1081, 902, 837, 795, 709	2923, 2854 (C-H); 1601 (ar. C=C) 1377 (C-N); 1286 (aryl-O) 1075 (alkyl-O); 541 (C-I)

		687, 594, 544, 541, 525, 508		
116d	NMe_2	3374, 2964, 2933, 2875, 2443, 2160, 1900, 1658, 1601, 1500, 1444, 1351, 1085, 989, 902, 794	2964, 2983, 2075, 2443, 2160, 1900, 1678, 1630, 1601, 1500, 1444, 1351, 1282, 1080, 988, 802	3374 (ar. C-H); 2964-2875 (C-H) 1601 (ar. C=C); 1351 (C-N) 1282 (aryl-O); 1085 (alkyl-O)
116e	H	2963, 2934, 2861, 2685, 2477, 2362, 2335, 2236, 2205, 2153, 2024, 2002, 1958, 1817, 1680, 1601, 1511, 1486, 1423, 1194, 1096, 989, 903, 834, 795	3191, 2951, 2913, 2850, 2603, 2217, 2157, 2024, 1971, 1528, 1501, 1466, 1426, 1379, 1266, 1210, 1115, 1001, 957, 927, 872, 815	2963-2934 (C-H); 1602 (ar. C=C) 1379 (ar. C-N)
116f	$O(CH_2CH_2O)_3CH_3$	3247, 2929, 2857, 2447, 2349, 2163, 2036, 1900, 1654, 1713, 1654, 1603, 1511, 1487, 1446, 1362, 1284, 1252, 1172, 1085, 989, 902, 794	3247, 2929, 2857, 2163, 1980, 1603, 1500, 1480, 1446, 1362, 1240, 1085, 989, 902, 794, 709	2929, 2857 (C-H); 1603 (ar. C=C) 1362 (C-N); 1284, 1252 (aryl-O) 1240 (ar C-O); 1085 (alkyl-O)
116g	OH	3400, 2960, 2932, 2859, 2726, 2650, 2291, 2121, 2109, 1666, 1603, 1512, 1487, 1444, 1285, 1252, 1169, 1086, 989, 903, 838	3704, 3221, 2962, 2934, 2752, 2589, 2263, 2050, 2018, 1982, 1512, 1487, 1444, 1084, 989, 902	3400 (OH, ar. C-H); 2960-2859 (C-H) 1603 (ar. C=C); 1252 (aryl-O) 1086 (alkyl-O)
116h	$CH_2P(O)(OEt)_2$	3215, 3020, 2964, 2936, 2877, 2778, 2163, 2031, 1980, 1793, 1657, 1602, 1511, 1487, 1445, 1355, 1276, 1218, 1062, 989, 902, 831	2942, 2880, 2163, 2031, 1940, 1656, 1602, 1487, 1445, 1357, 1192, 1017, 989, 902, 795, 709	3020-2876 (C-H); 1602 (ar. C=C) 1276 (aryl-O); 1217 (P=O) 1062 (alkyl-O); 1017 (P-OEt)
116i	NH_2	3404, 3280, 2962, 2874, 2778, 2652, 2362, 1978, 1794, 1725, 1602, 1630, 1657, 1511, 1487, 1445, 1354, 1314, 1217, 1062, 989, 903, 794, 709	3404, 3022, 2879, 2779, 1978, 1656, 1487, 1448, 1355, 1328, 1218, 1050, 989, 903, 831, 795, 709	3404, 3280, 3022 (N-H, ar. C-H) 2962-2874 (C-H); 1602 (C=C) 1328 (ar. C-N); 1217 (aryl-O) 1062 (alkyl-O)
116j	CH_2COOH	3396, 3020, 2962, 2938, 2875,	2971, 2879, 2162, 1979,	3396 (ar. C-H); 2962 – 2875(C-H)

		2361, 2162, 1979, 1793, 1723, 1602, 1487, 1511, 1353, 1315, 1063, 989, 902, 850, 794, 908	1805, 1602, 1487, 1354, 989, 902, 794, 708	3020 (O-H); 1723 (C=O) 1602 (ar. C=C); 1329 (ar. C-N) 1085 (alkyl-O)
116k	$CH_2P(O)(OH)(OEt)$	3246, 2929, 2857, 2606, 2348, 2388, 2262, 2039, 1735, 1602, 1457, 1298, 1252, 1174, 1081, 989, 960, 901, 835	3246, 2929, 2857, 2601, 2262, 2039, 1735, 1602, 1457, 1252, 1174, 1081, 1040 900, 837, 795, 708	2929, 2857 (C-H); 2606 (OH) 1602 (ar. C=C); 1298 (P=O) 1252 (aryl-O); 1081 (alkyl-O) 1040 (P-OR)
116l	$CH_2P(O)(OH)_2$	3396, 2931, 2859, 2600, 2457, 2224, 2827, 1602, 1520, 1487, 1446, 1351, 1252, 1171, 1083, 989, 902, 830	3396, 2931, 2859, 2601, 2232, 2027, 1602, 1520, 1487, 1446, 1352, 1083, 989, 902, 830, 795, 708	3396 (ar. C-H); 2931, 2859 (C-H) 2601 (O-H); 1602 (ar. C=C) 1298 (P=O); 1252 (aryl-O) 1081 (alkyl-O)
116m	$CH_2P(O)O_2Ca$	2930, 2859, 2728, 2268, 1979, 1741, 1654, 1601, 1511, 1487, 1446, 1252, 1170, 1084, 1018, 902, 795, 709	2931, 2859, 2617, 2161, 2027, 1979, 1601, 1520, 1446, 1252, 1084, 989, 822, 795	2859, 2728 (C-H); 2617(P(O)-O) 1601 (C=C); 1252 (aryl-O) 1084 (alkyl-O)

[a] Spectra of linker terminated **115** was subtracted.

Table 6.11: ATR-IR data for directly coupled materials.

Material	R	Raw data (cm^{-1})	Subtracted data (cm^{-1})[a]	Significant peaks
117a	*t*-Butyl	3279, 3021, 2967, 2940, 2692, 2324, 2236, 2116, 1979, 1711, 1659, 1631, 1603, 1512, 1486, 1445, 1360, 1275, 1087, 989, 903, 834, 795	3361, 2938, 2880, 2842, 2324, 2117, 1711, 1666, 1603, 1511, 1486, 1444, 1356, 1086, 989, 903, 835, 795	2967-2940 (C-H) 1603 (ar. C=C)
117b	C_6H_{13}	3338, 2929, 2856, 2445, 2285, 2163, 2036, 1980, 1743, 1649, 1467, 1379, 1156, 1679, 890, 722, 679	3345 (br), 2929, 2856, 2408, 2385, 2350, 2166, 2164, 2036, 1743, 1641, 1467, 1379, 1253, 1149, 1086, 1018, 903, 843, 790, 723, 681	2929, 2856 (C-H)

117c	I	3258, 2930, 2859, 2709, 2627, 2165, 1980, 1740, 1712, 1654, 1558, 1444, 1370, 1240, 1173, 990, 902, 793, 708	3268, 2930, 2859, 2709, 2628, 2166, 1980, 1713, 1655, 1444, 1370, 1279, 1048, 990, 903, 794, 709	2930, 2859 (C-H)
117d	NMe_2	3371 (br), 2973, 2938, 2910, 2257, 2039, 1657, 1604, 1511, 1486, 1445, 1087, 1047, 1989, 902, 880, 829, 794	3371, 2973, 2938, 2910, 2257, 2039, 1657, 1604, 1511, 1486, 1445, 1087, 1047, 989, 902, 880, 829, 794	2973-2910 (C-H) 1604 (ar. C=C)
117e	H	3366 (br), 3017, 2963, 2691, 2362, 1799, 1714, 1657, 1602, 1511, 1486, 1444, 1360, 1219, 1066, 989, 903, 831, 795, 709	3527, 2962, 2932, 2861, 2687, 2362, 2324, 2167, 2112, 1980, 1715, 1659, 1602, 1511, 1486, 1444, 1359, 1219, 1087, 989, 903, 834, 795, 709	2963, 2691 (C-H) 1602 (ar. C=C) (1360 ar. C-N)
117f	$O(CH_2CH_2O)_3CH_3$	3246 (br), 2957, 2930, 2858, 2167, 1979, 1739, 1653, 1540, 1510, 1486, 1443, 1251, 1149, 1083, 988, 903, 835, 792, 709	3246, 2929, 2859, 2719, 2628, 2167, 1979, 1663, 1510, 1446, 1251, 1080, 989, 903, 833, 709	2957, 2858 (C-H)
117g	OH	3020, 2974, 2941, 2883, 2934, 2036, 1796, 1631, 1603, 1512, 1487, 1443, 1087, 1018, 989, 902, 834, 795	3049, 3021, 2971, 2883, 2839, 1758, 1631, 1603, 1511, 1487, 1409. 1089, 1018, 989, 903, 834, 795, 708	3020 (O-H) 2974-2883 (C-H) 1603 (ar. C=C)
117h	$CH_2P(O)(OEt)_2$	3256 (br), 2930, 2857, 2436, 2163, 1979, 1640, 1560, 1298, 1150, 1049, 897, 683	3252, 2932, 2857, 2439, 2164, 1980, 1640, 1520, 1480, 1383, 1147, 1022, 920, 857, 739, 677	2932, 2903, 2857 (C-H)
117i	NH_2	3266 (br), 2930, 2858, 2740, 2655, 2349, 2299, 2163, 1979, 1744, 1468, 1353, 1083, 900, 795, 708	3266 (br), 2958, 2930, 2859, 2439, 2349, 2300, 2163, 2036, 1979, 1744, 1514, 1486, 1353, 1250, 1178, 1083, 1016, 990, 901, 837, 795, 708, 688	2930, 2858 (C-H)
117j	CH_2COOH	3257 (br), 2929, 2858, 2656, 2323, 2163, 1980, 1738, 1608, 1680, 1487, 1446, 1173, 989, 902, 794,	3326 (br), 2958, 2929, 2858, 2443, 2323, 2349, 2163, 1980, 1603, 1511, 1487, 1446, 1353, 1170, 1086, 989, 902, 794, 709	2929, 2858 (C-H)

		709		
117k	$CH_2P(O)(OH)(OEt)$	3242 (br), 2923, 2853, 2363, 2286, 2232, 2166, 2950, 1978, 1653, 1541, 1457, 1377, 1277, 1237, 1168, 1066, 990, 903, 836, 785, 709	3242, 2923, 2853, 2618, 2496, 2287, 2160, 2044, 1979, 1653, 1542, 1458, 1286, 1066, 990, 903, 835, 709	2923, 2853 (C-H) 1277 (P=O)
117l	$CH_2P(O)(OH)_2$	2345 (br), 2926, 2855, 2363, 2167, 1979, 1735, 1511, 1492, 1448, 1376, 1067, 988, 903, 834, 792, 709	3244 (br), 2926, 2855, 2363, 2168, 1979, 1735, 1511, 1447, 1276, 1249, 1156, 1068, 988, 903, 833, 791, 706	2926, 2855 (C-H) 1276 (P=O)
117m	$CH_2P(O)O_2Ca$	3368 (br), 2930, 2165, 1633, 1680, 1520, 1445, 1172, 1062, 989, 901	3367, 2930, 2165, 1980, 1633, 1520, 1480, 1446, 1080, 990, 903, 794, 709	2930, 2165 (C-H)

[a] Spectra of unmodified XAD-4 was subtracted.

Table 6.12: Summary of combustion analysis of linker coupled materials.

Material	**R**	**Combustion analysis data**	**mmol of nitrogen / g of polymer**	**mmol surface modification / g polymer**	**Molecules / g polymer**	**Molecules / cm^{2} [a]**	**Surface coverage (%)[b]**	**Coupling efficiency (%)**	**N[c]**
115	-	%C: 87.34 %H: 7.72 %N: 0.25	0.179	0.179	1.08×10^{20}	1.48×10^{13}	25	n/a	50
116a	*t*-Butyl	%C: 84.18 %H: 7.45 %N: 0.26	0.186	0.062	3.73×10^{19}	5.14×10^{12}	9	35	149
116b	C_6H_{13}	%C: 90.63 %H: 7.97 %N: 0.28	0.200	0.067	4.01×10^{19}	5.54×10^{12}	9	37	138

116c	I	%C: 87.60 %H: 7.88 %N: 1.5 %I: 1.66	1.071	0.357	2.15×10^{20}	2.97×10^{13}	51	200	20
116d	NMe_2	%C: 80.48 %H: 7.19 %N: 0.21	0.150	0.038	2.26×10^{19}	3.11×10^{12}	5	21	251
116e	H	%C: 89.78 %H: 8.14 %N: 0.7	0.500	0.167	1.00×10^{20}	1.38×10^{13}	24	93	52
116f	$O(CH_2CH_2O)_3CH_3$	%C: 88.35 %H: 7.67 %N: 0.52	0.371	0.124	7.46×10^{19}	1.03×10^{13}	18	69	71
116g	OH	%C: 83.86 %H: 6.99 %N: 0.24	0.171	0.057	3.44×10^{19}	4.75×10^{12}	8	32	163
116h	$CH_2P(O)(OEt)_2$	%C: 89.34 %H: 7.62 %N: 0.34 % P: 0.06	0.243	0.121	7.31×10^{19}	1.01×10^{13}	17	68	72
116i	NH_2	%C: 90.09 %H: 8.00 %N: 0.26	0.186	0.046	2.80×10^{19}	3.86×10^{12}	7	26	202
116j	CH_2COOH	%C: 89.76 %H: 7.92 %N: 0.22	0.157	0.052	3.15×10^{19}	4.35×10^{12}	7	29	178
116k	$CH_2P(O)(OH)(OEt)$	%C: 88.25 %H: 7.62 %N: 0.63 %P: 0.11	0.450	0.150	9.03×10^{19}	1.25×10^{13}	21	84	58
116l	$CH_2P(O)(OH)_2$	%C: 90.70	0.436	0.145	8.75×10^{19}	1.21×10^{13}	21	81	60

		%H: 7.84 %N: 0.61 %P: 0.71							
116m	$CH_2P(O)O_2Ca$	%C: 89.68 %H: 7.91 %N: 0.32 %P: 0.06	0.229	0.076	4.59×10^{19}	6.33×10^{12}	11	43	120

[a]Calculated on the basis of a bead surface area of $725 m^2/g$; [b]A limiting area of 1.71 nm^2/molecule is assumed as calculated using Chemicalize (www.chemicalize.com); [c]N is the ratio of unmodified sites to modified sites.

Table 6.13: Combustion analysis of directly coupled materials.

Material	**R**	**Combustion analysis data**	**mmol of nitrogen / g of polymer**	**mmol surface modification / g polymer**	**Molecules / g polymer**	**Molecules / cm^{2} [a]**	**Surface coverage (%)[b]**	**N[c]**
117a	*t*-Butyl	%C: 89.12 %H: 7.79 %N: 0.10	0.071	0.036	2.15×10^{19}	2.97×10^{12}	0.7	65
117b	C_6H_{13}	%C: 85.18 %H: 7.60 %N: 0.10	0.071	0.036	2.15×10^{19}	2.97×10^{12}	0.7	64
117c	I	%C: 83.97 %H: 7.40 %N: 0.89	0.636	0.318	1.91×10^{20}	2.64×10^{13}	6.2	4
117d	NMe_2	%C: 81.39 %H: 7.28 %N: 0.10	0.071	0.024	1.43×10^{19}	1.98×10^{12}	0.5	42

117e	H	%C: 82.45 %H: 7.48 %N :0.34	0.243	0.121	7.31×10^{19}	1.01×10^{13}	2.4	18
117f	$O(CH_2CH_2O)_3CH_3$	%C: 86.40 %H: 7.50 %N: 0.43	0.307	0.154	9.25×10^{19}	1.28×10^{13}	3.0	12
117g	OH	%C: 89.88 %H: 7.95 %N: 0.10	0.071	0.036	2.15×10^{19}	2.97×10^{12}	0.7	65
117h	$CH_2P(O)(OEt)_2$	%C: 89.67 %H: 8.00 %N: 0.15 %P: 0.04	0.107	0.054	3.23×10^{19}	4.45×10^{12}	1.0	41
117i	NH_2	%C: 77.76 %H: 6.85 %N: 0.04	0.029	0.010	5.74×10^{18}	7.91×10^{11}	0.2	110
117j	CH_2COOH	%C: 87.69 %H: 7.65 %N: 0.03	0.021	0.011	6.45×10^{18}	8.90×10^{11}	0.2	222
117k	$CH_2P(O)(OH)(OEt)$	%C: 89.66 %H:7.74 %N: 0.39 % P: 0.06	0.279	0.139	8.39×10^{19}	1.16×10^{13}	2.7	14
117l	$CH_2P(O)(OH)_2$	%C: 90.91 %H:7.84 %N: 0.46 %P: 0.09	0.329	0.164	9.89×10^{19}	1.36×10^{13}	3.2	12
117m	$CH_2P(O)O_2Ca$	%C: 89.89 %H: 8.01 %N: 0.49 %P: 0.10	0.350	0.175	1.05×10^{20}	1.45×10^{13}	3.4	10

[a]Calculated on the basis of a bead surface area of 725m^2/g; [b]A limiting area of 0.24 nm^2/molecule is assumed as calculated using Chemicalize (www.chemicalize.com); [c]N is the ratio of unmodified sites to modified sites.

Table 6.14: TGA and DSC thermal analysis.

Material	R	TGA decomposition temperature (˚C)				DSC thermal event (˚C)				
		Sample 1	Sample 2	Average	Standard deviation	Sample 1	Sample 2	Sample 3	Average	Standard deviation
XAD-4	-	473.74	476.20	474.97	1.74	103.86	97.41	100.65	100.64	3.23
115	-	474.48	472.20	473.34	1.61	105.44	104.58	-	105.01	0.61
116a	*t*-Butyl	472.87	473.63	473.25	0.54	91.78	100.33	100.55	97.55	5.00
116b	C_6H_{13}	472.37	474.95	473.66	1.82	89.68	90.26	102.62	94.19	7.31
116c	I	474.34	478.39	476.37	2.86	99.46	94.21	100.01	97.89	3.20
116d	NMe_2	475.26	477.68	476.47	1.71	99.42	95.15	95.89	96.82	2.28
116e	H	472.70	474.83	473.77	1.51	92.95	101.06	101.26	98.42	4.74
116f	$O(CH_2CH_2O)_3CH_3$	472.46	475.08	473.77	1.85	98.76	94.30	101.25	98.10	3.52
116g	OH	475.78	477.10	476.44	0.93	91.11	102.08	95.30	96.16	5.54
116h	$CH_2P(O)(OEt)_2$	475.63	478.53	477.08	2.05	99.90	90.72	99.73	96.78	5.25
116i	NH_2	476.75	473.34	475.05	2.41	90.16	99.95	91.93	94.01	5.22
116j	CH_2COOH	472.59	469.33	470.96	2.31	100.41	92.07	102.13	98.20	5.38
116k	$CH_2P(O)(OH)(OEt)$	477.52	475.63	476.58	1.34	101.61	93.28	101.07	98.65	4.66
116l	$CH_2P(O)(OH)_2$	474.83	471.49	473.16	2.36	94.01	100.79	92.66	95.82	4.36
116m	$CH_2P(O)O_2Ca$	475.04	472.89	473.97	1.52	90.42	101.41	96.30	96.04	5.50

6.4.3 Preparation and characterisation of Penicillin V loaded materials

Preparation of materials 121 and 122

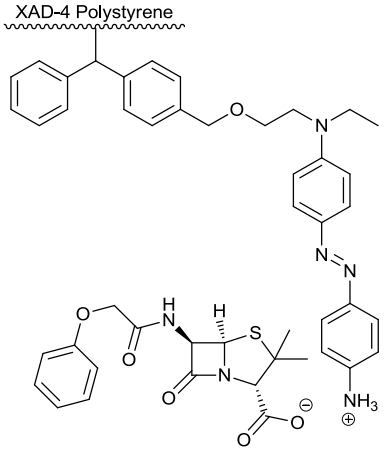

121

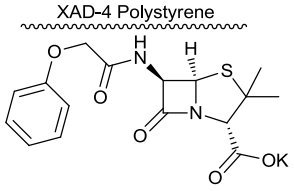

122

To generate **121** as pale green beads, amine modified beads **116i** was used. **122** was produced from unmodified XAD-4 and no colour change was observed.

The beads (**116i** or unmodified XAD-4) (1 g) were soaked in a solution of the potassium salt of penicillin V in phosphate buffered saline, pH 7.24, (25 ml, 5 μmol/ml) for 18 hours, if necessary a drop of EtOH was added to the mixture so that the beads did not rest on the surface of the solution. The beads were filtered and washed extensively with water then dried under vacuum. Table 6.15: Table displaying the combustion analysis data and surface loadings of penicillin V.

Table 6.16: Combustion analysis of penicillin loaded materials

Material	Combustion analysis data	Loading of Sulphur (mmol/g of polymer)	Molecules of Penicillin V per g of polymer	Molecules of Penicillin V per cm^2
121	C: 77.21 H: 6.96 N: 0.32 S: 0.45	0.14	8.45×10^{19}	1.17×10^{13}
122	C: 65.83 H: 5.97 N: 0.24 S:0.58	0.18	1.09×10^{20}	1.50×10^{13}

6.5 Chapter 5

Protein adsorption protocol: single incubation time[†]

The beads were sterilized in methanol then exposed to DPBS (physiological pH) for 18 hours, after which they were dried for 24 hours at 37 ˚C. The beads (2 mg) were placed in well plates with BSA-DPBS solution (1000 µl, 5 mg/ml). After incubation at 37 ˚C under constant shaking for 3 hours the remaining solution was removed, leaving behind the beads. A solution of 1% (w/v) SDS (sodium dodecyl sulphate) (1 ml) was added to each of the wells after which they were incubated for 1 hour at 37 ˚C. The SDS solutions were removed and the optical density of the solutions measured using a spectrometer at wavelength 280 nm. Using a calibration curve, the optical density measurements could be converted into the quantity of protein adsorbed onto the beads.

Protein adsorption protocol: multiple incubation times[†]

The beads were sterilised in methanol for 10 minutes, soaked in DPBS (physiological pH) for 18 hours and dried in the oven at 37 ˚C for 24 hours. For each material 5 experiments were performed according to the incubation times of 1, 3, 6, 12, and 24 hours with three replicas per experiment. The beads (2 mg) were added to the wells with BSA-DPBS solution (200 µl, 5 mg/ml) and the beads were incubated at 37 ˚C under constant shaking for the allotted time. At the end of the incubation time the remaining solution was removed from the well then the optical density of the solution measured with a spectrometer at 280 nm, the concentration of BSA remaining in the solution was found using a calibration curve. The quantity of protein adsorption by the beads was obtained by measuring the change in concentration of BSA in the PBS solution. The results are below in Table 6.18

Hole-plate bioassay

The bioassay plates were prepared by Wendy Sobey. Materials **121** and **122** were tested against *Staphylococcus Aureus* and *Escherichia Coli*. Various amounts of **121** and **122** were placed into wells cut out of bioassay plates, the beads sealed in with agar then the samples incubated overnight ay 37 ˚C. The diameters of the inhibition zones were measured and then the relative potency of the materials calculated from standards prepared using cephalosporin C, where a calibration curve had been prepared of zone size against the log of the molar concentration of cephalosporin C.

Table 6.17: Protein adsorption after incubation for 3 hours.

Functionality	Protein adsorption (mg/mg)	Adjusted protein adsorption (g/mmol of surface modification)
XAD-4	0.0265	N/A
115	0.0355	0.198
116a	0.02	0.323
116b	0.0365	0.547
116c	0.045	0.126
116d	0.015	0.400
116f	0.0305	0.246
116g	0.025	0.438
116h	0.033	0.273
116i	0.03	0.647
116j	0.0355	0.677
116k	0.095	0.633
116l	0.0375	0.259
116m	0.0495	0.650

Table 6.18: Average protein adsorption after incubation at various time intervals.

	Average concentration of protein adsorbed (mg/ml)					Average percentage of BSA adsorbed					Standard deviations				
Material	**1 hour**	**3 hours**	**6 hours**	**12 hours**	**24 hours**	**1 hour**	**3 hours**	**6 hours**	**12 hours**	**24 hours**	**1 hour**	**3 hours**	**6 hours**	**12 hours**	**24 hours**
Xad-4	0.057	0.070	0.071	0.082	0.106	5.12	6.31	6.34	7.34	9.50	0.03	1.87	1.22	1.14	2.58
115	0.084	0.064	0.053	0.045	0.067	7.56	5.78	4.76	4.06	6.03	1.25	1.19	3.88	1.75	1.65
116a	0.083	0.057	0.094	0.087	0.082	7.50	5.08	8.46	7.85	7.38	1.37	4.31	1.95	2.56	0.47
116b	0.065	0.068	0.084	0.102	0.107	5.88	6.14	7.59	9.18	9.60	4.47	0.92	1.62	0.01	0.97
116d	0.047	0.071	0.086	0.066	0.048	4.26	6.37	7.76	5.90	4.33	3.61	0.38	0.99	1.57	0.88
116f	0.084	0.085	0.075	0.053	0.054	7.50	7.67	6.74	4.78	4.81	0.47	0.69	3.50	1.69	0.34
116g	0.066	0.021	0.063	0.028	0.028	5.96	1.92	5.65	2.50	2.55	2.20	0.57	2.37	1.11	2.04
116h	0.098	0.037	0.116	0.123	0.072	8.79	3.36	10.42	11.03	6.47	2.90	0.11	4.44	5.55	1.60
116i	0.055	0.042	0.087	0.061	0.069	4.95	3.81	7.84	5.45	6.15	2.30	1.54	1.71	4.85	1.07
116j	0.069	0.087	0.113	0.099	0.096	6.15	7.79	10.17	8.85	8.65	3.69	0.87	0.55	0.98	0.31

Table 6.19: Data obtained from hole plate bioassay with *E. Coli.*

Material	Sample mass (mg)	Zone size (mm)	Equivalent nmol of cephalosporin c per well	µmol of Penicillin V per sample[a]	% Relative potency[b]	nmoles of penicillin V released	% Penicillin V released	% Relative potency[c]
121	7.6	19	0.95	1.06	0.089	0.90	0.085	105
	10.9	14	0.42	1.53	0.028	0.40	0.026	106
	15.7	25.5	2.70	2.20	0.123	1.55	0.071	174
	21.4	26	2.93	3.00	0.098	1.60	0.053	183
	26.7	26.5	3.17	3.74	0.085	1.65	0.044	192
	32	30	5.57	4.48	0.124	2.00	0.045	278
	40.7	30	5.57	5.70	0.098	2.00	0.035	278
	49.3	30.5	6.04	6.90	0.087	2.05	0.030	294
	55.4	31	6.54	7.76	0.084	2.10	0.027	312
	71.5	35	12.5	10.0	0.124	2.50	0.025	498
122	5.1	23	1.81	0.92	0.196	1.30	0.141	139
	10.7	26.5	3.17	1.94	0.164	1.65	0.085	192
	16.7	28	4.04	3.02	0.134	1.80	0.060	224
	19.9	34	10.6	3.60	0.294	2.40	0.067	442
	26.3	37	17.2	4.76	0.361	2.70	0.057	636
	31.4	38.5	21.9	5.68	0.385	2.85	0.050	768
	41.6	39	23.7	7.53	0.315	2.90	0.039	818
	49.7	42	38.4	9.00	0.427	3.20	0.036	1201
	61	41	32.7	11.0	0.296	3.10	0.028	1055
	69.6	42	38.4	12.6	0.305	3.20	0.025	1201

[a] Calculated using the loadings of penicillin V determined by combustion analysis; [b] based on the total available amount of penicillin V in the sample; [c] based on the amount of penicillin V released.

Table 6.20: Data obtained from hole plate bioassay with *S. Aureus.*

Material	Sample mass (mg)	Zone size (mm)	Equivalent µmoles of Cephalosporin C per well	µmoles of penicillin V in sample[a]	% Relative potency[b]
121	6.6	31	2.26	0.92	245
	11.1	36	5.60	1.55	361
	14.4	35	4.67	2.02	232
	26.3	39	9.66	3.68	262
	34.9	38	8.06	4.89	165
	42.7	45	28.7	5.98	480
	59.9	41	12.7	8.39	151
	71	41	13.9	9.94	140
122	7.1	38	8.06	1.29	627
	10	40	11.6	1.81	640
	16.3	42	16.6	2.95	564
	20.4	41	13.9	3.69	376
	26.8	42	16.6	4.85	343
	31.2	41	13.9	5.65	246
	42.5	46	34.4	7.69	447
	51.5	41	13.9	9.32	149
	63	46	34.4	11.4	302
	71.9	50	71.1	13.0	546

[a] Calculated using the loadings of penicillin V determined by combustion analysis; [b] based on the total available amount of penicillin V in the sample

Chapter 7: References

1. D. F. Williams, *Definitions in biomaterials: Progress in biomedical engineering 4*, Elsevier, Amsterdam, 1987.
2. B. D. Ratner and S. J. Bryant, *Annual Review of Biomedical Engineering*, 2004, **6**, 41-75.
3. M. Salta, J. A. Wharton, P. Stoodley, S. P. Dennington, L. R. Goodes, S. Werwinski, U. Mart, R. J. K. Wood and K. R. Stokes, *Philosophical Transactions of the Royal Society a-Mathematical Physical and Engineering Sciences*, 2010, **368**, 4729-4754.
4. A. Caro, V. Humblot, C. Methivier, M. Minier, M. Salmain and C-M. Pradier, *Journal of Physical Chemistry B*, 2009, **113**, 2101-2109.
5. L. Nordstierna, A. A. Abdalla, M. Masuda, G. Skarnemark and M. Nyden, *Progress in Organic Coatings*, 2010, **69**, 45-48.
6. L. K. Ista, M. E. Callow, J. A. Finlay, S. E. Coleman, A. C. Nolasco, R. H. Simons, J. A. Callow and G. P. Lopez, *Applied and Environmental Microbiology*, 2004, **70**, 4151-4157.
7. P. Vadgama, *Annual Reports Section C (Physical Chemistry)*, 2005, **101**, 14-52.
8. E. Moy, F. Y. H. Lin, J. W. Vogtle, Z. Policova and A. W. Neumann, *Colloid and Polymer Science*, 1994, **272**, 1245-1251.
9. M. Charnley, M. Textor and C. Acikgoz, *Reactive & Functional Polymers*, 2011, **71**, 329-334.
10. C.-K. Kang and Y.-S. Lee, *Journal of Materials Science-Materials in Medicine*, 2007, **18**, 1389-1398.
11. J. W. Costerton, P. S. Stewart and E. P. Greenberg, *Science*, 1999, **284**, 1318-1322.
12. S. Hou, E. A. Burton, R. L. Wu, Y.-Y. Luk and D. Ren, *Chemical Communications*, 2009, 1207-1209.
13. S. Dobretsov, M. Teplitski and V. Paul, *Biofouling*, 2009, **25**, 413-427.
14. E.-R. Kenawy, S. D. Worley and R. Broughton, *Biomacromolecules*, 2007, **8**, 1359-1384.
15. J. M. Schierholz, N. Yucel, A. F. E. Rump, J. Beuth and G. Pulverer, *International Journal of Antimicrobial Agents*, 2002, **19**, 511-516.
16. L. R. Hoffman, D. A. D'Argenio, M. J. MacCoss, Z. Y. Zhang, R. A. Jones and S. I. Miller, *Nature*, 2005, **436**, 1171-1175.
17. G. A. O'Toole and P. S. Stewart, *Nature Biotechnology*, 2005, **23**, 1378-1379.
18. D. Hames and N. Hooper, *Biochemistry*, 3rd edn., Taylor and Francis Group, UK, 2005.
19. W. Norde, *Pure and Applied Chemistry*, 1994, **66**, 491-496.
20. B. N. Johnson and R. Mutharasan, *Langmuir*, 2012, **28**, 6928-6934.
21. B. G. Keselowsky, D. M. Collard and A. J. Garcia, *Journal of Biomedical Materials Research Part A*, 2003, **66A**, 247-259.
22. K. M. Defife, K. M. Hagen, D. L. Clapper and J. M. Anderson, *Journal of Biomaterials Science-Polymer Edition*, 1999, **10**, 1063-1074.
23. T. Tsukagoshi, Y. Kondo and N. Yoshino, *Colloids and Surfaces B-Biointerfaces*, 2007, **54**, 101-107.
24. A. Kugel, S. Stafslien and B. J. Chisholm, *Progress in Organic Coatings*, 2011, **72**, 222-252.
25. R. G. Chapman, E. Ostuni, S. Takayama, R. E. Holmlin, L. Yan and G. M. Whitesides, *Journal of the American Chemical Society*, 2000, **122**, 8303-8304.

26. A. S. G. Curtis, J. V. Forrester, C. McInnes and F. Lawrie, *Journal of Cell Biology*, 1983, **97**, 1500-1506.
27. P. Kingshott, J. Wei, D. Bagge-Ravn, N. Gadegaard and L. Gram, *Langmuir*, 2003, **19**, 6912-6921.
28. U. Hersel, C. Dahmen and H. Kessler, *Biomaterials*, 2003, **24**, 4385-4415.
29. R. A. Gemeinhart, C. M. Bare, R. T. Haasch and E. J. Gemeinhart, *Journal of Biomedical Materials Research Part A*, 2006, **78A**, 433-440.
30. J. N. Baumgartner, C. Z. Yang and S. L. Cooper, *Biomaterials*, 1997, **18**, 831-837.
31. M. H. Lee, D. A. Brass, R. Morris, R. J. Composto and P. Ducheyne, *Biomaterials*, 2005, **26**, 1721-1730.
32. A. Joy, D. M. Cohen, A. Luk, E. Anim-Danso, C. Chen and J. Kohn, *Langmuir*, 2011, **27**, 1891-1899.
33. J. M. Li, M. J. Menconi, H. B. Wheeler, M. J. Rohrer, V. A. Klassen, J. E. Ansell, M. C. Appel and J. Cronenwett, *Journal of Vascular Surgery*, 1992, **15**, 1010-1017.
34. R. Vohra, G. J. L. Thomson, H. M. H. Carr, H. Sharma and M. G. Walker, *British Journal of Surgery*, 1991, **78**, 417-420.
35. M. Schuler, G. R. Owen, D. W. Hamilton, M. De Wilde, M. Textor, D. M. Brunette and S. G. P. Tosatti, *Biomaterials*, 2006, **27**, 4003-4015.
36. S. Venkataraman, Y. Zhang, L. Liu and Y.-Y. Yang, *Biomaterials*, 2010, **31**, 1751-1756.
37. G. Guangzheng, D. Lange, K. Hilpert, J. Kindrachuk, Z. Yuquan, J. T. J. Cheng, M. Kazemzadeh-Narbat, Y. Kai, W. Rizhi, S. K. Straus, D. E. Brooks, B. H. Chew, R. E. W. Hancock and J. N. Kizhakkedathu, *Biomaterials*, 2011, **32**.
38. K. Glinel, A. M. Jonas, T. Jouenne, J. Leprince, L. Galas and W. T. S. Huck, *Bioconjugate Chemistry*, 2009, **20**, 71-77.
39. R. de Nys and P. D. Steinberg, *Current Opinion in Biotechnology*, 2002, **13**, 244-248.
40. Y. Han, S. Hou, K. A. Simon, D. Ren and Y.-Y. Luk, *Bioorganic & Medicinal Chemistry Letters*, 2008, **18**, 1006-1010.
41. E. B. H. Hume, J. Baveja, B. W. Muir, T. L. Schubert, N. Kumar, S. Kjelleberg, H. J. Griesser, H. Thissen, R. Read, L. A. Poole-Warren, K. Schindhelm and M. D. P. Willcox, *Biomaterials*, 2004, **25**, 5023-5030.
42. R. Kuehl, S. Al-Bataineh, O. Gordon, R. Luginbuehl, M. Otto, M. Textor and R. Landmann, *Antimicrobial Agents and Chemotherapy*, 2009, **53**, 4159-4166.
43. N. Aumsuwan, S. Heinhorst and M. W. Urban, *Biomacromolecules*, 2007, **8**, 713-718.
44. N. Aumsuwan, R. C. Danyus, S. Heinhorst and M. W. Urban, *Biomacromolecules*, 2008, **9**, 1712-1718.
45. S.-H. Yang, Y.-S. J. Lee, F.-H. Lin, J.-M. Yang and K.-S. Chen, *Journal of Biomedical Materials Research Part B-Applied Biomaterials*, 2007, **83B**, 304-313.
46. M. C. Porte-Durrieu, C. Labrugere, F. Villars, F. Lefebvre, S. Dutoya, A. Guette, L. Bordenave and C. Baquey, *Journal of Biomedical Materials Research*, 1999, **46**, 368-375.
47. H. B. Lin, C. Garciaecheverria, S. Asakura, W. Sun, D. F. Mosher and S. L. Cooper, *Biomaterials*, 1992, **13**, 905-914.
48. M. W. Huh, I. K. Kang, D. H. Lee, W. S. Kim, L. S. Park, K. E. Min and K. H. Seo, *Journal of Applied Polymer Science*, 2001, **81**, 2769-2778.
49. O. Moreau, C. Portella, F. Massicot, J. M. Herry and A. M. Riquet, *Surface & Coatings Technology*, 2007, **201**, 5994-6004.

50. J. Vartiainen, M. Ratto and S. Paulussen, *Packaging Technology and Science*, 2005, **18**, 243-251.
51. S. G. Hu, C. H. Jou and M. C. Yang, *Journal of Applied Polymer Science*, 2002, **86**, 2977-2983.
52. B. Gottenbos, H. C. van der Mei, F. Klatter, P. Nieuwenhuis and H. J. Busscher, *Biomaterials*, 2002, **23**, 1417-1423.
53. R. A. Quirk, W. C. Chan, M. C. Davies, S. J. B. Tendler and K. M. Shakesheff, *Biomaterials*, 2001, **22**, 865-872.
54. K. O. V. Flores, A. P. de Aguiar, M. R. M. P. de Aguiar and L. C. d. S. Maria, *Materials Letters*, 2007, **61**, 1190-1196.
55. J. Bernard, C. Branger, T. L. A. Nguyen, R. Denoyel and A. Margaillan, *Reactive & Functional Polymers*, 2008, **68**, 1362-1370.
56. J. L. Boudenne, S. Boussetta, C. Brach-Papa, C. Branger, A. Margaillan and F. Theraulaz, *Polymer International*, 2002, **51**, 1050-1057.
57. M. G. Moloney, *Journal of Physics D-Applied Physics*, 2008, **41**, 174006-17414.
58. D. Leonard, M. G. Moloney and C. Thompson, *Tetrahedron Letters*, 2009, **50**, 3499-3502.
59. H. Wang, J.-P. Griffiths, R. G. Egdell, M. G. Moloney and J. S. Foord, *Langmuir*, 2008, **24**, 862-868.
60. K. M. Awenat, P. J. Davis, M. G. Moloney and W. Ebenezer, *Chemical Communications*, 2005, 990-992.
61. D. R. Braybrook, M. G. Moloney, H. M. I. Osborn and W. J. Norris, *Journal of Photochemistry and Photobiology a-Chemistry*, 1993, **70**, 171-178.
62. A. Blencowe, K. Cosstick and W. Hayes, *New Journal of Chemistry*, 2006, **30**, 53-58.
63. C. Choong, J. S. Foord, J.-P. Griffiths, E. M. Parker, B. Luo, M. Bora and M. G. Moloney, *New Journal of Chemistry*, 2012, **36**, 1187-1200.
64. D. Griller, A. S. Nazran and J. C. Scaiano, *Journal of the American Chemical Society*, 1984, **106**, 198-202.
65. D. Griller, M. Majewski, W. G. McGimpsey, A. S. Nazran and J. C. Scaiano, *Journal of Organic Chemistry*, 1988, **53**, 1550-1553.
66. K. B. Eisenthal, N. J. Turro, M. Aikawa, J. A. Butcher, C. Dupuy, G. Hefferon, W. Hetherington, G. M. Korenowski and M. J. McAuliffe, *Journal of the American Chemical Society*, 1980, **102**, 6563-6565.
67. S. B. Duckett, M. D. Galvez-Lopez, R. N. Perutz and D. Schott, *Dalton Transactions*, 2004, 2746-2749.
68. A. S. Nazran and D. Griller, *Journal of the American Chemical Society*, 1985, **107**, 4613-4615.
69. P. B. Grasse, B. E. Brauer, J. J. Zupancic, K. J. Kaufmann and G. B. Schuster, *Journal of the American Chemical Society*, 1983, **105**, 6833-6845.
70. Y. Z. Li and G. B. Schuster, *Journal of Organic Chemistry*, 1988, **53**, 1273-1277.
71. K. Hirai, K. Hatanaka, T. Yamaguchi, A. Miyajima, T. Kitagawa and H. Tomioka, *Journal of Physical Organic Chemistry*, 2011, **24**, 909-920.
72. K. Monguchi, T. Itoh, K. Hirai and H. Tomioka, *Journal of the American Chemical Society*, 2004, **126**, 11900-11913.
73. T. Itoh, Y. Nakata, K. Hirai and H. Tomioka, *Journal of the American Chemical Society*, 2006, **128**, 957-967.
74. H. Tomioka, E. Iwamoto, H. Itakura and K. Hirai, *Nature*, 2001, **412**, 626-628.
75. E. Iwamoto, K. Hirai and H. Tomioka, *Journal of the American Chemical Society*, 2003, **125**, 14664-14665.

76. H. Tomioka, *Research on Chemical Intermediates*, 1994, **20**, 605-634.
77. D. Griller, A. S. Nazran and J. C. Scaiano, *Tetrahedron*, 1985, **41**, 1525-1530.
78. J-P. Griffiths, D. M. L. Leonard, M. G. Moloney and N. J. Stratton, Journal of Molecular and Engineering Materials, submitted 2012.
79. D. Ke and W. Rizhi, *Journal of Materials Chemistry*, 2006, **16**, 2309-2321.
80. C. Choong, J.-P. Griffiths, M. G. Moloney, J. Triffitt and D. Swallow, *Reactive & Functional Polymers*, 2009, **69**, 77-85.
81. K. M. Awenat, *DPhil Thesis*, University of Oxford, 1998.
82. Vantamel.Ee, M. Davis and M. F. Deem, *Chemical Communications*, 1965, 71-72.
83. J. J. Looker, *Journal of Organic Chemistry*, 1967, **32**, 472-473.
84. H. Zollinger, *Color Chemistry*, 3rd edn., Wiley-VCH, Switzerland, 2003.
85. J. H. Gardner and L. Joseph, *Journal of the American Chemical Society*, 1935, **57**, 1.
86. G. P. Wild, C. Wiles, P. Watts and S. J. Haswell, *Tetrahedron*, 2009, **65**, 1618-1629.
87. C. H. Lee, J. S. Kim, S. Y. Park, D. J. Ahn and J.-M. Kim, *Chemistry Letters*, 2007, **36**, 682-683.
88. J. L. Bahr, J. P. Yang, D. V. Kosynkin, M. J. Bronikowski, R. E. Smalley and J. M. Tour, *Journal of the American Chemical Society*, 2001, **123**, 6536-6542.
89. T. Suzuki, O. Nagae, Y. Kato, H. Nakagawa, K. Fukuhara and N. Miyata, *Journal of the American Chemical Society*, 2005, **127**, 11720-11726.
90. S. Gester, J. Pietzsch and F. R. Wuest, *Journal of Labelled Compounds & Radiopharmaceuticals*, 2007, **50**, 105-113.
91. D. Leonard, *Part II Thesis*, University of Oxford, 2008.
92. Z. Heinrich, *Color Chemistry*, 3rd edn., Wiley-VCH, Switzerland, 2003.
93. G. S. Kumar and D. C. Neckers, *Chemical Reviews*, 1989, **89**, 1915-1925.
94. R. M. Silverstein, F. X. Webster and D. Kiemle, *Spectrometric identification of organic compounds*, 7th edn., Wiley, 2005.
95. G. E. Lewis, *Journal of Organic Chemistry*, 1960, **25**, 871-872.
96. B. B. Thompson and P. G. Kulkarni, *Journal of Pharmaceutical Sciences*, 1969, **58**, 623-625.
97. H. Mustroph and J. Epperlein, *Journal Fuer Praktische Chemie*, 1980, **322**, 205-313.
98. P. F. Gordon and P. Gregory, *Organic Chemistry in Colour*, Springer-Verlag, 1983.
99. J. Zhou, J. Zhang, Y. Ma and J. Tong, *Carbohydrate Polymers*, 2008, **74**, 405-410.
100. G. W. Nelson, M. Perry, S.-M. He, D. L. Zechel and J. H. Horton, *Colloids and Surfaces B-Biointerfaces*, 2010, **78**, 61-68.
101. Q-Sense, *www.q-sense.com*.
102. A. Dolatshahi-Pirouz, K. Rechendorff, M. B. Hovgaard, M. Foss, J. Chevallier and F. Besenbacher, *Colloids and Surfaces B-Biointerfaces*, 2008, **66**, 53-59.
103. A. A. Feiler, A. Sahlholm, T. Sandberg and K. D. Caldwell, *Journal of Colloid and Interface Science*, 2007, **315**, 475-481.
104. R. Zeng, Y. Zhang, Z. Liang, M. Tu and C. Zhou, *Science in China Series E-Technological Sciences*, 2009, **52**, 2275-2279.
105. Z. Yang and C. Zhang, *Applied Surface Science*, 2009, **255**, 4569-4574.
106. J. L. Jordan and E. J. Fernandez, *Biotechnology and Bioengineering*, 2008, **101**, 837-842.
107. H. Stadler, M. Mondon and C. Ziegler, *Analytical and Bioanalytical Chemistry*, 2003, **375**, 53-61.
108. F. Hook, J. Voros, M. Rodahl, R. Kurrat, P. Boni, J. J. Ramsden, M. Textor, N. D. Spencer, P. Tengvall, J. Gold and B. Kasemo, *Colloids and Surfaces B-Biointerfaces*, 2002, **24**, 155-170.

109. F. Hook, B. Kasemo, T. Nylander, C. Fant, K. Sott and H. Elwing, *Analytical Chemistry*, 2001, **73**, 5796-5804.
110. H. Xiao Min and D. C. Carter, *Nature*, 1992, **358**, 209-215.
111. J. Ghuman, P. A. Zunszain, I. Petitpas, A. A. Bhattacharya, M. Otagiri and S. Curry, *Journal of Molecular Biology*, 2005, **353**, 38-52.
112. M. R. Panjehshahin, M. S. Yates and C. J. Bowmer, *Biochemical Pharmacology*, 1992, **44**, 873-879.
113. C. M. Stiff, M. Zhong, R. W. Sarver, H. Gao, A. M. Ho, M. T. Sweeney, G. E. Zurenko and D. L. Romero, *Bioorganic & Medicinal Chemistry Letters*, 2007, **17**, 5479-5482.
114. G. L. Trainor, *Annual Reports in Medicinal Chemistry, Vol 42*, 2007, **42**, 489-502.
115. Rohm and Haas, *www.rohmhaas.com/ionexchange*.
116. Sigma-Aldrich, *www.sigmaaldrich.com*.
117. L. Sansom, *DPhil Thesis*, University of Oxford.
118. N. Ochoa, G. Baril, F. Moran and N. Pebere, *Journal of Applied Electrochemistry*, 2002, **32**, 497-504.
119. A. Vogel, *Vogel's Textbook of Practical Organic Chemistry*, 4th edn., Longman Group Limited, United States, 1978.
120. Perkin Elmer, *www.perkinelmer.com*.
121. K. S. Birdi, *Self-assembly monolayer structures of lipids and macromolecules at interfaces*, Springer, 1999.
122. ChemAxon, *www.chemicalize.org*.
123. EMD Chemicals, *www.emdchemicals.com*.
124. F. Boury, H. Marchais, J. P. Benoit and J. E. Proust, *Biomaterials*, 1997, **18**, 125-136.
125. P. R. Waghmare and S. K. Mitra, *Langmuir*, 2010, **26**, 17082-17089.
126. L. Aras and M. J. Richardson, *Polymer*, 1989, **30**, 2246-2252.
127. M. J. Richardson and N. G. Savill, *Polymer*, 1975, **16**, 753-757.
128. B. Wunderlich, D. M. Bodily and M. H. Kaplan, *Journal of Applied Physics*, 1964, **35**, 95-102.
129. J. Rieger, *Journal of Thermal Analysis*, 1996, **46**, 965-972.
130. M. M. Hann, A. R. Leach and G. Harper, *Journal of Chemical Information and Computer Sciences*, 2001, **41**, 856-864.
131. A. K. Ghose and G. M. Crippen, *Journal of Chemical Information and Computer Sciences*, 1987, **27**, 21-35.
132. V. N. Viswanadhan, A. K. Ghose, G. R. Revankar and R. K. Robins, *Journal of Chemical Information and Computer Sciences*, 1989, **29**, 163-172.
133. *Encyclopedia of surface science and colloid science*, 2nd edn., Taylor and Francis, 2006.
134. H. Noh and E. A. Vogler, *Biomaterials*, 2006, **27**, 5801-5812.
135. P. R. Babu and V. G. Gaikar, *Separation and Purification Technology*, 2001, **24**, 23-34.
136. J. Benavente, M. I. Vazquez, R. de Lara and P. Galan, *Colloids and Surfaces A (Physicochemical and Engineering Aspects)*, 2005, 270-271.
137. D. Rana and T. Matsuura, *Chemical Reviews*, 2010, **110**, 2448-2471.
138. Method developed by S. Hunter, Oxford Advanced Surfaces Ltd..
139. A. Vigroux, M. Bergon and C. Zedde, *Journal of Medicinal Chemistry*, 1995, **38**, 3983-3994.
140. D. Crich and X. L. Hao, *Journal of Organic Chemistry*, 1997, **62**, 5982-5988.
141. P. N. Juri and R. A. Bartsch, *Journal of Organic Chemistry*, 1979, **44**, 143-145.

142. T. W. Campbell, D. A. Young and M. T. Rogers, *Journal of the American Chemical Society*, 1951, **73**, 5789-5791.

Appendix I : Combustion analysis calculations

This is an example calculation demonstrating the methods followed to analyse the combustion analysis data. Material **116b** has been used as example.

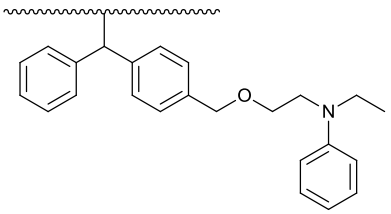

115

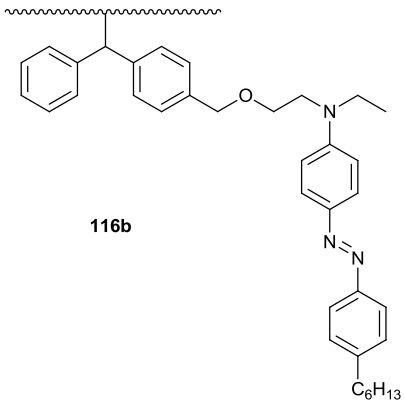

116b

Surface loadings:

%N = 0.23, as measured by combustion analysis.

Number of moles of N per gram of polymer

$$= \frac{\%N}{Mr(N)} \times 100 = \frac{0.24}{14} \times 100 = 1.79 \times 10^{-4}$$

Number of moles of surface modification per gram of polymer

$$= \frac{\text{moles N/gP}}{\text{atoms of N}} = \frac{1.79 \times 10^{-4}}{3} = 6.67 \times 10^{5}$$

Number of molecules of surface modification per gram of polymer

$$= \text{moles of surface modification} \times Av = (6.67 \times 10^{5}) \times (6.02214 \times 10^{23}) = 4.10 \times 10^{19}$$

Number of molecules of surface modification per cm^2 (where the literature surface area of XAD-4 is 725 m^2/g)

$$= \frac{\text{molecules/gP}}{725} / (100 \times 100) = (4.10 \times 10^{19}/725)/(100 \times 100) = 5.54 \times 10^{12}$$

Surface coverage:

Maximum number of molecules possible in 1 cm^2

$$= \frac{1}{\text{Ao}} = \frac{1}{1.71 \times 10^{-14}} = 5.85 \times 10^{13}$$

Ao is the limiting factor in cm^2, 1.17 nm^2/molecule

$$\% \text{ Surface coverage} = \frac{\text{actual number of molecules per cm}^2}{\text{maximum number of molecules per cm}^2} \times 100 = \frac{5.54 \times 10^{12}}{5.85 \times 10^{13}} \times 100 = 9.5\%$$

Efficiency of diazonium coupling method 1:

$$= \frac{\text{moles N/gP}}{\text{atoms of nitrogen} \times \text{moles N/gP on } \mathbf{115}} \times 100$$

$$= \frac{2.00 \times 10^{-4}}{3 \times 1.79 \times 10^{-4}} \times 100 = 37\%$$

Efficiency of diazonium coupling method 2:

Using **116l** as example.

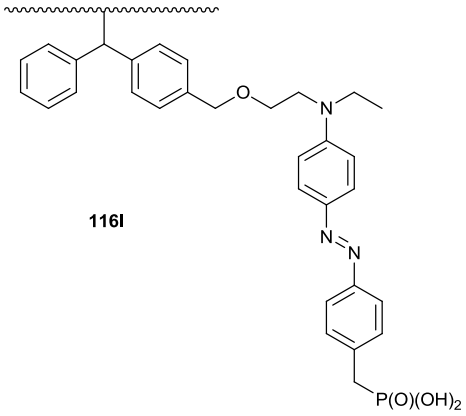

116l

%P = 0.17% = 0.055 mmol/g of P, %N = 0.61

$$\text{Expected \%P} = \frac{\%\text{N}}{3} = \frac{0.61}{3} = 0.203\% = 0.066 \text{ mmol/g P}$$

$$\% \text{ efficiency} = \frac{\text{actual}}{\text{expected}} \times 100 = \frac{0.055}{0.066} \times 100 = 83\%$$

N, the number of unmodified sites:

$$\%\text{N} = \frac{\text{Mass of N}}{\text{total mass}} \times 100$$

$$\%\text{N} = \frac{14x}{(Mr\ of\ 1\ modified\ monomer) + (N \times Mr\ styrene\ monomer)} \times 100$$

x = number of atoms of N

It is assumed that the number of unmodified monomers of polystyrene will much greater than the modified monomers so the number of modified monomers is always ~ 1. The M_r of a styrene monomer is 104.

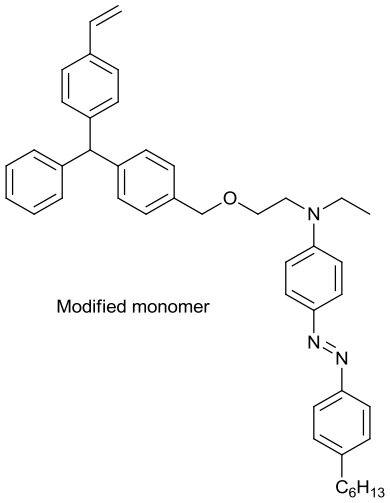

Modified monomer

This equation is rearranged to determine N. Using **116b** as an example,

$$\mathrm{N} = \left[\frac{14(3)}{0.23/100} - 637.9\right]/104 = 138$$

Appendix II : Protein Adsorption Correlations

Protein adsorption after three hours

As discussed in Chapter 5, the adjusted protein adsorption, after exposure to BSA for 3 hours, was compared with various cheminformatic parameters. Below are the remaining correlations not discussed in detail in the Chapter.

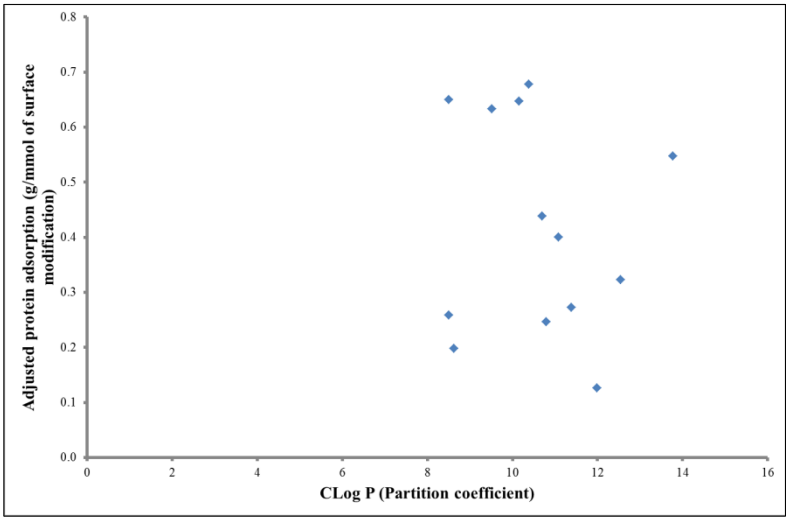

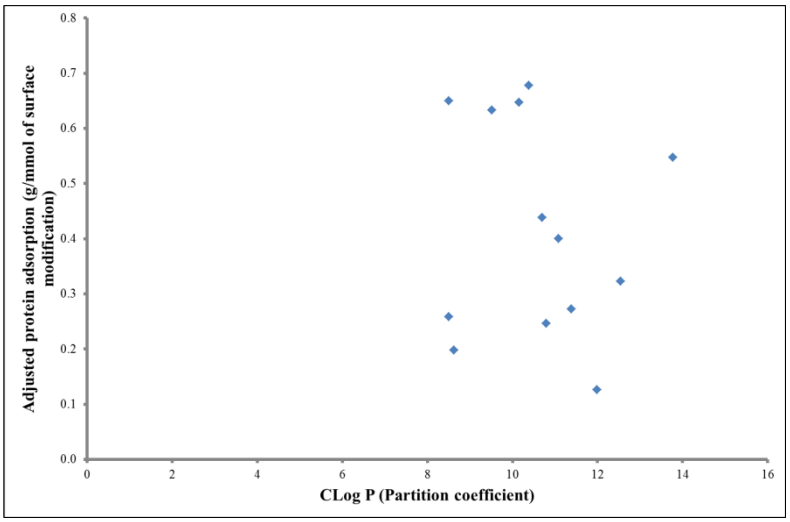

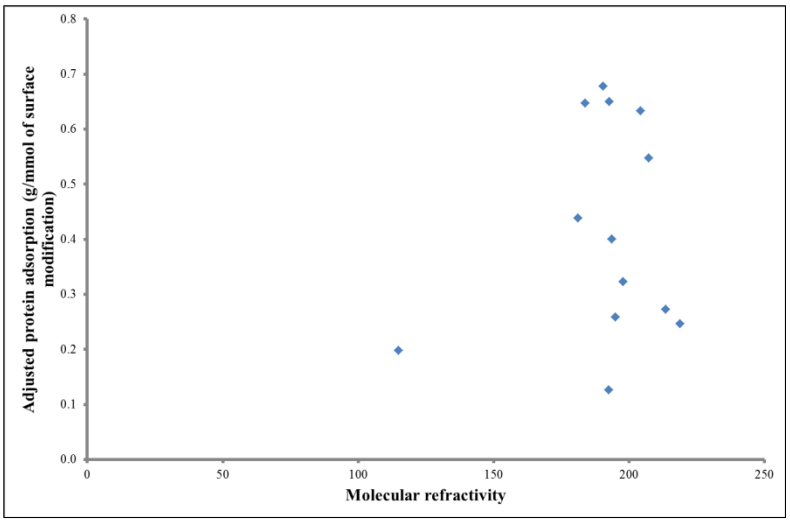
Adjusted protein adsorption (g/mmol of surface modification)
0.0
0.1
0.2
0.3
0.4
0.5
0.6
0.7
0.8
0
50
100
150
200
250
Molecular refractivity

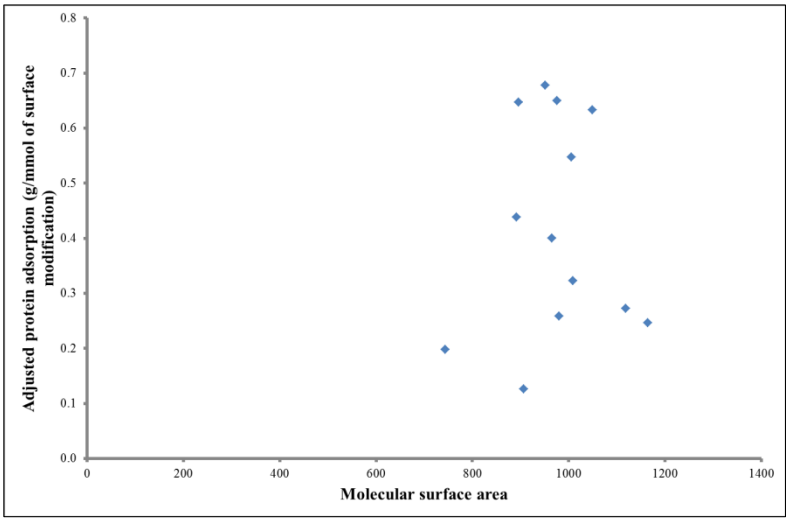
Adjusted protein adsorption (g/mmol of surface modification)
0.0
0.1
0.2
0.3
0.4
0.5
0.6
0.7
0.8
0
200
400
600
800
1000
1200
1400
Molecular surface area

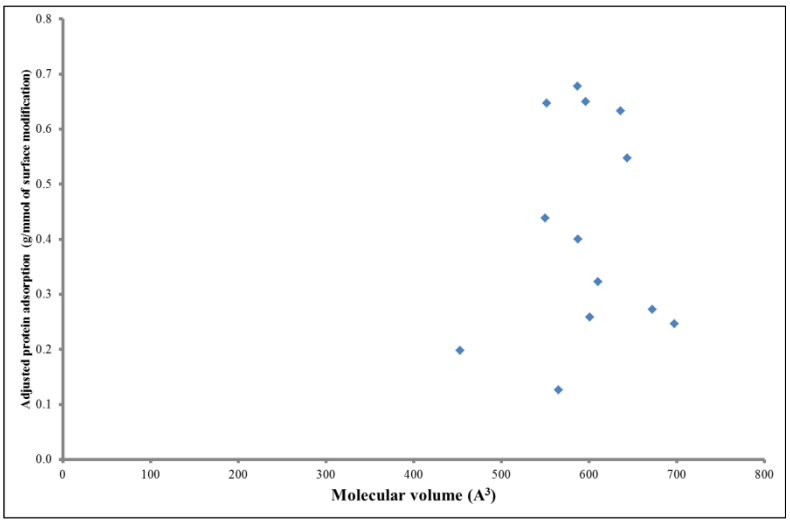
Adjusted protein adsorption (g/mmol of surface modification)
0.0
0.1
0.2
0.3
0.4
0.5
0.6
0.7
0.8
0
100
200
300
400
500
600
700
800
Molecular volume (A3)

Time-course protein adsorption

The adjusted protein adsorption after 1, 12 and 24 hours was compared with various cheminformatic parameters, below are the correlations not featured in Chapter 5.

1 hour

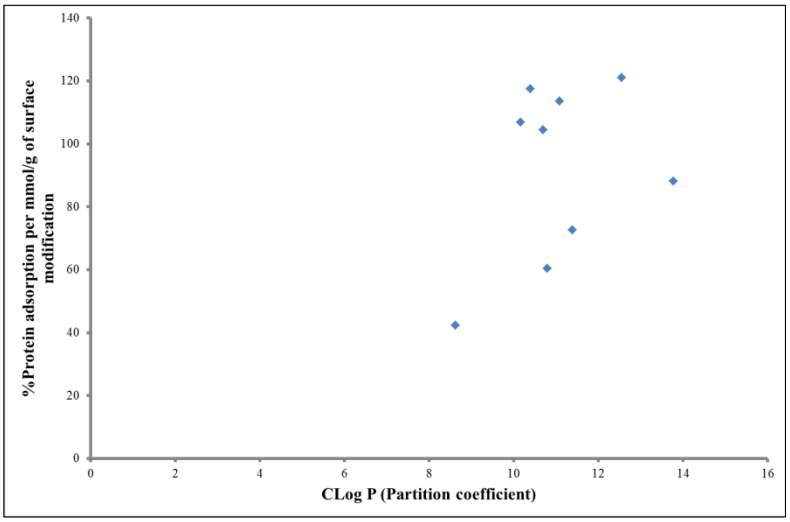

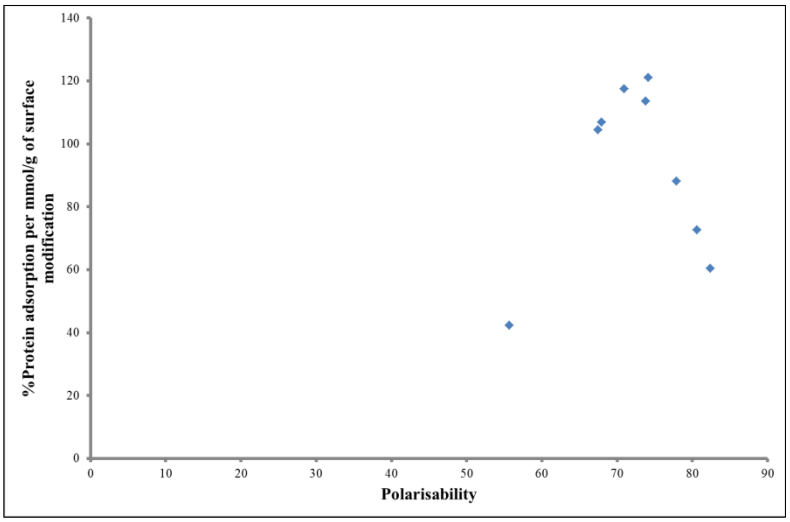

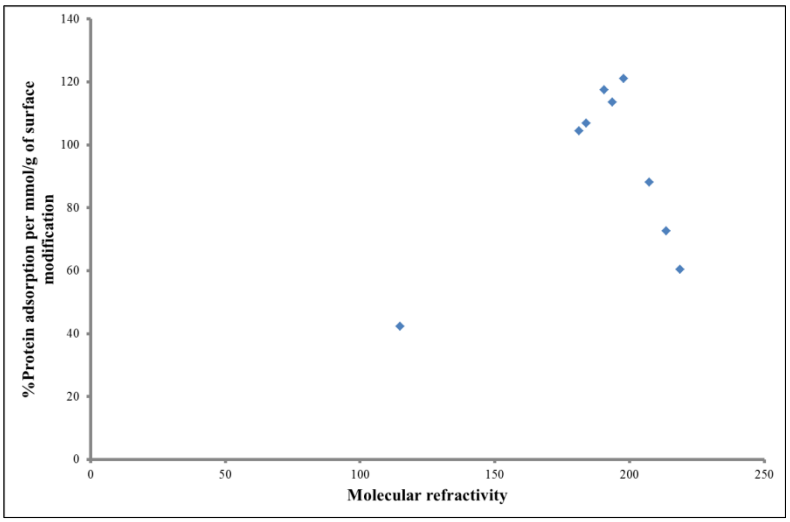
%Protein adsorption per mmol/g of surface modification
Molecular refractivity
0
20
40
60
80
100
120
140
0
50
100
150
200
250

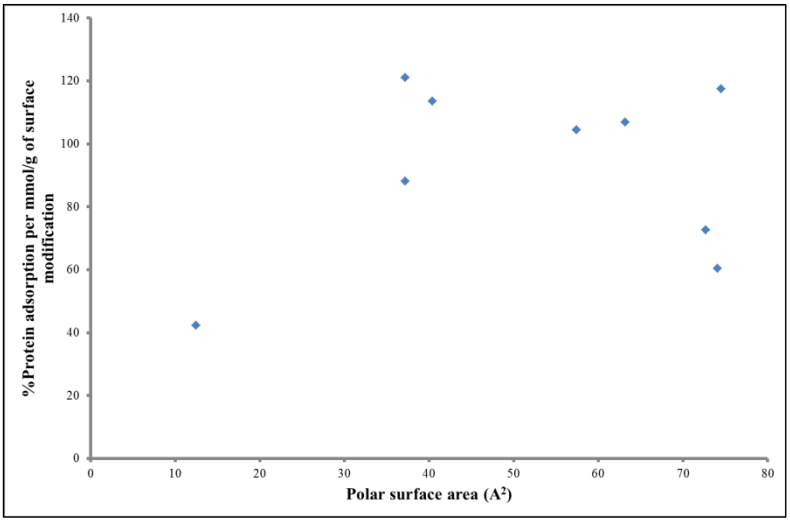
%Protein adsorption per mmol/g of surface modification
Polar surface area (A²)
0
20
40
60
80
100
120
140
0
10
20
30
40
50
60
70
80

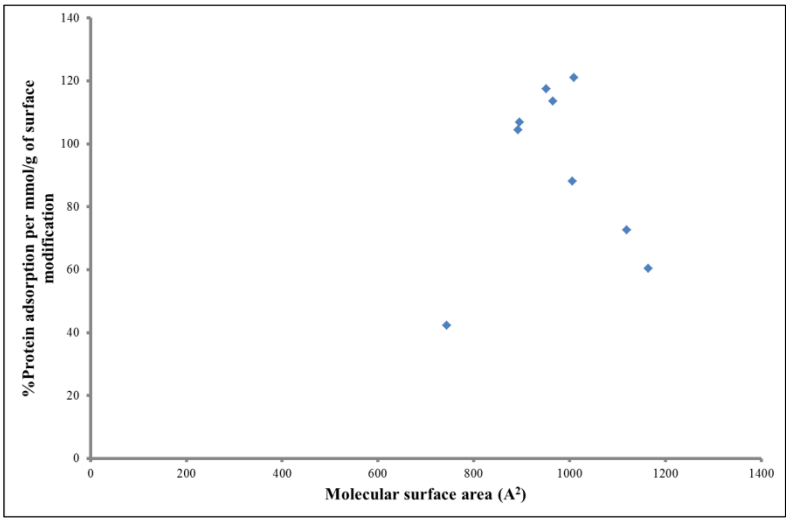
%Protein adsorption per mmol/g of surface modification
Molecular surface area (A²)
0
20
40
60
80
100
120
140
0
200
400
600
800
1000
1200
1400

12 hours

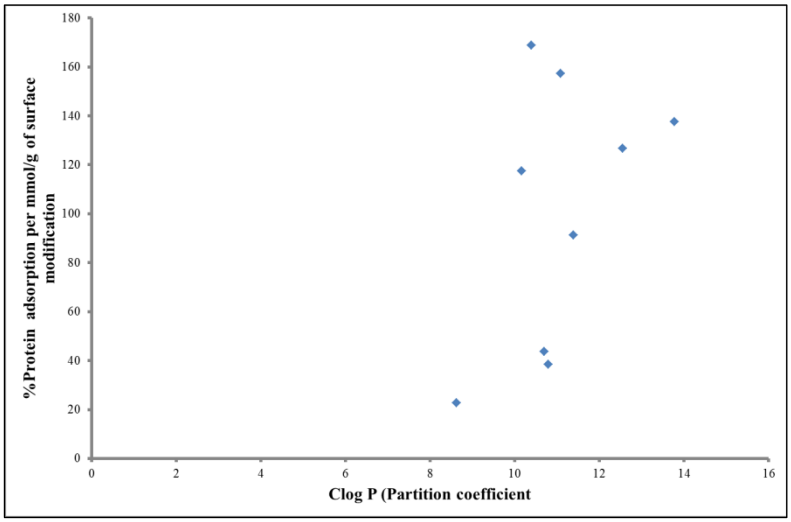
%Protein adsorption per mmol/g of surface modification
Clog P (Partition coefficient
0
20
40
60
80
100
120
140
160
180
0
2
4
6
8
10
12
14
16

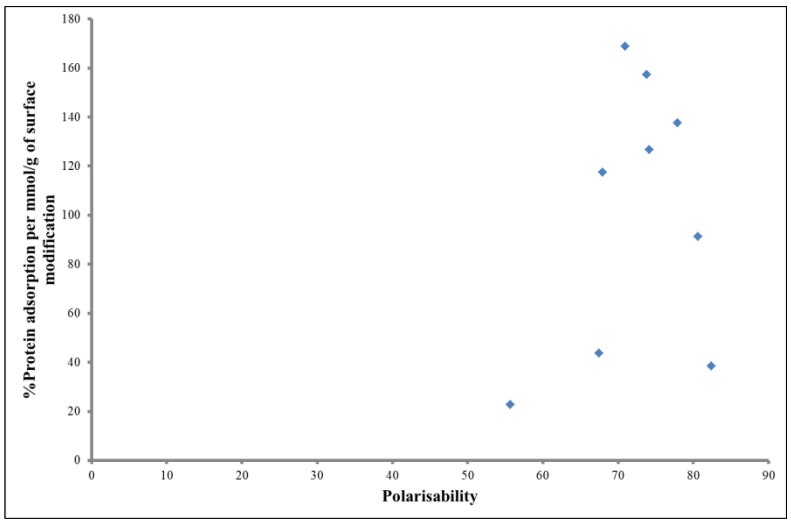
%Protein adsorption per mmol/g of surface modification
Polarisability
0
20
40
60
80
100
120
140
160
180
0
10
20
30
40
50
60
70
80
90

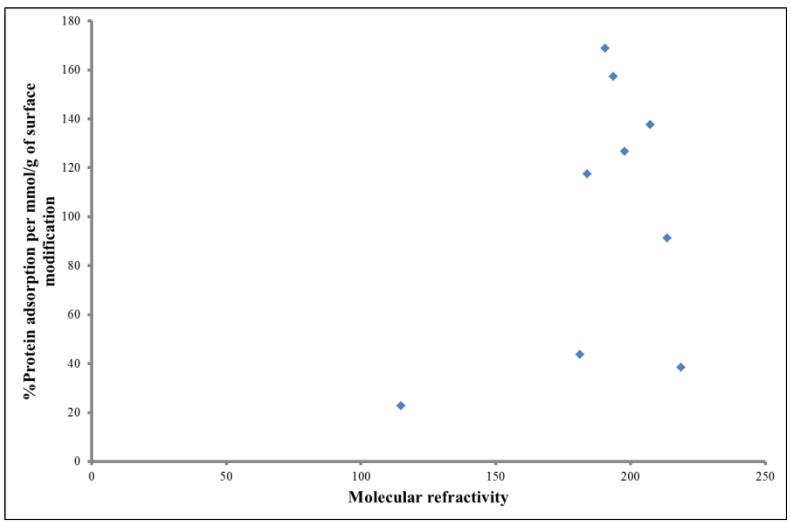
%Protein adsorption per mmol/g of surface modification
Molecular refractivity
0
20
40
60
80
100
120
140
160
180
0
50
100
150
200
250

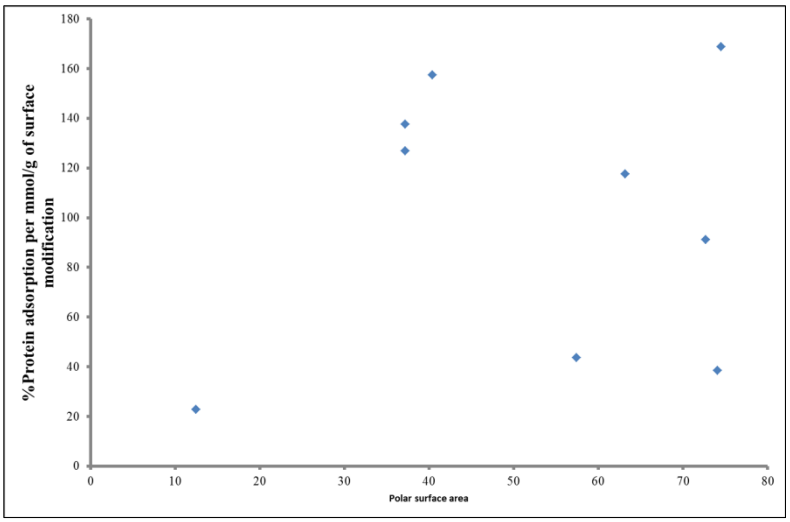
%Protein adsorption per mmol/g of surface modification
180
160
140
120
100
80
60
40
20
0
0
10
20
30
40
50
60
70
80
Polar surface area

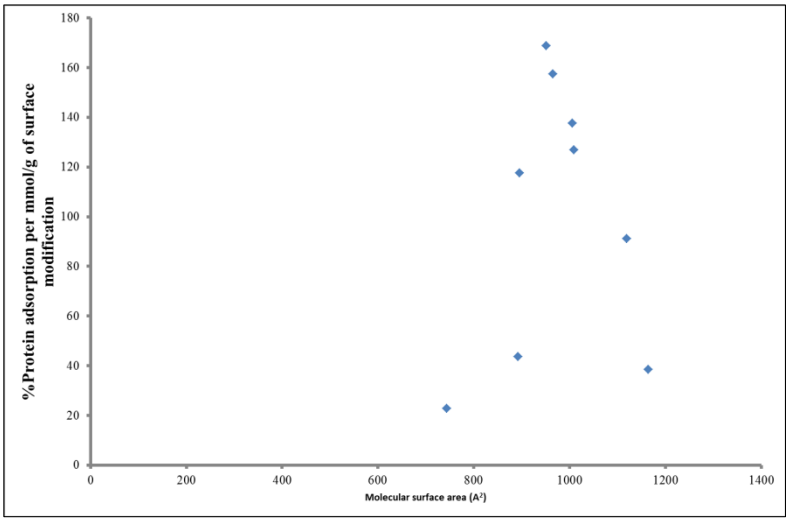
%Protein adsorption per mmol/g of surface modification
180
160
140
120
100
80
60
40
20
0
0
200
400
600
800
1000
1200
1400
Molecular surface area (A²)

24 hours

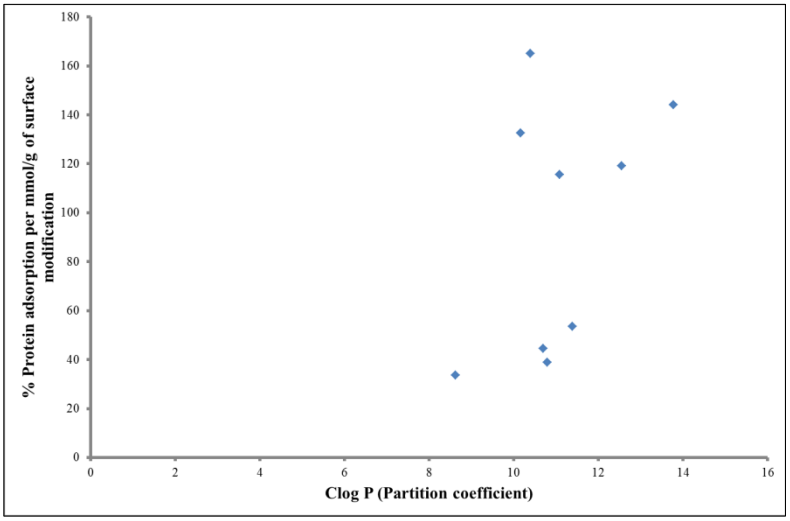
% Protein adsorption per mmol/g of surface modification
Clog P (Partition coefficient)

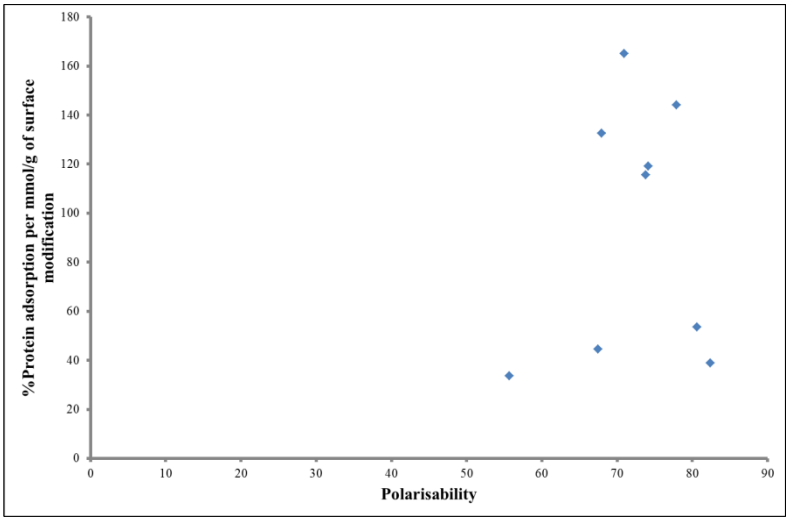
%Protein adsorption per mmol/g of surface modification
Polarisability

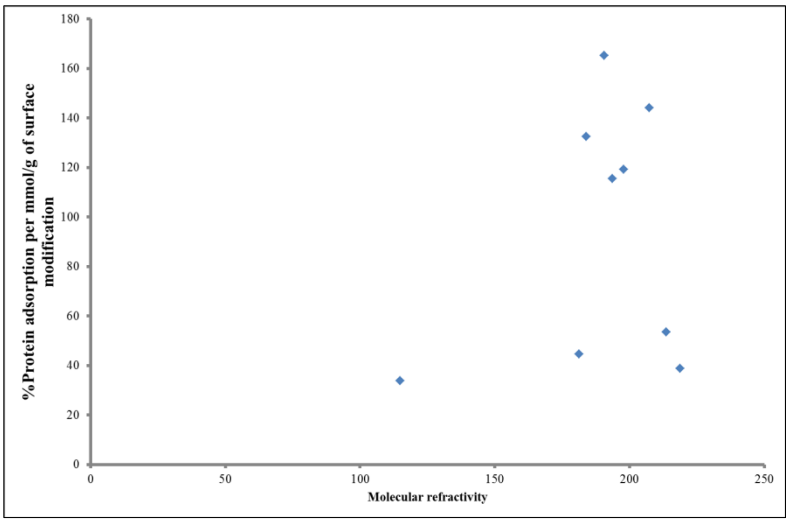
%Protein adsorption per mmol/g of surface modification
Molecular refractivity

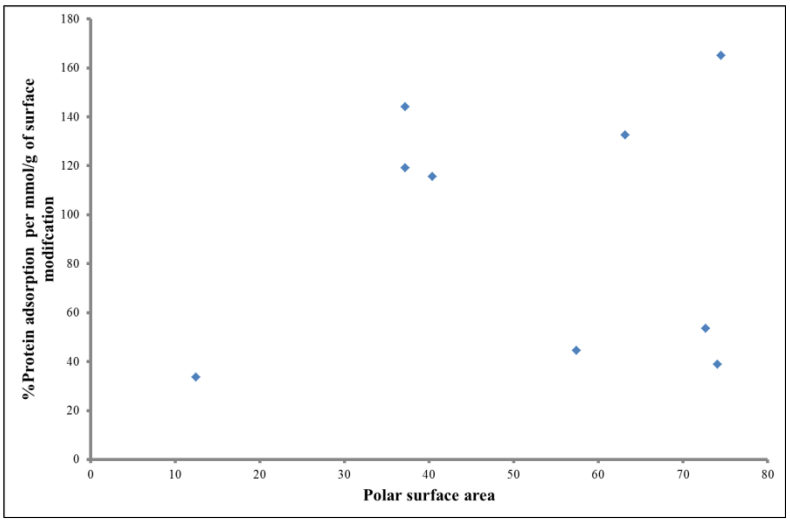
%Protein adsorption per mmol/g of surface modifcation
180
160
140
120
100
80
60
40
20
0
0
10
20
30
40
50
60
70
80
Polar surface area

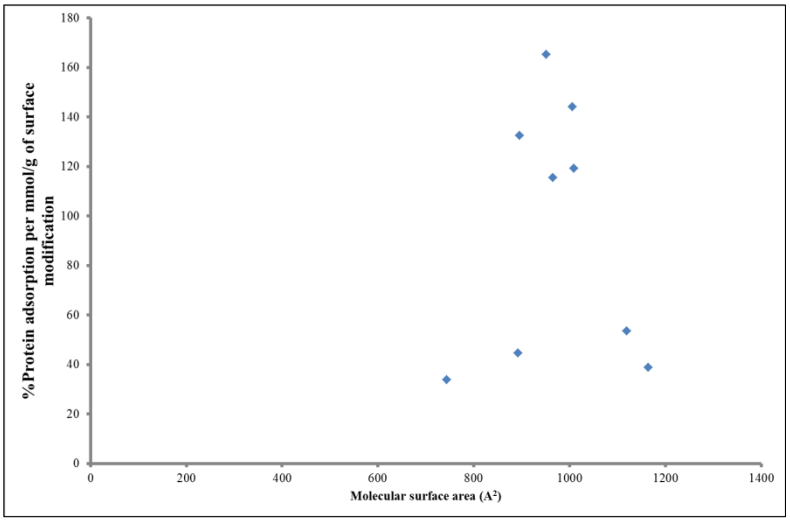
%Protein adsorption per mmol/g of surface modifcation
180
160
140
120
100
80
60
40
20
0
0
200
400
600
800
1000
1200
1400
Molecular surface area (A²)

Appendix III : Bioassay data and calibrations

Cephalosporin C (Ceph C) was used a reference in measuring the activity of the penicillin materials. Calibrations were carried out by Apichat Aphaiwong.

E Coli

Concentration of stock solution µg/mL	Volume Ceph C µL/well	Volume water mL/well	Mass Ceph µg/well	moles of Ceph C nmol/well	Zone size mm	log (nmoles of Ceph C/well)
10	20	80	0.2	0.48	13	0.32
	40	60	0.4	0.96	20	0.02
	60	40	0.6	1.44	22	0.16
	80	20	0.8	1.93	24	0.28
	100	0	1	2.41	27	0.38
100	20	80	2	4.81	29	0.68
	40	60	4	9.63	32	0.98
	60	40	6	14.44	36	1.16
	80	20	8	19.26	37	1.28
	100	0	10	24.07	39	1.38

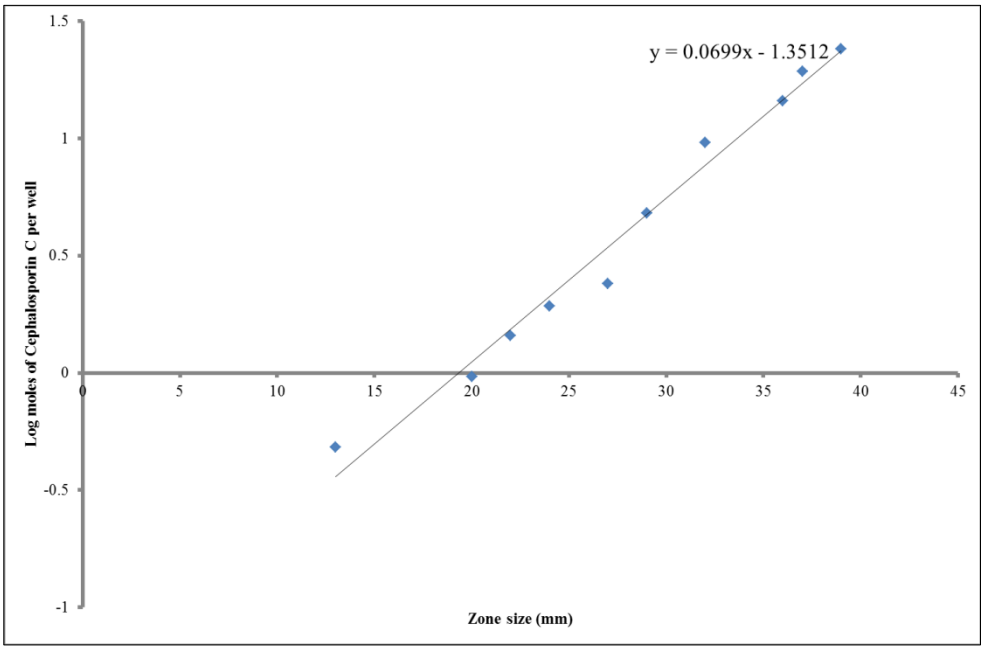

S. aureus

Concentration of stock solution µg/mL	Volume Ceph C µL/well	Volume water mL/well	Mass Ceph C µg/well	moles of Ceph C nmol/well	Zone size mm	log (nmoles of Ceph C/well)
1000	40	60	40	96.29	13.5	1.98
	60	40	60	144.44	16	2.16
	80	20	80	192.59	17.5	2.28
	100	0	100	240.73	18.5	2.38

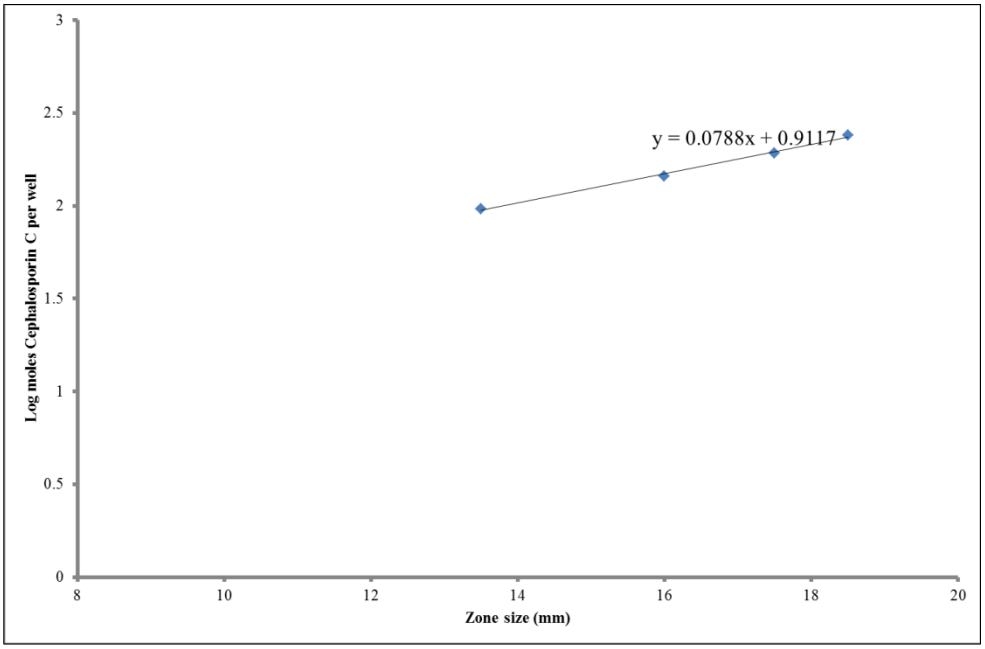

Hole plate assay of penicillin V

A hole plate assay of penicillin V was carried out by Apichat Aphaiwong and the results are presented below. The calibration used to determine the equivalent amount of the cephalosporin C reference is similar to that presented previously but not exactly the same.

Amount of penicillin V per well (mg)	nmoles of penicillin V	average zone size (mm)	Equivalent log ceph C	Equivalent nnoles of ceph C	% relative potency[a]
0.003125	8.95	33	1.30	19.99	223
0.001563	4.48	28.8	1.01	10.35	231
0.000781	2.24	27	0.89	7.80	349
0.000586	1.68	22.8	0.61	4.034	240
0.000488	1.4	22.5	0.59	3.85	275
0.000391	1.12	20.3	0.44	2.72	243
0.000293	0.84	18.8	0.33	2.16	257
0.000195	0.56	13	-0.06	0.87	155

[a]Relative potency = (moles cephalosporin c/moles penicillin V) × 100

The number of moles released by penicillin materials **121** and **122** was determined using the equation on the graph below.

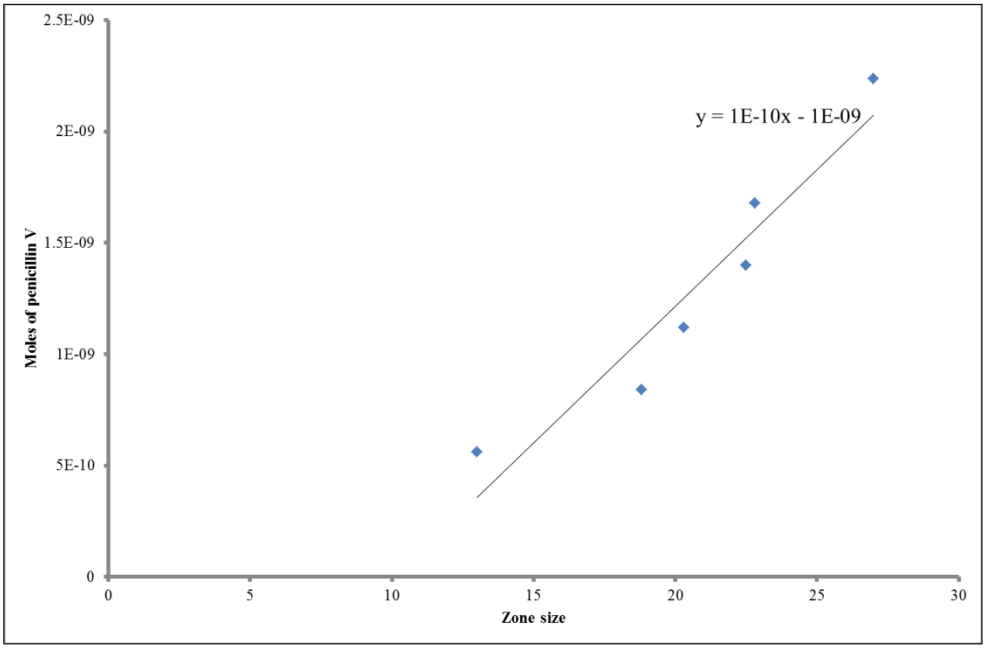

Appendix IV : XPS data on disc